GEOLOGICAL SURVEY OF CANADA

OPEN FILE 2983

Investigation of the space-time distribution of earthquakes in the Charlevoix Seismic Zone, Quebec

M. Eneva

1994

Natural Resources Canada | Ressources naturelles Canada

Canada

GEOLOGICAL SURVEY OF CANADA

OPEN FILE 2983

Investigation of the space-time distribution of earthquakes in the Charlevoix Seismic Zone, Quebec

M. Eneva

1994

Natural Resources Canada | Ressources naturelles Canada

Canada

INVESTIGATION OF THE SPACE-TIME DISTRIBUTION OF EARTHQUAKES IN THE CHARLEVOIX SEISMIC ZONE, QUEBEC

Mariana Eneva

Geophysics Division, Department of Physics
University of Toronto, 60 St George Street
Toronto, Ontario M5S 1A7

(under contract to Geophysics Division, Geological Survey of Canada)

Geological Survey of Canada Open File 2983

October 1994

ABSTRACT

A detailed analysis of earthquake activity in the Charlevoix Seismic Zone (CSZ) over the period October 1977 to July 1991 does not indicate any significant precursory changes in either the rate of seismic activity or in b-values. This contrasts with numerous reports of changes in these parameters prior to moderate and large events in other seismically active areas. It must be recognized however that the largest Charlevoix earthquake during the study period was only of magnitude 5.0, and occurred too early (August 1979) for extensive monitoring to be carried out beforehand. While spatially the activity was mostly random during the time period studied, the largest departure from this behaviour took place in late 1988, near the date of the M6.5 Saguenay earthquake. This event, the largest in eastern North America since 1925, was located 85 km to the northwest of the CSZ. The apparent connection between the Saguenay earthquake and reduced randomness, or greater clustering, in the CSZ suggest either stress changes in the CSZ as a result of the earthquake, or the simultaneous response of both the CSZ and the source area of the Saguenay event to a large-scale tectonic factor.

RÉSUMÉ

Une étude détaillée de la sismicité de la zone sismique de Charlevoix (ZSC) pour la période d'octobre 1977 à juillet 1991 ne montre aucune changement précurseur que ce soit en fréquence d'activité ou en valeur de b. Ce résultat contraste avec de nombreux rapports de changements de ces paramètres avant des tremblements de terre moyens et grands dans d'autres régions à sismicité elevée. Il faut tenir compte cependant que le plus grand séisme dans la ZSC pendant la période considérée n'a eu qu'une magnitude de 5,0 et s'est passé avant qu'on ait pu faire une surveillance prolongée (août 1977). Quoique la distribution spatiale de l'activité sismique était généralement aléatoire pendant la période d'étude, la plus grande exception s'est produit vers la fin de l'année 1988, autour de la date du tremblement de terre du Saguenay (M6,5). Cette événement, le plus grand dans l'est de l'Amérique du Nord depuis 1925, s'est produit au nord-ouest de la ZSC à une distance de 85 km. Le lien apparent entre le tremblement de terre du Saguenay et une diminution de la distribution aléatoire suggère soit une changement de contraintes dans la ZSC à la suite de ce tremblement de terre, soit une réaction simultanée de la ZSC et de la zone-source de l'événement du Saguenay en réponse à un facteur tectonique à grande échelle.

CONTENTS

CHAPTER 1. INTRODUCTION

1.1 Objective and Report Description

The Charlevoix Seismic Zone (CSZ)[1] is a seismically active area located in the valley of the St. Lawrence River, between Quebec City and the Sagueany River in Quebec (Figure 1.1.1). The level of current microseismic activity in the CSZ is the highest in eastern Canada. This zone is one of the few in eastern North America where large earthquakes have repeatedly occurred. Since the time intervals between the last four large events were smaller or comparable with the time that has elapsed since the last large earthquake in 1925, it is reasonable to expect another mainshock in the CSZ in a feasible future. This possibility, together with previous failure for any precursory phenomena to be identified in the zone, have inspired the present study of the spatial and temporal distribution of the Charlevoix microearthquakes. The techniques applied to study the CSZ earthquake catalogue are not the conventional ones and stemmed from recent similar studies of other seismically active areas (Eneva, 1984; Eneva and Pavlis, 1988; Eneva and Hamburger, 1989; Eneva et al., 1992c). The objective was to evaluate the long-term values of specific parameters describing and quantifying the space-time distribution of earthquakes in the CSZ, as well as their short-term variations in time. It was hoped that some previously unknown possibilities for earthquake forecasting might emerge in the course of this study. Alternatively, one might have to admit that the CSZ catalogue is useless in this respect, should it be the case (in agreement with previous studies). In any case, we aimed at obtaining information that is different from what was already known about the zone and is perhaps complimentary to the existing knowledge in a significant practical way.

The present Chapter features general information about the larger events in the area, the seismic stations used to record and analyze the CSZ earthquakes, previous studies in the zone, its tectonic setting, and the techniques used in this study. Chapter 2 provides detailed information about the earthquake catalogues used and the quality of data. Various visual displays are shown in this Chapter, such as cross-sections and X-Y plots featuring the temporal changes of the parameters included in the earthquake catalogues. Magnitude-frequency relationships are also shown. All these are of traditional type and are only used for general examination of the data. The next three chapters feature non-traditional techniques in the way the CSZ earthquake catalogue was examined (as intended when this study was proposed; see Eneva and Farquhar, 1991). Chapter 3 examines the changes in the rates of seismic activity in the CSZ using the technique of Habermann (1983, 1987). This technique makes it possible to distinguish between artificial and natural (man-made) rate changes (numbers of events per unit time) in many cases, as well as to identify the most probable cause for the artificial rate changes. Chapter 4 describes the application of the pair analysis technique (Eneva and Pavlis, 1988, 1991; Eneva and Hamburger, 1989; Eneva et al., 1992c) to the CSZ data. Chapter 5 shows results from the application of the correlation integral method (e.g., Hirata, 1989) to the earthquake data in the CSZ. Both Chapter 4 and 5 present results based on the study of interevent distances and time intervals. The characteristics provided allow us to utilize the catalogue information significantly

[1] Other names for the CSZ have been also used in some papers, such as La Malbaie area (e.g., Lyons et al., 1980; Stevens, 1980) and Charlevoix-Kamouraska area (e.g., Lamontagne et al., 1990)

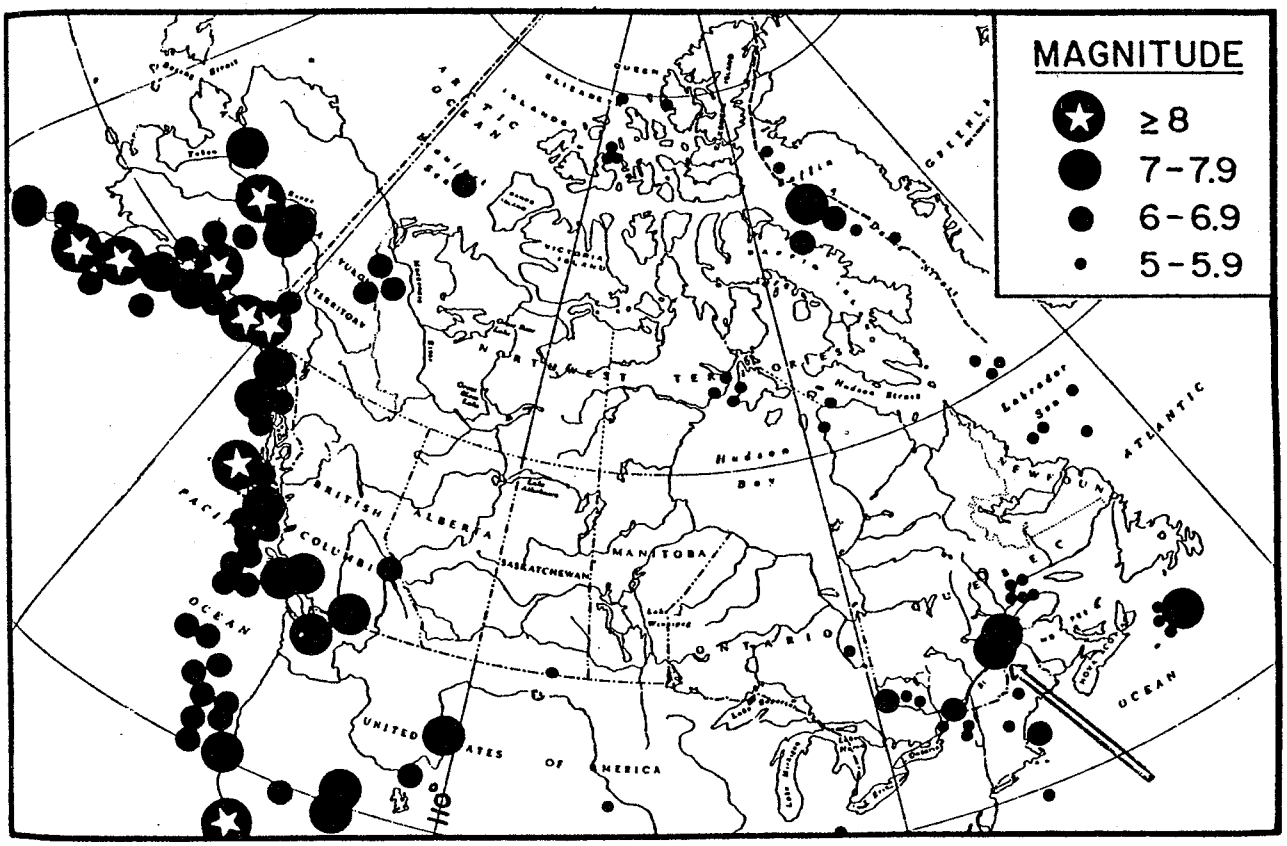

Figure 1.1.1 Significant historic earthquakes in Canada and adjacent regions (after Basham et al., 1985). Earthquakes with magnitudes $\leq$ 5.9 are shown only in the region east of 110°W. Arrow shows the location of the Charlevoix seismic zone (CSZ).

beyond the traditional studies of rates of seismic activity and b-values (the slopes of the magnitude-frequency relationships). Chapter 6 includes the description of some approaches that did not provide at this time any significant new insight into the space-time distribution of the CSZ earthquakes, but may have potential of doing so upon a more involved development of the related techniques. Chapter 7 features the main conclusions from this study and recommendations for further work.

1.2 Larger Events in the Area

The CSZ has been determined as one of the regions of higher seismic risk in Canada and certainly the highest risk in eastern Canada (Basham et al., 1985). M=7.5 is selected as the largest plausible earthquake in the intraplate environment of eastern Canada. Such an event would represent a rupture along most of the CSZ. Mainshocks of magnitudes about 6 and above, and perhaps as large as 7, have occurred at least five times over the last 300 years in the CSZ. Smith (1962) reported that large historic events occurred in 1663, 1791, 1860, and 1870 before the last large earthquake of magnitude about 6.5 in 1925. Other relatively recent moderate events in the CSZ were the M5.6, M5.2, and M5.0 earthquakes in 1939, 1952, and 1979, respectively (Adams and Basham, 1989). Stevens (1980) relocated earthquakes of magnitudes greater than 4.5 that were instrumentally recorded back to 1924 (Figure 1.2.1). Of 17 such events (including the largest of them in 1925), 11 were in the vicinity of Hare Island (Ile aux Lievres), or more precisely, to the southwest of this island. The remaining 6 events occurred in the vicinity of Ile aux Coudres, around the south-western boundary of the CSZ. These two locations are therefore perhaps the most likely sites of future larger events. To confirm this, the largest most recent earthquakes, a M5.0 event in 1979 and a M4.3/M4.4 doublet in March 1989 (Wetmiller and Adams, 1990) occurred in the northeastern location. For the period studied here, October 20, 1977 - July 31, 1991, 6 events of $M \geq 4.0$ have occurred in the CSZ, 4 of them at the same northeastern location.

A number of fault plane solutions have been calculated for the CSZ. Although the mechanisms of the older events are not well determined, Ebel et al. (1986) suggested that the relatively large 1925 and 1939 earthquakes were of thrust type with faulting on either NE or NW striking planes. The first well constrained CSZ mechanism was the one for the 1979 M5.0 event evaluated by Hasegawa and Wetmiller (1980); the preferred nodal plane solution for this event indicates a 46° east of north strike and a 76° dip to the southeast. Wetmiller and Adams (1990) provided fault-plane solutions for the M4.3/M4.4 doublet from March 1989; these solutions indicate thrust mechanism as well, although the planes of faulting are north-striking.

One of the largest earthquakes in eastern North America over the last 50 years occurred just about 80 km northwest from the CSZ on November 25, 1988 (Figure 1.2.2). This M6.5 event came to be known as the Saguenay event after the Saguenay Graben that is a structure almost normal to the St. Lawrence valley, intersecting it some 35 km northeast from the Hare Island (see also Figure 1.3.1). The Saguenay graben has not been considered to be seismically active (no events of magnitude greater than 3 had been recorded within 50 km of the epicentre) and the 1988 earthquake apparently occurred some 20 km to the south of the most southerly of the mapped faults considered to be associated with this graben (North et al., 1989). However, a recent reexamination of the available geological data seems to indicate a closer spatial relationship between the hypocentre and the Saguenay Graben (J. Adams, personal

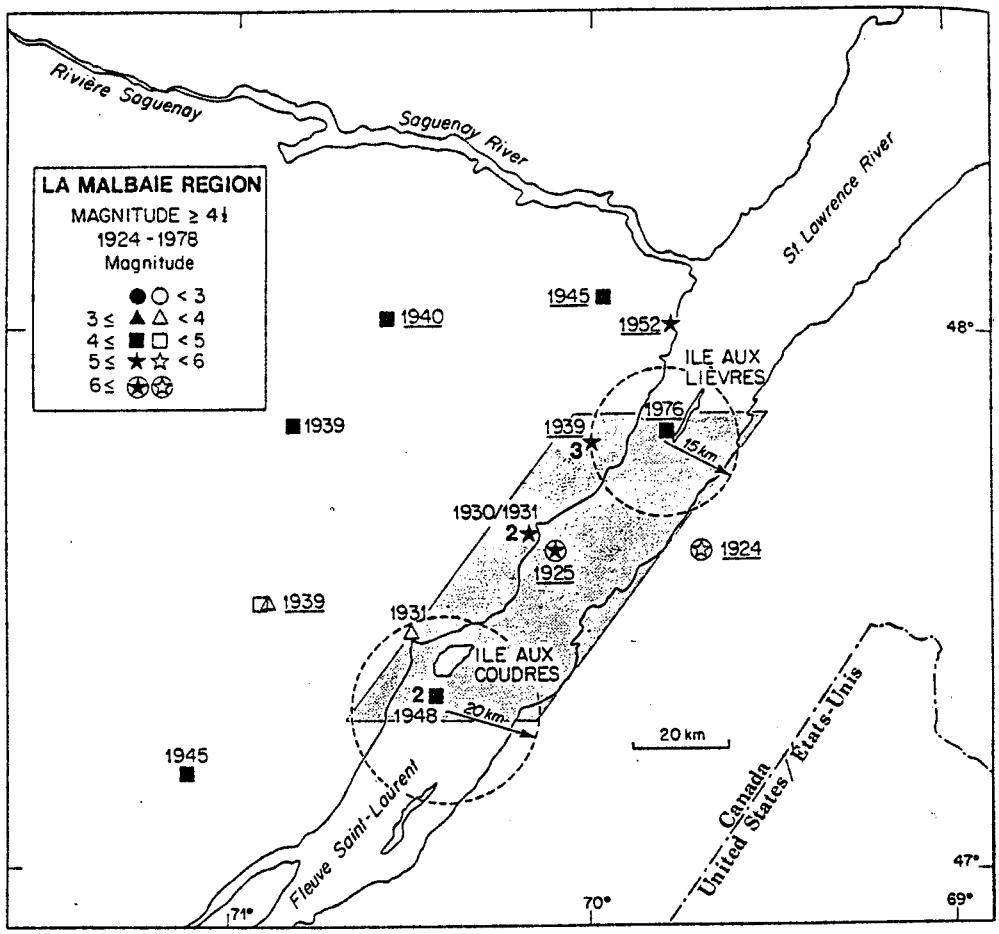

Figure 1.2.1 Epicentral map of all known earthquakes with magnitude $\geq$ 4.5 that occurred in the Charlevoix seismic zone (CSZ) during the period 1924-1978 (after Stevens, 1980). The approximate outlines of the CSZ are marked by the shaded area. Filled symbols indicate epicentral uncertainty $\leq$ 40 km, open symbols indicate larger uncertainty. Four-digit numbers show year of earthquake occurrence. The 11 epicenters marked by underlined years were relocated near Ile aux Lievres (Hare Island). The remaining 6 epicenters (the 1945 event excluded) were relocated near Ile aux Coudres. Dashed circles indicate the approximate source areas of the relocated events.

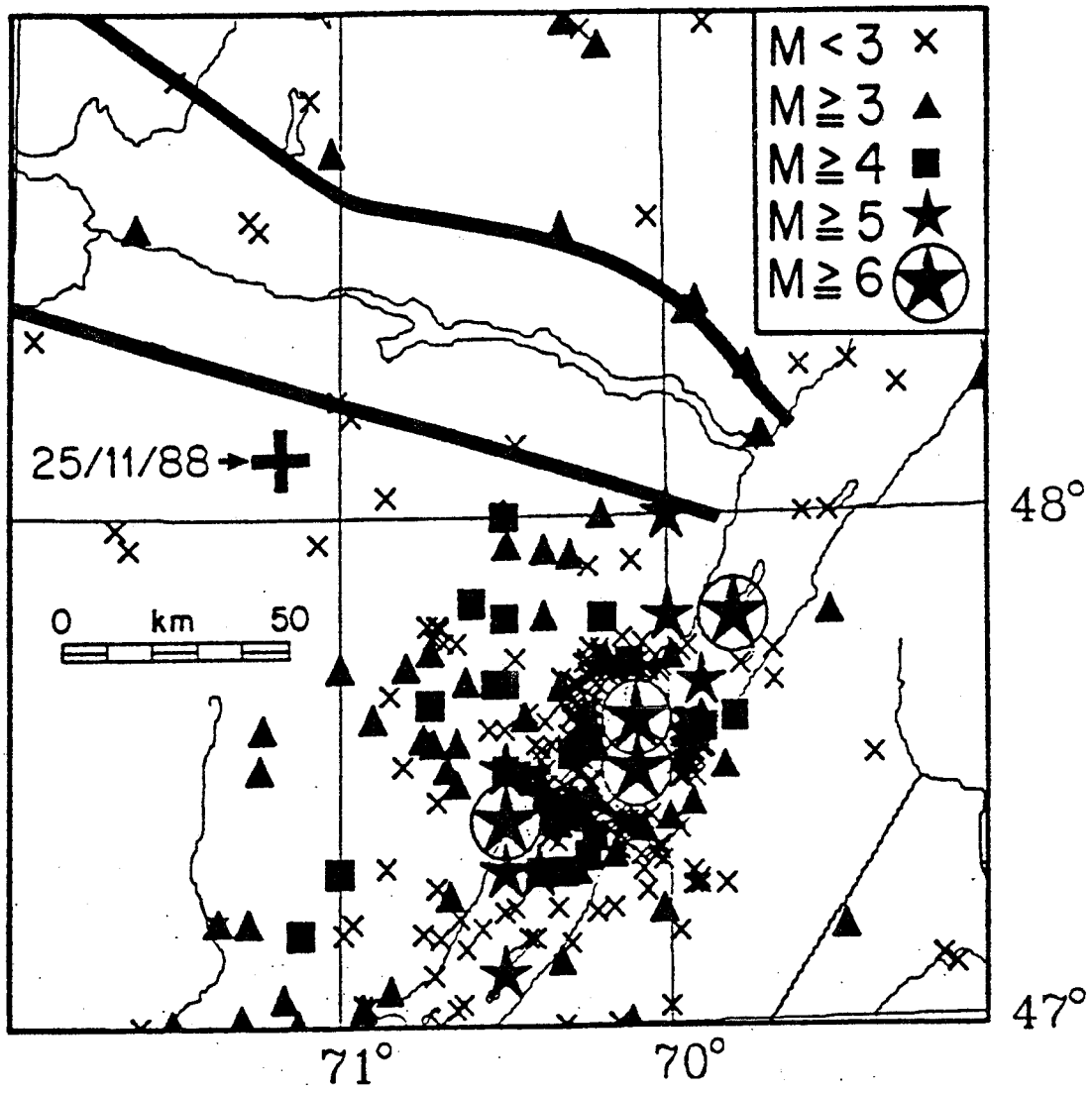

Figure 1.2.2 Epicentral map of the Charlevoix seismic zone (CSZ) together with the source area of the 1988 M6.5 Saguenay event marked by a large cross (after North et al., 1989). Heavy lines show the approximate limits of the Saguenay Graben. (Many of the epicenters in the northeastern part of the CSZ are for older events and are poorly located.)

communication). While outside the study area, this mainshock has to be considered in connection to the space-time distribution of earthquakes in the CSZ, as will be explained below. The Saguenay event had several interesting and even unusual features. Its magnitude of 6.5 is a m_{bLg}, but the estimates of m_b and the moment magnitude from teleseismic data are much smaller (about 6.0 and less). This testifies to one of the most unusual characteristics of the Saguenay event, i.e. the unexpectedly large amount of high frequency energy this earthquake produced. Another unusual characteristic was its depth of 29 km; such depth is significantly larger than the depths of other moderate earthquakes in eastern North America. The relatively large felt area and aftershock area, as well as the relatively small number of aftershocks associated with the Saguenay event contribute further to its being considered as an event that is significantly different from other intraplate mainshocks of the same size. The Saguenay earthquake was studied in great detail by North et al. (1989), Lamontagne et al. (1990), Somerville et al. (1990), Du Beger et al. (1991), Haddon (1992), Boore and Atkinson (1992).

1.3 Tectonic Setting

Figure 1.3.1 shows an epicentral map of all earthquakes recorded in the period October 20, 1977 - July 31, 1991, studied here. The dotted lines denote known faults in the region. The microearthquakes occur mostly at depth between 5 and 25 km. Since the Palaeozoic sediments that crop out on the south shore of the river are only few kilometres thick, Adams and Basham (1989) indicate that the earthquake activity is concentrated in the Precambrian basement. Anglin (1984) provides stereo plots of hypocentral cross-sections showing that most events occur on NE striking planes, steeply dipping to the southwest. In general, the seismic activity is concentrated between Palaeozoic rift faults along the north shore (see Figure 1.3.1) and a bathymetric feature (not shown) along the south shore. Thus, a large part of the microearthquakes occur under the St. Lawrence river. In addition to the controlling role of the northeast-striking rift faults, Anglin's (1984) stereo plots reveal that some northwest-striking transverse faults exercise partial control on the spatial distribution of seismic activity as well. In general, the fault-plane solutions of most CSZ earthquakes indicate thrust or thrust/strike-slip faulting. In addition to the mechanisms of the larger events (see 1.2), six mechanisms were determined in a 1974 microearthquake survey (Leblanc and Buchbinder, 1977). Lamontagne (1987) derived composite mechanisms from more than 100 CSZ events, and Adams et al. (1988) determined the mechanisms of other recent relatively small events. The fault-plane solutions for the CSZ earthquakes are a natural consequence of the orientation of the deviatoric compressive stress axis in the region, similar to the mechanisms of other earthquakes in eastern North America (e.g., Wahlstrom, 1987).

The CSZ represents an area of very concentrated seismic activity, since there are very few earthquakes outside the boundaries naturally outlined on the basis of the visible epicentres. The Gouffre Fault along the north shore (Figure 1.3.1) clearly forms the northwest boundary of the CSZ. The Saguenay Graben faults, such as the Palissades fault perhaps control the NE boundary when intersecting with the faults parallel to the north shore of the St. Lawrence river. Further NE, however, significantly beyond the CSZ boundaries, the microearthquake activity reappears along the lower St. Lawrence valley, closer to the mouth of the river (Figure 1.1.1). While no events of $M \geq 5.0$ are likely to have occurred there, M3.0 and M4.0 events are as frequent as in the CSZ.

Neotectonic processes due to a variety of geophysical processes apparently control the seismic activity (e.g., Hasegawa, 1988). Along the St. Lawrence valley, faults from previous

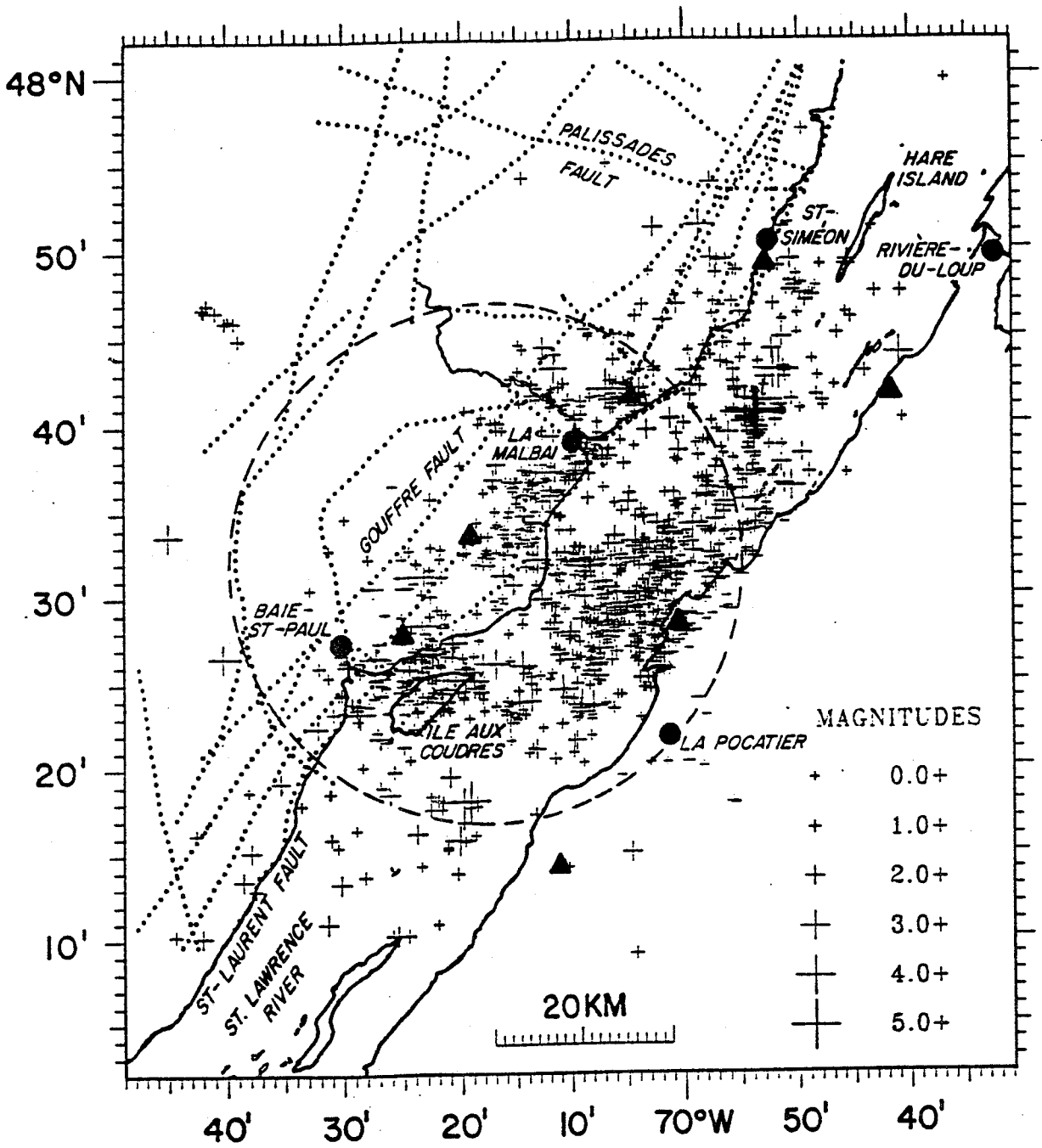

Figure 1.3.1 Epicentral map of the events that occurred in the CSZ during the period October 20, 1977 - July 31, 1991. Large cross shows the epicenter of the August 19, 1979 M5.0 event, the largest in the study period. Dotted lines mark known faults in the area. Triangles denote the stations of the local array. Dashed circle marks the Charlevoix impact structure. Data provided by A.M. Franklin, R.G. North, and J. Adams (Geological Survey of Canada; personal communication).

tectonic orogeneis such as the opening of the Proto-Atlantic Ocean (Kumarapeli and Saull, 1966) are reactivated by the neotectonic stress field. These authors consider the St. Lawrence valley system as a North American equivalent of the East African rift. The ancient rift faults behave mostly as thrust faults under the present high compressional stress field that is prevalent in eastern North America (Adams, 1989). Description of different fault systems in the CSZ, more specifically the times of their formation, is given by Lamontagne (1987) among others. Details on the specific faults mapped in Figure 1.3.1 were discussed by Rondot (1979), while Anglin (1984) provides a detailed comparison between the hypocentral distribution of earthquakes in the CSZ and individual faults. Similar to other areas in eastern Canada (e.g., Forsyth et al., 1983; Hasegawa, 1988) the reactivation of these ancient zones of weakness is considered to be the major reason for the seismic activity in the CSZ. However, the plate tectonic driven compressional stresses (i.e., opening of the mid-Atlantic ridge), are not sufficient to explain the seismic activity concentrated in only few areas, while the rift zone extends along the whole valley. Sanford et al. (1984) used satellite imagery and seismicity patterns along the St. Lawrence river to delineate observed and assumed block boundaries. These authors hypothesize that block tilting and rotation due to underlying viscoelastic processes could also contribute to the seismic activity. Developing an earlier idea (Hasegawa et al., 1985), Yamazaki and Hasegawa (1990) used numerical simulations of stress migration in a lithosphere with non-uniform viscosity to suggest that vertical upward migration of the horizontal tectonic component significantly enhances the upper crustal stress in the CSZ. They model the CSZ with a wedge inserted between two geologic provinces: the high heat-flow Palaeozoic Appalachian province to the southeast and the low heat-flow Grenville province of the Canadian shield to the northwest. A quasi-ductile surface layering in the CSZ (indicated by lack of earthquakes) represents an additional stress amplifier in the underlying layer. These authors conjecture that this enhanced stress could cause stable sliding along pre-existing faults in the middle and lower crust which results in a further stress concentration and sudden slip along locked faults.

None of the above factors, however, explain why seismic activity is present in the CSZ and in the lower St. Lawrence valley, but is absent in most other parts of the St. Lawrence rift system. An additional factor causing the seismic activity in the CSZ could be the ring faulting due to the impact crater of a late Devonian, 350 Ma old, meteorite (see dashed circle in Figure 1.3.1). In a search for an explanation why seismic activity is not evident along the whole valley of the St. Lawrence river, some authors argue that the CSZ activity is influenced by the crater (Roy and Du Berger, 1983; Lamontagne, 1987). Readily observable relationship is apparently absent, but Lamontagne (1987) suggests that at least the fault-plane solutions of the CSZ earthquakes seem to be affected by the impact zone: events inside this zone seem to be characterized by more variable orientations, while the earthquakes outside it are more similar in their focal mechanisms. Adams and Basham (1989), however, note that the impact structure hardly represents a controlling factor in the seismicity, since many of the CSZ earthquakes occur downriver beyond the impact zone and the hypocentral trends suggest only reactivation of the rift faults.

The seismic activity in the CSZ poses some questions that have been associated with the intraplate seismic activity in the whole region of eastern Canada (e.g., Yang and Aggarwal, 1981), as well as elsewhere in the world. Clear link between the earthquake activity and particular faults is not easy to observe. Details on possible additional causative factors for the

intraplate seismicity in eastern Canada are given by Hasegawa et al. (1985), Hasegawa (1988) and Yamazaki and Hasegawa (1990).

1.4 Network

The Geological Survey of Canada operates over 150 seismograph stations throughout Canada (North, unpublished manuscript). Of these, some 50 stations produce digital data that is subsequently telemetered to central acquisition systems. The *standard network* that was installed in the 1960's initially consisted of 25 stations equipped with three-component short- and long-period seismometers. Because the operation of these stations was expensive, 18 of them were closed and replaced by *regional* stations. Over 50 regional stations are deployed throughout Canada. They measure vertical short-period component data only and, while inexpensive to operate, provide only the most basic information in analog form.

In the most densely populated seismically active areas, southwestern B.C. and the St. Lawrence valley, telemetered networks now provide real-time digital data from 20 sites in each area to acquisition systems in the Pacific Geoscience Centre (Western Canadian Telemetered Network, WCTN) and Ottawa (*Eastern Canadian Telemetered Network*, ECTN). Clones of the ECTN system, i.e., *local telemetered networks*, have been installed at Charlevoix, Quebec (CLTN) and Sudbury, Ontario (SLTN). These are aimed at assuring detailed monitoring of the high microearthquake activity in the CSZ and the mining activity around Sudbury.

The earliest microseismicity study conducted near the CSZ took place in 1968 when 3 stations were operated in the region for a brief period of time (Milne et al., 1970). The first microearthquake survey of the CSZ was carried out in 1970 (Leblanc et al., 1973), followed by a second one in 1974 (Leblanc and Buchbinder, 1977). Up to 19 stations were used in 1974. At that time, the Charlevoix Seismic Observatory was established on the north shore of the St. Lawrence river for continuous recording of various geophysical parameters (Buchbinder et al., 1988). In October 1976, a regional station (LMQ) was installed at this observatory (between Bai-St-Paul and La Malbaie, see Figure 1.3.1). This station is very important for determining the magnitudes of the CSZ microearthquakes. A radio-telemetered analog tape recording array of 7 seismometers was deployed in late 1977 (Anglin and Buchbinder, 1981). It used the same array sites as in 1974, with the addition of another station near LMQ. The array was reduced to 6 elements in July 1980. The original analog array was converted to a wide dynamic range digital network in October 1987 (Wetmiller and Adams, 1990). Current monitoring of the microseismicity in the CSZ is essentially based on this 6-station telemetered network, one analog seismograph station and one ECTN station.

The period studied here starts on October 20, 1977 (when the array was established) and ends on July 31, 1991 (the end of the data available at the time of preparing this report).

1.5 Variations in Geophysical Parameters From Previous Studies

Following the first (Leblanc et al., 1973) and the second (Leblanc and Buchbinder, 1977) microearthquake surveys in 1970 and 1974, respectively, extensive geophysical monitoring was carried out in the CSZ from 1974 to 1985/86 (Buchbinder et al., 1988) with the long-term aim of determining the background level and fluctuations in activity and with the hope that precursory phenomena prior to moderate or large earthquakes may be identified. In addition to microseismicity, other parameters were also studied, such as the following: P-travel times from

explosions; earthquake P- and S-waves; crustal deformation (vertical and horizontal movements, tilt, gravity change); magnetoteluric parameters (electric impedance and potential); and water level change in wells. In addition to the work cited above, other publications also discussed results from various studies in the CSZ zone. These were related to the crustal structure in the region (Lyons et al., 1980), velocity changes (Buchbinder, 1981), shear-wave splitting and anisotropy (Buchbinder, 1989), tidal and coseismic well-level observations (Bower, 1989), and gravity data (Lambert and Liard, 1981).

No clear precursors were identified before the largest local earthquake during the observation period (August 19, 1979; M5.0) or any other event in the CSZ. In particular, no unusual seismicity patterns were observed at that time, as evidenced by the spatial and temporal distribution of earthquakes (Anglin and Buchbinder, 1981; Anglin, 1984; Buchbinder et al., 1988). Rates of seismic activity were observed to fluctuate a lot, but without association with the presumed preparation time of any particular event. Quiescence patterns, i.e. precursory decrease of seismicity rate (e.g., Wyss and Habermann, 1988; Reasenberg and Matthews, 1988), have not been observed in the CSZ. Precursory changes in b-values were not observed either, although b-values have been reported to change before larger events elsewhere (e.g., Smith, 1986). In fact, it seems there were no time periods in the CSZ when the magnitude-frequency relationships formed straight segments with easily identifiable slopes. Since changes in seismicity rates and b-values are the parameters most commonly used when analyzing earthquake catalogues, these negative observations seemed to render the CSZ catalogue non-informative in this respect. Unless some other types of parameters are extracted from the catalogue, one may have to abandon the idea that the microearthquake record can be of any help. On a less pessimistic note, however, the fact that no obvious precursors were observed before a M5.0 event still does not mean that precursors would not be observed before the next moderate to large events in the CSZ. In the light of the above, the monitoring of traditional parameters should continue along with monitoring of other parameters that might be adopted from the catalogue of CSZ earthquakes.

1.6 Main Techniques Used

Previous studies of seismicity data (e.g., Anglin and Buchbinder, 1981; Anglin, 1984; Buchbinder et al., 1988) apparently revealed useful information about the possible relationship between the spatial distribution of earthquakes and the known tectonic features in the CSZ. This information, however, remains of qualitative type and is therefore unsuitable for quantitative estimates and monitoring in time. Although estimates of seismicity rates do provide some quantitative information, additional considerations are necessary in this respect before rate changes can be used (e.g., Chapter 3).

After analyzing the data by simple inspection of plots featuring various catalogue parameters (Chapter 2), three main quantitative techniques were applied in order to study the space-time distribution of CSZ earthquakes:

(1) The first one examines *rates of seismic activity* and their changes in time (Chapter 3). It was previously applied to various teleseismic and local catalogues (e.g., Habermann, 1983, 1986, 1987, 1991; Eneva et al., 1992b). An important feature of Habermann's approach is that changes in seismicity rates are examined depending on magnitude. This can help distinguish between artificial rate changes, due to changes in the network, and natural rate changes, due to real physical processes. It is also possible to distinguish between different types of artificial rate

changes. One might expect that no artificial changes have taken place in the CSZ, since the 6-element array has been fairly stable during the study period. While rate changes in the CSZ that can be interpreted as artificial are indeed much smaller than the ones in other active areas (e.g., Eneva et al., 1992b), they are still present. It is shown below that as many as 5 of the 6 larger rate changes identified in the CSZ might be artificial rather than natural.

(2) The second major technique applied is *pair analysis*. It is based on a specific type of study of interevent distances and time intervals. This technique was developed and applied to study the spatial and temporal distribution of earthquakes in seismically active areas of various sizes and tectonic settings (Eneva and Pavlis, 1988, 1991; Eneva and Hamburger, 1989; Eneva et al., 1991; Eneva et al., 1992a; Eneva et al., 1992c). The basis of pair analysis is comparison between frequency distributions of interevent distances and time intervals for the observed data with the same distributions for synthetic data. The latter represent randomly generated catalogues including the same number of events and covering the same three-dimensional volumes and time periods as featured by the real data. Previous results from the application of pair analysis suggest that spatial distribution of earthquakes is particularly informative in evaluating non-random patterns in seismic activity. Non-randomness dominates in the spatial distribution of earthquakes at all scales and tectonic settings. Different non-random features were found to characterize strike-slip and thrust tectonic environments. The study of groups of events at various stages of the earthquake process around the times of mainshocks revealed significant differences: the degree of spatial non-randomness increases before large earthquakes, reaches its highest values during aftershock sequences, and gradually decreases afterwards. This observation can be readily associated with the degree of heterogeneity in the stress field in the study areas and its changes in time. In the case of the CSZ long-term values characterizing the degree of non-randomness in earthquake spatial and temporal distribution are estimated from the whole data set. These are compared with short-term values obtained from groups of events covering various periods of time. On the basis of this comparison, it is evident that interevent distances are much more informative than the interevent time intervals. The temporal changes in the degree of spatial non-randomness are characterized by higher values during three distinct time periods. One of them is notably before the largest local event that occurred in the study period (M5.0, August 19, 1979), while another is more or less co- and post-seismic to the nearby Saguenay event (M6.5, November 25, 1988). These results allow us to speculate about the cause of changes in stress heterogeneity in the CSZ. More important, they point to the usefulness of the degree of spatial non-randomness in monitoring the changes in seismicity. It is to be noted that this parameter is different from the traditional seismicity rates and b-values and does not depend on them in any direct way. The degree of spatial non-randomness appears to be at least as useful a parameter as the well-known seismicity rates and b-values, and is in fact devoid of some of their shortcomings. The present study attempts to promote the idea, that while no single parameter can be used in earthquake forecasting, monitoring of a number of diverse seismicity parameters is ultimately necessary if any use is to be made of the existing earthquake catalogues.

(3) The third technique applied has been previously developed to study the chaotic properties of non-linear dynamic systems. It is based on the estimates of the so-called *correlation dimensions* (e.g., Grassberger, 1983; Grassberger and Procaccia, 1983; Goodings, 1991). These are represented by the slopes of the straight segments in the double logarithmic plots of the correlation integrals. Similar to pair analysis, correlation integrals can be calculated on the basis

of both interevent distances and time intervals. The correlation dimensions are widely used as lower bounds for the fractal dimensions of strange attractors in non-linear systems. They were applied to the spatial distribution of earthquakes by Hirata (1989a). Correlation dimensions have been found to indicate increasing spatial clustering to precede large events. Like pair analysis, correlation analysis of interevent distances in the CSZ yields more information than the interevent time intervals. Comparison of the short-term versus long-term correlation dimensions indicates the existence of periods of anomalous values. For example, a higher degree of clustering is evident around the time of the nearby Saguenay event.

Both pair analysis and correlation dimensions appear to provide useful integral measures of the distribution of seismic activity, allowing us to evaluate non-random patterns and their changes in time.

CHAPTER 2. DESCRIPTION OF DATA AND ITS QUALITY

2.1 Earthquake Catalogues Used

Two catalogues were used in this study of the CSZ earthquakes:

(1) The first catalogue includes events located using the arrivals at the local array stations. This catalogue was provided by F.M. Anglin from the Geological Survey of Canada (GSC) and will be referred to as the *Anglin catalog*ue. Only the following events were included in the list until some time in 1983: with hypocentres determined from at least 5 stations (LMQ and LPQ included); with at least 8 phases read; and with latitude standard deviations (STD) $\leq$ 0.004° and longitude STD $\leq$ 0.006°. After 1983, events determined from fewer than 5 stations and 8 phases were also included. The general purpose of including in this catalogue only more precisely located events was to use these data to create stereo plots of hypocentral cross-sections. If the visualized data is less noisy, such plots can greatly aid in the delineation of the active structures in the zone. New stereo plots were provided by Anglin (personal communication), while previous plots of this type were published by Anglin (1984).

(2) The second catalogue used will be referred to as the *PIK catalog*ue. It has been extracted for the same period (October 20, 1977 - July 31, 1991) from the so-called PIK file provided by the GSC (R.G. North, personal communication). This file contains four types of records: the earthquake solution record (ESR), the earthquake comment record (ECR), the observed data record (ODR), and the calculated data record (CDR). The program producing the PIK file is the CANSESS MULTILAYER epicentre location program. Unlike the previous catalogue for which mostly array data are used to locate the Charlevoix earthquakes, records from the regional Eastern Canada Telemetered Network (ECTN) were used for the locations in the PIK catalogue.

The PIK catalogue apparently includes more events than the Anglin catalogue. This is due to the lack of restrictions in terms of location precision and number of phases for the events to be included in the PIK catalogue. While the Anglin catalogue would be better suited for the study of the spatial distribution of earthquakes, it omits too many events for the temporal distribution to be properly studied. It seemed, therefore, reasonable to combine the two types of catalogues. Two combinations were further used:

(1) The first combined catalogue used the PIK catalogue as a basis (96.4% of the events)

and included those events in the Anglin catalogue which were absent from the PIK catalogue (the remaining 3.6% of the events). This catalogue will be referred to as the PA catalogue (for PIK-Anglin). Two events from the two catalogues were considered to be "identical" if they were located within 30 s and 2 km of each other. This means that 96.4% of the events were included in both catalogues, but the PA catalogue used the locations and the times given in the PIK catalogue. The PA catalogue is apparently not very different from the original PIK catalogue.

(2) The second combined catalogue is referred to as the AP catalogue (Anglin-PIK), since it uses the Anglin's catalogue as a basis (82% of the events) and included those of the PIK events which were not in the Anglin catalogue (18% of the events; these were the ones located not precisely enough to be included in the Anglin catalogue). Since 82% of the events in the AP catalogue keep the locations given in the Anglin catalogue, the AP catalogue generally features more precise locations than the PA catalogue. For this reason, after an initial examination of both combined catalogues, the AP catalogue is the one to be primarily used.

Both the AP and PA catalogues contain 1211 events each.

2.2 Quality of Primary Data and its Change in Time

The plots shown further represent simple graphical displays that allow us to evaluate data quality in various aspects and its change in time. These plots are shown for the PA, AP, and the Anglin catalogues.

(1) Standard deviations (STD) of latitudes (Figure 2.2.1) and longitudes (Figure 2.2.2) of hypocentral locations. The difference between the AP and the Anglin catalogues is well seen in the addition of the less precisely located events from the PIK catalogue. Note that STD=0.0 come from the PIK events before some time in 1986, for which STD were not listed for the locations. The discrete appearance of the AP plots (middle frames) in the period 1979-1982 is due to STD's given with precision to one digit after the decimal point for the events in the PIK catalogue.

(2) Number of stations used to locate earthquakes (Figure 2.2.3). It is apparent that at least 3 stations were used at all times for the PIK catalogue (hence, for the PA catalogue). The Anglin catalogue first featured events determined from 5 stations (until some time in 1983), but started including events determined from only 3 or 4 stations after that time.

(3) Number of phases used to locate earthquakes (Figure 2.2.4). At least 4 phases are used in the PIK/PA catalogues. In contrast, the Anglin catalogue features events determined from at least 8 phases before the same time in 1983 as above. After that, at least 6 phases are used (with the exception of few cases when 5 and 4 phases were used).

(4) Number of amplitudes used to determine magnitudes (Figure 2.2.5). The Anglin catalogue does not list this number before 1986, hence the 0's at these times. In the same period, the magnitudes in the PIK/PA catalogues were apparently determined from 1 or 2 amplitude readings most of the time. The same information is given throughout 1986 and 1987 in the Anglin file. A major change took place on November 1, 1987 (Anglin, personal communication). Prior to this date, the Charlevoix phase readings were taken from paper records produced by vertical component instruments. The data was digitized from analog tapes. While these phases were used for hypocentre location, amplitudes (needed to determine magnitudes) were not measured from these records. Instead, amplitudes and periods were obtained from LMQ paper records for small events, while ECTN (where seen) and primarily LPQ data were used for larger events. The former type of magnitude is the so-called *local magnitude*, and the latter type - the

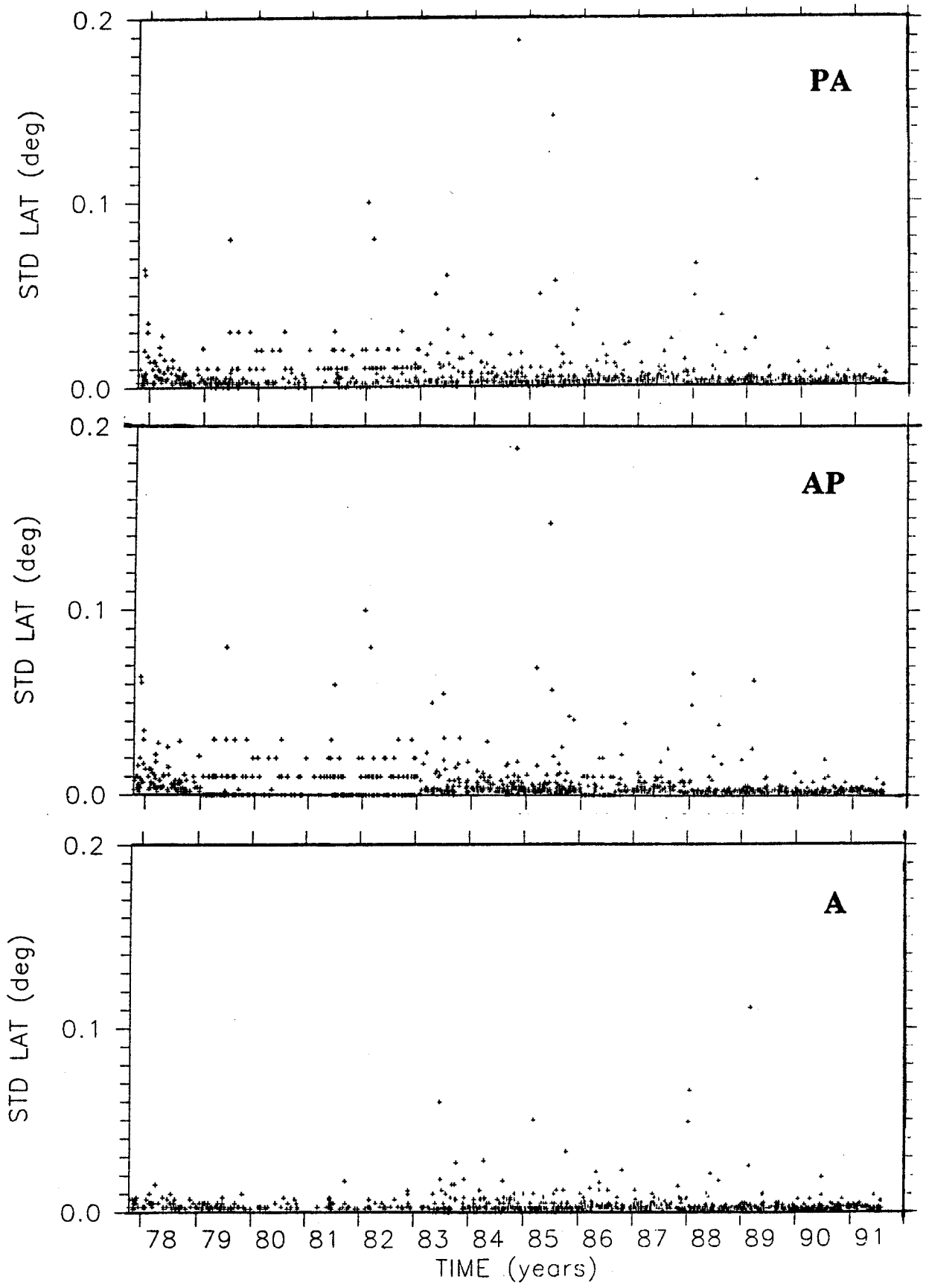

Figure 2.2.1 Standard deviations of latitudes of epicentral locations versus time. From top to bottom: PA, AP, and Anglin (A) catalogues.

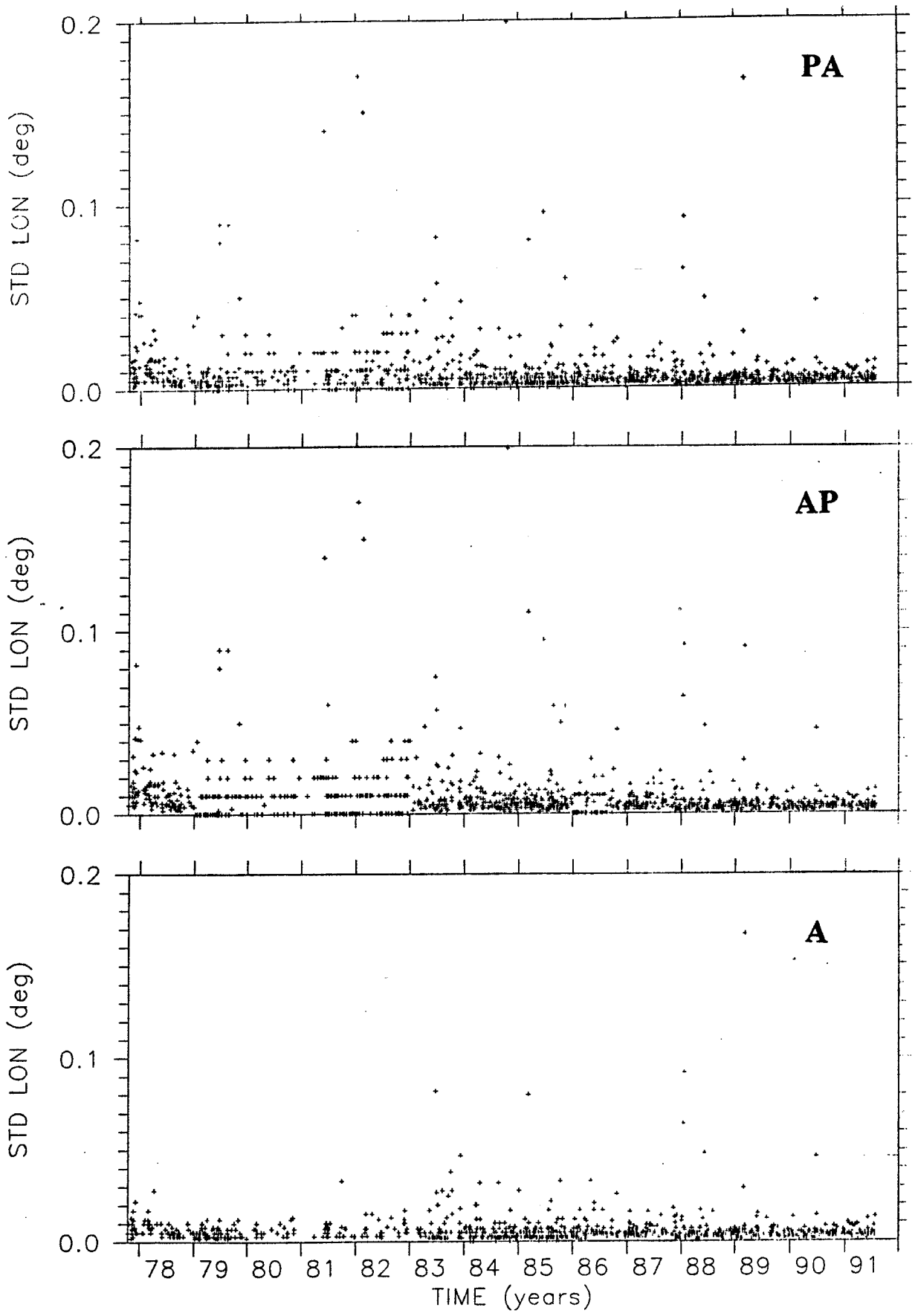

Figure 2.2.2 Standard deviations of longitudes of epicentral locations versus time. From top to bottom: PA, AP, and Anglin (A) catalogues.

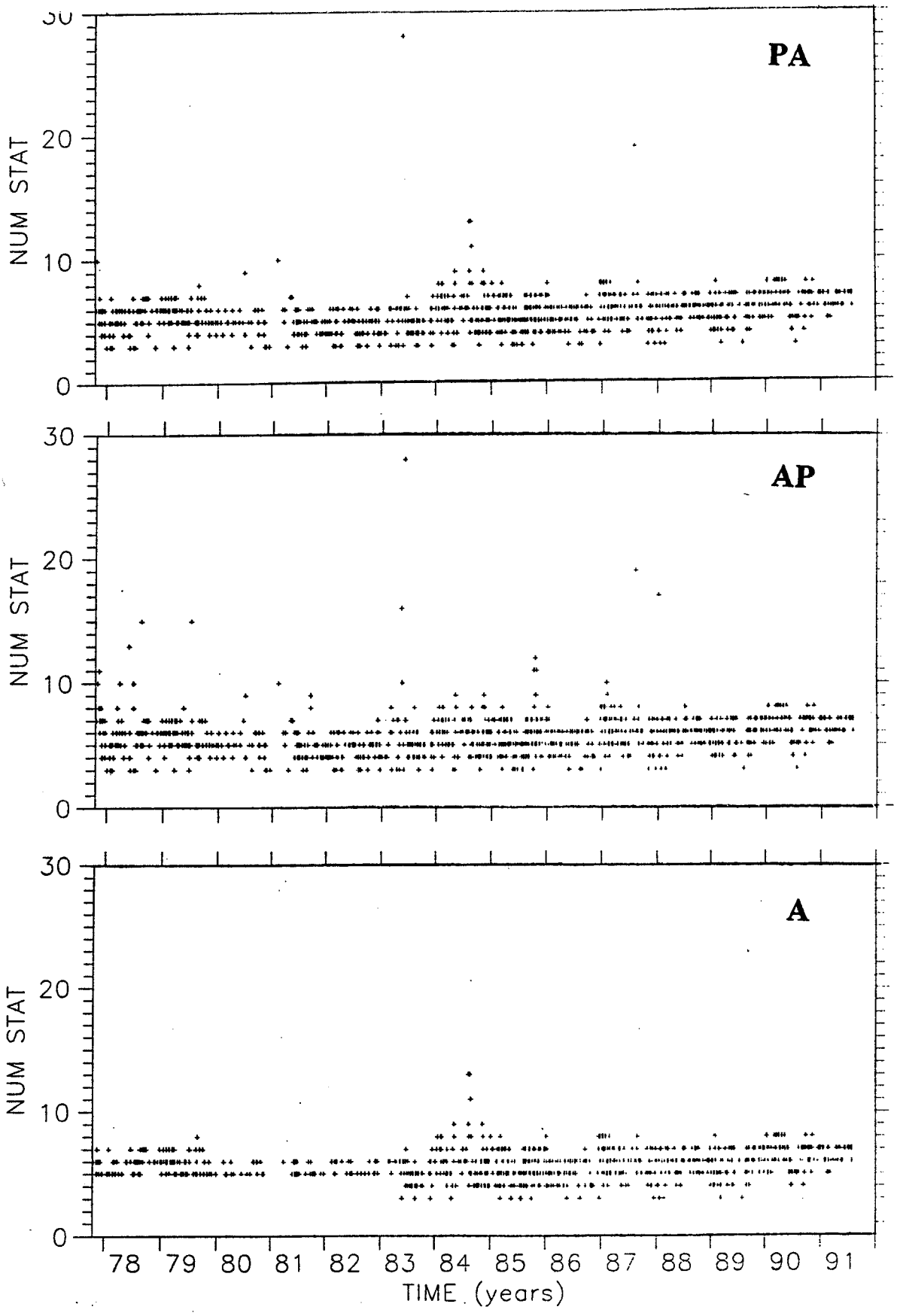

Figure 2.2.3 Number of stations used to locate events versus time. PA, AP, and A as before.

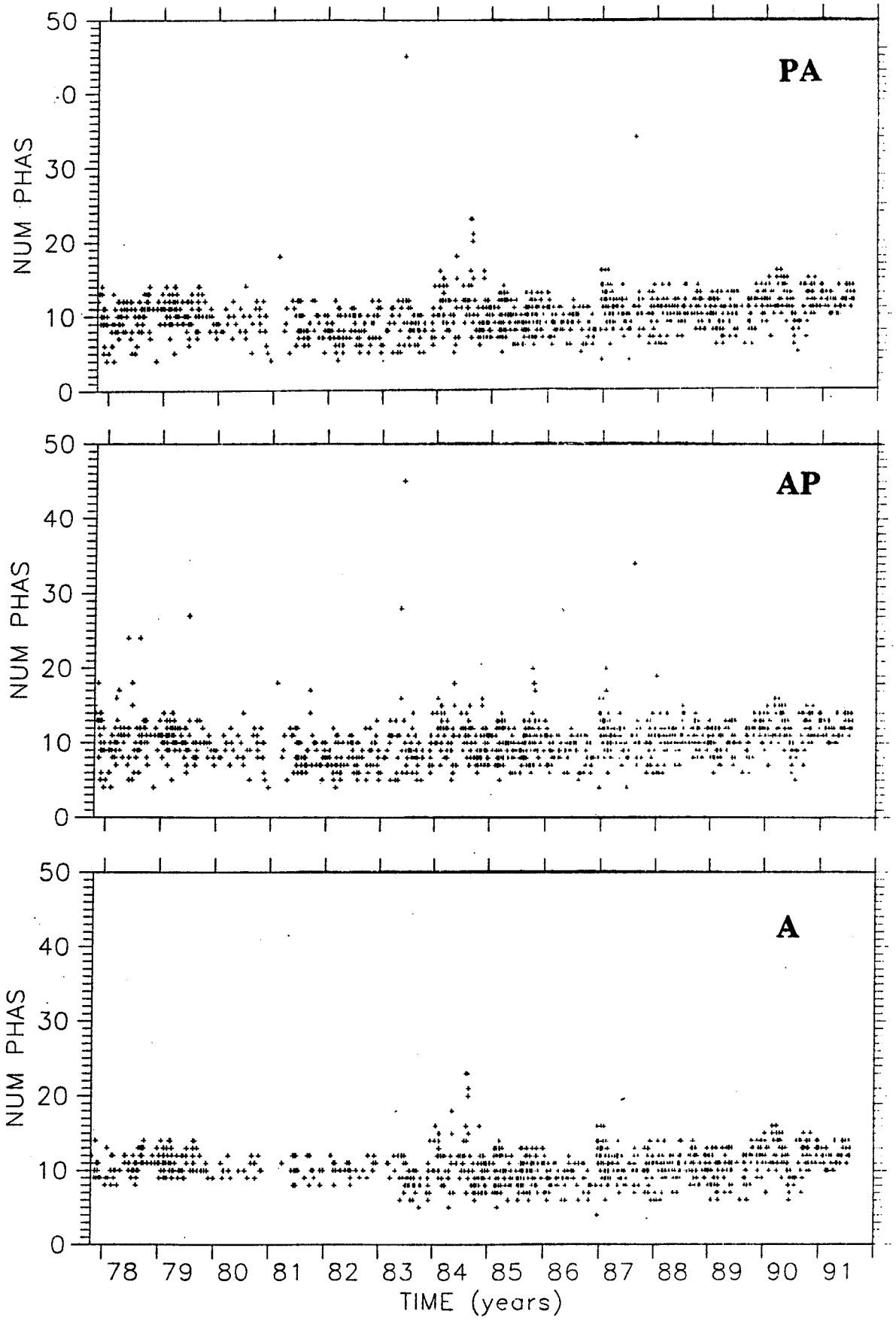

Figure 2.2.4 Number of phases used to locate events versus time. PA, AP, and A as before.

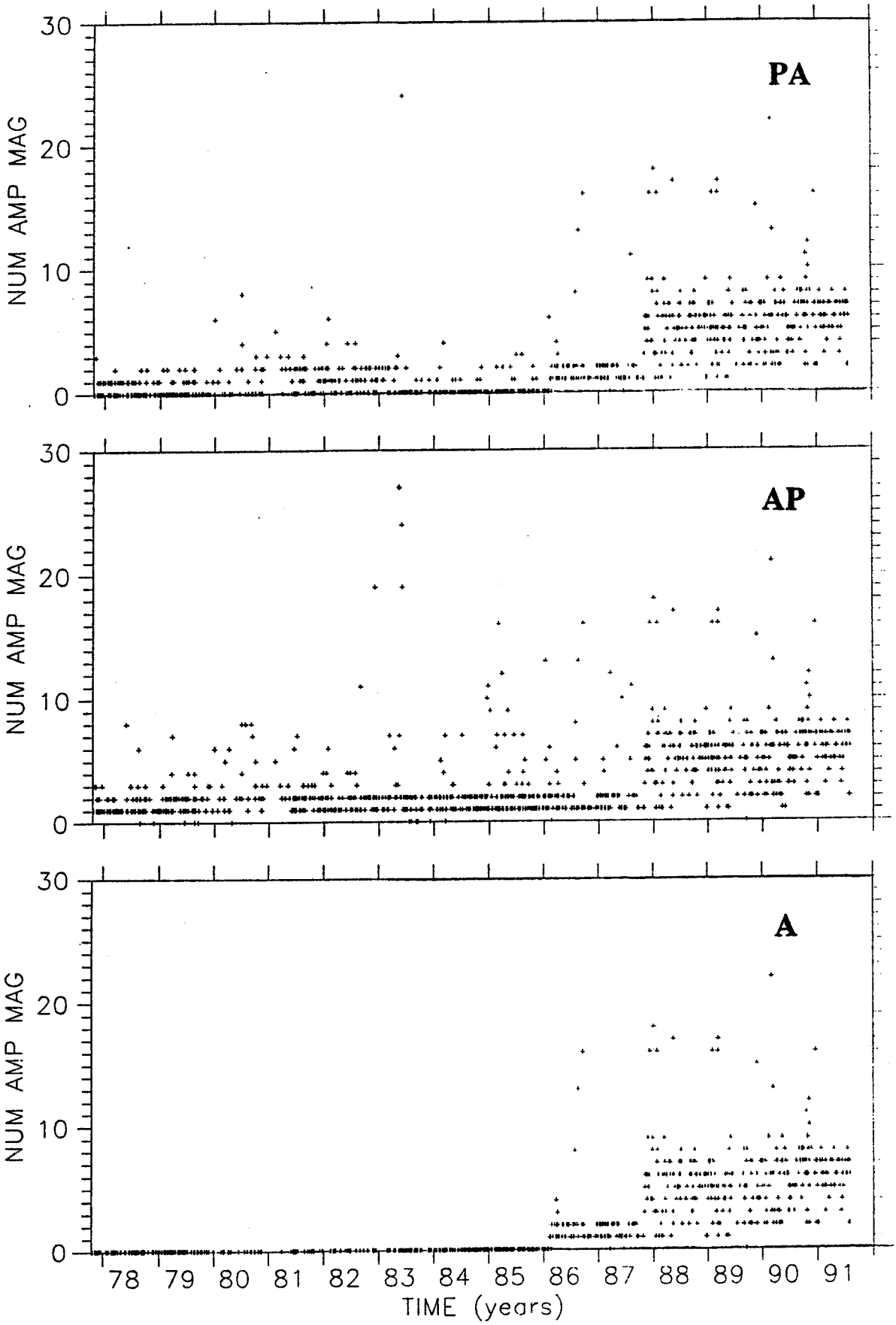

Figure 2.2.5 Number of amplitudes used to determine magnitudes versus time. PA, AP, and A as before.

so-called *Nuttli's magnitude* (Nuttli, 1973). It is evident from the plot that this situation changed drastically after November 1, 1987. Much more amplitudes were generally used after this date for magnitude determination.

(5) STD in magnitude determination (Figure 2.2.6). In the PIK/PA catalogues, 0's generally show that only one amplitude measurement was used. Similar to the previous plot, 0's in the Anglin file before 1986 indicate the absence of this type of information. Most magnitude STD's are apparently ≤ 0.5.

(6) RMS residuals, or root-mean-square time residuals in seconds (Figure 2.2.7). This information was not given in the Anglin catalogue prior to March 1986, hence the 0's in this period.

2.3. Magnitudes

The following plots focus on further details about magnitudes. The two different types of magnitudes, local magnitude (ML, used for the smaller events, and Nuttli's magnitude (MN), used for the larger events (Nuttli, 1973), are shown in all these figures with different symbols (open and filled squares, respectively). Figure 2.3.1 shows the primary magnitude listed in the AP catalogue versus time. ML was primary for 78.3% of the events and MN - for the remaining 21.7%. The term "primary magnitude" designates the first, or preferred, magnitude in the catalogue, since both ML and MN were shown for some events in the PIK catalogue. The figure clearly shows what is generally already known: the smaller events are shown with primary ML's and the larger events - with primary MN's. This plot, however, shows two main features, which are otherwise not easy to detect. The first one indicates a strong "human" factor that changed unpredictably. It is evident that the demarcation point between the two types of magnitudes changed in time; an entirely artificial (man-made) change in the catalogue. While this demarcation point was about 2.0 before 1982, it dropped to 1.3 and even 1.0 after this time. It is not clear how and why this decision was made. However, if the second period features a better choice, quite a few of the events of $M \geq 1.5$ before 1982 should be assigned MN's. It will become clear later that this would move all these points by almost one magnitude unit up. A second conspicuous feature suggested by this plot is the apparent relative "gap" between the two bands featuring the two magnitude types. The number of larger events is naturally smaller than the number of smaller events. Yet, the number of points does not decrease smoothly as the magnitude increases. This observation already indicates qualitatively that if both ML and MN are determined for the same event, ML is likely to be smaller than MN. In reality, it is not possible to determine from this limited study which magnitude is "better".

It is possible, however, to estimate the average relationship between the two types of magnitude. Figure 2.3.2 shows MN's versus ML's for the events for which both magnitudes were listed in the PIK catalogue. This information was given for 309 events (with non-zero magnitudes), i.e., for 25.5% of all events. The following regressions were found between the non-zero ML's and MN's:

$$MN = (0.992 \pm 0.026) + (0.791 \pm 0.018)ML$$

$$ML = (-0.992 \pm 0.051) + (1.094 \pm 0.025)ML$$

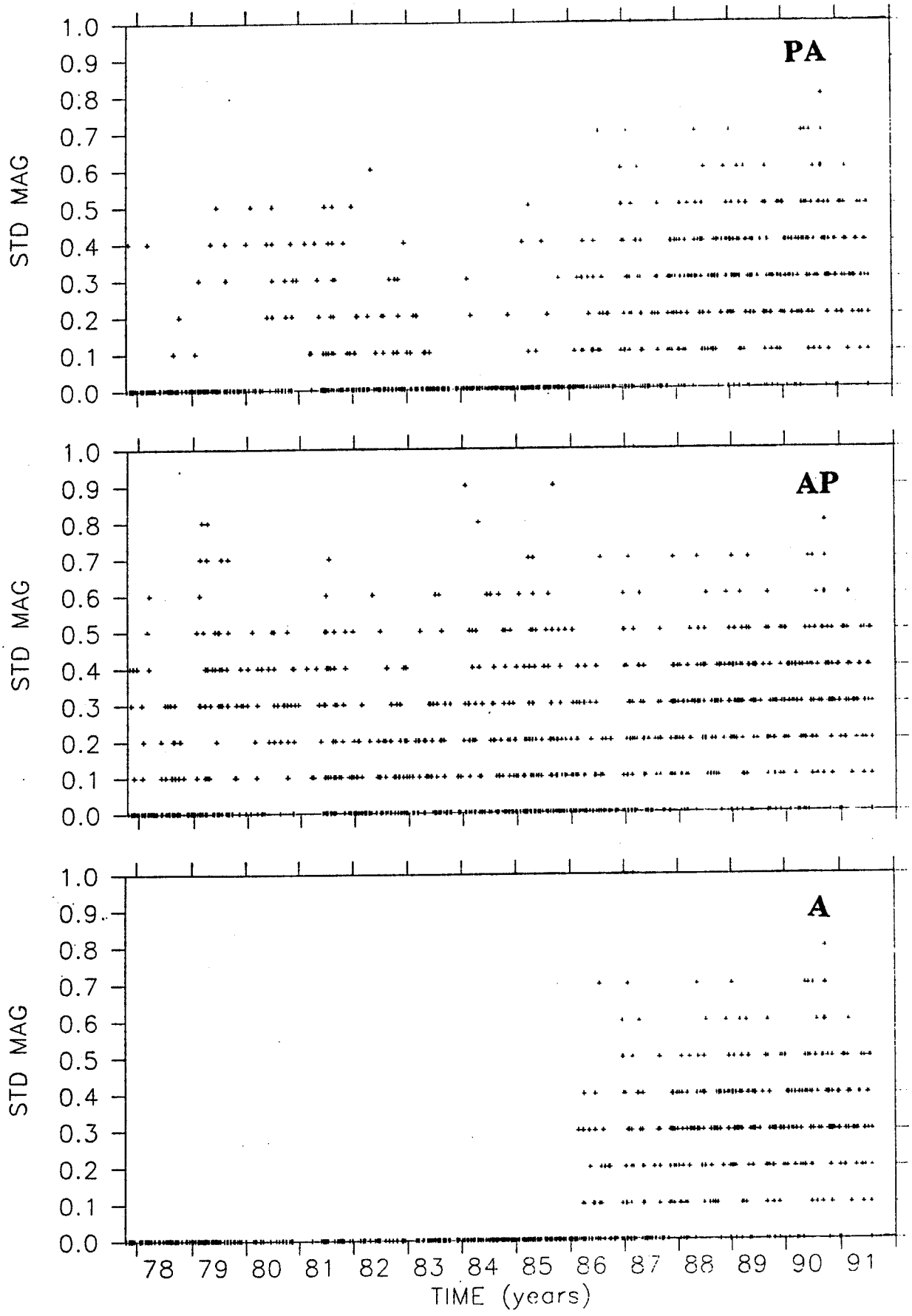

Figure 2.2.6 Standard deviations in magnitude determination versus time. PA, AP, and A as before.

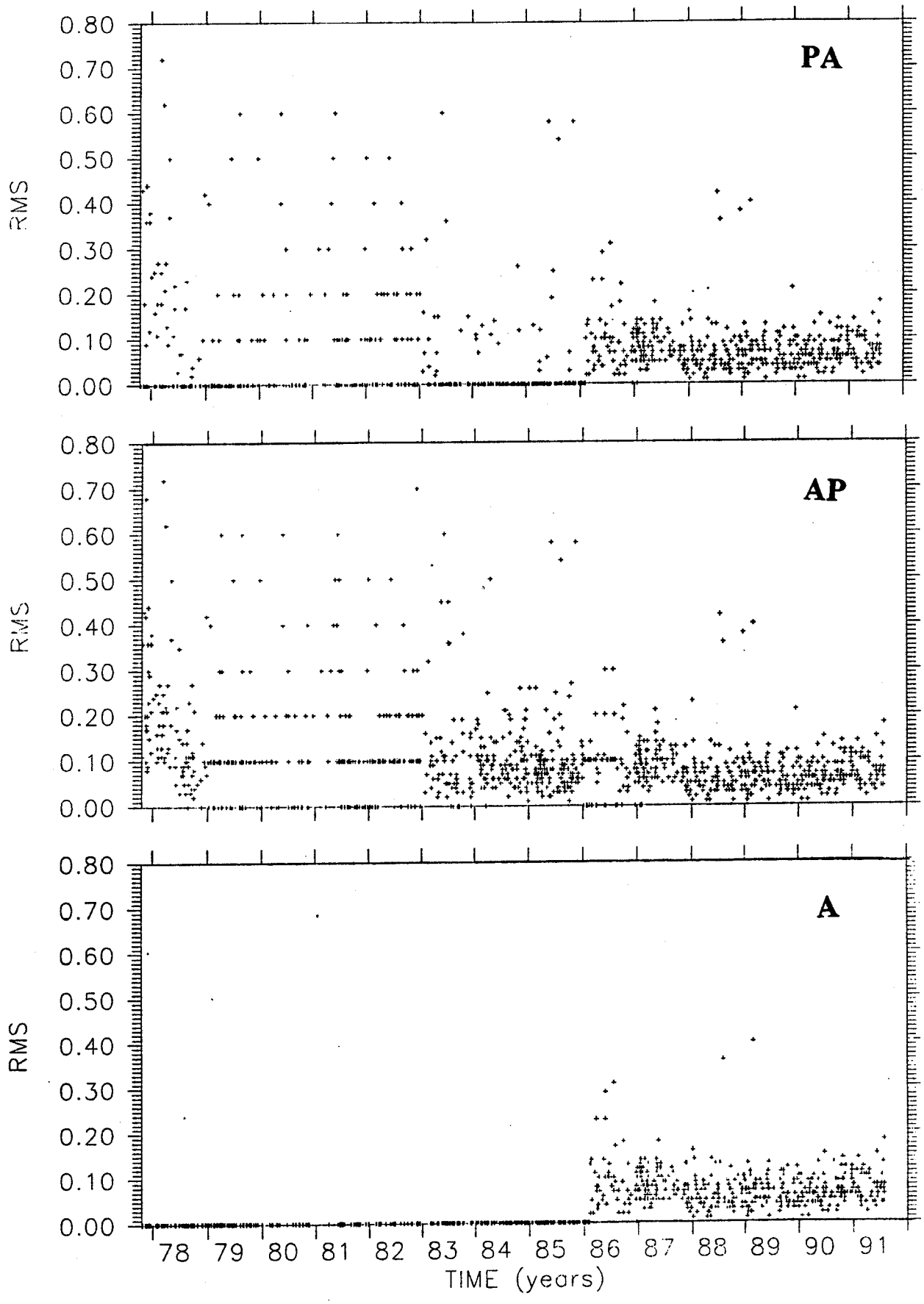

Figure 2.2.7 RMS residuals (root-mean-square time residuals in seconds) versus time. PA, AP, and A as before.

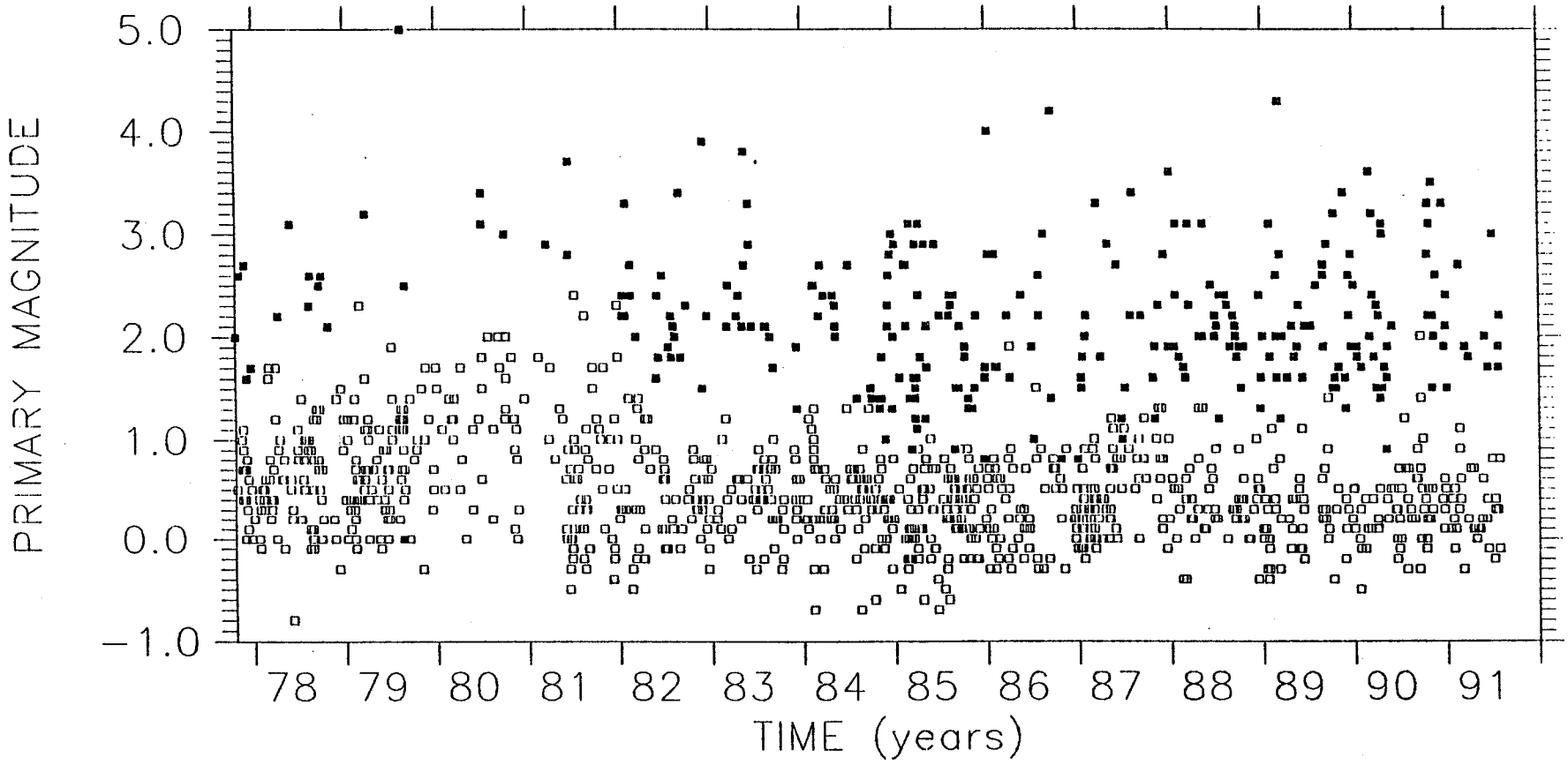

Figure 2.3.1 Primary magnitude listed in the AP catalogue versus time. Filled squares mark magnitudes MN, open squares denote magnitudes ML. See text for more detail.

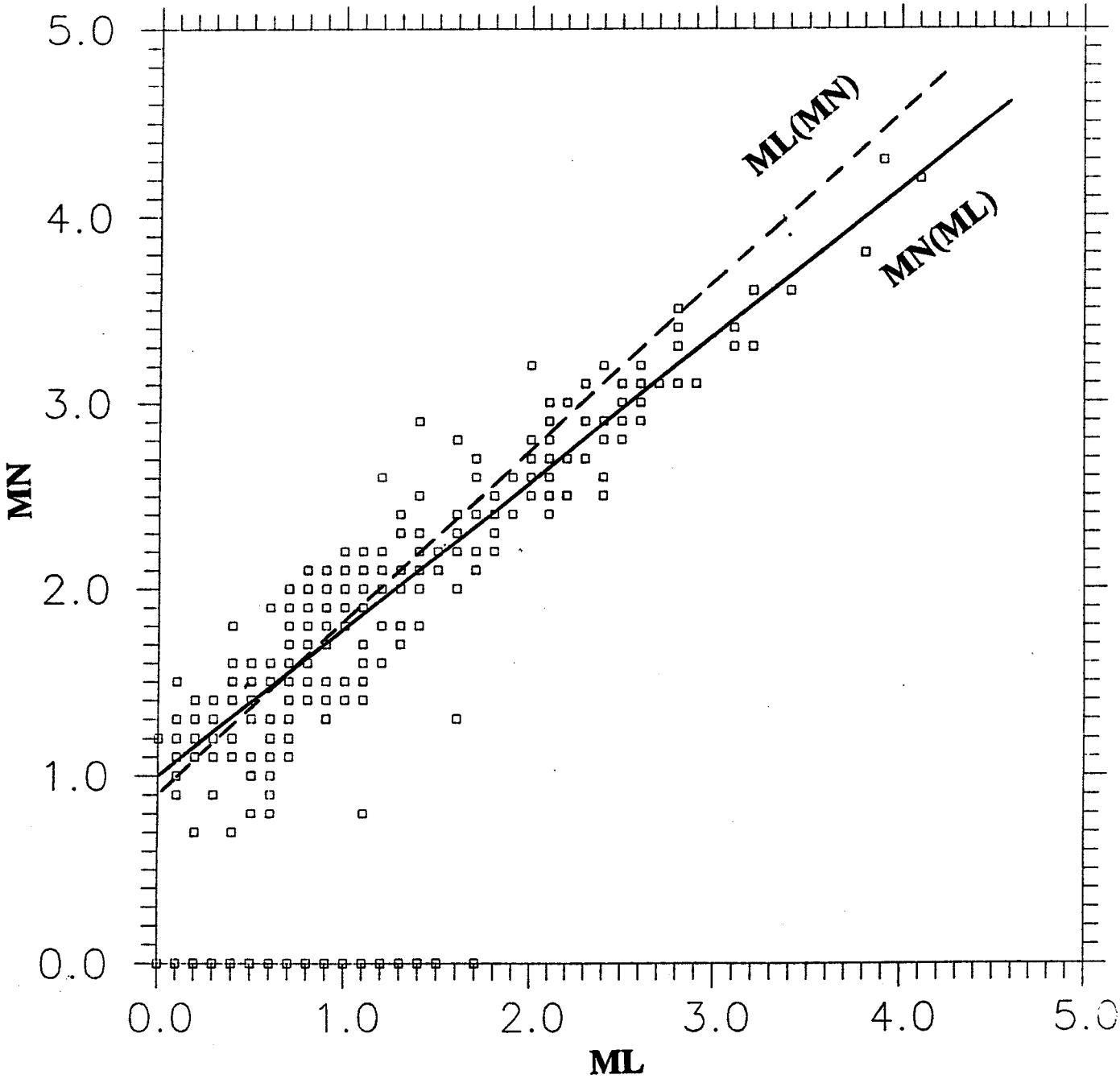

Figure 2.3.2 Empirical relationships between magnitudes MN and ML. Each pair of MN and ML is listed for the same event in the PIK file. Lines mark regressions from the text: solid line for MN=f(ML) and dashed line for ML=f(MN).

These formulae cannot be derived from each other, because they are empirical, not functional. That is, one needs individually derived formulae for either MN=f(ML) or ML=f(ML). These relationships quantitatively represent the observation made from Figure 2.3.1, according to which MN's are larger than ML's for the same events.

These relationships were independently confirmed in a study directed by G. Buchbinder (personal communication). In this study amplitudes were measured for 294 Charlevoix events that occurred in the period from November 1987 (when 3-component stations were installed) until April 1991. These were events for which (a) amplitudes could be read from the records of at least 5 stations; and (b) amplitudes could be read in both the 0-50 km (for ML's) and > 50 km (for MN's) distance ranges. The coefficients of the linear relationship ML=f(MN) were estimated in four depth ranges: 0-9 km, 9-12 km, 12-16 km, and > 16 km. The slope of this relationship increases with depth: 0.904 ± 0.062, 0.922 ± 0.051, 1.065 ± 0.059 (the closest to the slope of the ML=f(MN) estimated in the present report), and 1.120 ± 0.055, respectively. The estimates of the intercept also change with depth: -0.911 ± 0.116 (the closest to the estimate here), -0.901 ± 0.105, -1.183 ± 0.123, and -1.232 ± 0.113, respectively.

The next two figures provide additional information about the two types of magnitudes. Figure 2.3.3 shows the number of amplitudes used to determine magnitudes versus time (top frame) and versus magnitude (bottom frame). The plot in the top frame is different from the plot in Figure 2.2.5 in the way magnitudes are shown; different symbols are used for ML's and MN's. As it could be expected, generally more amplitudes were used at later times (bottom frame) and more amplitude readings were generally used for larger events (top frame). Figure 2.3.4 shows the STD's in the magnitude determinations versus time (top frame) and versus magnitude (bottom frame). Different symbols are again used for ML's and MN's. Both frames of this figure indicate that STD's > 0.5 m.u. are generally encountered for the ML's. Note that a 0 in both Figure 2.3.3 and Figure 2.3.4 indicates that either only a single magnitude determination was used or that the STD was not listed.

2.4 Magnitude-Frequency Relationships

An important empirical observation dating back to the 1940's was the discovery that the number of earthquakes in general decays exponentially with earthquake size (the so-called Gutenberg-Richter law). This exponential decay is translated into a linear relationship on a double logarithmic plot, i.e. in which logarithm of the number of events is shown versus magnitude (a logarithmic measure of energy). Estimates of the slope of this linear relationship (the so-called b-value) have been made in hundreds of publications. These estimates range mostly between 0.5 and 1.5 (Utsu, 1971). The physical meaning of the generally linear shape of the magnitude-frequency relationship in various seismically active areas has been interpreted in terms of self-similarity in earthquake distribution in respect to event size (e.g., King, 1983; Rundle, 1989).

No attempts were reported (Buchbinder et al., 1988) that made use of the magnitude-frequency relationships in the CSZ. This is perhaps due to the fact that these relationships are substantially curved at all times that makes it difficult to estimate their slopes (the b-values). It is otherwise well known that temporal changes in b-values were reported to have preceded large events in other parts of the world (e.g., Smith, 1986). The CSZ magnitude-frequency plots in Figure 2.4.1 are shown with open squares for the case when magnitudes are taken from the catalogue as they are (i.e., unchanged); one plot is shown for the whole period and 15 more plots

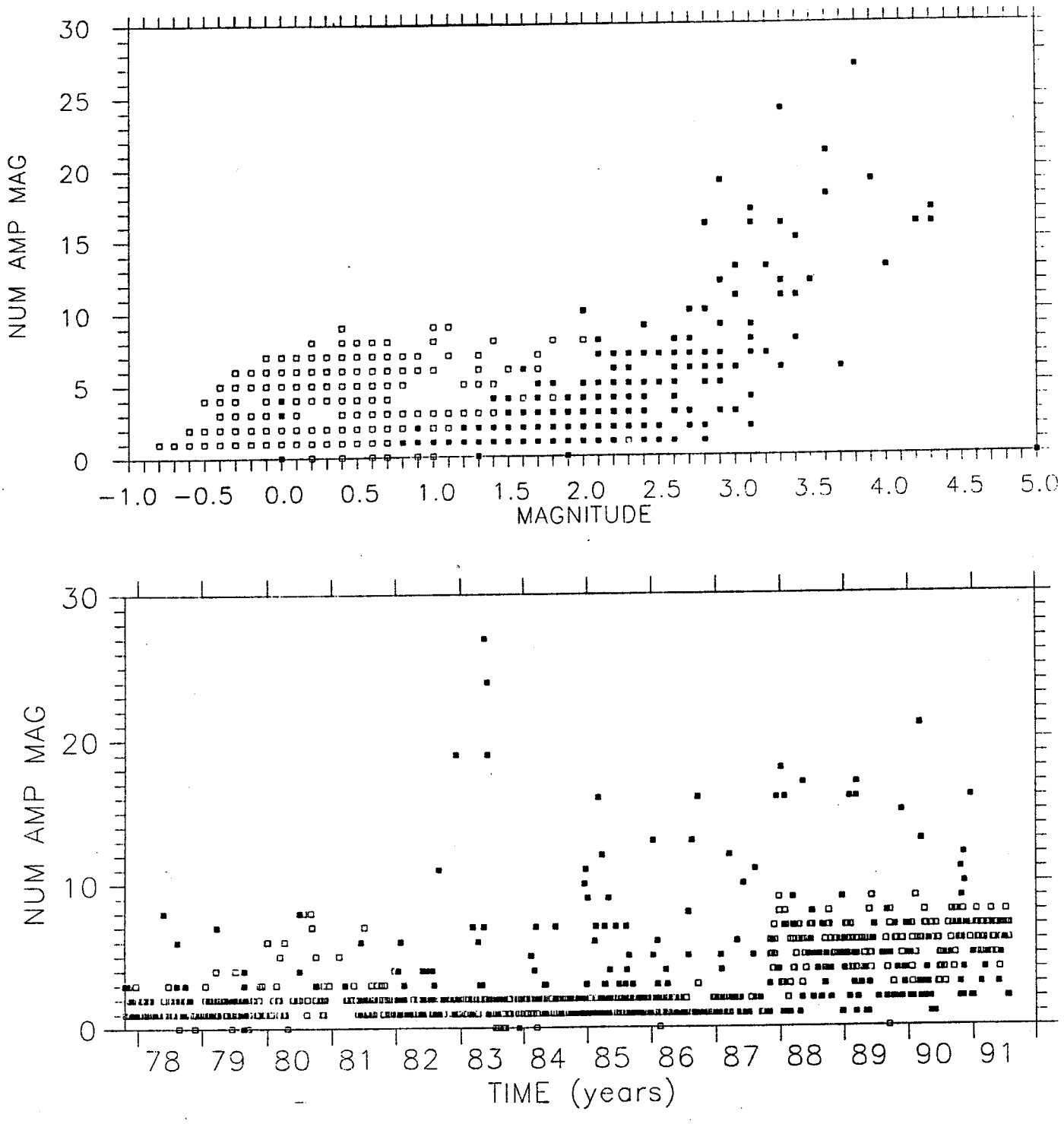

Figure 2.3.3 Number of amplitudes used to determine magnitudes versus magnitude (upper frame) and versus time (bottom frame). Filled and open squares as in Figure 2.3.1.

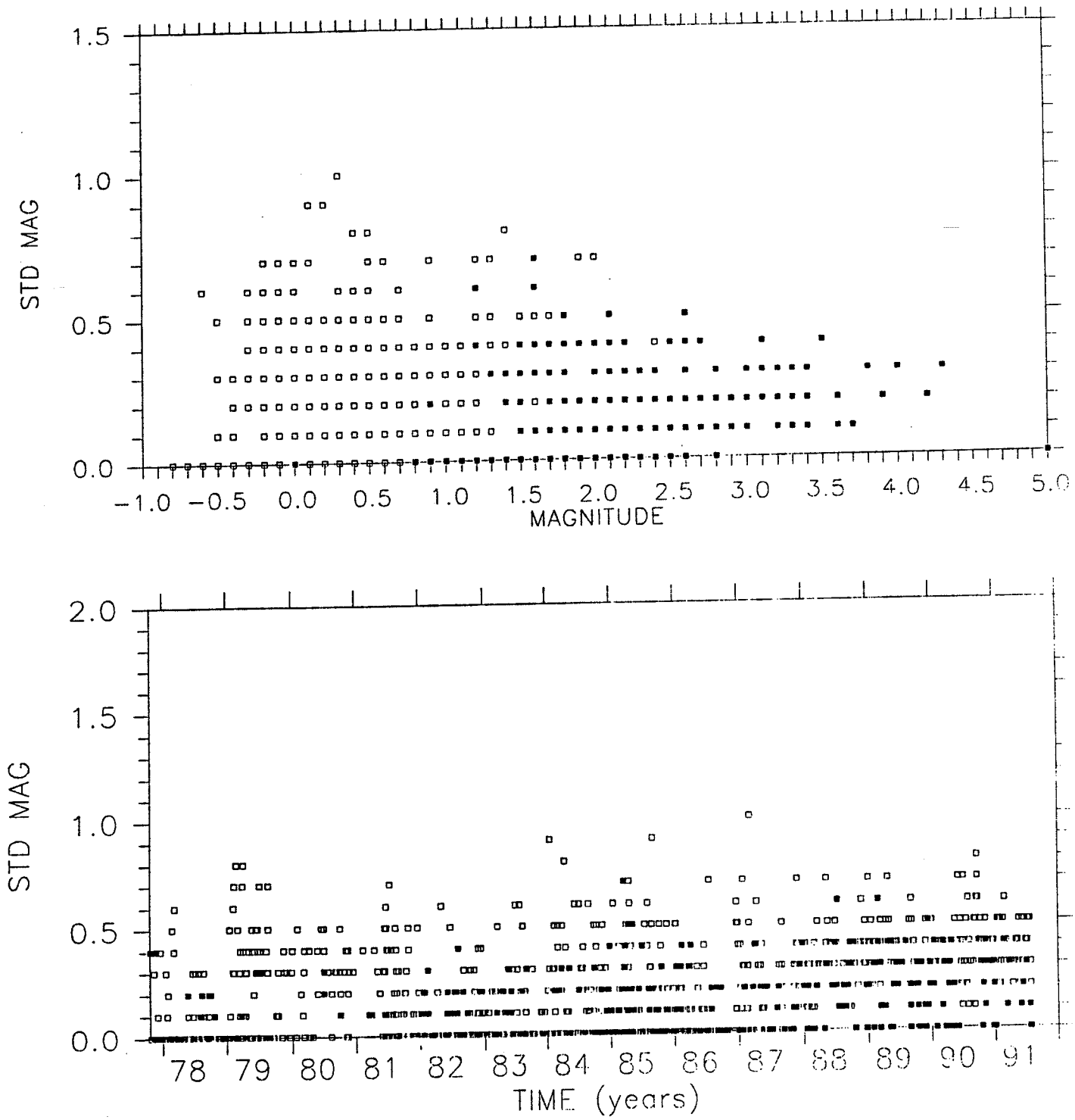

Figure 2.3.4 Standard deviations in magnitude determinations versus magnitude (top frame) and versus time (lower frame). Filled and open squares as in Figures 2.3.1 and 2.3.3.

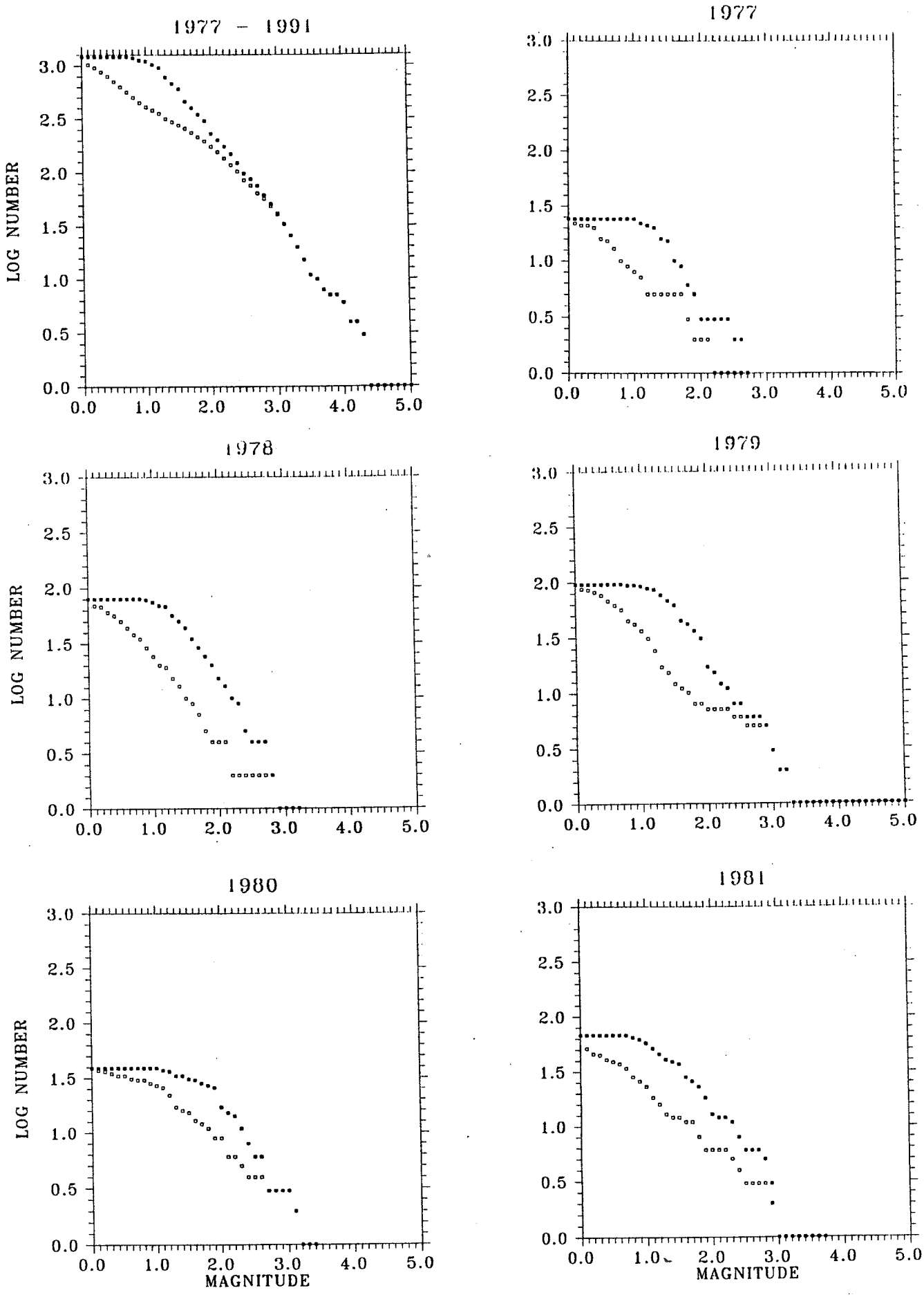

Figure 2.4.1 (Continued on next pages.)

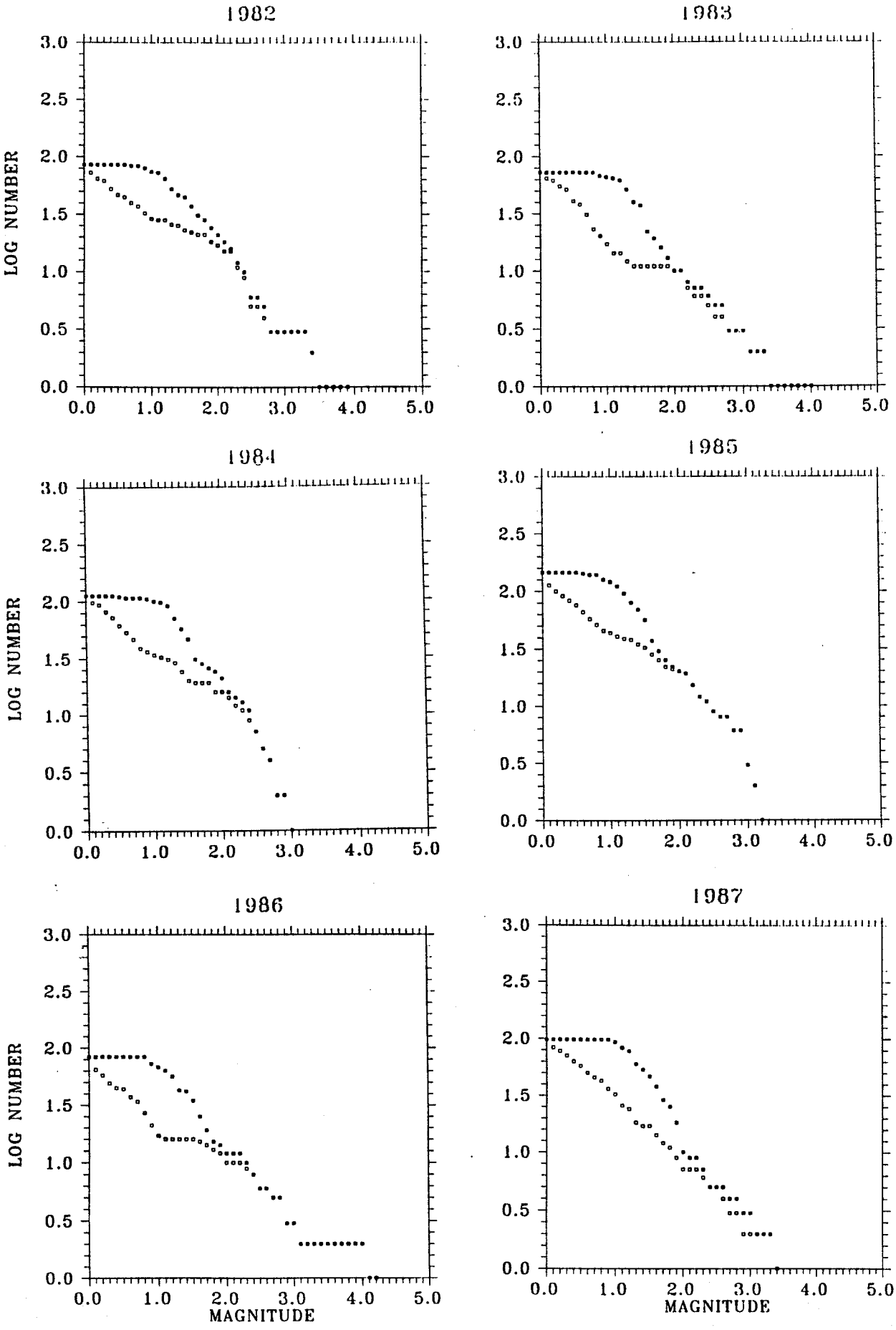

Figure 2.4.1 (Continued on next page.)

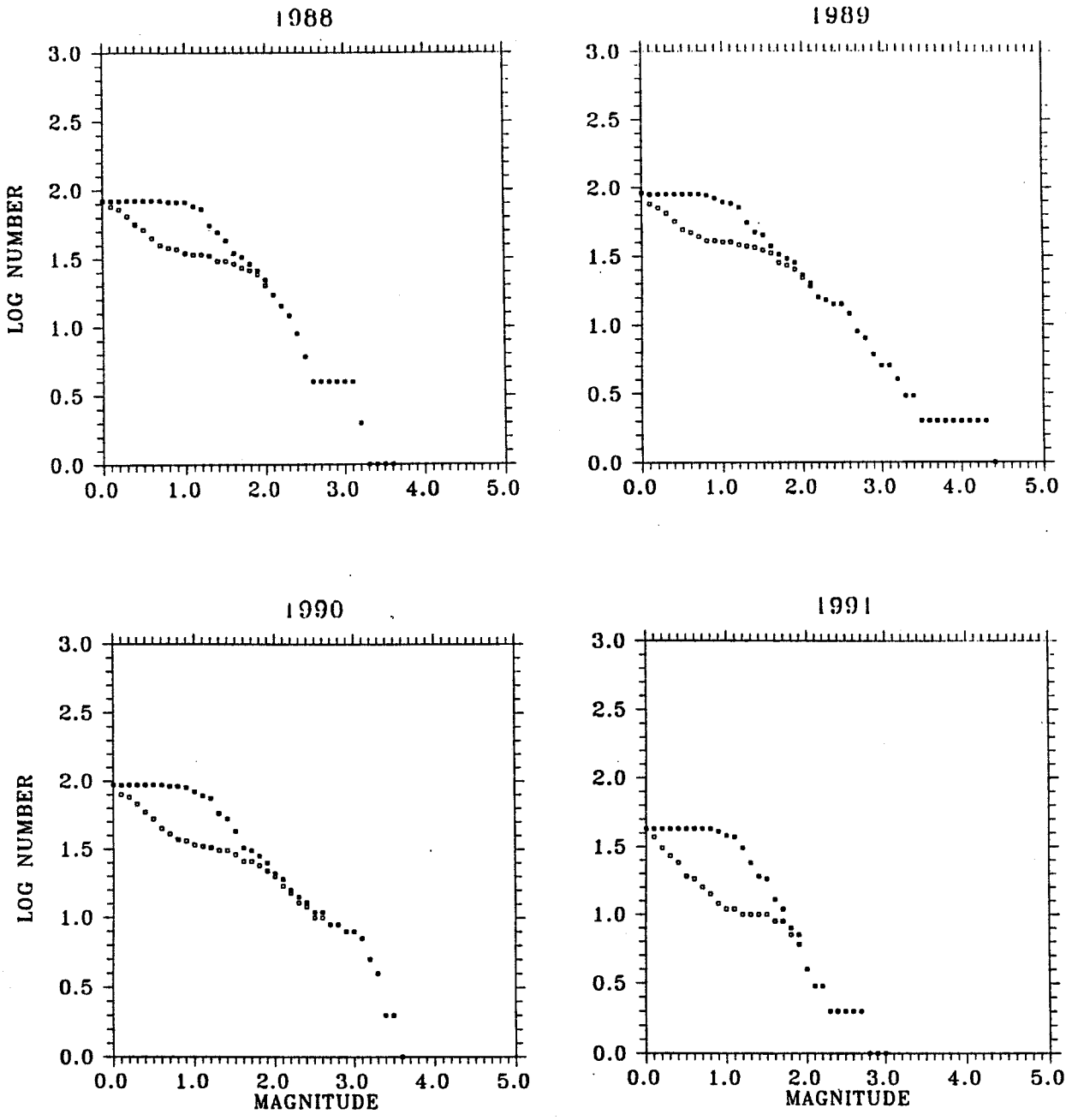

Figure 2.4.1 (Continued from two previous pages.) Magnitude-frequency relationships for the whole period and for each year; years marked on top of the plots. Open squares mark the relationships when the primary magnitude is used (ML for smaller events and MN for larger events). Filled squares denote the relationships when only magnitude MN is used (for the events given with primary magnitude ML, MN's are calculated using the empirical relationship between MN=f(ML); see text for more detail).

- for each year of the period of observation. Significant "bumps" are seen for most of these curves, generally around magnitude 2.0 and below. These "bumps" are particularly prominent from 1982 on. This is in agreement with what was observed in Figure 2.3.1; i.e., that the demarcation point between the two types of magnitudes changed around that time. It appears, however, that the magnitude-frequency curves are significantly straightened out when only one type of magnitude is used. The curves marked with filled squares were obtained after all ML's in the AP catalogue were converted to MN's using the above empirical relationship between ML and MN (see Figure 2.3.2). All this points to another artificial (man-made) feature in the data that has nothing to do with physical processes in the Earth; that is, significantly enhanced curvature of the magnitude-frequency relationship due to the use of two different types of magnitude.

Since the linearity of the magnitude-frequency relationship has been previously related to self-similarity in earthquake size distribution, breaks in this linearity were consequently interpreted as violation of this self-similarity. There have been numerous recent reports arguing that such breaks reflect real physical phenomena; that smaller events (e.g., M around 3.0 and smaller) originate from a population different from the one of the larger events (e.g, Pavlis et al., 1989). While this may be the case in many areas, the example of the CSZ points to an artificial cause that may be present in relationships from other areas as well.

In addition to curvatures discussed above, there is always a curvature for the smallest magnitudes that is due to their incomplete recording. A straightforward crude technique of determining the magnitude of complete recording is to look where the linearity breaks at the left side of the magnitude-frequency plots. If the magnitudes of completeness are estimated from yearly magnitude-frequency relationships, the largest of these can be considered as a conservative magnitude threshold valid for the whole period of observation (e.g., Eneva et al., 1992c). The corrected curves in Figure 2.4.1 (filled squares) can be readily used in this respect. It seems that MN=1.4 (ML=0.5) is safe to use as a completeness magnitude over the whole period, since the yearly relationships do not curve until smaller magnitudes are reached.

The above magnitude of completeness was determined in respect with time, but it may not be suitable in space (i.e., in all subareas of the CSZ). Figure 2.4.2 shows magnitudes versus latitude (top frame) and versus longitude (bottom frame), the two types marked with open (ML's) and filled (MN's) squares as before. Because of the specific SW-NE orientation of the CSZ, the left sides of both plots in this figure represent the SW part of the zone, while the right sides represent its NE part. Figure 2.4.2 makes it clear that the magnitude of completeness most probably varies in space, being lower in the middle of the zone. There may be a natural tapering off of the seismic activity at the edges, but it can be argued that the lowest recorded magnitude in these parts of the zone is the upper limit of the magnitude of completeness. Indeed, since the array has been essentially the same during the whole period of observation, there is no reason that a magnitude recorded at least once at a given spot would be missed at another time. On the basis of these considerations, ML=0.5 (MN=1.4) appears to be safe to use throughout the zone, i.e, in respect to both space and time. The MN $\geq$ 1.4 events are 56% of all events.

2.5 Epicentral Maps, Space-Time Plots, and Cross-Sections

Similar to Figure 1.1.1, Figure 2.5.1 shows an epicentral map of the CSZ together with the major fault traces and the outlines of the St. Lawrence river. However, only M $\geq$ 2.0 events are shown here. This allows us to see where the larger seismic activity takes place.

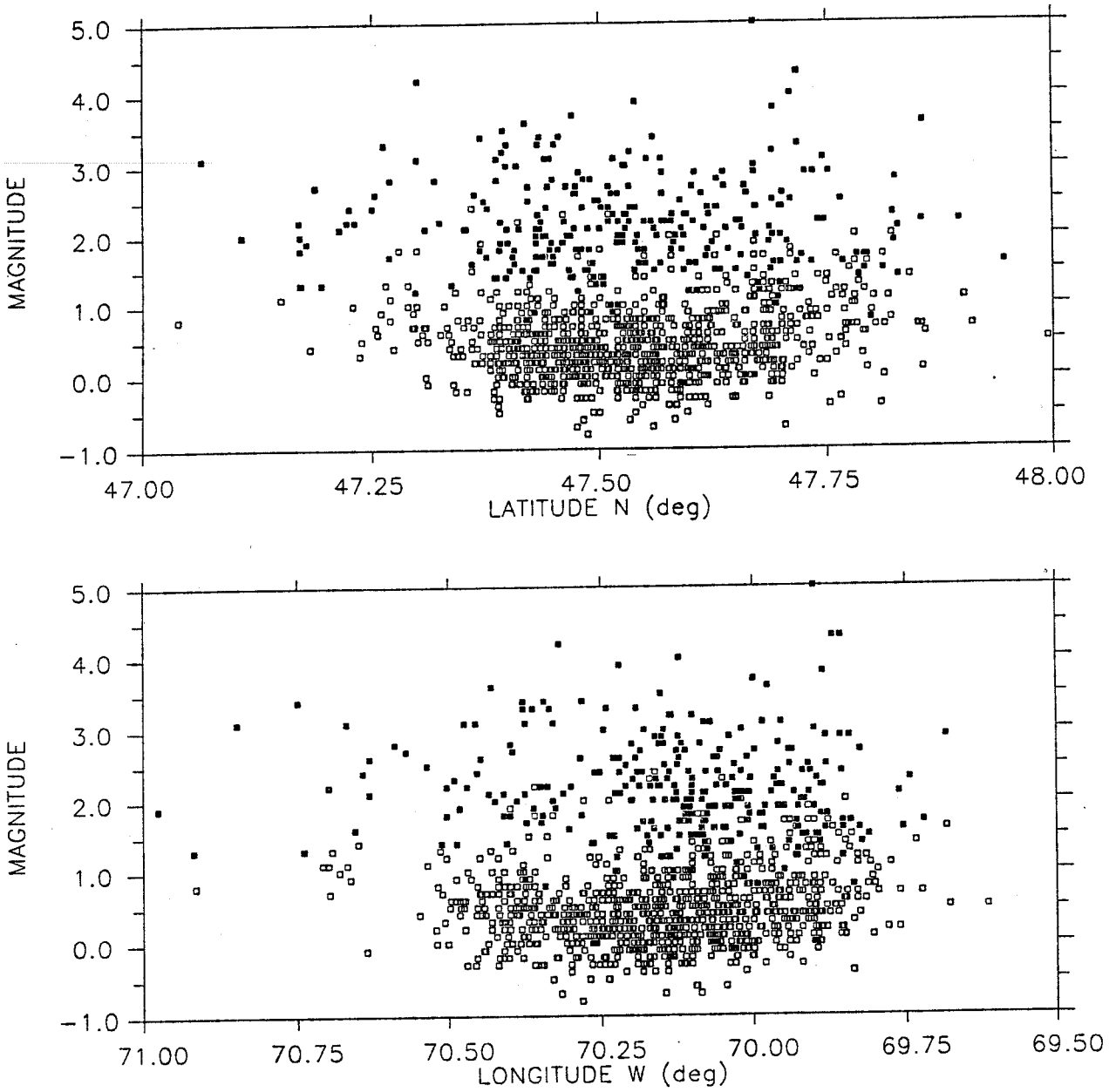

Figure 2.4.2 Spatial distribution of magnitudes: magnitudes versus latitude (top frame) and versus longitude (bottom frame). Filled squares mark MN's and open squares denote ML's (as in Figure 2.3.1).

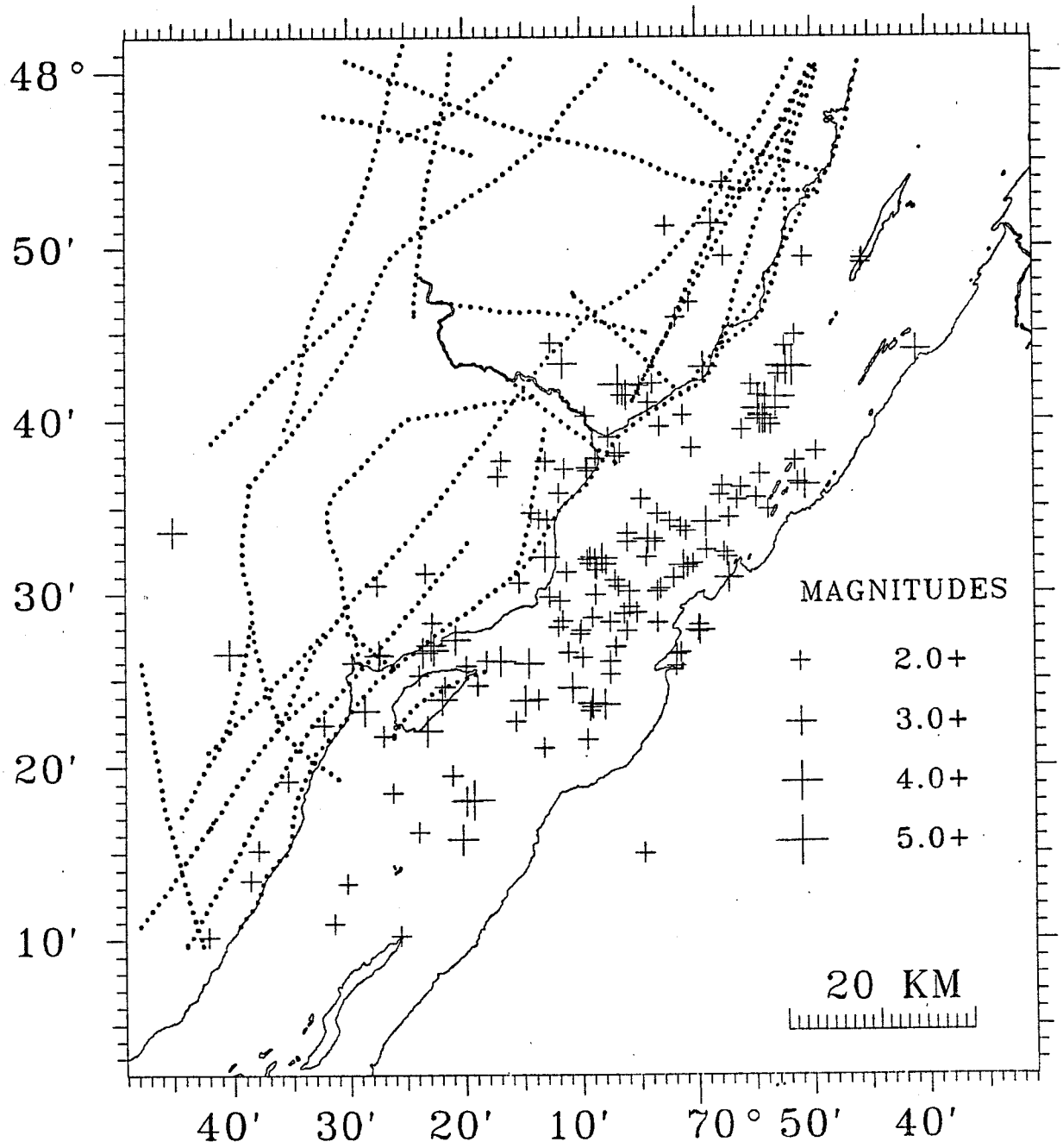

Figure 2.5.1 Epicentral map of the M ≥ 2.0 events that occurred in the CSZ in the period October 20, 1977 - July 31, 1991. Dotted lines show fault traces (same as in Figure 1.3.1).

Figure 2.5.2 on the other hand, shows an epicentral map on the top and a cross-section on the bottom. Both feature all events recorded within the study period. Two polygons are outlined in the top frame. The outer one encompasses most of the activity recorded, while the inner one delineates the area of more substantial concentration of seismic events. The inner area is the one that is traditionally associated with the CSZ and only the events within this polygon will be studied further. The space-time plot in the bottom frame features distance along profile PP' (across the zone in the top frame) versus time. The small cluster in the upper left is associated with the largest local event to take place in the study period (M5.0) that occurred in August 1979.

Figure 2.5.3 shows cross-sections (depth versus distance) along profiles normal to the PP' profile used in the previous figure. Nine boxes are outlined in the epicentral map; the nine cross-sections show the hypocentres in each of these boxes. This allows us to see features in depth which cannot be seen as clearly on either the epicentral map or the cross-section for the whole CSZ. These features have already been discussed in detail by Anglin (1984). The structures outlined by the seismic activity generally dips to SE, the dipping angle somewhat changing from SW to NE. Another conspicuous feature is the existence of a relatively aseismic area in depth that splits the activity into two branches. In some places the two branches seem to merge at depths > 13 to 15 km (C), but in other places they stay separated (F). These trends can be even more easily distinguished in stereo-plots (Anglin, 1984) not shown here.

2.6 Histograms of Number of Events and Plots of Cumulative Number of Events

A popular type of display giving information about earthquake distribution in time are histograms like the ones shown in Figure 2.6.1. The number of events per unit time (seismic activity rate) is shown versus time on these plots. The choice of lower magnitude cut-off and the length of the time unit for the counts is arbitrary. It is usually based on the subjective judgement about what is "reasonable". For example, small unit times are not reasonable for counts of larger events, since many of the time intervals will contain only very few events, if any. The magnitude thresholds and the size of the time interval for counting are shown in the upper left corners of the plots in Figure 2.6.1. Magnitudes are ML's for smaller events and MN's for larger events, as originally given in the AP catalogue.

Figure 2.6.2 shows a histogram of the number of $M \geq 0.5$ events per 30 days for the study period, October 20, 1977-July 31, 1991. The arrows indicate the times of occurrence of $M \geq 4.0$ events, including the M5.0 event in August 1979 and the M4.3/M4.4 doublet in March 1989. The dashed arrow indicates the time of the November 1988 M6.5 Saguenay earthquake which occurred outside the CSZ. It is evident that temporal variations of several times the average rate of activity are common. However, except for the aftershocks of the 1979 M5.0 event, the largest peaks or troughs of this histogram do not seem to be clearly associated with the times of occurrence of larger events. No rate larger or lower than the average one is uniquely observed before any of these events without being seen at many other times. A similar observation has already been indicated by Buchbinder et al. (1988) whose search for precursory quiescence failed to identify such a pattern.

Another way to display the same information is to plot the cumulative number of events versus time. Examples are shown in Figure 2.6.3. In the ideal case when the rate of seismic activity is constant, such plots simply feature straight lines. A significant change in the slope

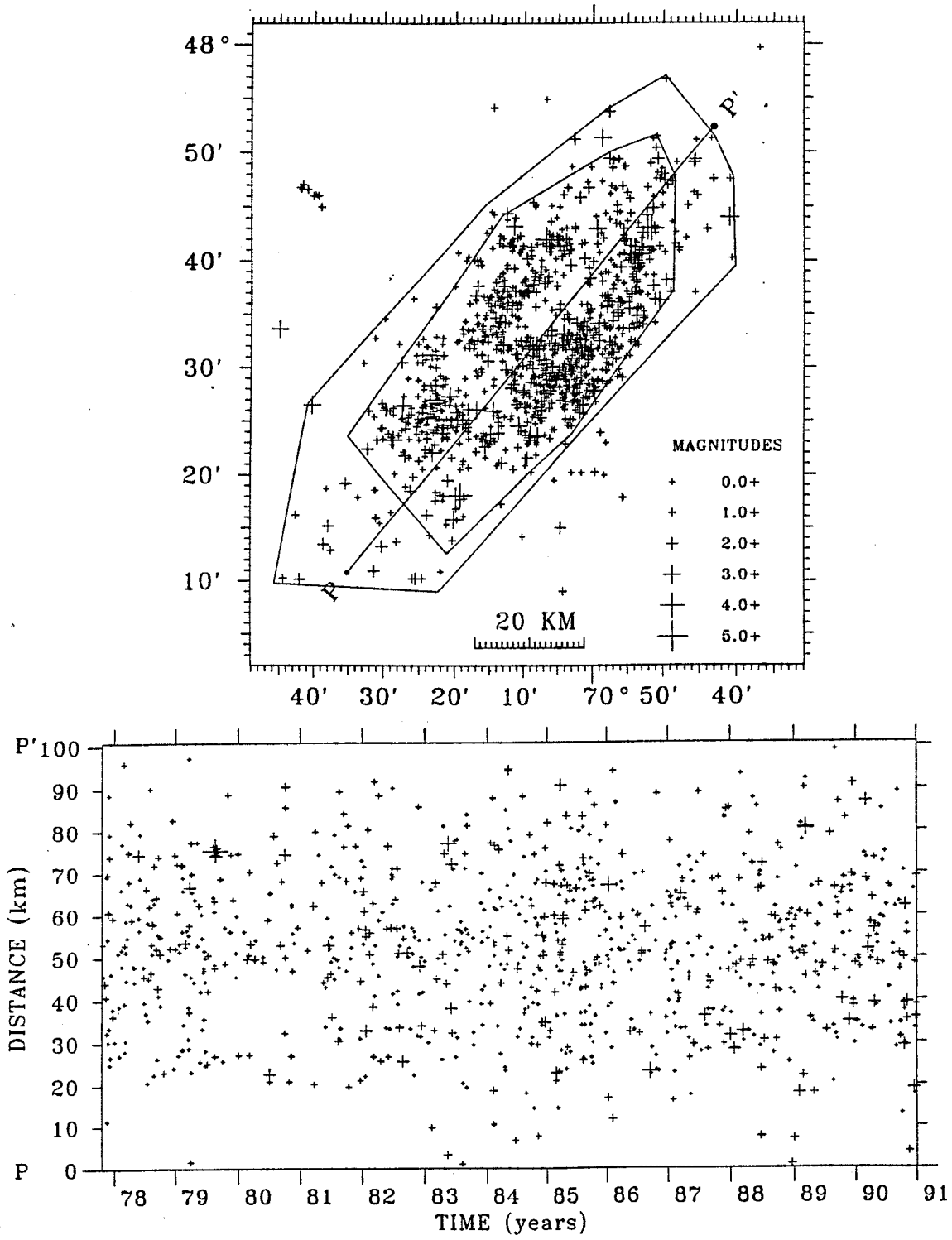

Figure 2.5.2 Epicentral map (top frame) and hypocentral cross-section along profile PP' (bottom frame). All events recorded in the period October 20, 1977 - July 31, 1991 are shown. Polygons in upper frame are explained in the text.

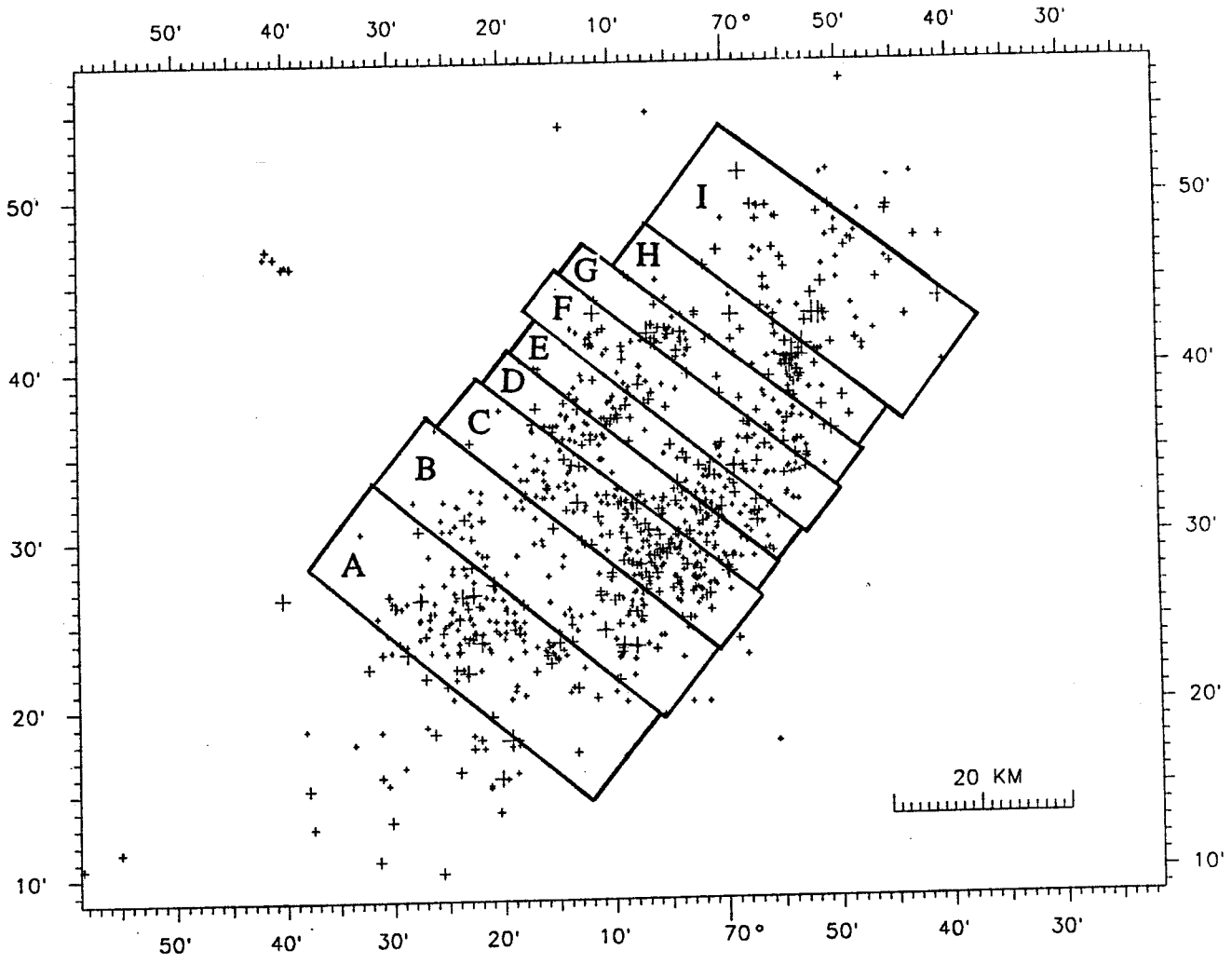

Figure 2.5.3 Depth distribution of the events in nine adjacent subareas covering the CSZ from southwest to northeast. Subareas are outlined by nine boxes and are marked with letters A to I. Figure continued on next page with cross-sections from the nine boxes. Each cross-section is marked with the same letter as the respective box.

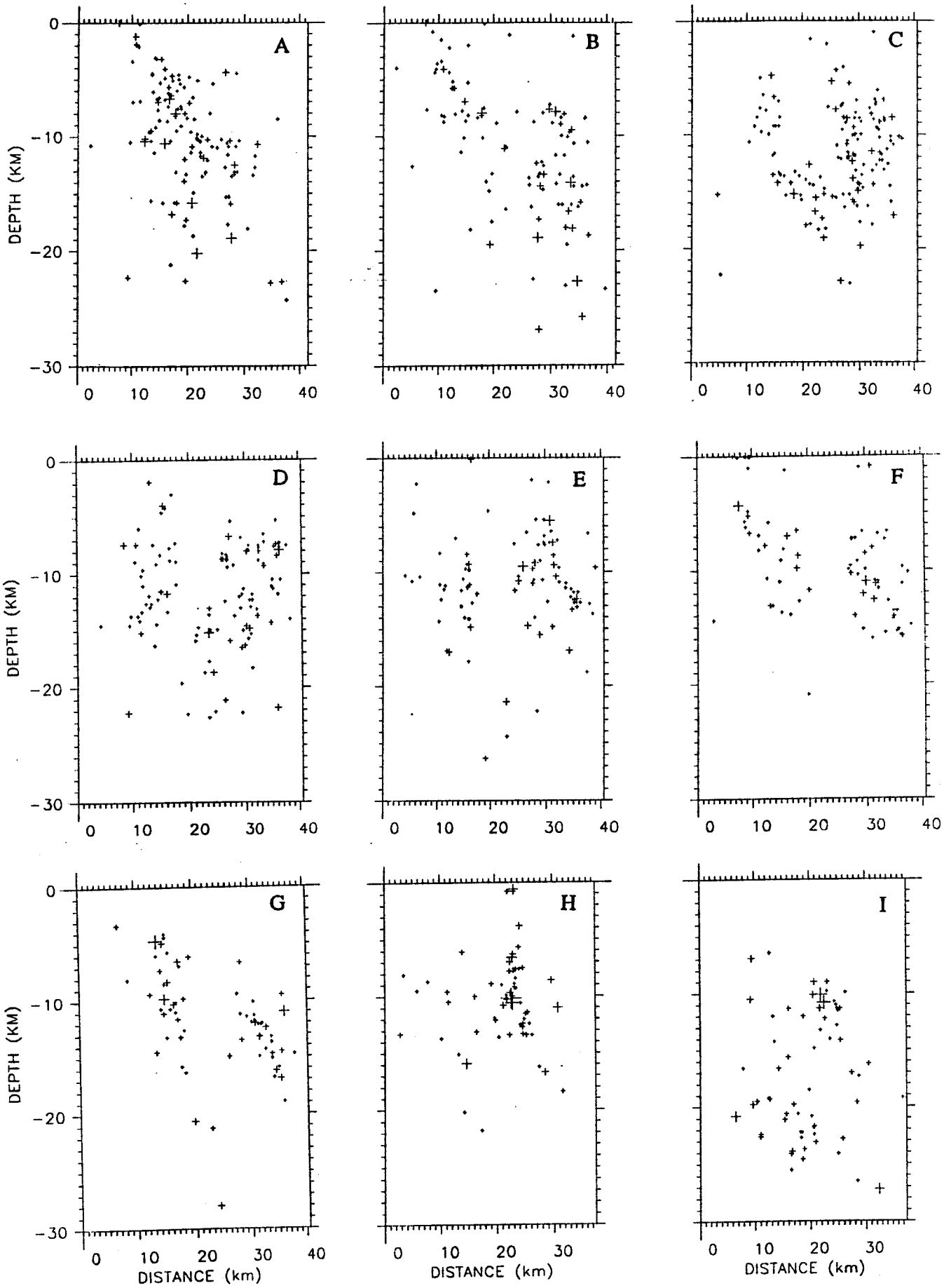

Figure 2.5.3 (Continued from previous page).

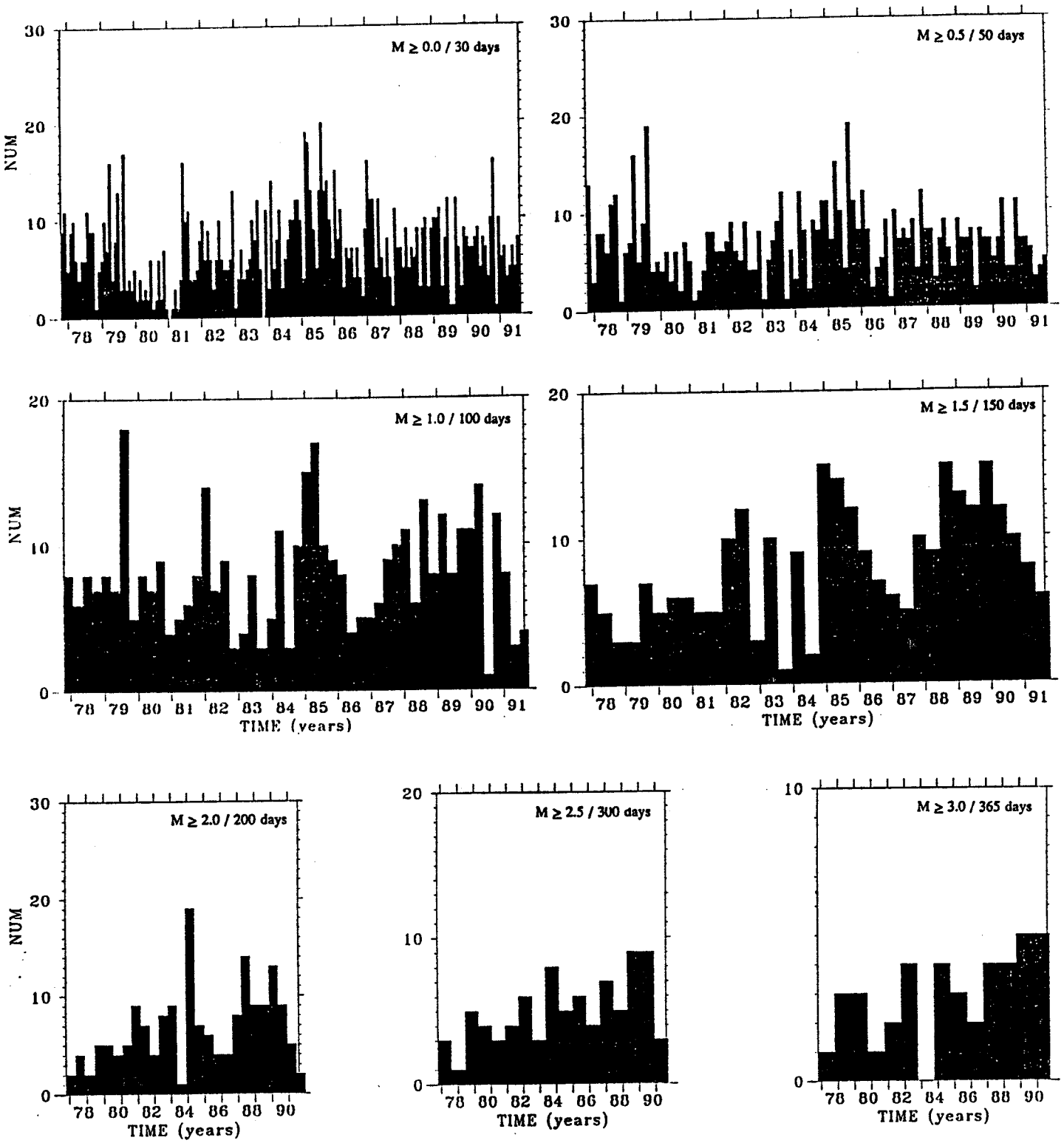

Figure 2.6.1 Histograms of number of events per unit time. Lower magnitude cut-off above which events are counted and the size of unit time are shown in upper right corners of the plots.

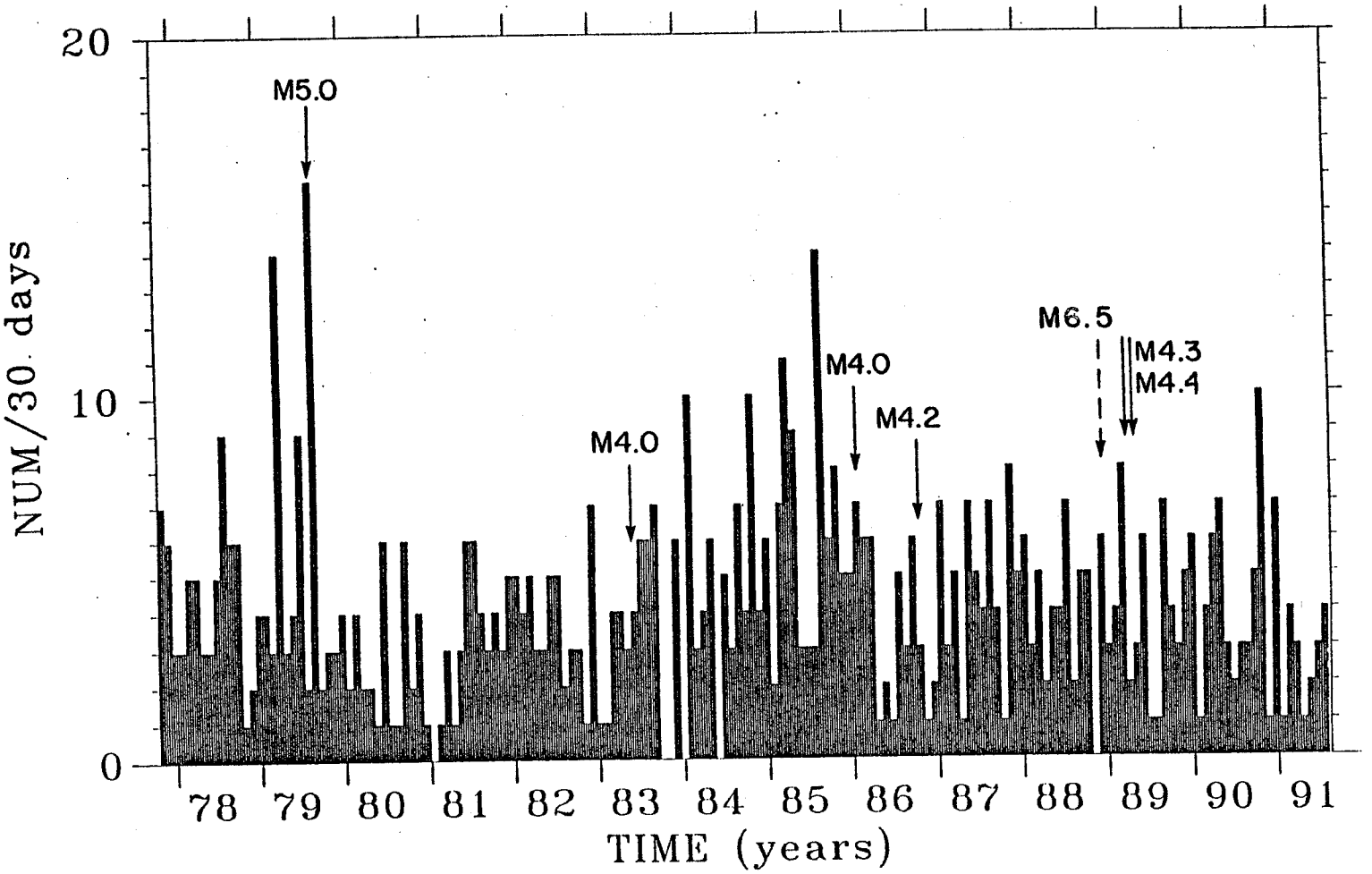

Figure 2.6.2 Histogram of number of ML $\geq$ 0.5 (MN $\geq$ 1.4) events per 30 days. Arrows show times of occurrence of M $\geq$ 4.0 earthquakes. Dashed arrow shows the time of the 1988 Saguenay event which occurred outside the CSZ.

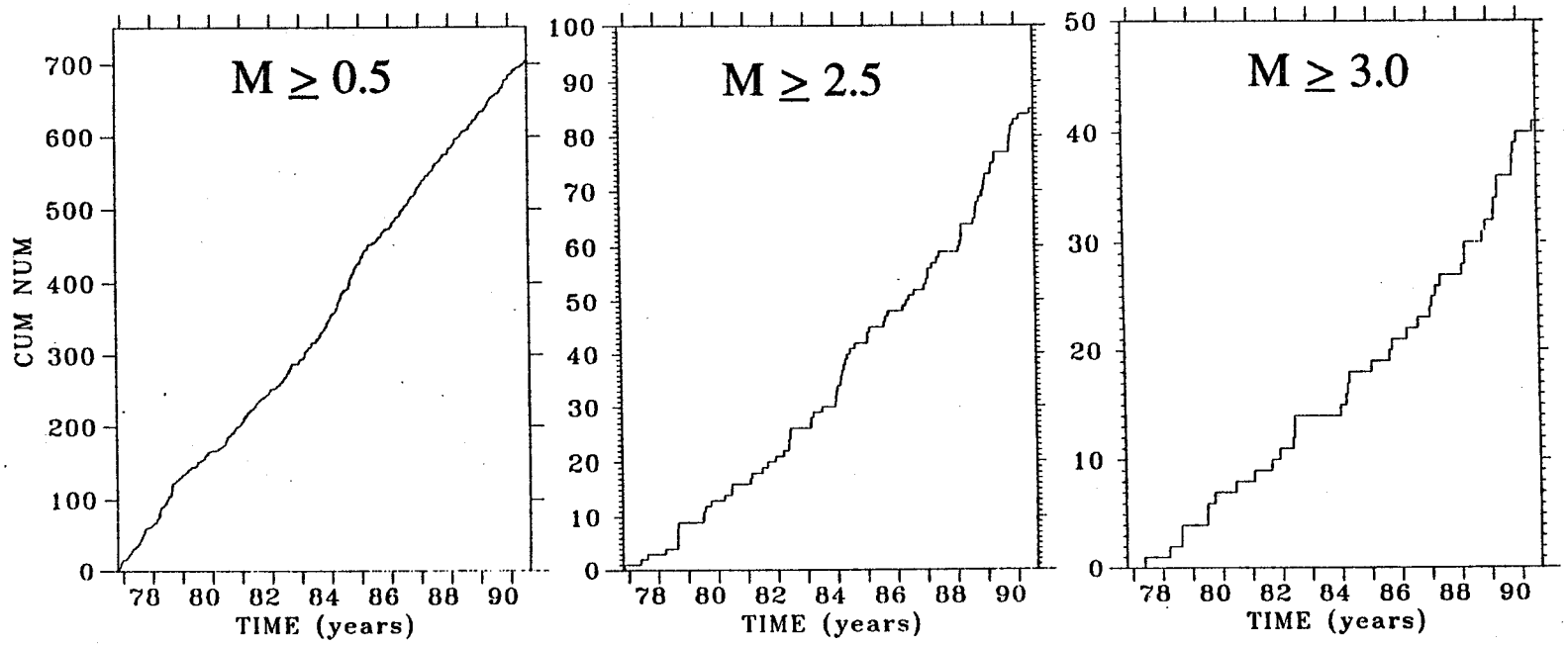

Figure 2.6.3 Cumulative numbers of events in three magnitude bands. Magnitudes indicated in the title are the primary magnitudes listed in the AP catalogue, i.e. M≥0.5 are mostly ML's (MN≥1.4), while M≥2.5 and M≥3.0 are mostly MN's. Note the appearance of ever-increasing rates of the larger events, which is most probably an artifact of the changes in the demarcation point between the two types of magnitudes (see text).

indicates a rate change. Often decreases in rate observed from such plots have been associated with quiescence preceding large events. Habermann (1987, 1991) showed, however, than only a limited number of such rate changes are likely to be natural, and that many of them are in fact artificial (man-made). At this point it is already known that one potential man-made problem in the Charlevoix catalogues is the varying demarcation point between the two types of magnitudes used for smaller and larger events. Figure 2.6.3 apparently indicates that the rate of small events has been much more constant than the rate of larger events. In fact, the rate of larger events (plots in the middle and on the right) looks ever increasing, or at least, characterized by not fewer than three different slopes at various times. This is quite a suspicious observation; we already know, indeed, that events which have been previously assigned magnitudes between 1.5 and 2.0 (ML's) appear with magnitudes by close to 1 m.u. higher after 1982 (MN's). Such an artificial change in the way magnitudes are determined can easily cause apparent rate change. Seismicity rates are studied in a more quantitative way in the next Chapter 3, applying the Habermann's technique.

It is to be noted that the visual displays shown until this point provide a valuable information about the earthquake distribution in space and time. This information, however, remains qualitative. Various subjective choices are always made when such displays are prepared. Their visual inspection can be misleading in the way certain features are reenforced, while others become suppressed. In contrast, the next three chapters concentrate on various non-traditional quantitative aspects of spatial and temporal distribution of earthquakes.

CHAPTER 3. CHANGES IN THE RATES OF SEISMIC ACTIVITY

Variations in seismicity rates, i.e. number of earthquakes per unit time, have great potential for providing information in many seismotectonic and earthquake prediction studies. Quiescence in seismic activity taking place prior to larger events is perhaps the precursor most frequently reported among precursors based on earthquake catalogues (e.g., Wyss and Habermann, 1988). Alternatively, increasing seismicity rates, have been also associated with forthcoming large events (e.g., Shaw et al., 1992).

3.1 Natural Versus Artificial Rate Changes

Seismologists rely on seismicity catalogues in order to examine variations in seismicity rates. These catalogues, however, contain a mixture of natural and artificial variations. For example, recent more rigorous studies, indicate that quiescence may not be as wide spread as initially believed (e.g., Reasenberg and Matthews, 1988) and what is even worse, there have been cases when rate changes due solely to changes in the seismic networks were mistakenly attributed to quiescence (Habermann, 1991). For this reason, establishing a seismicity rate change is not sufficient to assume that it reflects a natural process. The artificial rate changes are related to ever-present changes in the size and configuration of seismic networks and in the analytical and computational procedures used to compile the catalogues. The principal types of artificial changes that have been recognized and described are *detection changes* and *magnitude shifts*. These types of changes must be identified and understood before natural rate variations can be examined. The CSZ catalogue is analyzed for seismicity rate changes using techniques developed by Habermann

(1983, 1987) and previously applied to many regional and teleseismic catalogues (Wyss and Habermann, 1988; Wyss, 1991; Habermann, 1991; Eneva et al., 1992b).

3.2 Types of Artificial Rate Changes

The two most commonly observed artificial rate changes are *detection changes* and *magnitude shifts*. The artificial rate change that is most easily understood is the *detection change*. These changes are concentrated in the smaller events. The installation of new stations in a given region usually results in a detection increase. Closure of stations on the other hand can cause a detection decrease, which seems to be more common than previously recognized (Habermann, 1987). Detection changes may also result from changes in instrumentation, changes in gains, changes in ambient noise level, policy decisions, or other, more obscure reasons. For example, a detection decrease in one region can be related to the installation of new stations in another region and the associated increase of workload. Similarly, temporary detection decreases may be associated with natural increases of activity in surrounding regions (such as aftershock sequences) that cause increased amount of work. Artificial changes in catalogues due to changes in workload or personnel most probably would remain unaccounted for even if comprehensive information about the changes in the network were available.

It has also been shown that systematic changes in magnitude determination, the so-called *magnitude shifts* (Habermann, 1987), can cause rate changes. Systematic shifts in magnitude estimates can be caused by changes in instrumentation or changes in gains. Magnitude estimates can systematically change with changes in station distribution even if the method of calculating the magnitudes does not change. North (1977) has reported such a change in PDE data caused by the closure of the VELA arrays. Examples of magnitude shifts were shown by Habermann (1986, 1987) and Habermann and Craig (1988), the latter unexpectedly seen at the times of occurrence of aftershock sequences. Magnitude decreases can be particularly troublesome because they can cause apparent decrease in seismicity rate above certain magnitude cut-off. If one happens to examine the events only above such a cut-off (as it is usually done), rate changes may be mistakenly interpreted as real quiescences before large events.

3.3 Identification of the Times of Rate Changes

The first step in any study of seismicity rates is to determine the times at which they change. These times generally depend on the magnitude band considered. The general approach used here consists of quantitative comparison of mean rates of seismic activity from different periods of time. The mean rates are calculated separately for various magnitude bands. Only the original Habermann's approach is used here, although newer modifications are already available (Eneva et al., 1992b). The technique is described in detail by Habermann (1983, 1987); it was called the GENAS technique after the "general AS(t)" function used in this work. It is based on systematic comparisons of rates using the z-test for calculating the difference between the means of two samples (e.g., Meyer, 1975). The difference between the mean seismicity rates $\mathbf{m_1}$ and $\mathbf{m_2}$ in two consecutive periods can be measured by:

$$z = (m_1 - m_2) / ((s_1^2/n_1) + (s_2^2/n_2))^{1/2},$$

where $\mathbf{s_1}$ and $\mathbf{s_2}$ are the standard deviations of the mean rates, and $\mathbf{n_1}$ and $\mathbf{n_2}$ are the numbers of

samples in the two periods used to determine the mean rates. Values of $|z| \geq 1.96$ indicate 95% confidence and $|z| \geq 2.57$ - 99% confidence.

The z-values are calculated with a sliding dividing point between two endpoints. These endpoints are iterated until a set of periods of constant rate are identified. Negative z-values indicate rate increases and positive z-values indicate rate decreases. Numerous times of rate changes can be identified in this way, but only those for which the |z|-values exceed a preliminary chosen *alarm level* in at least several magnitude bands are considered to be significant. Rates are calculated after binning the data into time intervals of a given length, called the *sample length* (e.g., 1 week, 1 month, etc.). Another parameter is the *buffer length*: the minimum number of samples from which a mean rate is calculated. The buffer length is the shortest period allowed between two successive rate changes to be examined. The lengths of the periods around a given time of rate change vary, but are larger than or equal to the buffer length. The alarm level, the window length, and the buffer length are chosen arbitrarily. The optimum set of these three parameters varies from catalogue to catalogue, depending on how high the observed seismicity rates are and how variable the catalogue is. One usually makes a decision based on the degree of detail preferred for the identification of rate changes. Similar arbitrary choices are made in the application of any technique that is based on data sampling. Reasonable variations in the sample length (i.e., allowing for a sufficient number of events per sample) are not that crucial to the identification of the times of the main rate changes. The role of the buffer length, however, is more decisive. For this reason, a somewhat different technique is applied by Eneva et al. (1992b) where times of rate changes are identified by calculating z-values for sliding points in time which divide two periods of fixed length (*window length*). The present study, however, makes use only of the original GENAS technique. While the original technique does have some limitations as does any other technique that involves division of data into samples, the main rate changes are usually identified around the same times as long as the choices of parameters (sample length, buffer length, and alarm level) stay within reasonable limits. What is "reasonable" may vary from catalogue to catalogue, depending on numbers of events and desired detail of study. Experimenting with several choices of parameters should point to the rate changes that reappear consistently, regardless of these choices.

If a rate change is gradual as opposed to relatively abrupt one, it most probably would not be identified by the GENAS technique. What is "gradual" depends on the interplay between sample length and buffer length. The technique used identifies more or less abrupt changes. More details on the limitations of the Habermann's technique are given by Eneva et al. (1992b).

3.4 Identification of the Source of Rate Changes

The identification of the times of rate changes is only the first step in this analysis. It is furthermore important to distinguish between natural and artificial rate changes, as well as to analyze the types of artificial changes. Significant understanding of the possible causes of seismicity rate variations can be gained from examining these variations in a number of magnitude bands. In addition to the traditional bands of events with magnitudes greater than or equal to given magnitude thresholds (e.g., $M \geq 2.0$, $M \geq 3.0$, etc.), bands of events with magnitudes smaller than these thresholds (e.g., $M < 2.0$, $M < 3.0$, etc.) also contain information about the cause of an observed change. These are referred to as the *and aboves* and the *belows*, respectively.

The magnitude distribution of an observed rate change is described by plots of the z-

values associated with a given change as a function of magnitude band. These plots are called *magnitude signatures*. The z-values for the magnitude signatures are determined by comparing rates in each magnitude band during two time periods surrounding the time of the rate change being characterized. Magnitude signatures which are associated with particular types of changes have characteristic shapes described in detail by Habermann (1987, 1991). The magnitude signatures shown in Figure 3.4.1 demonstrate the relationship between type of rate change and shape of magnitude signature (after Eneva et al., 1992b). To create these magnitude signatures a portion of the catalogue used by Eneva et al. (1992b) was extracted that was apparently free of rate changes for all magnitude bands. The particular catalogue used is not important for the shapes of the magnitude signatures to be understood. Figure 3.4.1-A shows a magnitude signature comparing the first and second halves of this period. The lack of rate change is indicated by a magnitude signature around the zero line when these two halves are compared. The subsequent plots in Figure 3.4.1 show the shapes of magnitude signatures after changes are artificially introduced in the second period. The changes introduced mimic the following: B and C - pure detection changes (twice increase or decrease) over a certain magnitude range (M<2.0); D and E - pure magnitude shifts for all magnitudes (+0.2 m.u. or -0.2 m.u.); F to I - combinations of these; and J and K - natural rate changes over all magnitudes (twice increase or decrease). Since the original mean rates compared were not perfectly equal (as it would be in any real catalogue) the shapes of the magnitude signatures obtained after the manipulation of the second period are not perfectly smooth. Details describing these shapes are given in the caption of Figure 3.4.1. The main features to be used in the interpretation of the CSZ magnitude signatures in the next paragraph are the following: (a) a pure detection change is characterized by z-values of the same sign throughout the magnitude signature and z's around 0 for data sets with magnitudes larger than some threshold (see Figure 3.4.1 - B, C); and (b) a pure magnitude shift is indicated by z-values of different sign on both sides of the central vertical line, and z=0 where the magnitude signature crosses this line (see Figure 3.4.1 - D, E).

The cause of rate changes cannot be determined in a non-unique way only on the basis of the technique described. The magnitude signatures in Figure 3.4.1 are obtained from solving a forward problem, that is, finding the shape of magnitude signature when the source of rate change is known. The practical problem is the inverse one. An implicit assumption is made here that if the shape of a given magnitude signature matches one of the shapes shown in Figure 3.4.1, then the source of the respective rate change is most probably the same as the one used to produce the reference magnitude signature. This is not necessarily true, but seems to be a good working assumption.

Eneva et al. (1992b) used randomized catalogues in order to further constrain the possibilities when identifying the cause of a rate change. These are not used here. In general, the Habermann's technique considers a rate change to be "natural" if it manifests itself over all magnitudes. This is not to say that natural rate changes cannot take place only for some magnitudes, but these are much more ambiguous. In particular, cases of rate changes only for small events are assumed to be of artificial origin in this study following the previous works of this type (Habermann, 1983, 1987, 1991; Eneva et al., 1992b). If one examines only the catalogues, it is not possible to distinguish between a detection change and a natural rate change that takes place only for the small events. For example, the magnitude signature for a hypothetical detection decrease of M<2.0 events cannot be distinguished from the magnitude

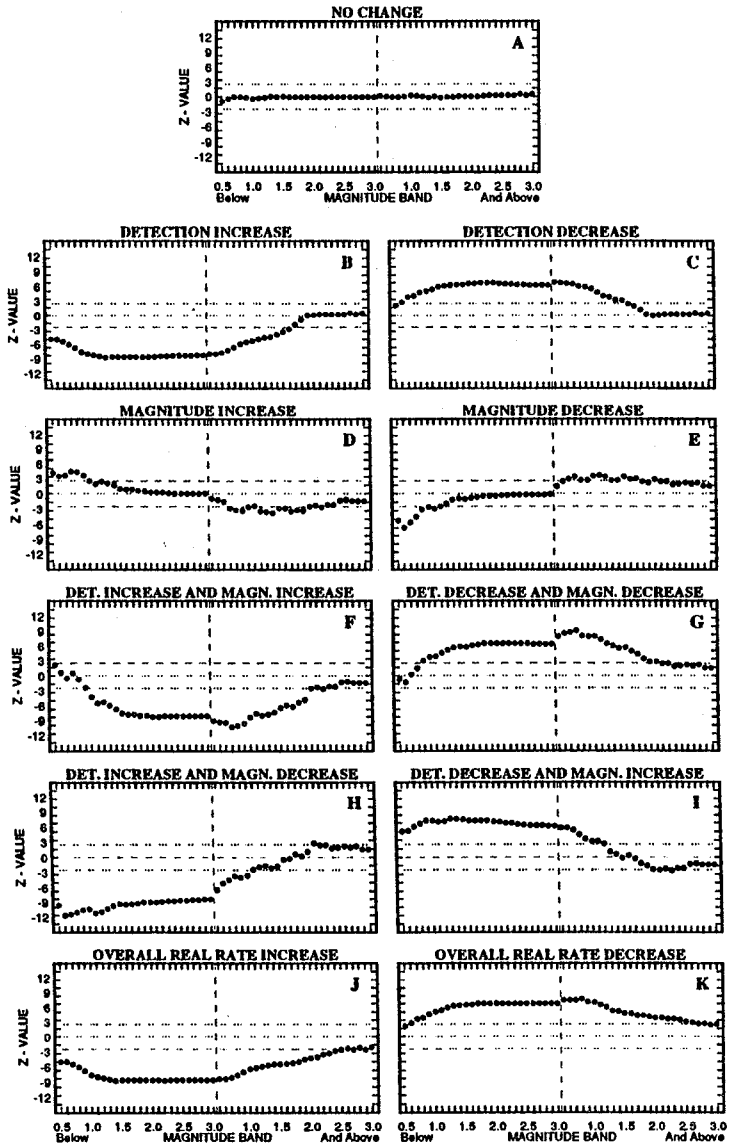

Figure 3.4.1 Examples of magnitude signatures comparing the rates between two periods that did not show a rate change in a real catalogue (after Eneva et al., 1992b). Frame A shows the comparison of the two periods for the original data. Because of the lack of a rate change in the original data, the z-values are around 0. Synthetic artificial and "natural" rate changes were introduced into the second period in order to illustrate the relationship between the shape of the magnitude signatures and causes of the rate changes. Horizontal dashed lines at 2.57 show nominal 99% confidence limits. B, C) *Detection Increase / Decrease* - indicated by the "plateaus" of negative/positive z-values for bands with upper cut-offs (on the left side of the plot) and lack of change (z-values near 0), for bands with lower cut-offs (on the right side of the plot). Note that z-values do not change signs throughout a given magnitude signature. D, E) *Magnitude Increase / Decrease* - indicated by z-values with different signs on opposite sides of the magnitude signature. F) Combination of *Detection Increase and Magnitude Increase* - sum of the magnitude signatures in Frames B and D. It is similar to the detection increase in Frame B, but is tilted, i.e., the z-values are increased on the left and decreased on the right. This combination can be misinterpreted as natural overall increase (Frame J). It shows, however, a rate decrease for the very small events (positive z's) and a jump around the vertical line in the centre, neither of which is observed in Frame J. G) Combination of *Detection Decrease and Magnitude Decrease* - sum of the magnitude signatures in Frames C and E. This change could easily be misinterpreted as a natural overall rate decrease as it causes apparent rate decreases in all magnitude bands (compare with Frame K). The significant jump in the signature as the vertical line in the centre is crossed and the presence of negative z's for the smallest events to the left are features not observed in Frame K. H) Combination of *Detection Increase and Magnitude Decrease* - the plateau of negative z's on the left indicates the detection increase, while the presence of z's of different sign indicates the magnitude decrease. I) Combination of a *Detection Decrease and Magnitude Increase* -the plateau of positive z-values on the left of the magnitude signature indicates the detection decrease, and the negative z-values on the right side of the plot indicate the magnitude increase. J, K) *Natural Rate Increase / Decrease* over all magnitudes - generally indicated by negative/positive z-values across the magnitude signature and looks substantially different from simple detection or magnitude changes. It may be difficult to distinguish between these natural changes and the combined artificial changes in Frames F and G.

signature for a natural rate decrease only for events of M<2.0. It is assumed, however, that the latter is much less likely to occur; it is necessary to check in such cases whether there were some network changes at the same time.

Figure 3.4.1 shows that it may be difficult to distinguish between natural overall decrease (K) and a combination of negative magnitude shift and detection decrease (G). The situation is similar for a natural overall rate increase (J) and a combination of artificial magnitude increase with detection increase (F). Other ambiguous combinations are also possible. An example would be a combination of detection (or natural) increase below some magnitude cut-off and a natural rate decrease above certain magnitude threshold. This may mimic a combination of detection increase and magnitude decrease (H). The use of randomized signatures may help to analyze some of these cases as discussed by Eneva et al. (1992).

In the light of the above, the approach used in the present work to distinguish between artificial and natural rate changes is rather conservative: a rate change is assumed to be artificial unless it is observed in all magnitude bands as an overall rate change. The source of a rate change affecting only smaller events is considered to be an artificial one. A rate change only for the larger events would be a candidate for a natural rate change under some circumstances, but no such changes were observed in the CSZ catalogue.

3.5 Results from the CSZ

The catalogue examined was the AP catalogue after all ML's were converted to MN's according to the ML=f(MN) empirical relationship obtained in 2.3 and illustrated by Figure 2.3.2. The following times of rate changes were identified in the CSZ using the GENAS technique: September/October 1979, May/June 1981, July/August 1984, April/May 1986, May/June 1987, and October/November 1988. Note that none of these times is associated with the change of the demarcation point between ML's and MN's (discussed in 2.3). The parameters used were: sample length = 1 month (168 samples for the period October 20, 1977 - July 31, 1991), buffer length = 12 months, and alarm level = 2.5. The number of magnitude bands considered was 32: MN<1.0, MN<1.1, MN<1.2, ..., MN<2.5 (the *belows*) and MN$\geq$1.0, MN$\geq$1.1, MN$\geq$1.2, ..., MN$\geq$2.5 (the *and aboves*). MN$\geq$1.4 was determined as the magnitude of complete recording in time and space for the CSZ (see 2.4 and Figures 2.4.1 and 2.4.2). Habermann's technique, however, uses all magnitudes; hence, the use of magnitude bands such as MN<1.0, 1.1, etc., and MN$\geq$1.0, M$\geq$1.1, etc.

The above choices mean that rates were obtained as numbers of events per month (separately for each of the 32 data sets featuring different magnitude bands), that mean rates were calculated from at least 12 samples, and that only those times of rate changes were considered for which |z|-values exceeded 2.5 in several data sets. It should be noted that the z-values calculated at the first run of the GENAS programme are only used as a general indication of the possibilities for significant rate changes. Each prospective time of a significant rate change is subsequently examined by comparing the two periods on its sides. The z-values obtained at this stage are not necessarily of the same significance as the ones from the first stage and some of the times might have to be dropped out. The times of rate changes listed above are only the times for which the magnitude signatures definitely indicated significant rate changes.

Figure 3.5.1 shows these magnitude signatures. They can be readily compared with the shapes in Figure 3.4.1. This comparison indicates that only the rate decrease (positive z-values)

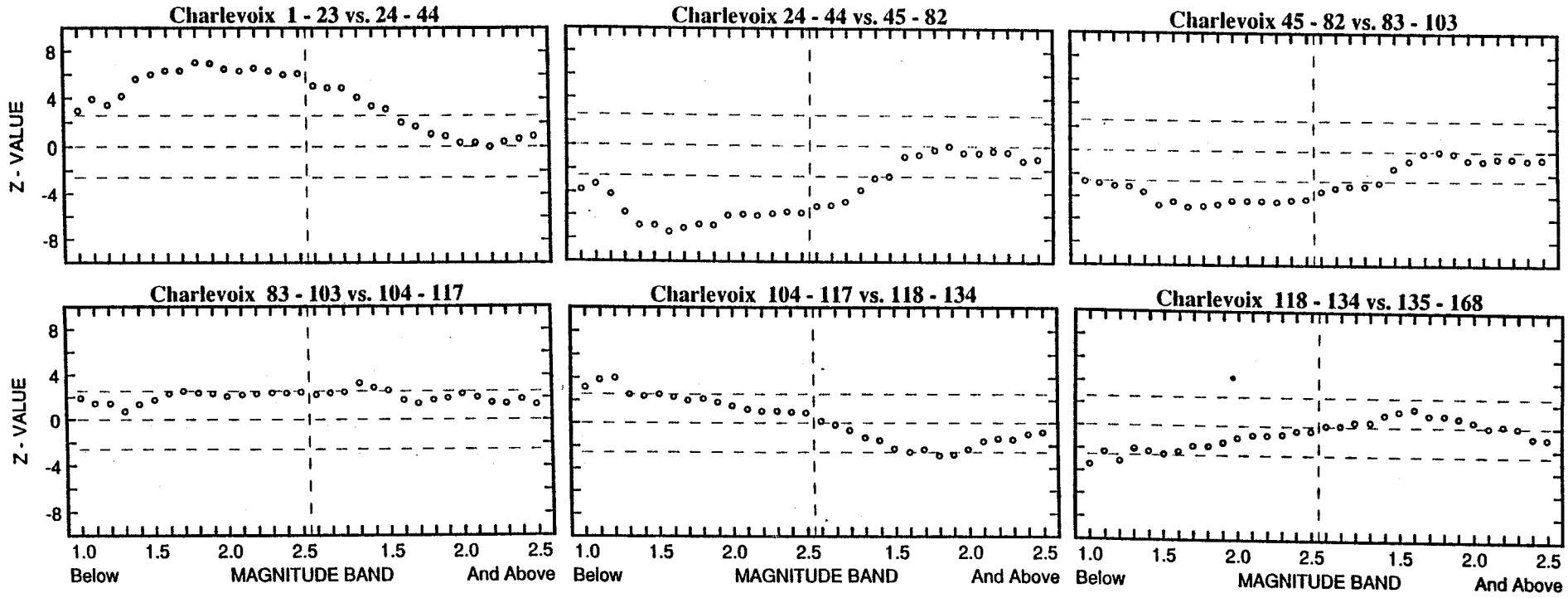

Figure 3.5.1 Magnitude signatures for the main rate changes in the CSZ. The numbers in the titles indicate months counted from October 20, 1977 on. For example, the first magnitude signature compares the period between the first and the 23-th month with the period between the 24-th and the 44-th months. Comparing this Figure with Figure 3.4.1, pure detection changes are indicated by the magnitude signatures shown in the top row, while a natural rate decrease and two opposite pure magnitude shifts are indicated by the magnitude signatures in the lower frames. See text for more discussion of these rate changes.

in April/May 1986 (104-th month; lower frame on the left) appears to be overall and therefore, perhaps natural, in the more strict sense described above. The first three changes all appear like detection changes, since z-values are around 0 for magnitudes above certain thresholds. A detection decrease (positive z-values) might have taken place in September/October 1979 (24-th month) for M<2.0 events. Coincidentally, this takes place after the M5.0 local event occurred on August 19, 1979. If the array had been down for some time, larger events would still be reported from the ECTN, while the reporting of smaller events would decrease. As long as this is not known to the author at this time, a natural rate change cannot be ruled out. Detection increases are indicated in May/June 1981 (45-th month) and July/August 1984 (83-th month) for M<1.7-1.8 events. The first of these is larger (smaller negative z-values). Detection increases could be associated with times after periods during which the array had been down. Because this information is not available at present, real rate changes cannot be ruled out at these times either.

The last two changes seem to be of a different character altogether. Since they involve positive and negative z-values for the same magnitude signature, magnitude shifts are indicated. The May/June 1987 (118-th month) apparent magnitude increase might be related to the changes in the network in October 1987; the identified times of rate changes could be somewhat offset in some cases, as discussed by Eneva et al. (1992b). The original analog network was converted to a wide dynamic range digital network in October 1987 (Wetmiller and Adams, 1990). As already discussed in 2.2, prior to November 1, 1987, the magnitudes for small events were calculated only from the amplitudes and the periods read from the paper records of station LMQ. For larger events, LPQ data were used, and where seen, ECTN data (Anglin, personal communication). These changes were already discussed above (see 2.2). The last rate change, in October/November 1988 (135-th month), appears to somewhat reverse the previous magnitude increase. It is not clear why such a magnitude decrease would have occurred. This is also the time of the nearby Saguenay event (November 25, 1988), yet the shape of the magnitude signature is very different from what would be observed for a natural rate change. Even if we abandon the strict sense in which only overall rate changes are assumed to be natural, this magnitude signature, similar to the previous one, indicates pure magnitude decrease (curves cross the 0,0-point at the centre of the plots). A hypothetical case of natural rate decrease for smaller events and natural rate increase for larger events would make the magnitude signature offset downwards at the centre (vertical dashed line) and would look very much like Figure 3.4.1-H (not as E), as discussed in more detail by Eneva et al. (1992b).

The possible artificial rate changes identified for the CSZ are far from being as large as the ones identified in other catalogues (for example, Eneva et al., 1992b). In fact, they also look rather simple by comparison with other networks for which combinations of detection changes and magnitude shifts make the interpretation more complicated. Unfortunately, very little is known to the author at present about the network changes at Charlevoix and more definite conclusions are not possible. In view of this, although Habermann's technique also uses a modelling procedure (Habermann, 1987), it is not applied here. It is worth, however, briefly describing this procedure. It involves manipulating the *background* (the period before the time of a given rate change) until the *foreground* (the period after the change) is satisfactorily matched. The amounts of detection changes, magnitude shifts, or natural rate changes determined from the modelling procedure are only average, or predominant. This can by no means replace much more accurate procedures, such as adopting appropriate station magnitude corrections for

each period between network changes. The systematic application of such corrections is very uncommon, however, even for networks with well documented changes, and nearly impossible for networks with poor documentation. All this makes Habermann's technique a minimum requirement for any study of seismicity rate changes.

CHAPTER 4. PAIR ANALYSIS

4.1. Quantities Studied

Conventional methods to study earthquake distribution usually make an extensive use of epicentral maps and hypocentral cross-sections for the spatial distribution of earthquakes and seismicity rates for their temporal distribution. Consequently, earthquake catalogues have been traditionally used to produce various visual displays, to study seismicity rates, and to evaluate the slopes of the magnitude-frequency relationships (b-values). While temporal distribution of earthquakes has been described quantitatively, using distributions such as Poisson distribution and Markov chains, the spatial distribution has been studied mostly by examination of various visual displays. Only recently, quantitative approaches have been applied to the spatial distribution of earthquakes as well (Kagan and Knopoff, 1980; Matsumura, 1984; Sadovsky et al., 1987; Hirata, 1989a; Hirata and Imoto, 1991; Frohlich and Davis, 1990; Eneva, 1984; Eneva and Pavlis, 1988; 1991; Eneva and Hamburger, 1989; Eneva et al., 1992).

The results presented in this chapter are based on different parameters which, similarly to the seismicity rates and b-values, are derived from the catalogues alone, but utilize the catalogue information differently. These parameters are based on the hypocentral distances and time intervals between the events grouped in pairs, hence pair analysis. This approach extends the scope of the information that can be extracted from the catalogues. An attempt is made to find baseline values describing the zone as a whole and then to identify what variations from these base values took place and when. Although no precursors were previously found before the local M5.0 event, a specific attention is paid to the periods preceding and following this earthquake and other larger events.

The quantities studied using the pair analysis technique are: *hypocentral distances*, *time intervals* between events, and *products* of distances and time intervals. These are further referred to as interevent distances, times, and products. The use of distance-time interval product represents an attempt to adopt a joint space-time parameter. Other combinations of time and distance, different from their product, may be also useful, and perhaps even more appropriate, but we do not consider these here.

Three types of pairs are used in the present study. (1) The first type is conditionally called "all" pairs, since all possible pairs are formed between the events in a data set. If the data set consists of **N** events, pairs are formed between the first and the second event, the first and the third, the first and the fourth, etc., until the first and the **N**-th event. Pairs are further formed between the second and the third event, the second and the forth, etc., until the second and the **N**-th event. This process continues until **N(N-1)/2** pairs without repetition are formed. (2) The second type of pairs are conditionally called "next" pairs. Pairs are formed only between the events successive in time; i.e., between the first and the second event, the second and the third, the third and the forth, etc., until the **(N-1)**-th and the **N**-th. A date set of N events produces N-1 "next" pairs. (3) The third type of pairs are also **N-1** from **N** events; the same number as the

"next" pairs. These pairs are formed between events which are both successive in time and closest in space; that is, these pairs are both "next" and "near", but are further called "near" pairs for the sake of brevity.

Each quantity (distance, time interval, and product) is measured for each type of pairs (all, next, and "near"); this yields nine different parameters for each data set.

The data sets studied are formed in two major ways. First, the data set for the whole study period is considered. This data set includes the events of ML$\geq$0.5 (MN$\geq$1.4) that occurred in the period October 20, 1977 - July 31, 1991. It was previously explained that this magnitude is considered to be the magnitude of complete recording in both space and time (see 2.4). N=623 for this data set. The values of the parameters measured from this data set are considered to be the *long-term* values. The whole data set is further split into overlapping groups of constant number of events; 27 groups are formed of 100 events each. Each group moves forward in time by 20 events; that is, two consecutive groups overlap by 80 events. The periods covered by these groups are shown in the Table. It is evident that these periods are of different length: the lower the activity, the longer the period within which 100 events occur. The values of the parameters estimated from these groups are the *short-term* values that are compared against the long-term ones.

4.2 Use of "Random" Catalogues

A major feature of the approach used, is a quantitative comparison of the observed catalogue with catalogues, which are conditionally called "random". Figure 4.2.1 shows a map of the epicentres within the study polygon (the same as the inner polygon in Figure 2.5.2), and two cross-sections along two perpendicular profiles, YY' and XX'. The events within $\pm$ 20 km around YY' and $\pm$ 25 km around XX' are shown on these sections. The distance in km is along the horizontal axes of the cross-sections and the depth is along the vertical axes. Each random catalogue used for reference, is obtained by a random generation of the same number of events as in the observed catalogue within the same three-dimensional volume where the real events occurred (Figure 4.2.2). The epicentral map and cross-sections of the random catalogue are visually different from the observed ones. Uniform distribution is used for the random generation, i.e., the randomly generated points fall with equal probability anywhere in the volume. It is to be emphasized that the three-dimensional volume used is of irregular shape closely following the natural outlines of the seismically active volume. The random generation of depths is performed between two non-planar surfaces following the upper and lower limits of the seismogenic volume. Details can be found in Eneva and Pavlis (1991) and Eneva et al. (1992c). The two major techniques used to compare observed and randomly generated distributions are pair analysis (this chapter) and estimates of correlation dimension (next chapter). Both of these allow us to assign certain quantitative characteristics to the earthquake distribution in the CSZ and to examine their changes in time, if any.

4.3 Pair Analysis Technique

Pair analysis is a technique which has been developed and applied to data from central California (Eneva and Pavlis, 1988; 1991) and Soviet Central Asia (Eneva and Hamburger, 1989; Eneva et al., 1992). The next three figures feature the original application of pair analysis when all possible pairs between the events in a data set are considered. The principle used for the

Table. Beginning and ending dates of periods covered by the groups used. (Dates are determined by the origin times of the first and the last event of each group.)

Begining and ending date	Group number
10/20/77 04:07 08/15/79 16:43	1
03/17/78 14:31 11/30/79 10:57	2
08/03/78 08:48 07/25/80 22:24	3
12/24/78 22:00 05/07/81 03:41	4
04/14/79 20:42 09/28/81 13:39	5
08/17/79 05:56 02/15/82 10:53	6
12/18/79 09:14 08/29/82 02:07	7
08/14/80 20:30 04/12/83 22:04	8
05/17/81 18:56 08/22/83 17:59	9
09/30/81 07:14 03/24/84 14:44	10
03/05/82 09:26 09/26/84 17:08	11
09/01/82 04:24 01/15/85 20:32	12
04/18/83 07:16 04/28/85 07:37	13
08/23/83 00:09 08/17/85 12:43	14
03/29/84 14:14 11/15/85 15:12	15
09/30/84 01:46 03/27/86 20:28	16
01/20/85 21:28 09/29/86 15:37	17
05/02/85 09:13 03/29/87 12:02	18
08/22/85 23:23 08/25/87 02:19	19
11/20/85 02:40 01/24/88 01:07	20
03/30/86 08:05 07/03/88 03:25	21
10/18/86 22:00 12/25/88 20:35	22
04/29/87 18:27 08/22/89 17:38	23
08/25/87 20:28 01/11/90 07:15	24
01/24/88 04:33 05/30/90 02:50	25
07/09/88 06:24 11/06/90 11:30	26
02/01/89 05:38 07/23/91 01:03	27

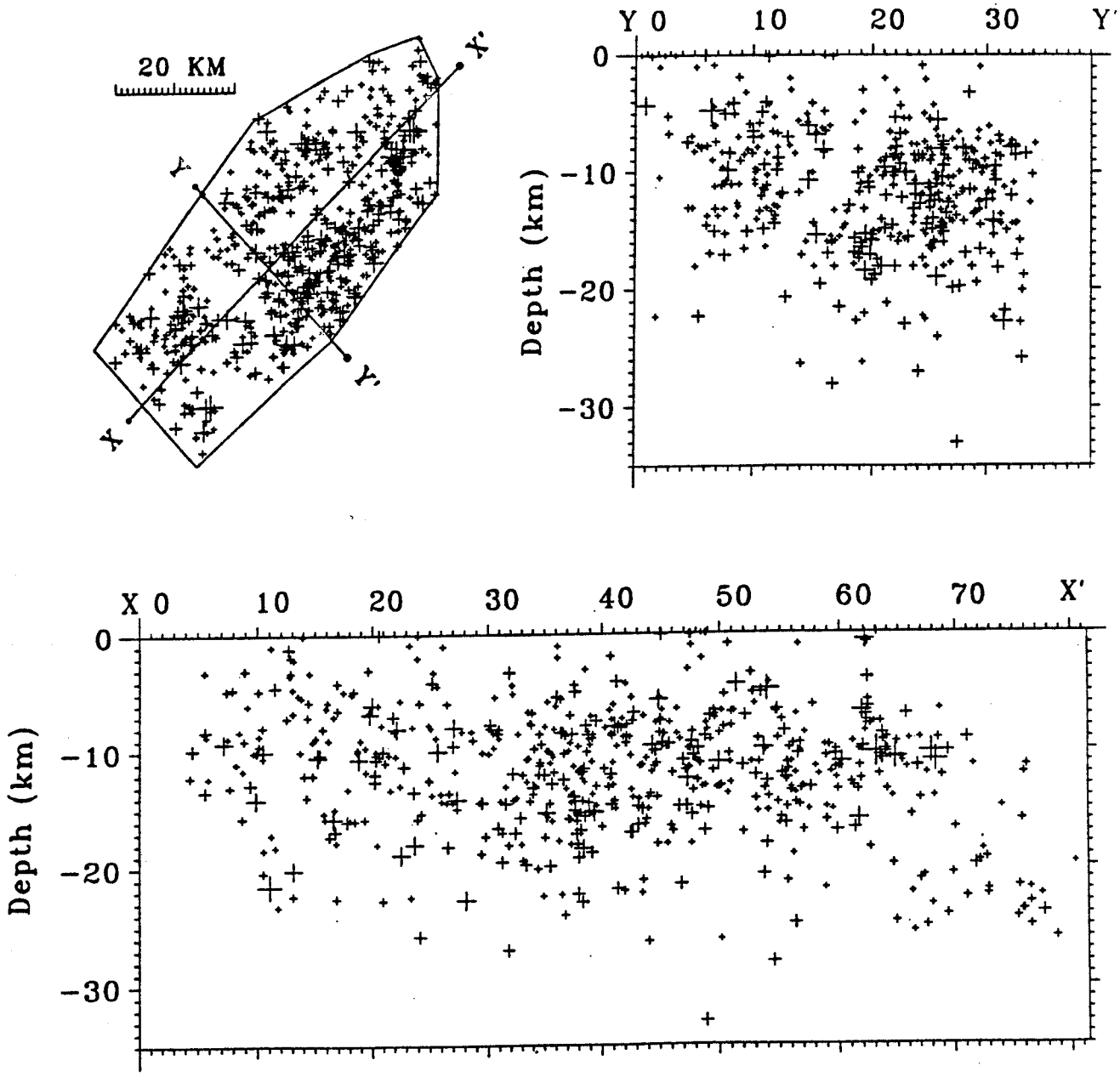

Figure 4.2.1 Epicentral map and two cross-sections of the observed catalogue along profiles XX' and YY' marked on the epicentral map. Polygon is the same as the inner polygon in Figure 2.5.2. See text for more detail.

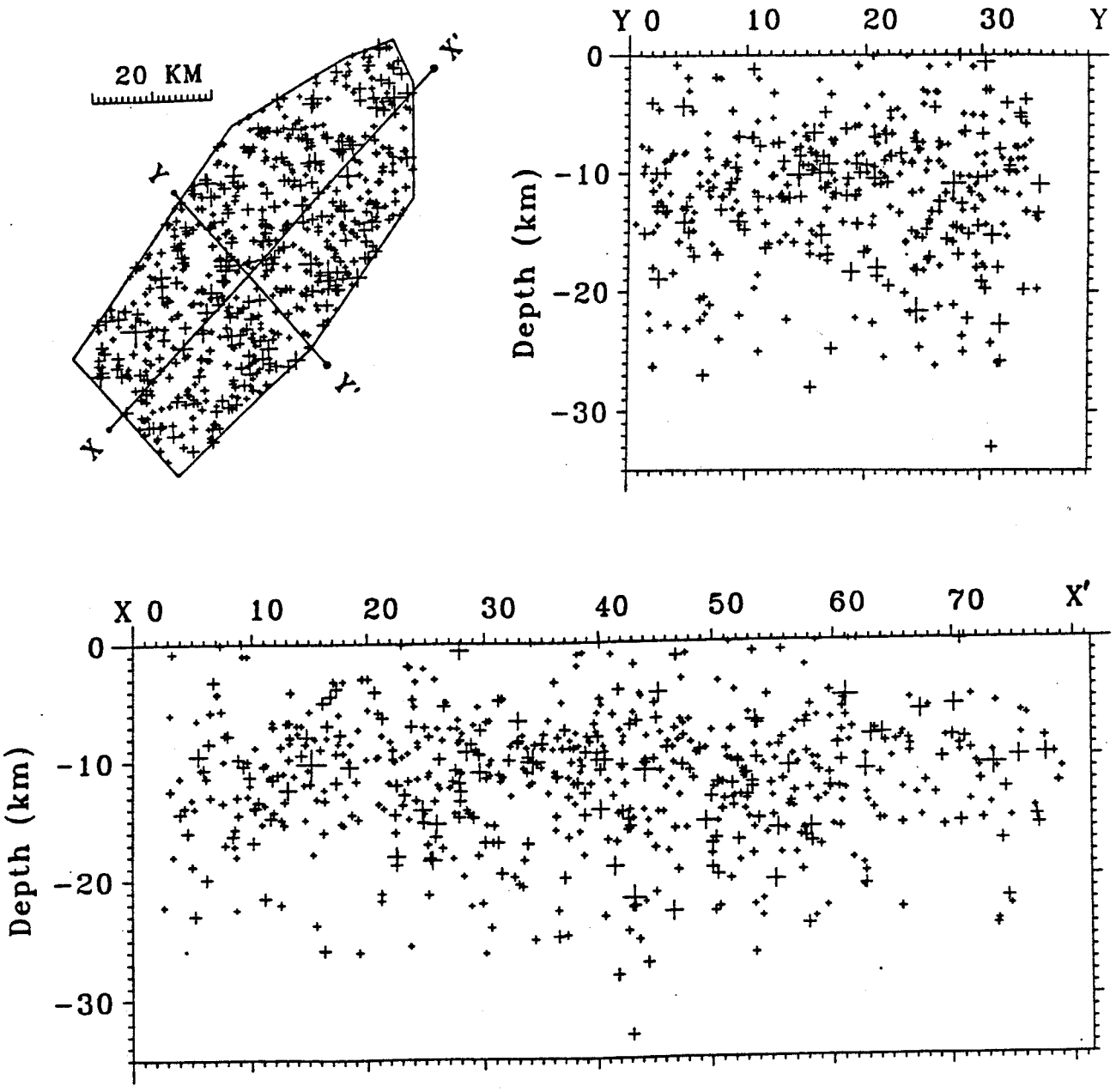

Figure 4.2.2 Same as Figure 4.2.2, but data is from a randomly generated catalogue. See text.

spatial distribution of earthquakes is illustrated in Figure 4.3.1. The observed frequency distribution of distances between the events is shown on the top. Distances are along the horizontal axis, frequency of distances (number of earthquake pairs with a certain distance divided by the total number of pairs) is along the vertical axis. The middle plot shows an expected distribution obtained as an average from the distributions derived from many random catalogues (as previously described). The general decaying trend for distances larger than 25 km in both the observed and the expected distributions is due to the limited size of the area and its specific aspect ratio. When the expected distribution is subtracted from the observed distribution, a residual distribution is obtained (bottom frame). The edge effect is eliminated from the residual distributions for all practical purposes, and the features seen reflect only patterns in the spatial distribution. Positive values mean excess of number of pairs, negative values mean deficiencies, and 0 values mean no difference from randomness. That is, the residual distribution can be used to quantitatively measure the *degree of spatial non-randomness* over certain distance ranges. For example, the hatched area above the distance range **[a,b]** in this Figure shows the percentage of pairs that is anomalously clustered over this distance range. The square root of this amount transforms the degree of non-randomness in terms of pairs into a degree of non-randomness in terms of events. Details about how the degree of non-randomness is measured can be found in Eneva and Pavlis (1988) and Eneva and Hamburger (1989). The dashed lines are tolerance limits which cover with 95% confidence 90% of the frequencies from the random trials. These can be used as a conservative measure of significance. 50 randomly generated catalogues are used in our study to obtain each of the expected distributions. Values outside the tolerance limits are definitely significant, but values inside them cannot be attributed to randomness; it rather remains unknown whether the deviations from the 0-line are random or non-random fluctuations. In the case of the CSZ, this approach readily provides a measure of relative clustering over distances smaller than 29 km (i.e., **a**=0 km and **b**=29 km), since an excess of pairs is observed over this distance range. The spatial non-randomness in the CSZ represents basically clustering, as opposed to other seismically active areas, such as central California, where long-distance anomalies were also observed (Eneva and Pavlis, 1988, 1991). On the other hand, similar to the CSZ, mostly short-distance anomalies (clustering) were observed in other non-strike slip areas, such as Coalinga in central California (Eneva and Pavlis, 1991), and Tadjikistan (CIS) in central Asia (Eneva et al, 1992c). In the particular case of the CSZ, the square root of the percentage of pairs with distances smaller than 29 km represents the percentage of events involved in the clustering over this distance range. The example in Figure 4.3.1 indicates that about 40% of the events are involved in anomalous non-random pattern (clustering) at distances smaller than 29 km, as compared with random distribution of hypocentres within the study volume. It is to be emphasized that the term "clustering" is used only in a relative sense. Excessive number of pairs can be associated with either too many pairs formed by hypocentres occurring spatially close to each other (which coincides with the intuitive perception of clustering) or/and too many pairs formed by hypocentres distant from each other (which increases the relative number of pairs with smaller distances). Although the parameter thus described measures non-randomness in a non-unique way, it provides a convenient and useful characteristic of the overall spatial distribution of earthquakes in a given seismically active volume.

The same principle can be applied to interevent times and products. Figure 4.3.2 shows examples of observed, expected and residual distributions for the time intervals. Figure 4.3.3

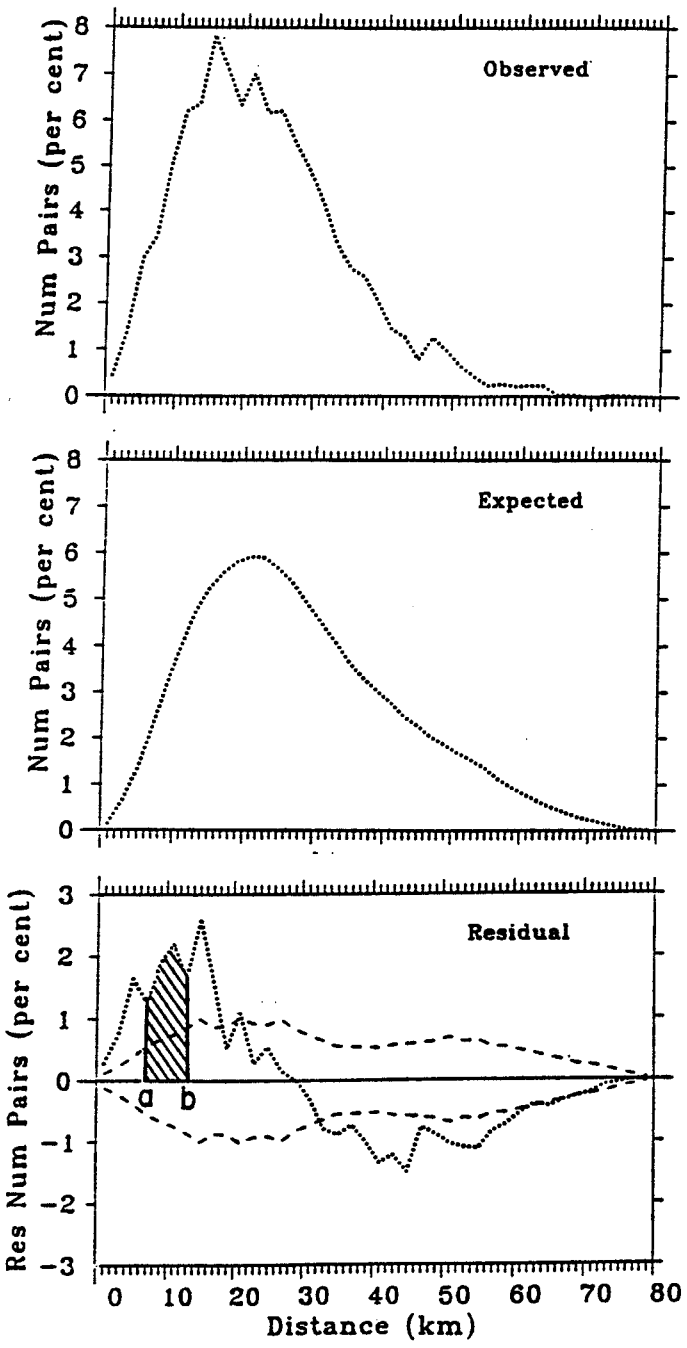

Figure 4.3.1 Schematic representation of the pair analysis for interevent distances. Expected frequency distribution of interevent distances (middle frame) is subtracted from the observed distribution (top frame) in order to obtain a residual distribution (bottom frame). Hatched area (bottom frame) under the residual curve over distance range [a,b] is used to measure the degree of spatial non-randomness over this distance range. Dashed lines mark tolerance limits that cover 90% of the frequencies from all random catalogues with confidence of 95%. See text for more detail.

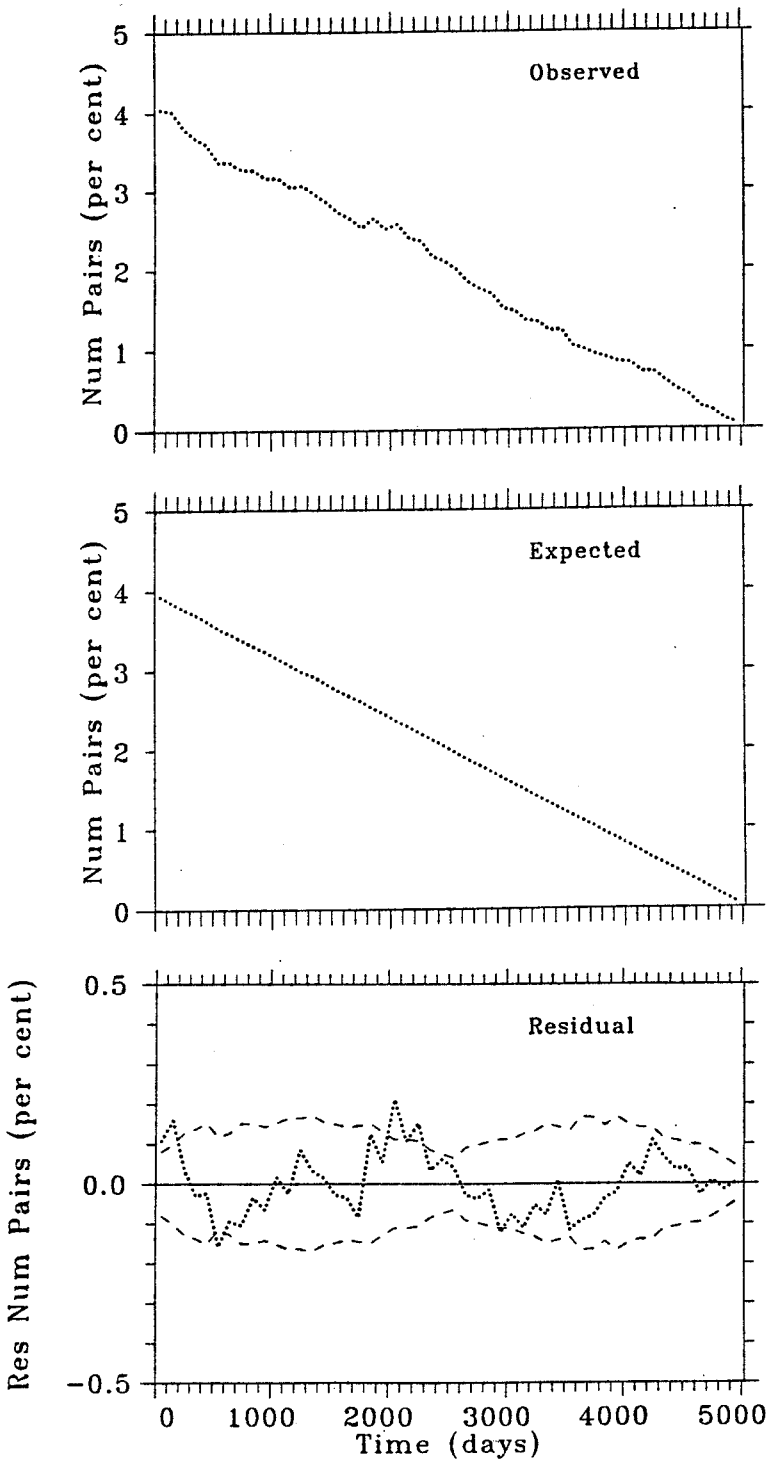

Figure 4.3.2 Pair analysis of interevent times. Notations the same as in Figure 4.3.1.

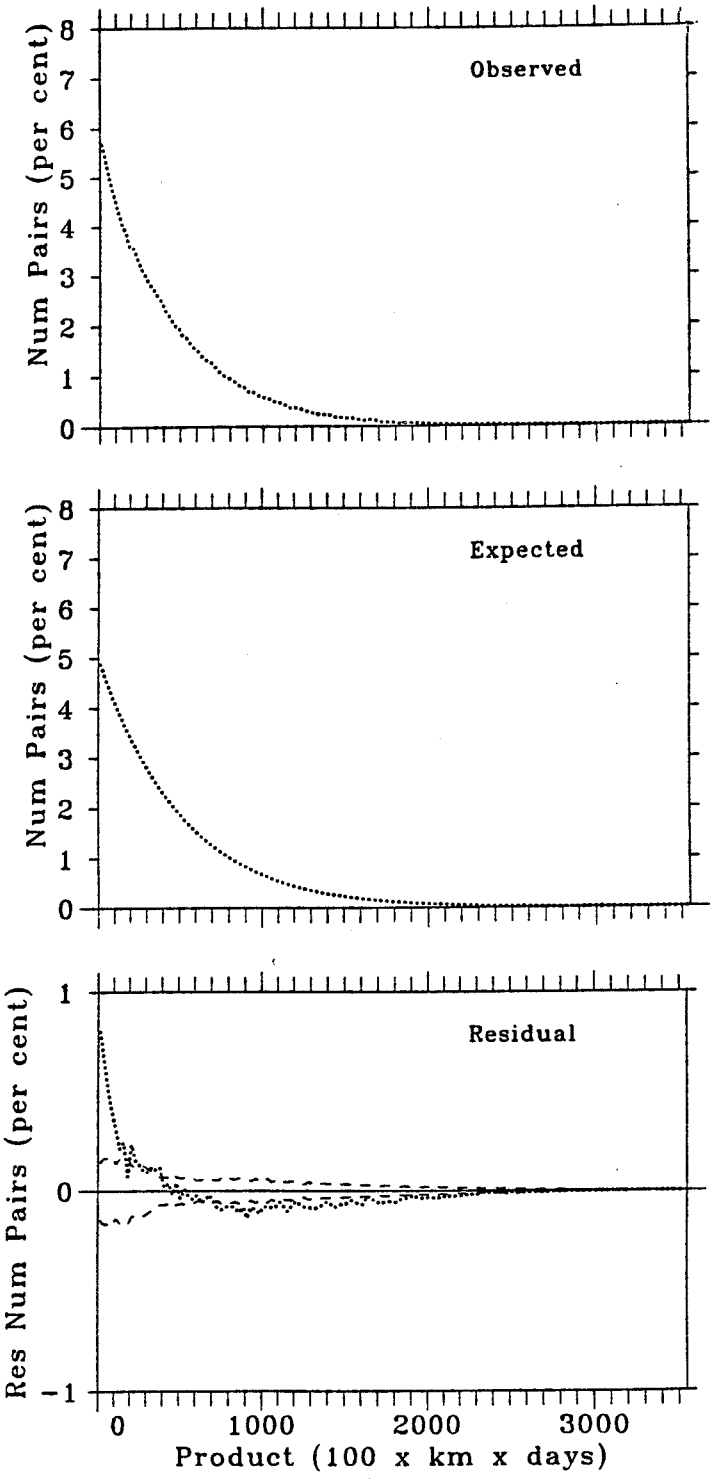

Figure 4.3.3 Pair analysis of interevent products (product equals distance multiplied by time interval). Notations the same as in Figures 4.3.1 and 4.3.2.

shows the same for the distance-time interval products. It is evident that the shapes of the expected distributions for the interevent times and products are different from the shape of the distance expected distribution. The expected distribution for the interevent times has a linear decaying shape, while the one for the products indicates a power type decay.

4.4 Results From "All" Pairs

(A) Interevent distances. The residual spatial distributions for each of the 27 groups (100 events per group, 4950 pairs) are shown in Figure 4.4.1, as well as the residual curve for the whole study period (623 events, 193753 pairs). The step of pair counting is 1 km, which is comparable with the relative location error for the CSZ catalogue. Since the maximum interevent distance is determined by the maximum size of the study volume (about 80 km for the CSZ), each residual curve is formed by about 80 points. The group residual curves are predictably less smooth than the overall residual distribution. The tolerance band for the groups are wider than the one for the whole period, due to the smaller number of pairs for the groups. It appears that the anomaly over distances < 29 km varies from group to group, as seen from the varying size of area between the residual curves and the 0-line (our measurement for degree of spatial non-randomness). The shape of this anomaly appears to vary in time as well; some of the residual curves indicate more or less clear splitting of the anomaly into two peaks (e.g., groups 4, 5, 6, 13), while others are more readily perceived as unimodal (e.g., groups 25 and 26). Shape variations are not examined here, but the temporal variations in the overall degree of non-randomness are closely studied.

Figure 4.4.2 represents the variations of the degree of spatial non-randomness over distances <29 km as measured from the residual curves of each of the 27 groups. The horizontal axis shows the time in years, the vertical axis shows the percentage of events associated with clustering over distances smaller than 29 km. 27 points are shown for the 27 groups. The times at which they are placed coincide with the times of the 50-th event in each group, which are not necessarily in the middle of the respective periods. The 27 horizontal bars in the top part of the figure represent the periods covered by each group. For example, it is seen that the 100 events in the first group occurred within an almost 2 year time interval, starting in the beginning of the study period and ending just before the time of occurrence of the local M5.0 mainshock in August 1979. Because the groups are overlapping by 80 events (out of 100), if certain event falls at the end of a given group, it is present in the next four groups gradually moving towards their beginnings. That is, each event is included in at most five consecutive and overlapping groups. The times of occurrence of $M \geq 4.0$ earthquakes are shown with arrows; the dashed arrow denotes the M6.5 Saguenay earthquake as before. The solid line at about 29% shows the percentage of events that are anomalously clustered in the whole data set (623 $ML \geq 0.5/MN \geq 1.4$ events in the period October 20, 1977 - July 31, 1991). This can be assumed to be the long-term value for the zone, or the baseline value against which the degree of non-randomness at various times is to be compared.

The numbers shown along the curve in Figure 4.4.2 are the sequential numbers of some characteristic groups being representative for specific changes, such as local maxima and minima. Epicentral maps for the same groups are shown in Figure 4.4.3. The epicentral maps are arguably not at all informative in discerning features suggested by Figure 4.4.2.

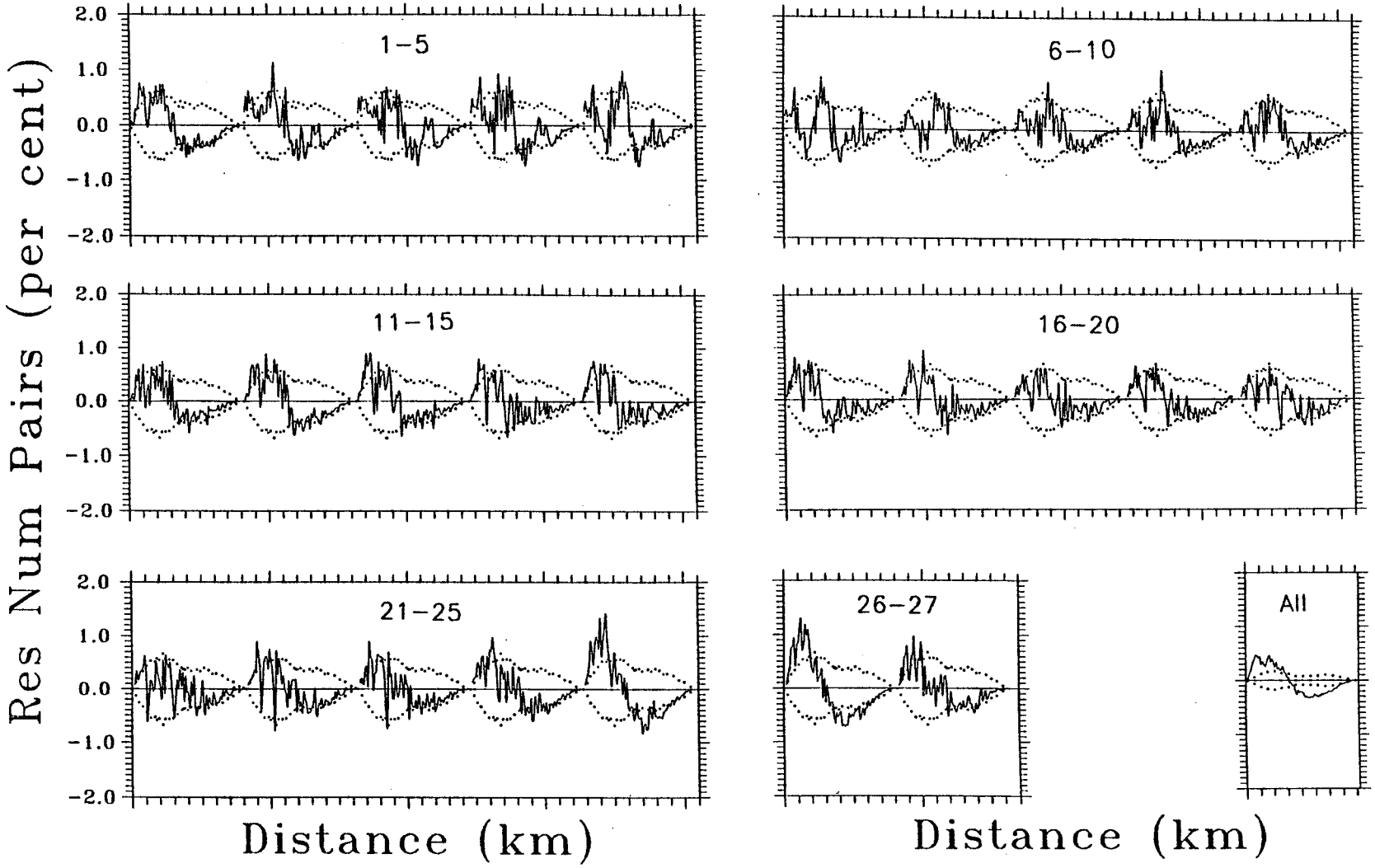

Figure 4.4.1 Group residual distributions of interevent distances for the 27 groups described in the text. Each frame features the residual curves from five groups, except for the frame in the bottom right corner that shows the distribution for the whole catalogue. Group numbers are shown on the top of each frame. Dotted lines mark tolerance limits. Each residual curve covers maximum distance of 80 km . See text for more detail.

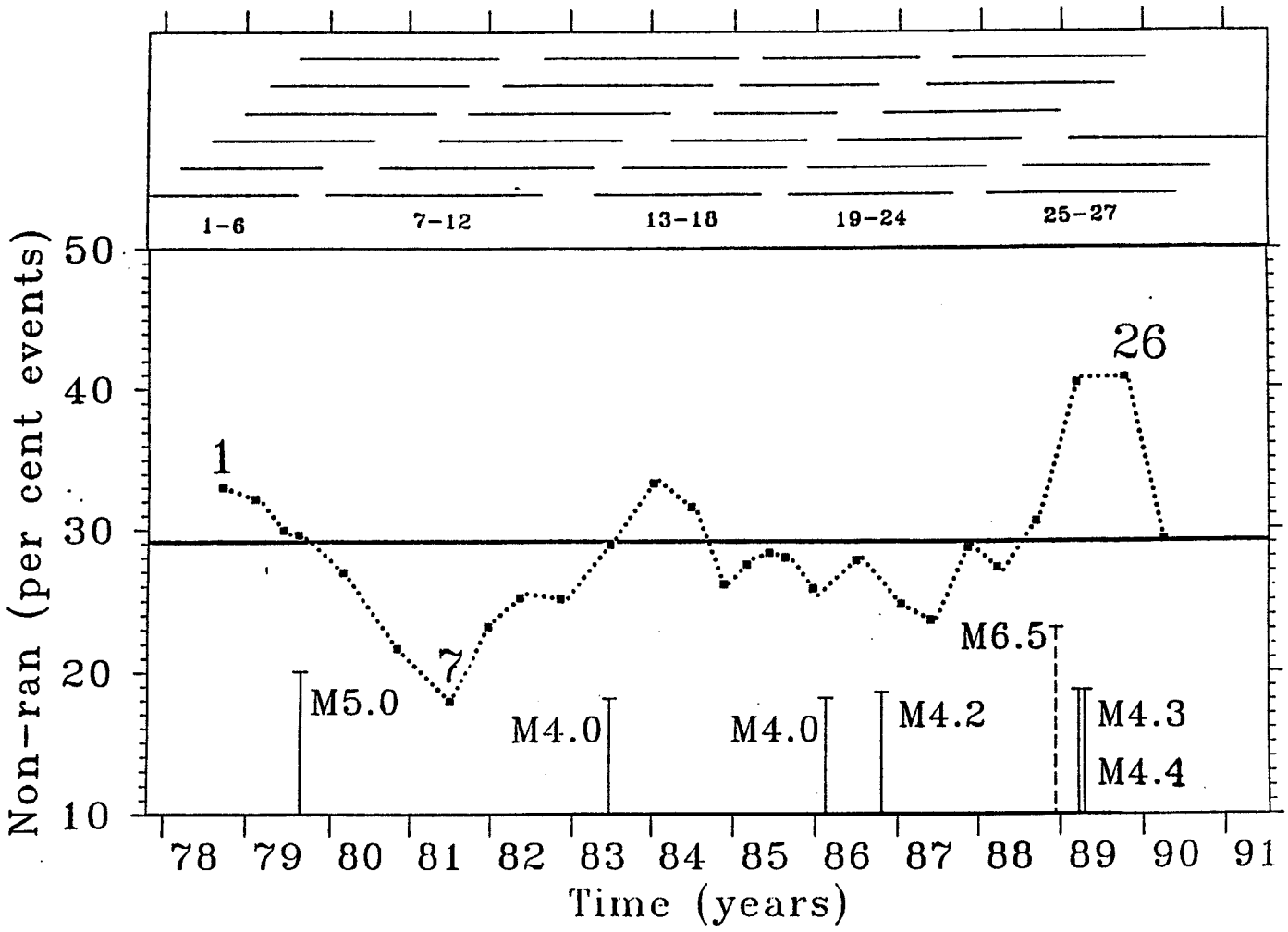

Figure 4.4.2 Temporal variation of the degree of spatial non-randomness in the 0-29 km distance range. Horizontal heavy line at about 29% shows the long-term degree of spatial non-randomness evaluated from the residual curve for all events. Each point represents a measurement of the short-term degree of spatial non-randomness from one of the 27 residual curves shown in Figure 4.4.1. Horizontal bars on the top indicate the lengths of the group periods; the group numbers are shown under these bars. Vertical bars denote the occurrence times of the $M \geq 4.0$ local events; the dashed bar shows the time of the nearby Saguenay event. The lengths of the bars vary according to magnitude as marked. Numbers 1,7, and 26 show characteristic groups; the epicentral maps of the events in these groups are shown in the next figure.

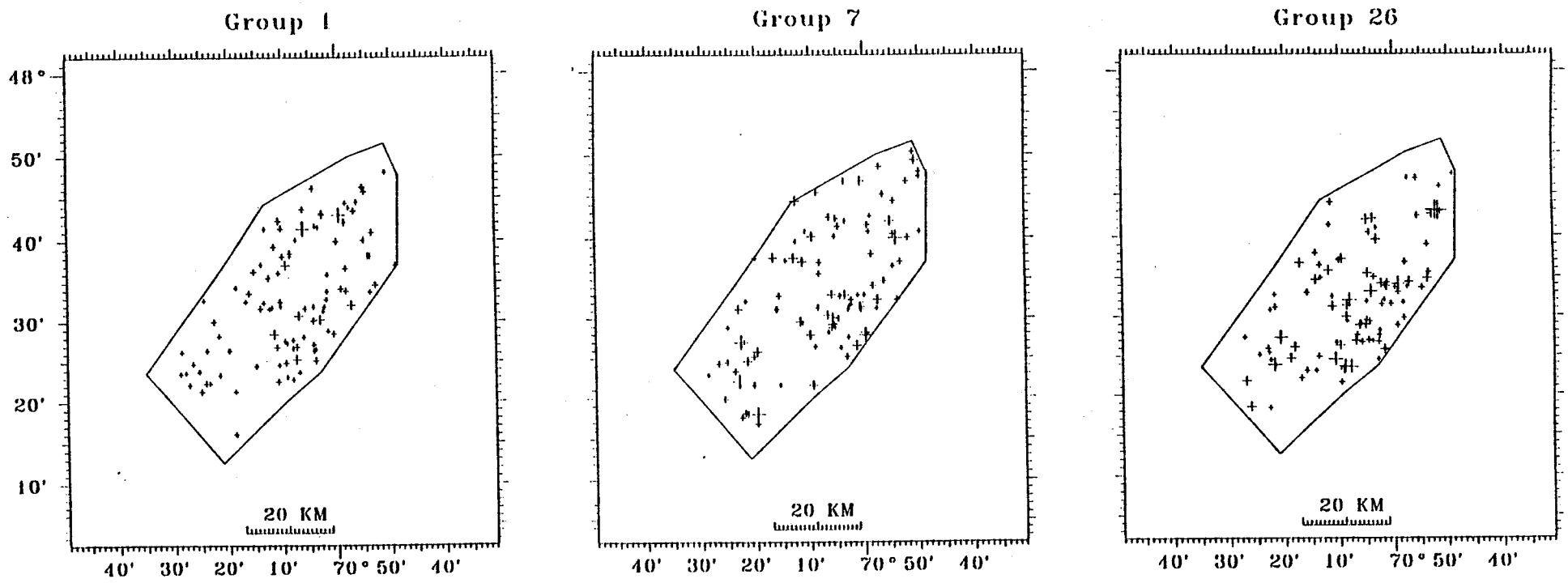

Figure 4.4.3 Epicentral maps of the events from three characteristic groups as marked in the previous figure (Figure 4.4.2). Note that there is little visual difference between these maps.

Three distinct time periods are observed in Figure 4.4.2 when the clustering in the groups is higher than the average. Since the M5.0 event in August 1979 is # 102 in the catalogue, only the first group of 100 events covers a period which precedes the time of mainshock occurrence. The times of the mainshock and its ML$\geq$0.5 (MN$\geq$1.4) aftershocks (their number is only ten) are included in the next five groups, 2-nd to 6-th, and the 7-th group is the first one to cover a period unaffected by the sequence (the 7-th group covers the period from the 121-th to the 220-th event). It is not particularly interesting that the groups from the 2-nd to the 6-th show an elevated clustering, because the aftershocks of the M5.0 mainshock are included in these groups. The first group is the only one for which a relative clustering larger than the average is observed before the mainshock. While the anomaly at this time is not the largest one, this is certainly an important observation given the limitations of the data, i.e., the M5.0 earthquake occurred too early in the catalogue for more extensive observations to be made before its occurrence and the total number of events in the catalogue is quite small. It is noteworthy that changes in spatial patterns prior to large events were observed in other seismically active areas as well, such as central California (Eneva and Pavlis, 1988, 1991) and in central Asia (Eneva et al., 1992c). Of these, two mainshocks in central Asia were preceded by an increasing degree of spatial clustering, a pattern similar to the one before the 1979 M5.0 event in the CSZ. Higher values are also observed here for the groups centred around 1983-1984 and 1989, which do not seem to either precede or follow local larger events. If we assume that the first of these may be somehow related to the 1983 M4.0 event, then it remains unclear why the 1986 M4.0 and M4.2 local earthquakes were not associated with increased values. The 1989 peak is the most prominent of the three local maxima. In order to explain it, we first turn to the M4.3/M4.4 doublet that occurred in March 1989. However, there is no feasible reason that this doublet would cause such a large effect, while the other M $\geq$ 4.0 events do not. Even the larger 1979 M5.0 event that occurred just about 5 km away from the doublet was not associated with such a large increase. It is therefore to be assumed that the reason for these two increases in the degree of spatial non-randomness, if any, may not be local.

In the search for a possible external cause for the anomalies centred around 1983-1984 and 1989 one is led to turn to the most prominent close event, the November 1988 M6.5 Saguenay earthquake. Its time of occurrence can certainly be associated with the anomaly centred around 1989, the largest of the three local maxima. It is to be recalled that this is not an observation of a larger number of events, since each group consists of 100 events, but of a specific spatial redistribution of the earthquakes in the CSZ zone. The largest values, exceeding 40%, are associated with the 25-th and the 26-th groups which cover periods starting before the Saguenay event, but ending well beyond it (the 25-th group covers the period from 10 months before the Saguenay event until 18 months after it; the 26-th group - from 5 months before until 23 months after). That is, the changes in the CSZ can be more readily classified as co-seismic and/or post-seismic to the Saguenay earthquake rather than precursory to it. However, the character of the present type of study makes it difficult to pinpoint the moment when a certain change started. Note that the residual curves for the 25-th and 26-th groups in Figure 4.4.1 distinctly indicate that the anomalies are the largest at this time. Figure 4.4.2, however, gives a better idea about the variations in time, since the residual curves for other groups are not that obvious.

One way to attempt to explain the highest degree of spatial clustering is to assume a

direct triggering effect from the Saguenay event on the CSZ. The latter is to be understood in terms of microearthquake redistribution in the CSZ, not in terms of occurrence of more events over the whole zone. The histogram in Figure 2.6.2 did not demonstrate any significant change in the activity rates of microearthquakes in the CSZ around the time of the 1988 Saguenay event. When rate changes were considered depending on magnitude (Chapter 3), there was evidence that the rate of small events increased, while the rate of larger events decreased (see 3.5 and Figure 3.5.1 - 135-th month). This change, as discussed in 3.5, is most probably an artificial rather than natural rate change. The observation that the overall seismicity rate did not change (naturally), does not preclude the possibility that the seismicity rates did increase in some subareas and decreased in other subareas of the zone, causing the degree of non-randomness identified by the pair analysis to increase. Splitting the CSZ into smaller subareas and looking for changes in seismicity rates in them is unlikely to be statistically significant. In this respect, the spatial degree of non-randomness provides an opportunity to monitor the spatial distribution of earthquakes in the whole zone without specifying what happened exactly and where. This procedure effectively avoids some of the major shortcomings of seismicity rates.

The epicentre of the Saguenay event was located about 80 km northwest from the boundary of the CSZ. Such a distance does not preclude a possible stress change that expanded as far as the CSZ. For example, Reasenberg and Simpson (1992) reported that the static stress changes after the October 1989 Loma Prieta event in California apparently affected the seismic activity on faults up to 100 km away. Without rejecting entirely this possibility in the case of the CSZ, it does not seem that such a triggering effect is particularly supported by the data. Because of the unusually high content of high frequencies, the magnitude of the Saguenay event measured from the Lg waves is quite high (6.5), while the magnitude more appropriate for estimates of the moment and of the stress changes following the event is around 6.0 (Huddon, 1992). This magnitude is perhaps too low to cause a significant stress change as far as the CSZ. S. Gross (personal communication) evaluated the stress changes from the Saguenay event on the territory of the CSZ and found that they hardly exceeded 0.1 mbar (Figure 4.4.4). This estimate is about a thousand times smaller than the one reported by Reasenberg and Simpson (1992) to have caused changes in seismicity rates in California.

Another explanation is also plausible. It may be that the source area of the Saguenay event and the changing pattern of microseismicity in the CSZ are not causally related, but are instead independent responses to a large-scale regional stress factor. In support of this hypothesis, a four-month period after the Saguenay earthquake was apparently characterized by a dramatic increase of the number of larger events ($M \geq 4.0$) in the whole region of eastern Canada (Wetmiller and Adams, 1991). The local M4.3/M4.4 doublet in the CSZ occurred in this period. It has not been studied how the microactivity in other seismically active areas in eastern Canada behaved around this time; so it is not known whether a similar tendency for greater degree of non-randomness (relative clustering) might have been present elsewhere. It would be necessary to study the microseismicity at least in the Western Quebec zone to search for changes in microseismicity distribution and their possible association in time with the same four-month period.

The latter explanation fits better the anomaly centred around 1983-1984. Note that the local maximum is observed for the 12-th group; the events in these group occurred between the second half of 1982 and the end of 1984. The 13-th group was also characterized by an elevated

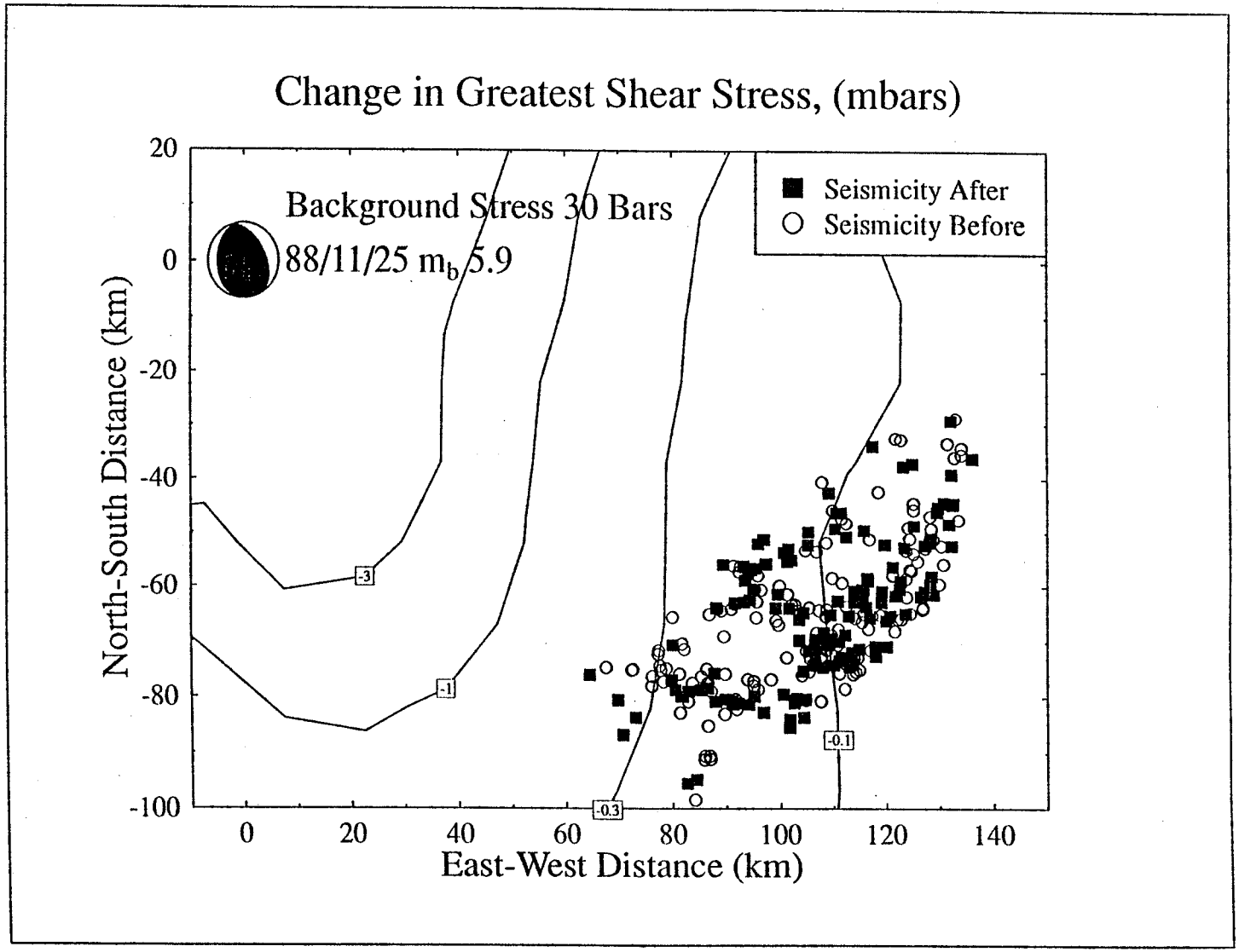

Figure 4.4.4 Stress changes produced by the 1988 Saguenay event. Numbers in boxes show shear stress changes in mbars. Note that isolines crossing the CSZ indicate stress changes of only -0.1 and -0.3 mbars. Figure provided by S. Gross (personal communication).

value; this group extends into 1985. There are no local or close large events to have occurred at this time. However, looking at larger distances (Adams and Basham, 1989), it is evident that a fairly unusual seismic activity took place in the Northern Appalachians (200-250 km east-southeast from the CSZ). In January 1982 the Miramichi sequence in New Brunswick started of magnitudes up to 5.7 (Wetmiller et al., 1984). Aftershocks of magnitudes up to 4.1 were observed until 1988. There were other events, like the 1982 M4.7 Throusers Lake event and a swarm of six M3.0 earthquakes in 1983-1984 in the Passamaquoddy Bay (about 350 km southeast-south from the CSZ). More moderate events also occurred in 1982 and 1983 in the Western Quebec zone and its extension into the Adirondacks, New York state (more than 300 km southwest from the CSZ): the M4.3 Timiskaming earthquake, the M4.1 North Gower event, and the M5.2 Goodnow event. The distances between the CSZ and all these areas are obviously too large to assume a possible triggering effect. However, if all these earthquakes reflect the effect of a large-scale stress factor, the question of distance is less relevant.

In the light of the above, the hypothesis for a large-scale tectonic factor affecting a number of seismically active areas in a given region, seem to be a likely explanation for the relatively high degrees of spatial non-randomness at some times. Yet, such a suggestion is at its arm-waving stage at this time. It may be that the microseismic activity in a given area becomes increasingly sensitive to outside influences during the preparation stage of a local large earthquake. That is, the same area may respond differently to large-scale tectonic factors at different times, according to how close it is to its next large local event. Most authors have been reluctant to assume that signs of preparation processes may be observed as a result of the influence of factors outside the future source area(e.g., Wyss, 1991). A few, however, have discussed such possibilities (e.g., Reyner, 1981; Ishibashi, 1988). Regardless of the speculative nature of such arguments, it appears increasingly important to monitor the temporal changes in microseismic activity in as many ways as possible. The spatial degree of non-randomness seems to be very promising in this respect. While it is also possible that no connection exists between these relatively high values and the state of the local and surrounding stress, it seems reasonable to monitor the spatial degree of non-randomness and watch for high values, since these may be associated with future local large events.

Periods of degree of spatial non-randomness, lower than the long-term baseline value, are also observed in Figure 4.4.2. Local minima were reached twice. First, this happened after the M5.0 mainshock (7-th group), which is consistent with previous observations in other seismically active areas in the world (central California and Soviet Central Asia, see Eneva and Pavlis (1991), Eneva et al. (1992c)). The 7-th group of events is beyond the end of the M5.0 sequence (it covers the period of the 121-th to the 220-th event). The second lowest value, is indicated by the 21-st group. This is the last group that contains only events preceding the time of the 1988 Saguenay earthquake. The five groups afterwards all cover periods which include the date of this event. Note, that the last group (the 27-th), is the first group following the Saguenay event and not including its date. A sharp decrease is observed, as if either the influence of the Saguenay event, or of the possible large-scale tectonic factor, has already ceased.

It is important to emphasize that neither the epicentral maps in Figure 4.4.3, nor even the residual distributions in Figure 4.4.1 convey as easily the temporal variations in the degree of spatial non-randomness, as Figure 4.4.2 does. The maps are particularly useless in this respect; it is evident that visual perception of seismic activity cannot provide the type of insight that the

quantitative approach can.

There have been reports of changes in spatial pattern before large events elsewhere (Ouchi and Uekawa, 1986; Hirata, 1989; Wirdlaw et al., 1991). These reports were based on techniques different from pair analysis. Yet, distances between events were used in one way or another in some of these techniques as well.

The following figures are intended to demonstrate the significance of the results suggested by Figure 4.4.2 and their stability with the variation of some parameters. Figure 4.4.5, for example, shows the original curve from Figure 4.4.2 (filled squares, dotted line) together with another curve (open squares, solid line). The residual distributions used for the former curve were obtained with a counting step of 1 km. The residual distributions for the latter curve were obtained with a larger counting step, 2 km. The effect of using a larger increment in distance is apparently somewhat smoothing, but seems negligible for all groups, except for the ones containing the M5.0 event and its aftershocks.

Figure 4.4.6 presents three curves for different choices of the number of events per group and number of events of overlap between two successive groups. The original choice of 100 events per group and 80 events of overlap used in the previous figures is shown here with the dotted line. The solid line traces the curve from 35 groups, for which the number of events per group was 80 and the number of overlapping events was 65. This curve is predictably less smooth than the original one. The local minima are the largest for this choice of parameters. Finally, the dashed line is obtained from 17 groups, 120 events each, 90 overlapping events. This is the smoothest curve of the three. There are differences between these curves in the details, but the main shape is apparently preserved. We can be quite confident that the same conclusion would follow for any reasonable choice of the number of events per group and the number of overlapping earthquakes.

Figure 4.4.7 illustrates an extremely conservative measure of significance. The original curve from Figure 4.4.2 is shown together with a dashed line obtained from the upper tolerance limit. The same procedure applied to measure the degree of spatial non-randomness over distances < 29 km using the residual curves is now applied to the upper tolerance limit. The dashed line shows the level that can be reached by randomly generated distributions of 100 events per group, in 50 different catalogues per group, in the extreme case. The anomaly for the 25-th and 26-th groups still stands out. The significance of the other ones, however, is somewhat questionable. I note that the level that covers with 95% confidence 90% of the 50 catalogues generated for 623 events (not 100) is about half that much (17%), which makes the deviation from randomness significant at any time.

The figures above illustrated the variation of the degree of spatial non-randomness over the distance range < 29 km. The same type of estimates can be made for other distance ranges as well. Figure 4.4.8 shows the original spatial non-randomness curve together with a curve (open squares, solid line) representing the variation of the spatial degree of non-randomness over the distance range 1 to 10 km (a=1 km and b=10 km; see Figure 4.3.1). The bold solid line shows the long-term degree of spatial non-randomness for the 0-29 km distance range as before, while the thin horizontal line shows the long-term value for the 1-10 km distance range. The two curves are apparently very close in shape, although the highest degree of spatial clustering over the range 1-10 km is less prominent than in the case of the 0-29 km range. The inset in the upper left of this figure shows the high degree of correlation between the measures in the two different

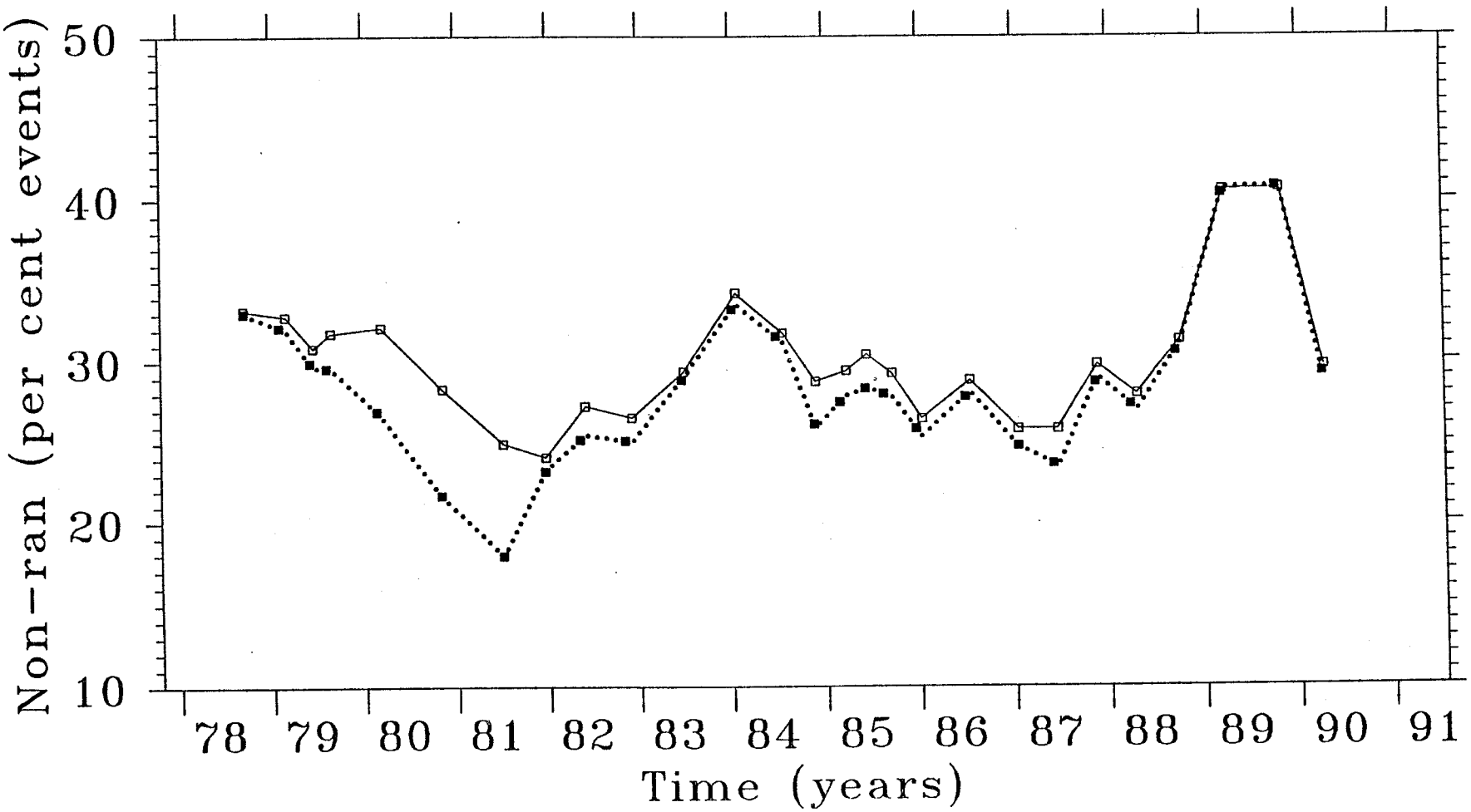

Figure 4.4.5 Temporal variation of the degree of spatial non-randomness in the 0-29 km distance range derived from residual curves obtained with step of counting 1 km (filled squares, dotted line; same as in Figure 4.4.2) and 2 km (open squares, solid line).

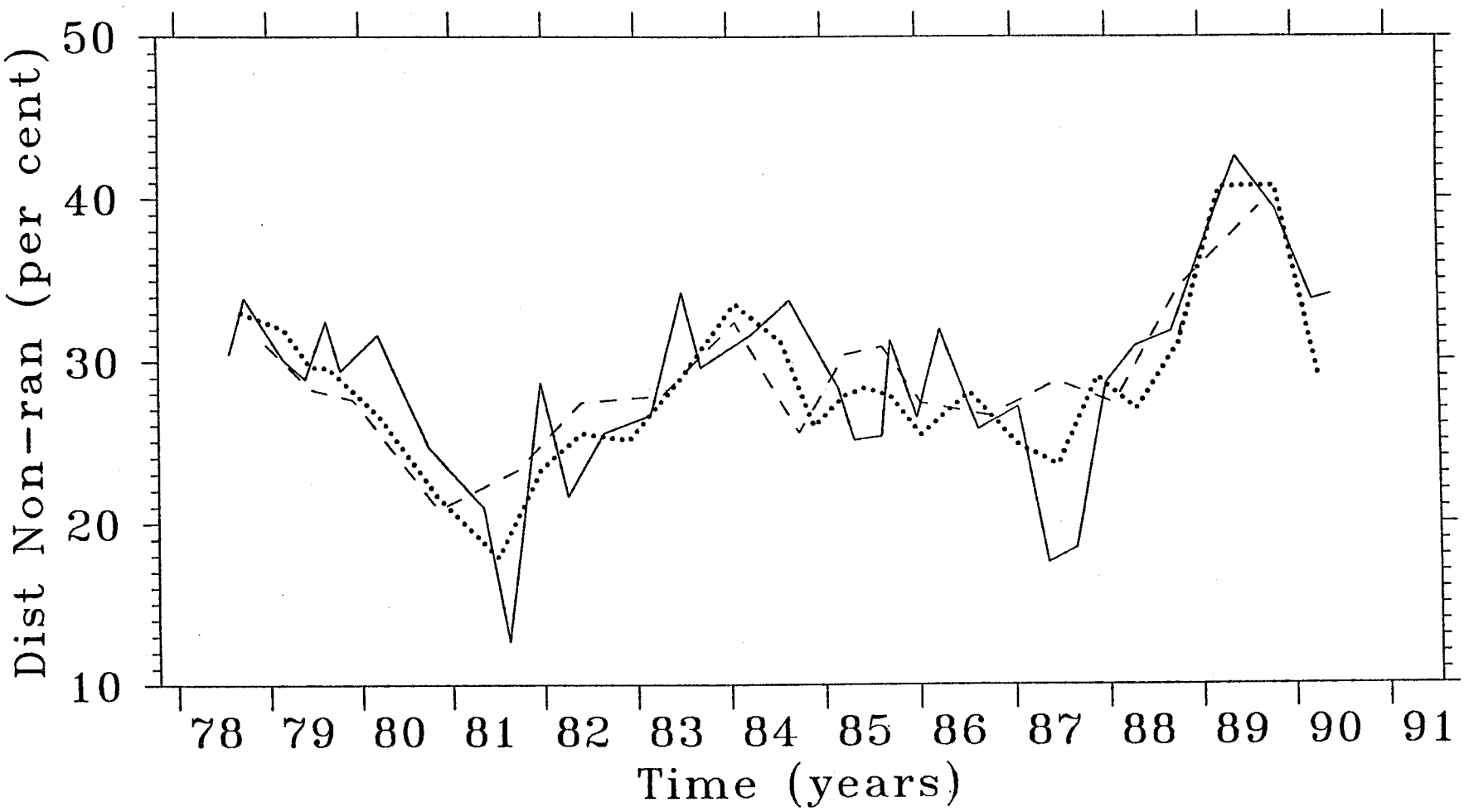

Figure 4.4.6 Temporal variation of the degree of spatial non-randomness in the 0-29 km distance range for different choices of the number of events per group and the number of overlapping events: 100 events per group and 80 overlapping events (dotted line; same as the original choice in Figure 4.4.2); 80 events per group and 65 overlapping events (solid line); and 120 events per group, 90 overlapping events (dashed line).

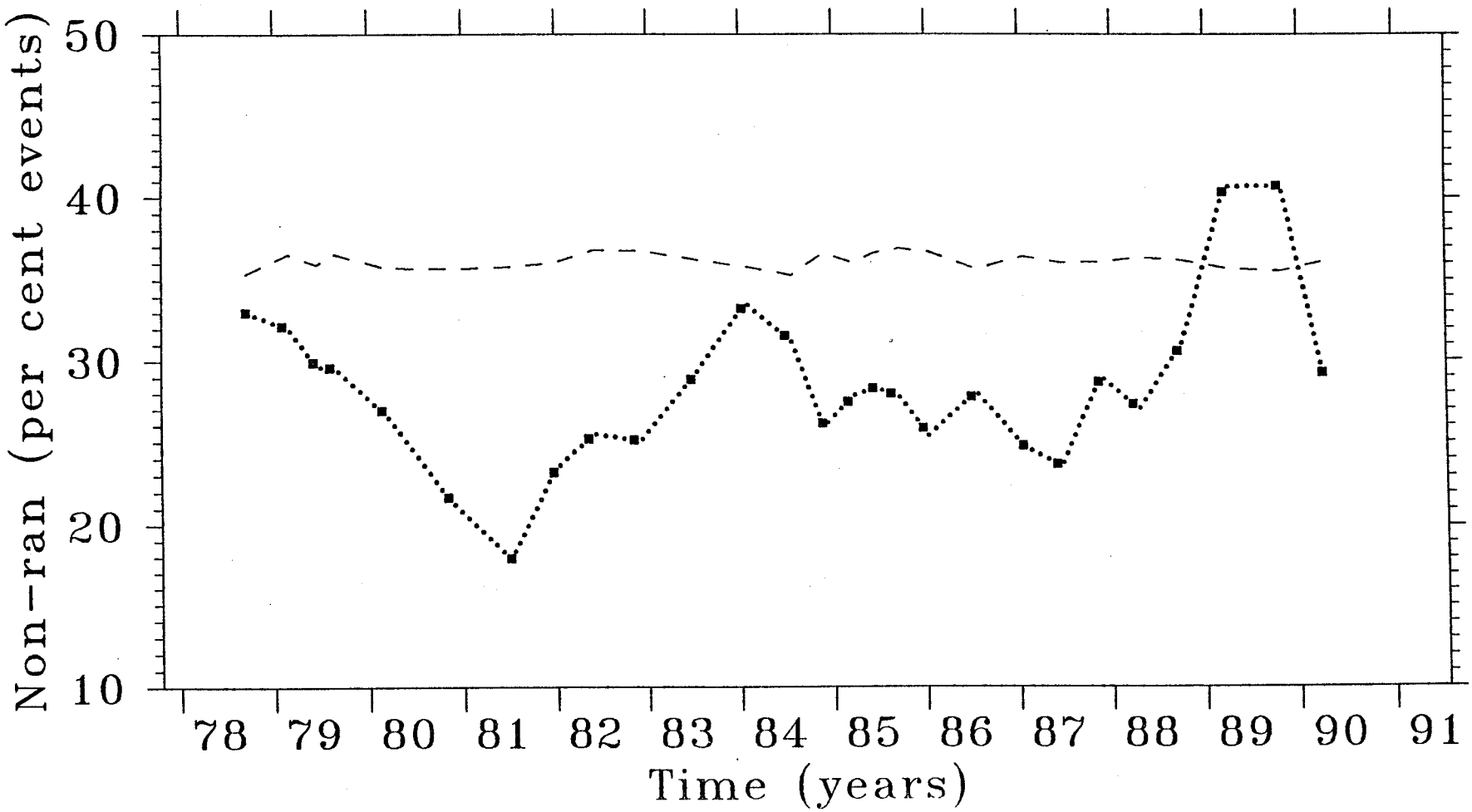

Figure 4.4.7 Temporal variation of the 0-29 km spatial non-randomness (dotted line, same as in Figure 4.4.2) shown together with the temporal variation of the upper tolerance limits (dashed line). See text for more details.

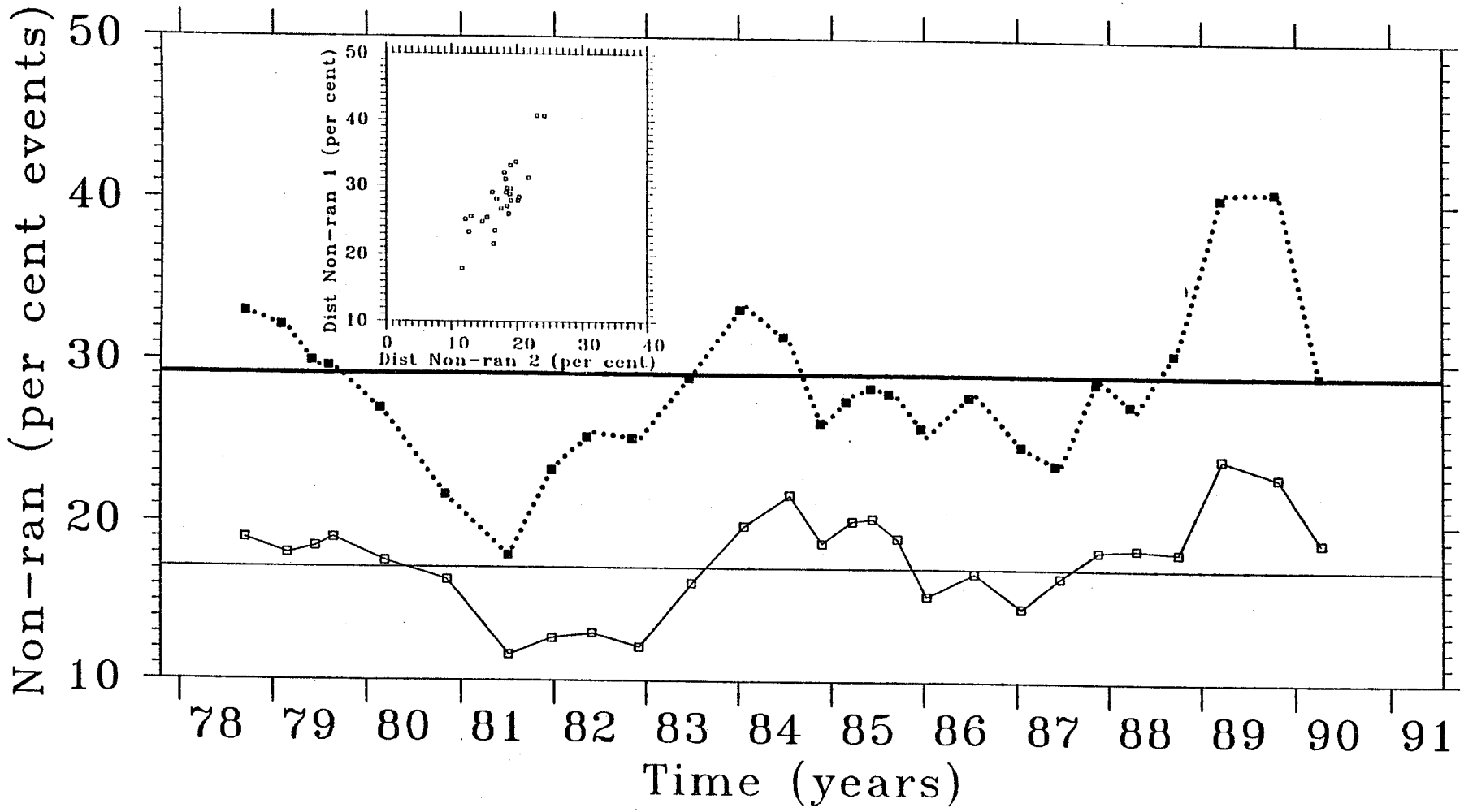

Figure 4.4.8 Temporal variation of the degree of spatial non-randomness in the distance ranges 0-29 km (filled squares, dotted line; same as in Figure 4.4.2) and 1-10 km (open squares, solid line). Bold horizontal line at about 29% shows long-term degree of spatial non-randomness in the distance range 0-29 km (same as in Figure 4.4.2). Thin horizontal line at about 17% shows the same for the 1-10 km distance range. Inset in upper left shows a scatter plot of the 0-29 km spatial non-randomness (marked with number 1) versus the 1-10 km spatial non-randomness (marked with number 2).

ranges. This correlation is not at all surprising, but it is not necessarily expected either; the 1-10 km distance range is just 1/3 of the 0-29 km range and had the other 2/3 behaved differently, such high correlation would not be observed. The next two figures are similar to Figures 4.4.6 and 4.4.7 above, but applied to the 1-10 km distance range. Figure 4.4.9 shows three different curves for the same choices of number of events per groups and number of events of overlap as above. The comparative characteristics are similar to the ones for the 0-29 km distance range; the general shape of the curves is the same, although the details are somewhat different. The variation curve for the 1-10 km distance range and the level that covers with 95% confidence 90% of the estimates from 50 catalogues for each group (dashed line) are shown in Figure 4.4.10. All three periods of higher degree of spatial clustering appear to be significantly above this level.

Figure 4.4.11 shows the original curves in the two distance ranges examined against the curves obtained after the removal of the aftershocks of the M5.0 event. Only 10 aftershocks of ML$\geq$0.5 (MN$\geq$1.4) seem to have occurred over the first eight days after the mainshock. These aftershocks outline quite small volume, with a vertical size exceeding its horizontal size several times; the maximum epicentral distance between an aftershock and the mainshock was 1.8 km with its respective hypocentral distance = 6.6 km. There are later events that might have been aftershocks too, occurring in (or close to) the initial aftershock volume 3 months, 4 1/3 months, 1 year, and 1 year 1/3 months after the mainshock. Since these cannot be considered as aftershocks with high confidence, only the 10 aftershocks from the first 8 days after the main event were removed. This reduced the original data set to 613 events. In order to examine groups as similar as possible to the original 27 groups, 93 events per group were considered with 73 events for the overlap. The curves for the whole data set and for the one with the ten aftershocks removed are not significantly different. In fact, the aftershock removal is important only in groups 2-nd to 6-th; the slight differences between the two curves for later groups are simply due to the difference in the events involved. Aftershocks apparently did not play any significant role in forming these curves. This lack of significant difference should not be attributed to the apparently small number of aftershocks removed; 10 aftershocks made 10% of the 100 events in the groups that originally included them. In terms of pairs, their contribution was 19.1% of all the 4950 original pairs per group (100 events make 100x99/2 = 4950 pairs). It will be shown below that the removal of the same aftershocks made much more difference in the next application (correlation dimensions; Chapter 5).

Finally, the two frames in Figure 4.4.12 show scatter plots of the degree of spatial non-randomness versus the length of the group period for the 0-29 km and 1-10 km distance ranges. In both cases, a tendency for lower degree of spatial non-randomness is observed for longer group periods, that is, for lower rates of seismic activity (since it takes longer for 100 events to occur). This appears to indicate that when events occur more frequently, they are more likely to be relatively more clustered in space; an observation that is in good agreement with what might be intuitively expected. This tendency is somewhat more clearly indicated for the smaller distance range (1-10 km).

B. Interevent Times. The same type of analysis was performed with the interevent times. The results do not seem to be very useful at this stage of study. Figure 4.4.13 shows the residual distributions for the same 27 groups. The step of counting is 30 days. Unlike the distance residual curves that covered always the same maximum distance, the time residual curves are

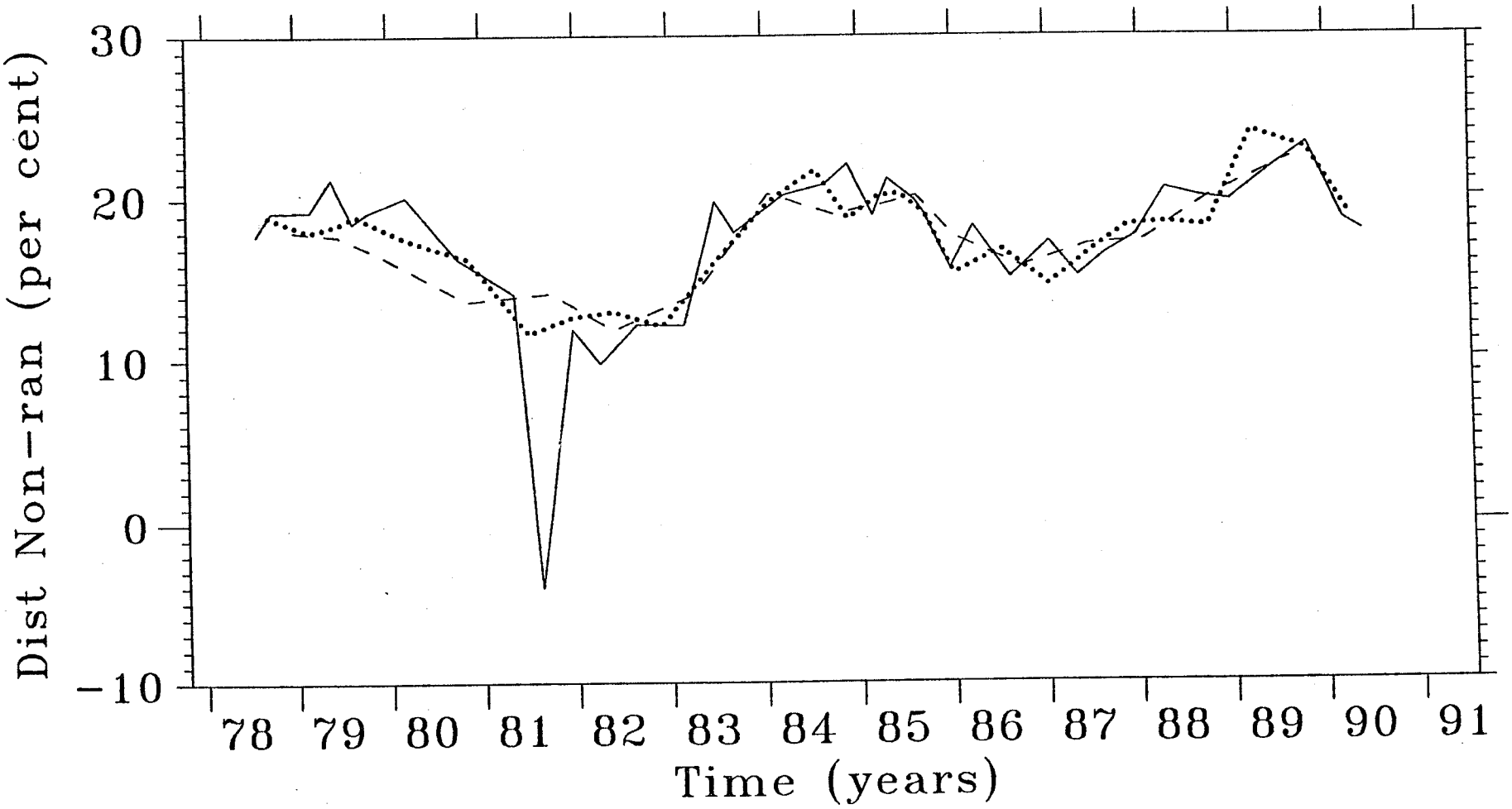

Figure 4.4.9 Temporal variation of the degree of spatial non-randomness in the 1-10 km distance range for different choices of the number of events per group and the number of overlapping events. Notations are same as in Figure 4.4.6.

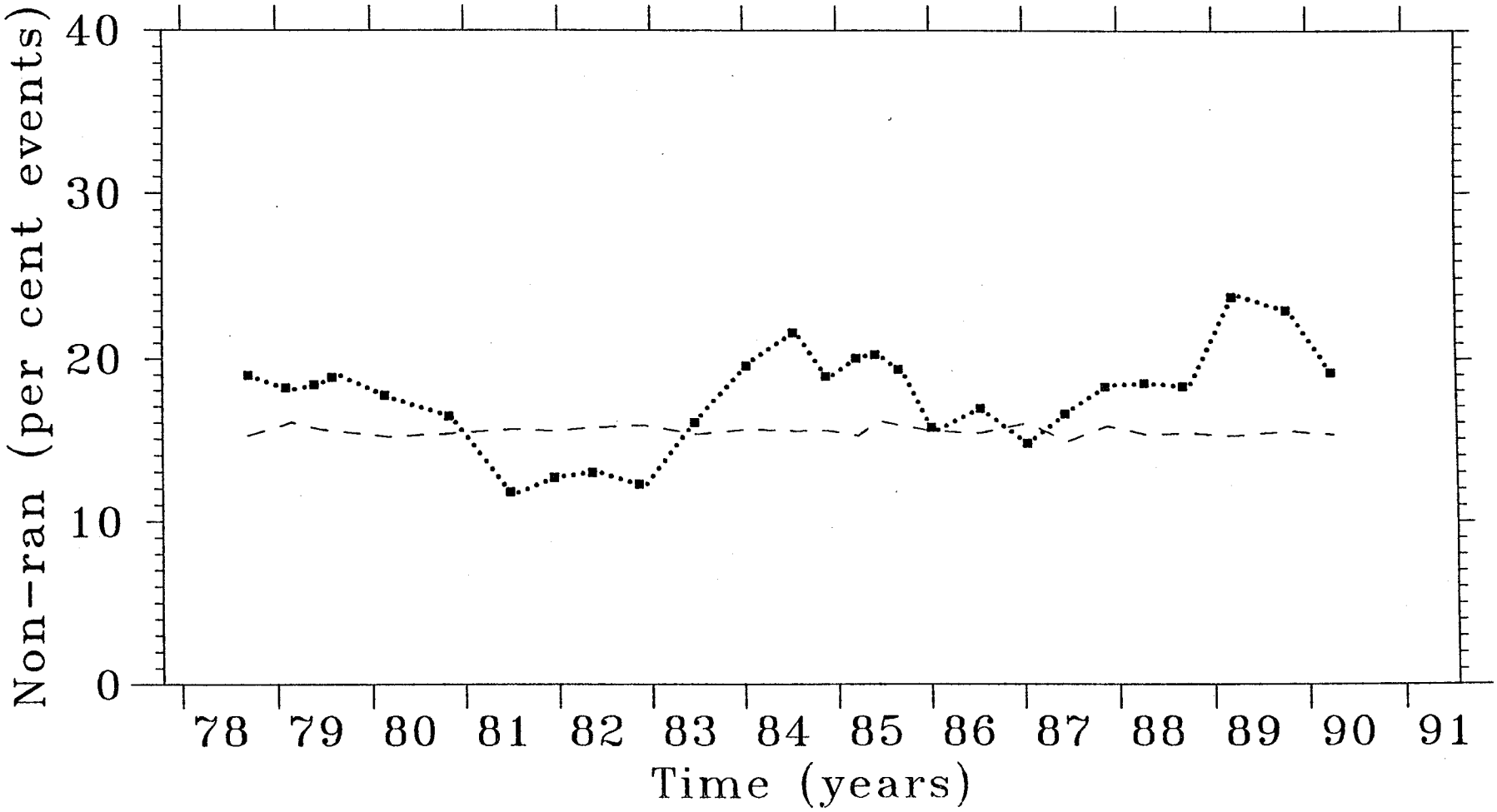

Figure 4.4.10 Temporal variation of the degree of spatial non-randomness in the distance range 1-10 km shown together with the upper tolerance limits (similar to Figure 4.4.7).

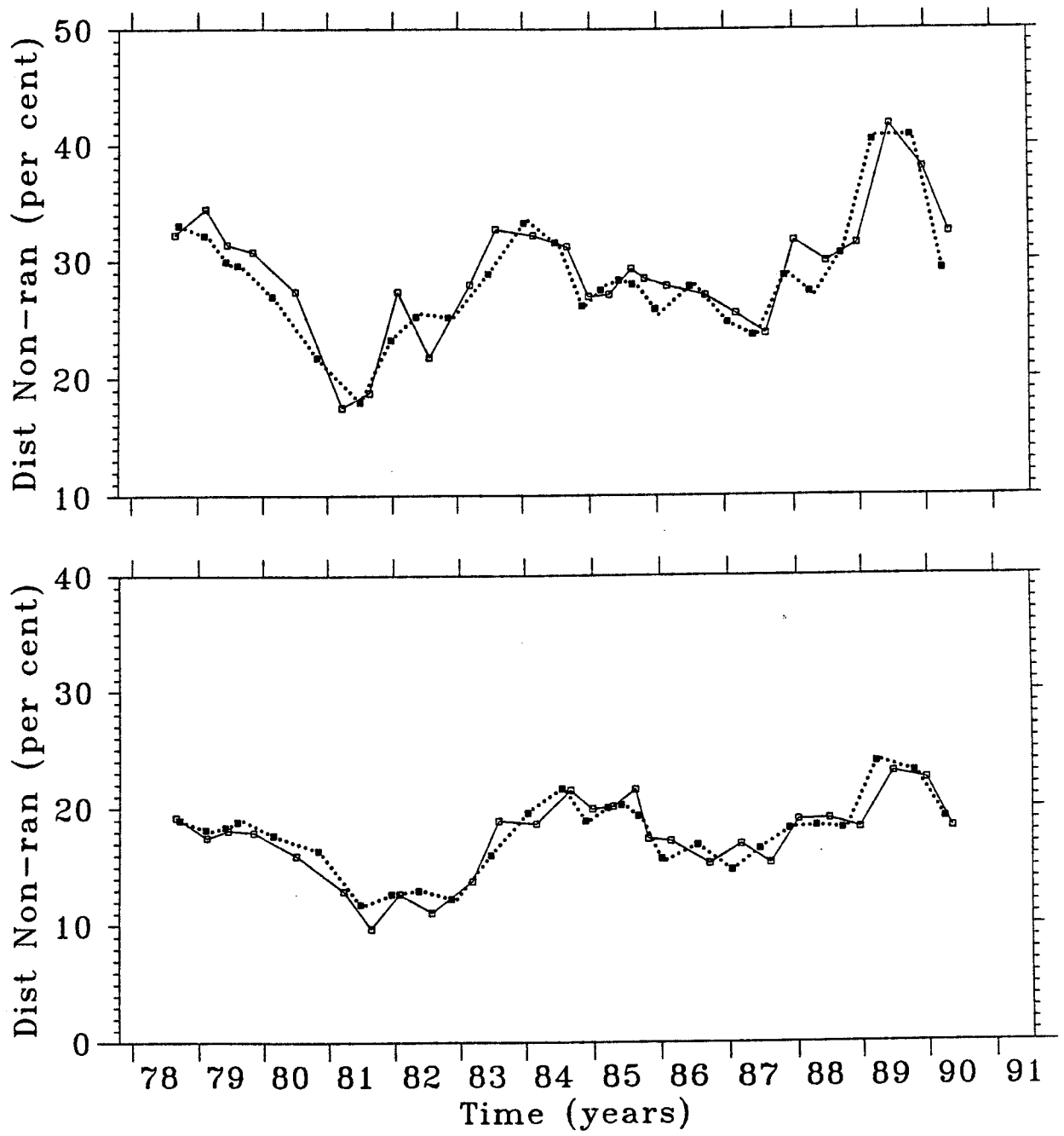

Figure 4.4.11 Temporal variation of spatial non-randomness from all events (filled squares, dotted lines) and with aftershocks removed (open squares, solid lines). The distance range 0-29 km is featured in the top frame and the 1-10 km distance range - in the bottom frame.

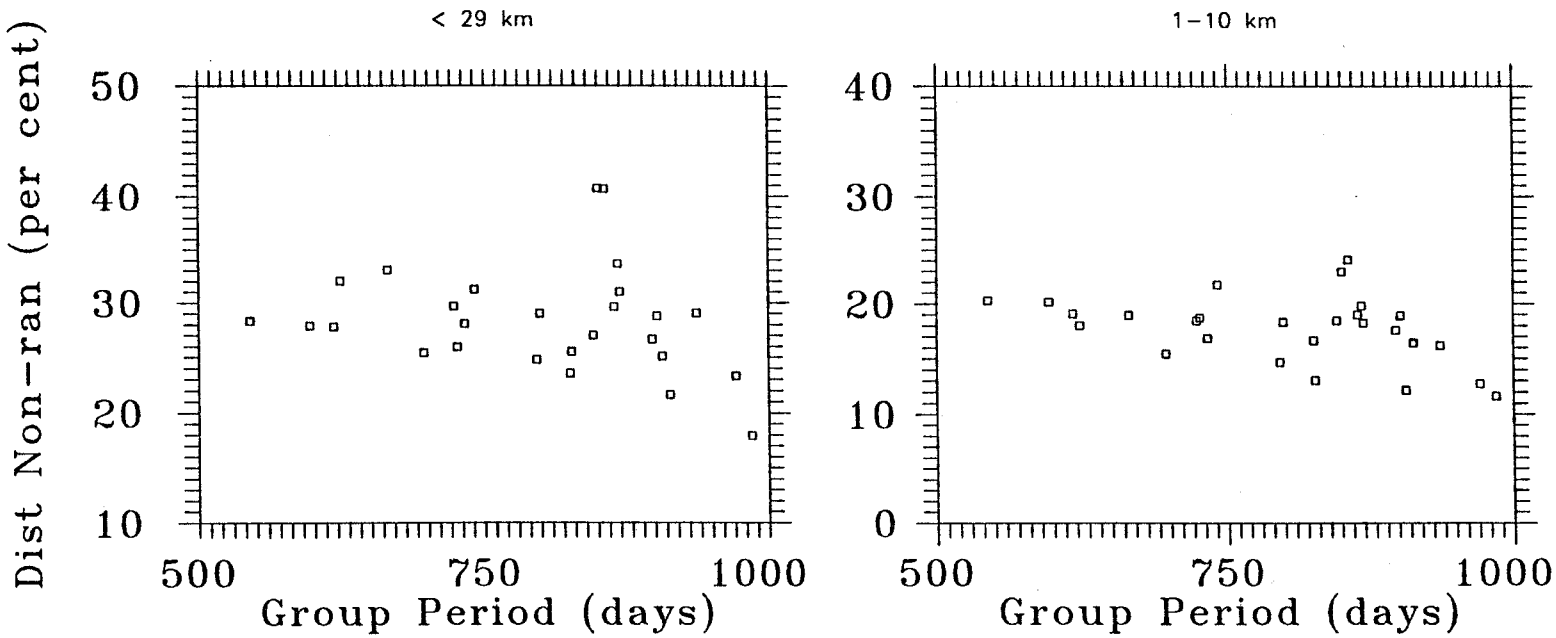

Figure 4.4.12 Scatter plots of the degree of spatial non-randomness versus length of group period. Left frame shows the 0-29 km distance range and right frame shows the 1-10 km distance range.

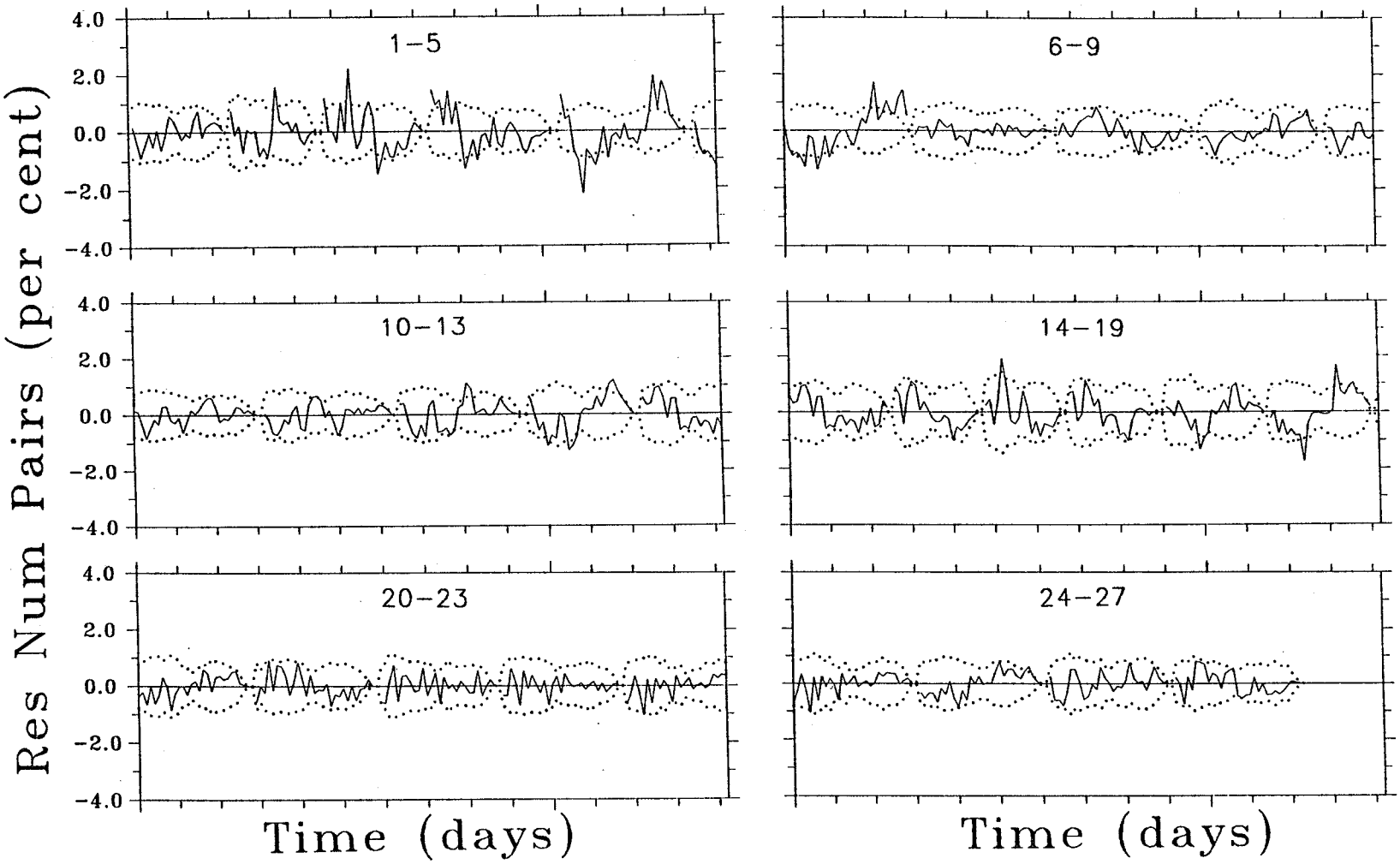

Figure 4.4.13 Group residual curves for the time intervals. Group numbers are shown on the top of each frame. Unlike the spatial residual curves in Figure 4.4.1, time residual curves span different maximum interevent times due to the different length of group periods; from 544 days (the shortest group period) to 985 (the longest group period). Notations are the same as in Figure 4.4.1.

characterized by different maximum time intervals. This is due to the fact that the groups span different time periods, from 544 to 985 days. For the individual lengths of the 27 time periods refer to the Table in 4.1 and to the horizontal bars in the upper part of Figure 4.4.2. Figure 4.4.14 shows two long-term residual curves for the whole period, estimated with counting step 30 days and 100 days, respectively. None of these figures is particularly enlightening. For example, it is seen from Figure 4.4.13 that with the exception of the groups including the aftershocks of the M5.0 event in 1979 (groups 2 to 6), the residual curves stay essentially within the tolerance limits. They are fluctuating so much around the 0-line that it is very difficult to pinpoint a time range over which it would be reasonable to evaluate the temporal degree of non-randomness. The plots with the long-term residual curves (Figure 4.4.14) do not suggest obvious significant features either. Both long-term residual curves slightly suggest a period of about 2000 days or more, but it is impossible to draw meaningful conclusions in this respect.

An intuitively interesting time range over which the degree of temporal non-randomness can be evaluated is the one that includes events closer in time, although the appearance of the group residual curves is particularly discouraging. Figure 4.4.15 shows a variation curve featuring the degree of temporal non-randomness versus time. The time range over which the values along the vertical axis were estimated is < 90 days. It is obvious that the long-term value, at less than 4%, is quite low. The fluctuations of the degree of temporal non-randomness are larger than for the spatial non-randomness; Figure 4.4.16, however, confirms the above considerations about the significance of these fluctuations and demonstrates that it is highly questionable. The dashed lines in this Figure indicate the tolerance bands for time range < 90 days. Since these represent a very conservative evaluation of significance, it may be still instructional to note what this curve indicates. Its characteristics are very much in counter-phase with the spatial non-randomness, suggesting a relative lack of pairs with interevent times < 90 days before the M5.0 event and around the time of the Saguenay event. The high values for the 2-nd to the 5-th groups, are not particularly interesting, since they belong to the groups containing the aftershocks of the M5.0 mainshock.

In a further search for useful (although arguably marginal) meaning of these results, Figure 4.4.17 shows scatter plots of the degree of spatial non-randomness in the 0-29 km (top left) and the 1-10 km (top right) distance ranges versus the temporal non-randomness in the 0-90 days range. The bottom frame of this Figure shows a scatter plot of the degree of temporal non-randomness versus the length of group period. None of these plots, however, show any signs of meaningful correlations. This is not surprising in view of the general insignificance of the pair analysis results in respect to interevent times. Yet, it is somewhat surprising that spatial non-randomness seems to be negatively correlated with group period, while the temporal non-randomness which should be naturally much more relevant in this respect, does not show any such tendency. I note, however, that a time lag between 1.5 and 2 years between the variation curves for spatial (see, for example, Figure 4.4.2) and temporal (Figure 4.4.16) non-randomness results in an apparent negative correlation between these two quantities. As it was previously mentioned, the respective time series are too short to be meaningfully examined in this respect and no figures to support such correlation are shown. It would be useful to examine the data for such cross-correlations in other areas, for which longer time series can be adopted. In general, given that larger degrees of spatial clustering are observed for smaller group periods (more frequent events), one could expect positive correlation between spatial and temporal non-

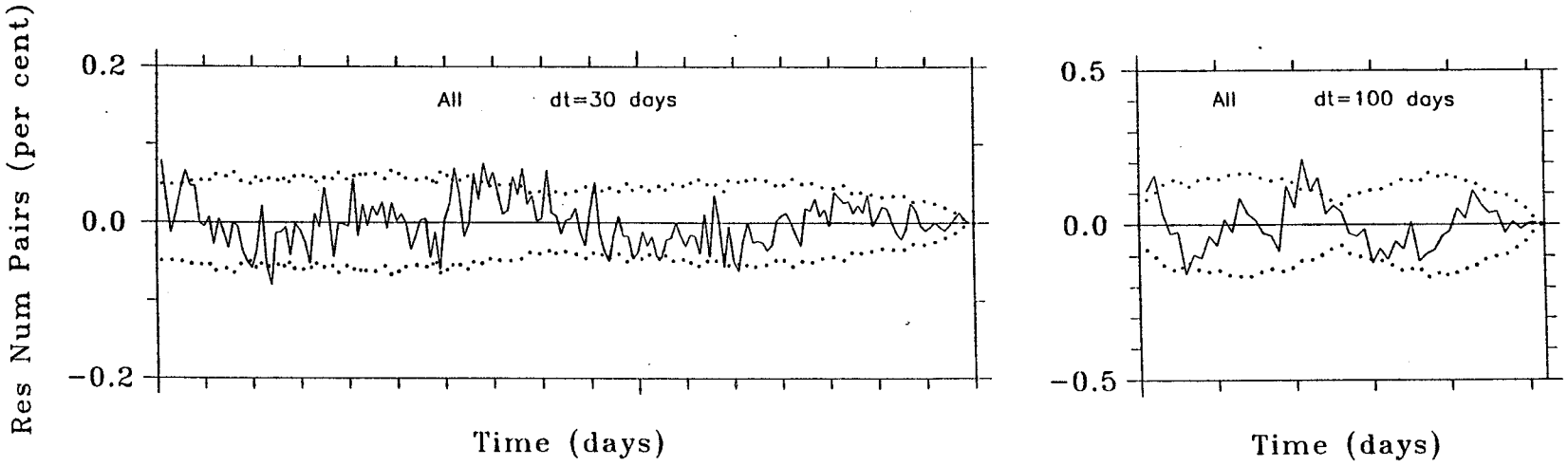

Figure 4.4.14 Long-term residual curves obtained from the whole period with steps of counting 30 days (left frame) and 100 days (right frame). Maximum interevent time is 5100 days. Dotted lines show tolerance limits as before.

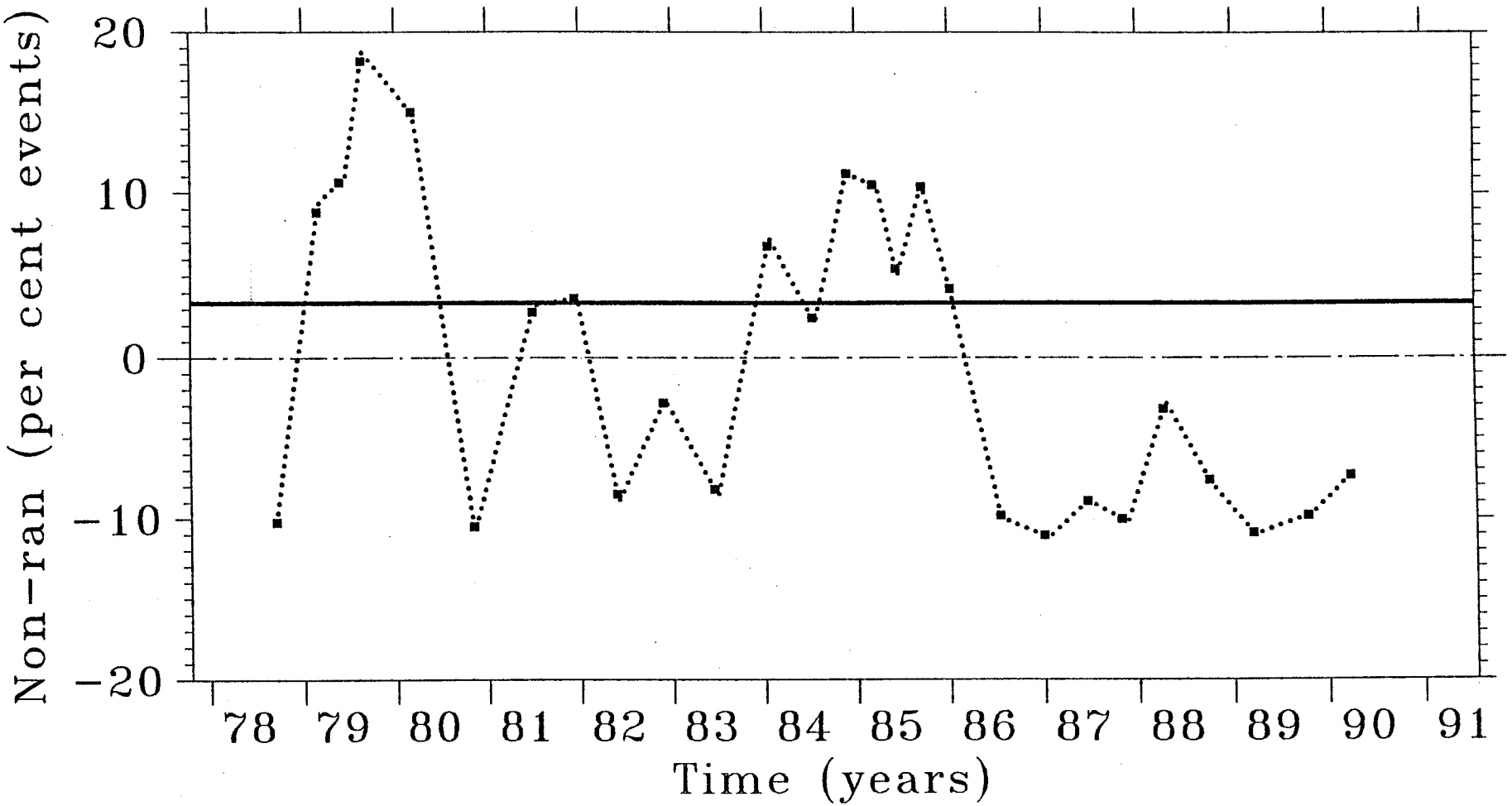

Figure 4.4.15 Temporal variation of the degree of non-randomness of interevent times evaluated from the residual curves in Figure 4.4.13 in the time range 0-90 days. Horizontal bold line at about 4% is the long-term value derived from the residual curve for the whole period shown in the left frame of Figure 4.4.14.

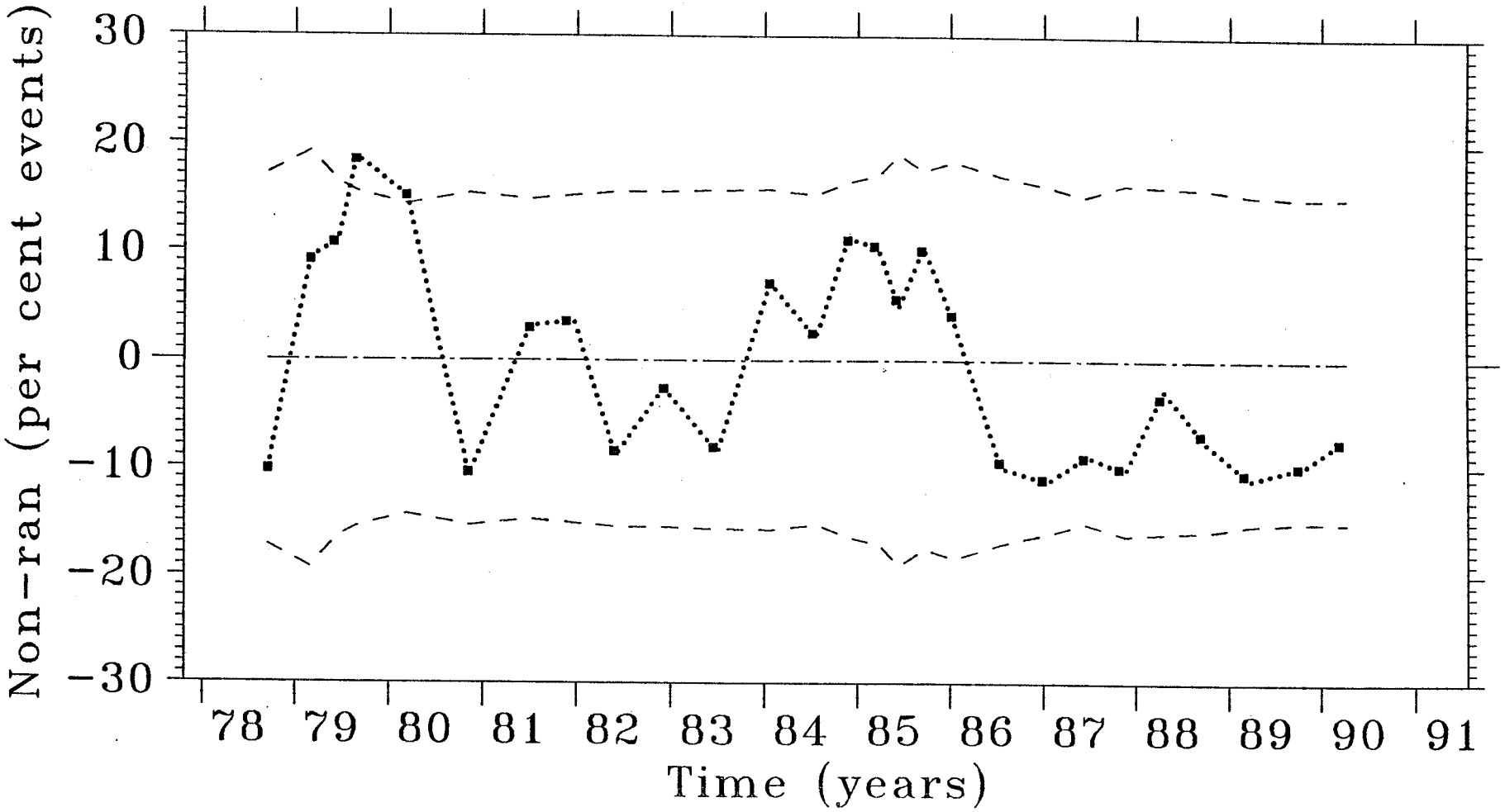

Figure 4.4.16 Temporal variation of the degree of non-randomness of interevent times (same as in Figure 4.4.15) shown together with the variation of the upper and lower tolerance limits (dashed lines).

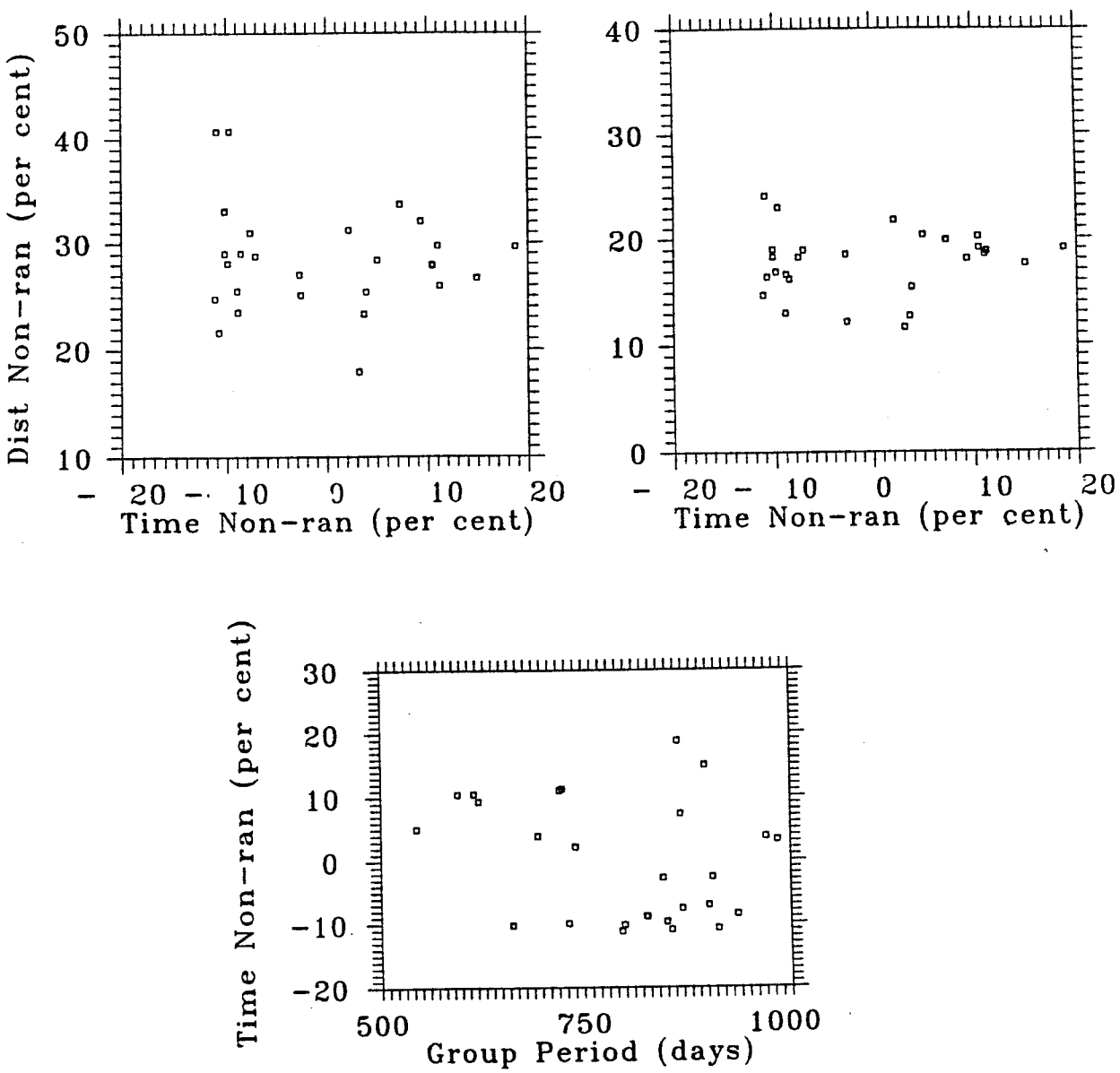

Figure 4.4.17 Scatter plots of the degree of spatial non-randomness versus non-randomness of interevent times (top frames) and the non-randomness of interevent times versus length of group period (bottom frame). Upper frames feature 0-29 km (left) and 1-10 km (right) distance ranges.

randomness: more frequent in time events, more spatially clustered events. The present observations do not support this expectation.

C. Interevent Distance-Time Interval Products. Figure 4.4.18 shows the group residual curves for the products. The interval of counting was 2500 km x days. Since the largest anomaly concentrates in the first interval (i.e, for products < 2500 km x days), the variation curve in Figure 4.4.19 shows group estimates from this interval only. The horizontal bold line at 12.1% shows the long-term degree of product non-randomness against which the short-term values are to be compared. Similar to the spatial degree of non-randomness, the product non-randomness shows values higher than the long-term one around the same three periods. Figure 4.4.20 shows the same curve together with the limits estimated from the tolerance bands. The high product values during the three periods indicated are apparently all significant. The interevent products do not, however, add new information to the features already suggested by the interevent distances. Figure 4.4.21 shows four scatter plots relating the product non-randomness with the 1-10 km (upper left) and the 0-29 km (upper right) distance non-randomness, as well as with the 0-90 days temporal non-randomness (lower left) and the length of group period (lower right). Positive correlations with the spatial degree of non-randomness is predictably indicated, but not with the temporal one. As could be expected, the correlation with the length of the group period is negative, similar to the correlation between the spatial degree of non-randomness and the group period.

4.5 "All" Pairs and b-Values

Figure 4.5.1 shows the original variation curve in the upper frame and the b-value variation curve in the bottom frame. The bold horizontal line and the two thin horizontal lines in the lower frame describe the long-term b-value and its standard deviation: 0.866 ± 0.068. The dashed lines outline the standard deviations of the short-term b-values, which were estimated as the slopes of the magnitude-frequency curves for the same 27 groups as before. The b-value estimates were maximum likelihood ones, using the Aki's formula (Aki, 1965; see also Utsu, 1971) for the CSZ events with $ML \geq 0.5$ ($MN \geq 1.4$). The standard deviations are quite large; this is due to the fact that the magnitude-frequency relationships are still curved, although their curvatures are smaller than the curvatures before the conversion to a single type of magnitude (MN). It appears from Figure 4.5.1 that the b-values are marginally low after both the local M5.0 event and the nearby Saguenay event. Low b-values mean relatively more larger events (or relatively fewer smaller events) when compared with the larger-to-smaller-events ratio at times of average b-values. The apparent increase in the number of larger events at such times cannot be distinguished from a suppression of the smaller events if only the b-values are considered. On the other hand, it appears that the b-value was marginally higher than the average before the local M5.0 event, as well as before the Saguenay earthquake. This would indicate more smaller events (or fewer larger events) by comparison with the average b-value.

The present study does not indicate any obvious correlation between the degree of spatial non-randomness estimated from pair analysis and the b-values. Figure 4.5.2 features two scatter plots showing the degree of spatial non-randomness versus the b-values for the two distance ranges (<29 km and 1-10 km). With the exception of the points at 40% (around the time of the Saguenay event), there might be a slight positive correlation (at best) between the b-values and

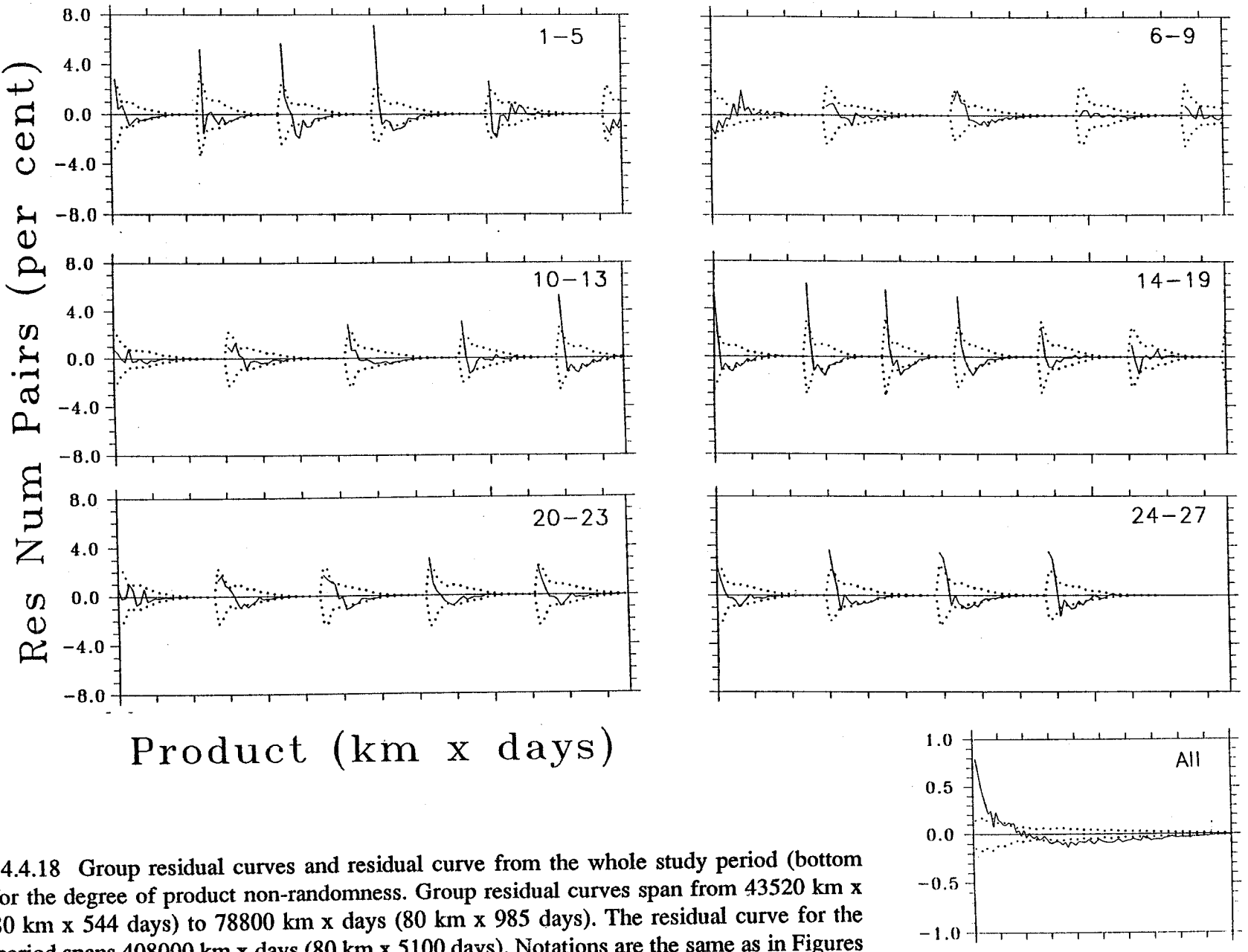

Figure 4.4.18 Group residual curves and residual curve from the whole study period (bottom right) for the degree of product non-randomness. Group residual curves span from 43520 km x days (80 km x 544 days) to 78800 km x days (80 km x 985 days). The residual curve for the whole period spans 408000 km x days (80 km x 5100 days). Notations are the same as in Figures 4.4.1 and 4.4.13.

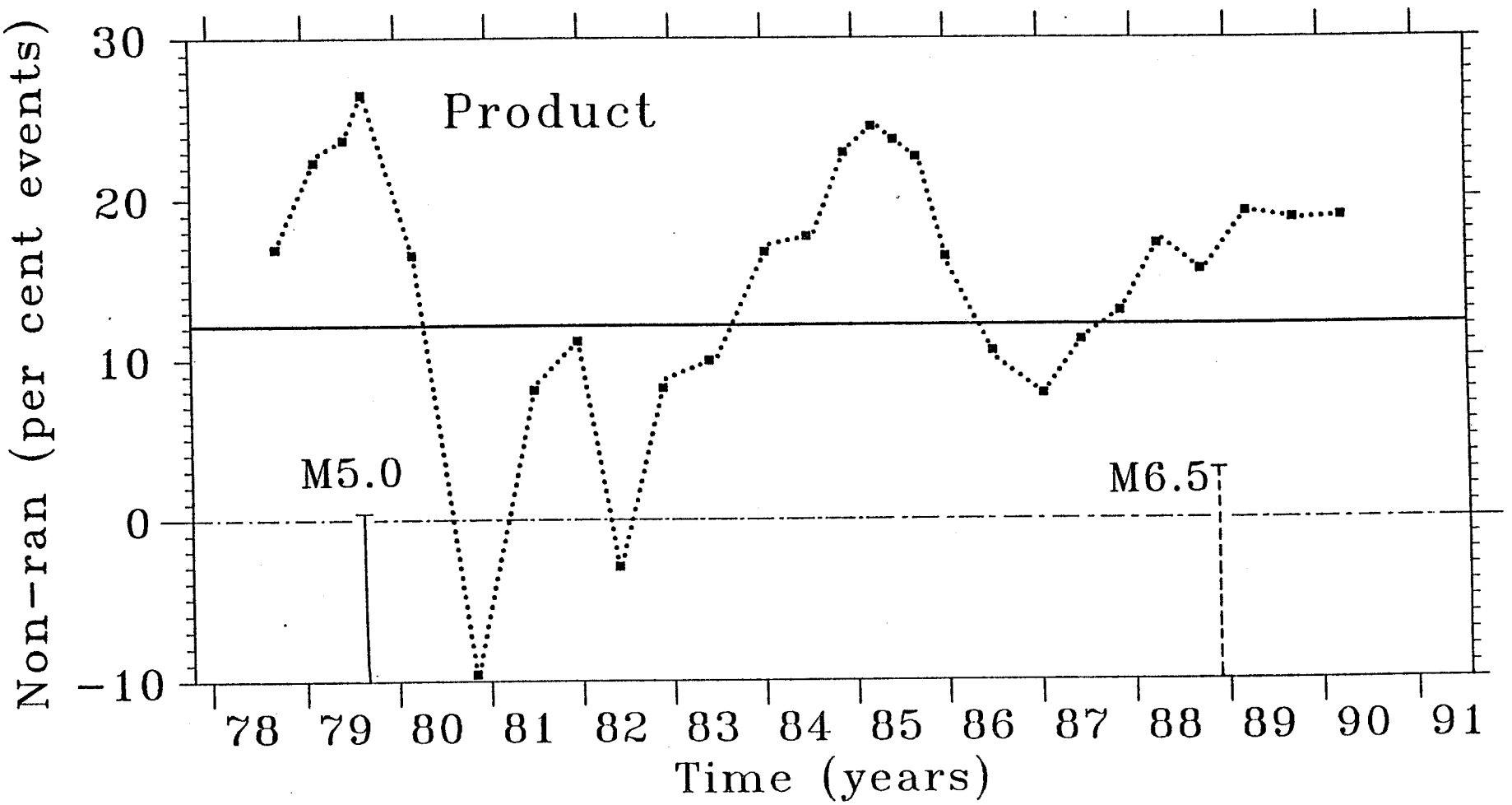

Figure 4.4.19 Temporal variation of the degree of product non-randomness in the product range 0-2500 km x days. Bold horizontal line at about 12% shows long-term value derived from the whole study period. Vertical bars show times of occurrence of the largest events in the region (solid pattern for the local M5.0 event and dashed pattern for the nearby Saguenay event).

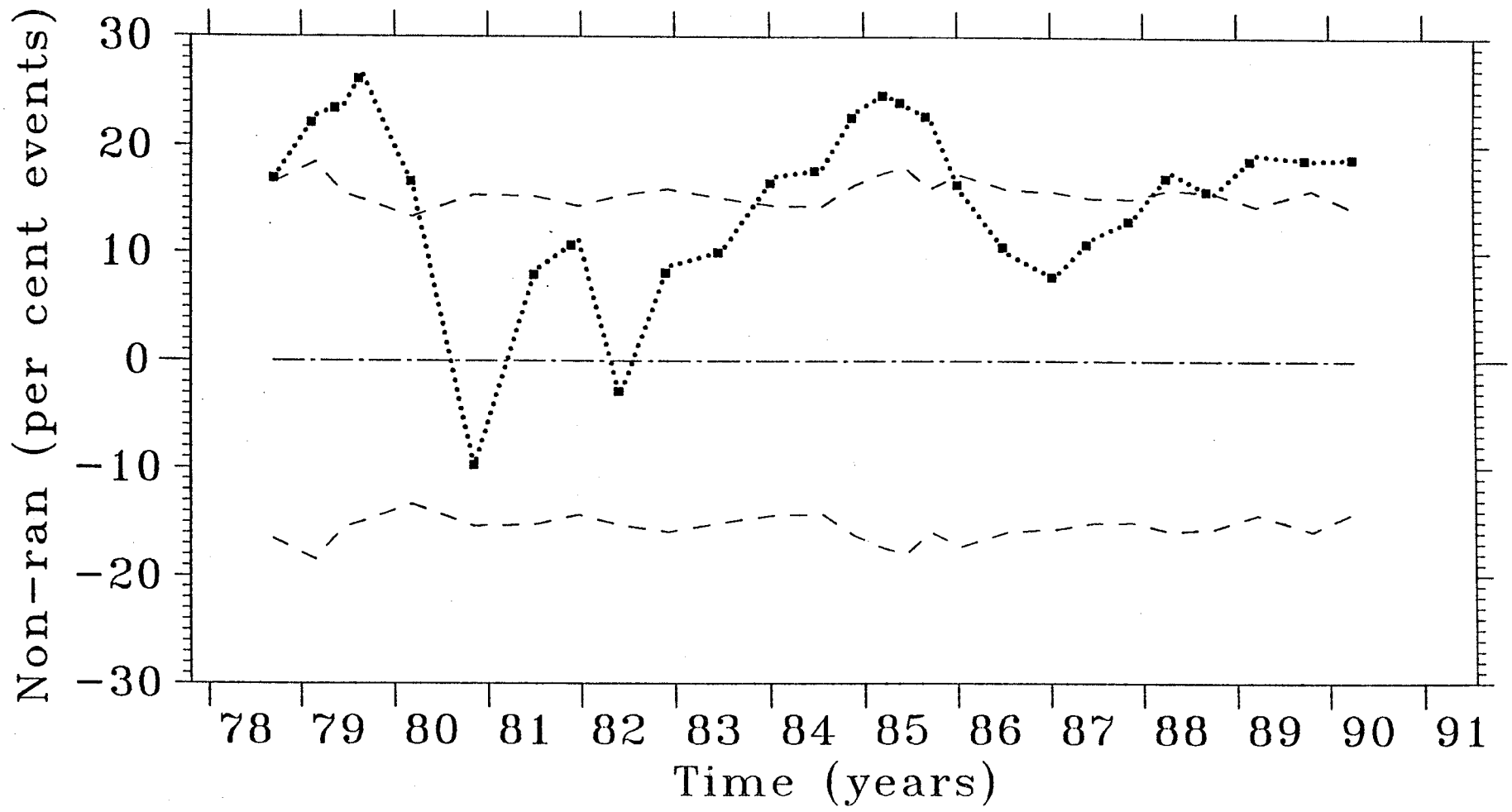

Figure 4.4.20 Temporal variation of the degree of product non-randomness (same as in Figure 4.4.19) shown together with the estimates from the tolerance limits (dashed lines).

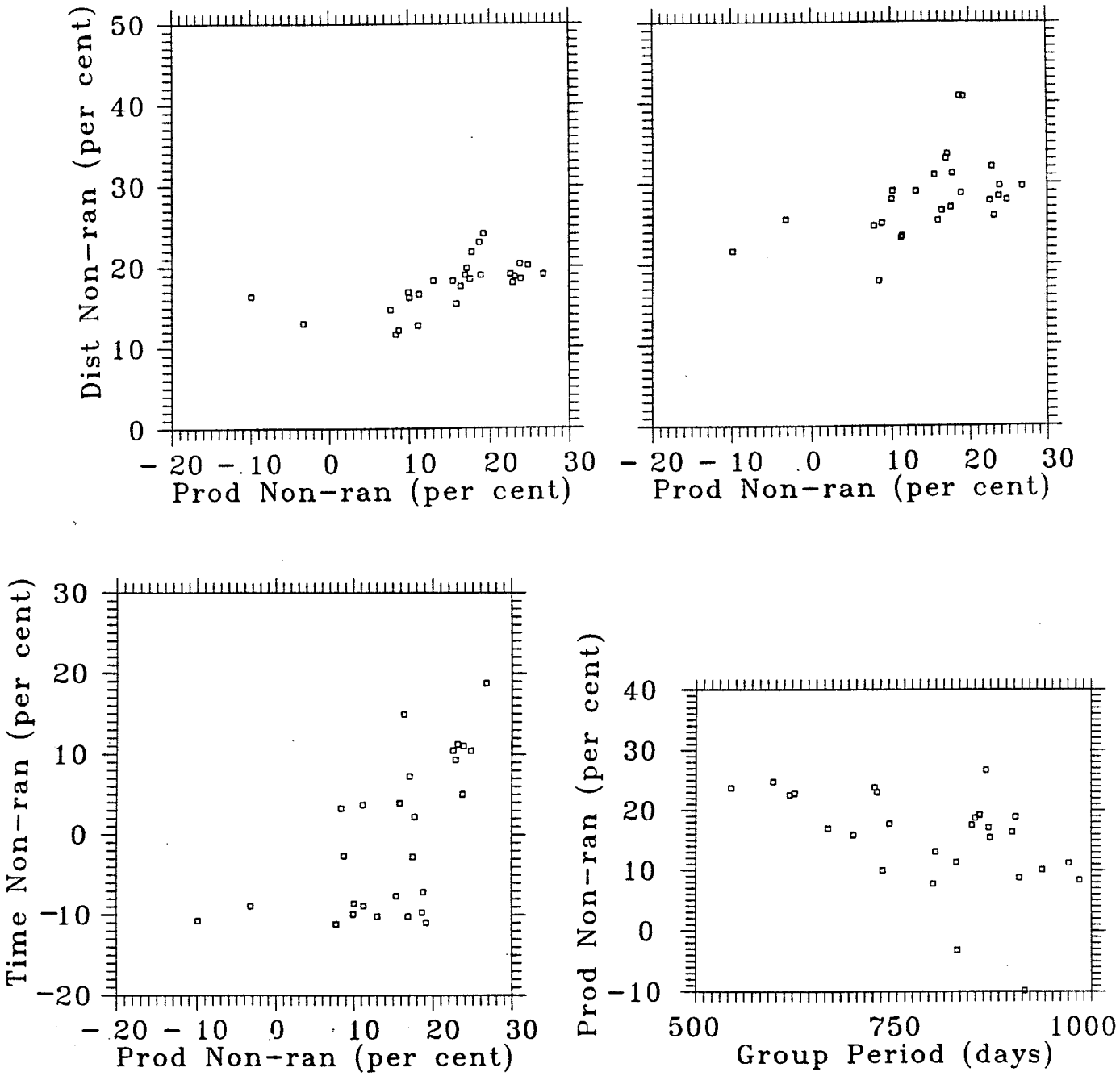

Figure 4.4.21 Scatter plots relating the product non-randomness to the spatial (top frames) and temporal (lower left frame) non-randomness, as well as with the length of group period (lower right frame). Plots on the top feature 1-10 km (left) and 0-29 km (right) distance ranges for the spatial non-randomness shown along the vertical axes.

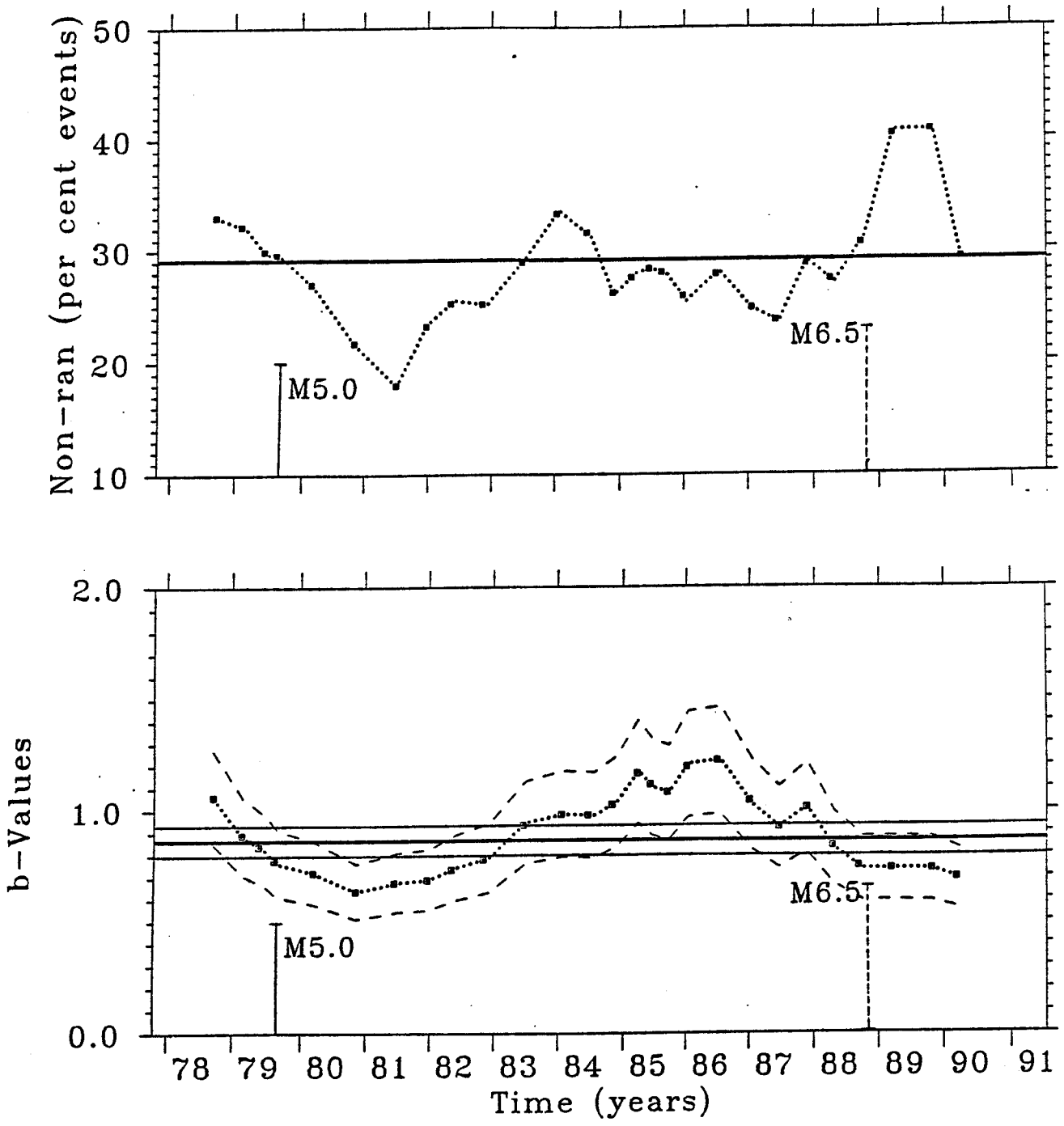

Figure 4.5.1 Temporal variation of the degree of spatial non-randomness in the 0-29 km distance range (top frame, same as in Figure 4.4.2) shown together with the temporal variation of the b-values from the magnitude frequency relationship (bottom frame). Bold horizontal lines in both frames show long-term values derived from the whole data set. Thin horizontal lines in the bottom frame show the standard deviation of the long-term b-value. Dashed lines in bottom frame show the standard deviations of the short-term b-values estimated from the 27 groups. Vertical bars indicate times of occurrence of the largest events.

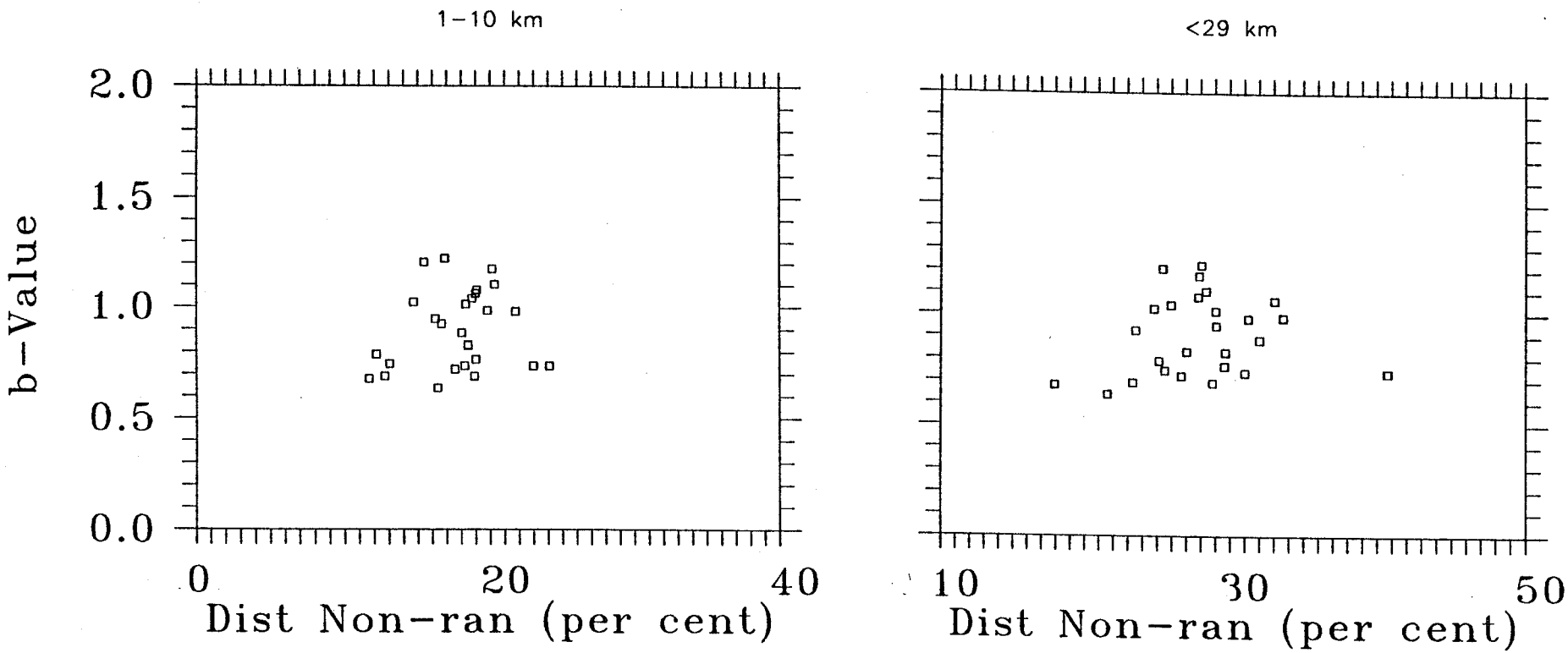

Figure 4.5.2 Scatter plots of group b-values versus group spatial non-randomness in the 1-10 km (left frame) and the 0-29 km (right frame) distance ranges.

the non-randomness in the larger distance range (0-29 km). This feature seems very weak, however, and no signs of correlation are present for the smaller, 1-10 km, distance range. The two time series are too short to be meaningfully studied for correlations at various time lags. This lack of correlation differs from the findings of Hirata (1989a) who used a different method to evaluate the spatial distribution of earthquakes in Japan. He reported a correlation between the spatial parameter he used and the b-values from the magnitude-frequency relationships at various times.

In a search for any meaningful correlation between the variations of the b-values in the CSZ and the other parameters being considered here, scatter plots of the b-values versus temporal and product non-randomness, as well as versus period length, were also examined (Figure 4.5.3). The only apparent correlation is the weak negative correlation with the length of group period. Since a longer period means less frequent events, such a correlation indicates that the large-to-small-events ratio is larger (i.e., the b-value is smaller) when events are less frequent. This is a valuable observation if this effect is real. At least for some groups, however, it is possible that the array did not operate for some short intervals of time. Larger events would continue to be reported during such intervals, because they are recorded by the ECTN network, but smaller events would not be reported. This may cause an apparent increase of the large-to-small-events ratio. The times when the array was down are not known to the author at present and it is difficult to decide whether the apparent negative correlation is an artificial effect. Since at least 2/3 of the groups suggest this trend (right-hand side of the bottom frame on the right), one would be inclined to assume that there is a significant real component to this observation. Although the groups are overlapping, the array would have to have been down too many times for this correlation to be entirely artificial.

4.6 Results from "Next" Events

Figure 4.6.1 shows distances (top frame), time intervals (middle frame) and products (bottom frame) versus sequential number of "next" pairs. Examples are given only from the first seven groups out of the same 27 groups as before. Since each group consists of 100 events, the number of "next" pairs is 99 per group. Values near 0 indicate successive events which occurred vary close in space and/or time. For example, a narrow trough appears at the end of the second group (top frame), since this is when the M5.0 event and its aftershocks occur. This trough persists in the next four groups as well, since they are overlapping. It gradually moves towards the beginning of these groups until it disappears in the 7-th group, which is the first one to become free of the aftershock sequence. The same feature, although less clear, can be also seen in the time intervals and the products, since the aftershocks occur at both small distances and small time intervals.

Note that the largest time intervals between two successive events may sometimes simply indicate that the seismic array was down. This may also result in large products when the respective distances are large, while the distances alone are completely uninformative in this respect. For this reason, as long as the times when the array was down are unknown at this time, one has to be cautious interpreting large time intervals and products between "next" events as indicative for a real quiescence in seismic activity. In contrast, the smaller time intervals and products are free from such an artificial effect. The same consideration affects the plots in Figure 4.6.2, which are the same as the ones in the previous figure, but illustrate the whole data set.

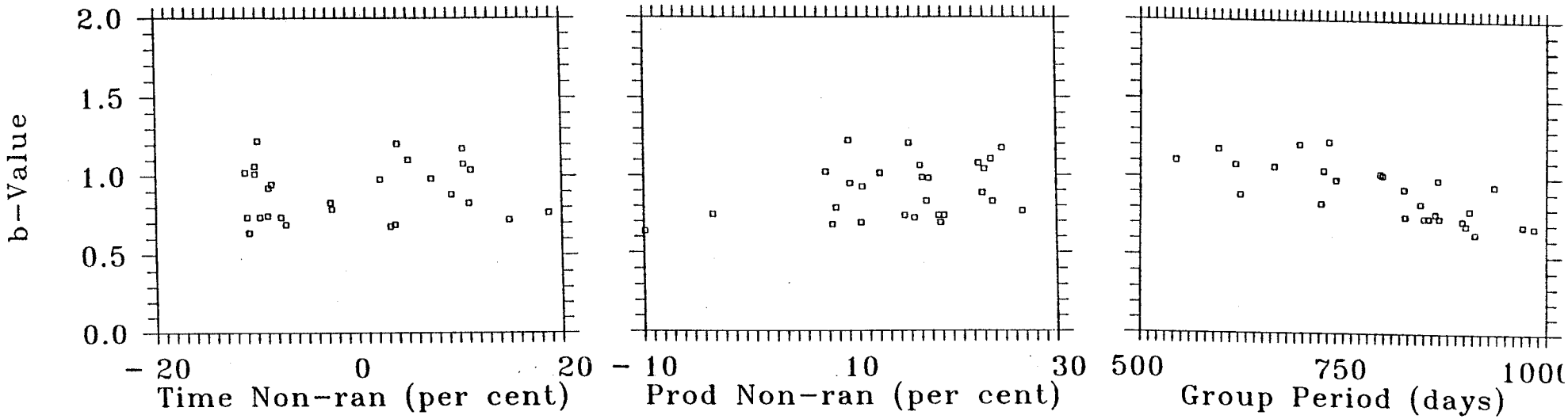

Figure 4.5.3 Scatter plots of the group b-values versus group temporal (left frame) and product (middle frame) non-randomness, as well as versus length of group period (right frame).

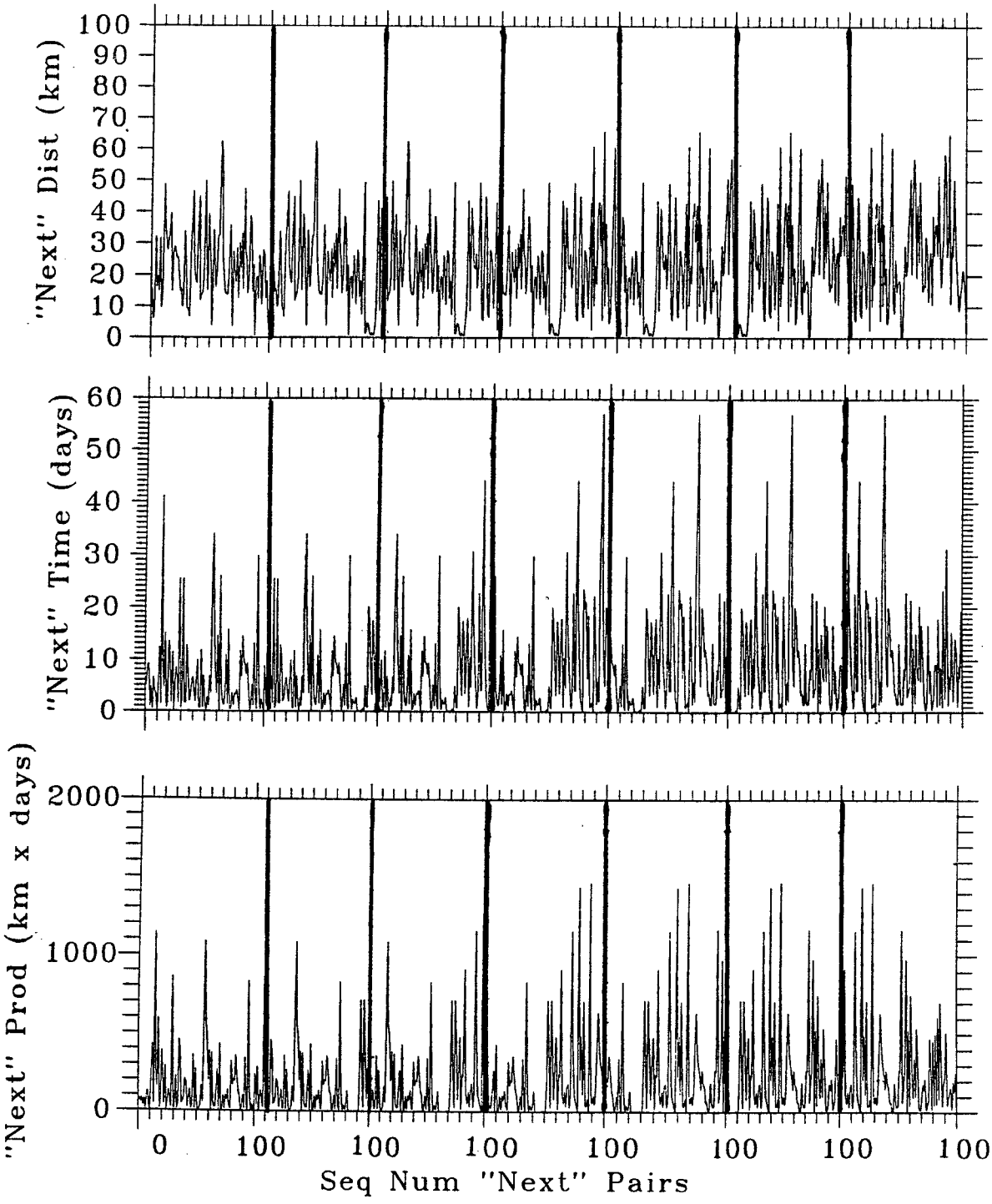

Figure 4.6.1 "Next" parameters versus pair sequential number shown for the first seven of the 27 groups. From top to bottom: distances between successive events, time intervals between successive events, and products of these. Bold vertical lines separate groups. Each group features 99 pairs. See text for more details.

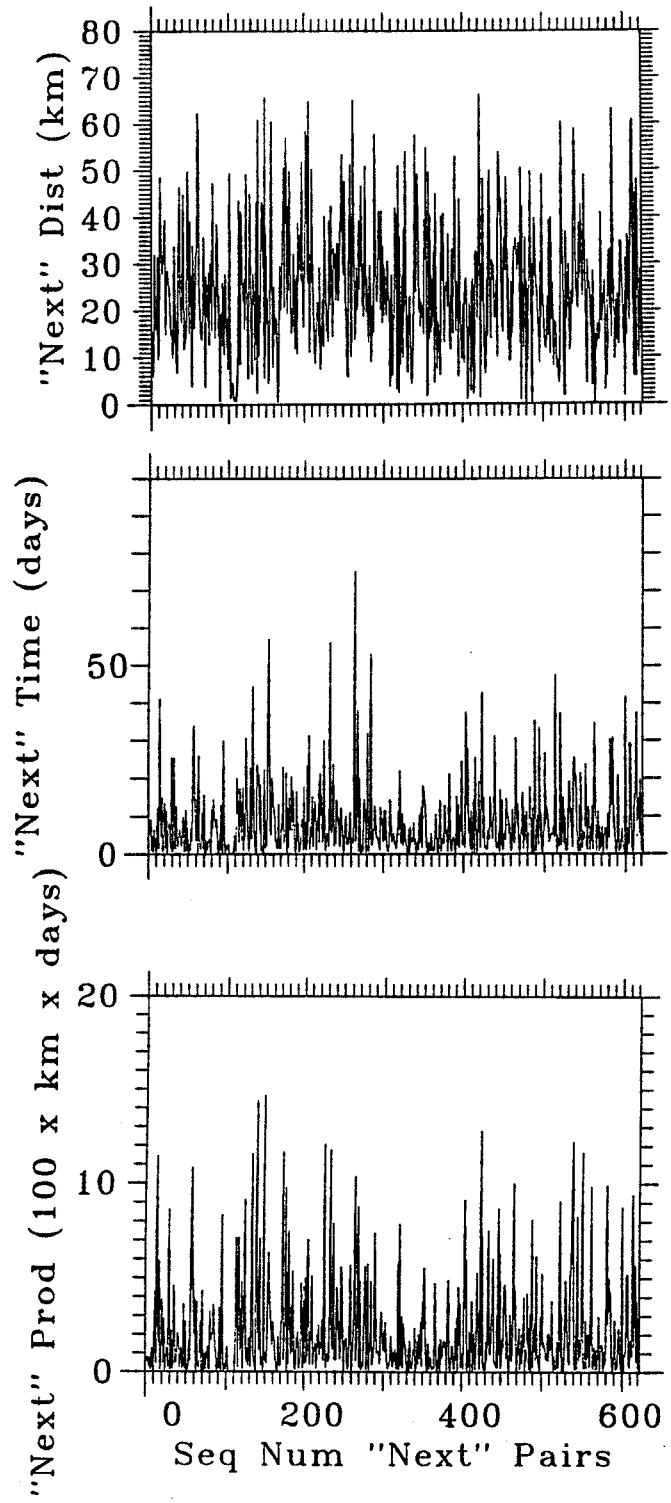

Figure 4.6.2 "Next" parameters versus pair sequential number for the whole data set (622 pairs). From top to bottom: interevent distances, times, and products.

Since the events in the whole data set are 623, the number of "next" pairs is 622 in all three frames of Figure 4.6.2.

None of the above two figures suggest any clear temporal change. Temporal variations are depicted in Figure 4.6.3. The top frames show the average distances, time intervals, and products for the "next" pairs. Each group is characterized by three average values (one for each of the three parameters). Each average value is calculated from 99 "next" pairs. The lower frames show the standard deviations of these means. The bold horizontal line in each of the top frames shows the long-term average determined from 622 "next" pairs, while the bold horizontal line in each of the lower frames shows its respective long-term standard deviation. The thin horizontal lines show the long-term average values from random catalogues and their standard deviations. These are calculated from 622 "next" pairs for 623 randomly generated events.

Similar to the results of pair analysis, the long-term average distance of 24.5 ± 13.7 km indicates some spatial clustering (closer events) by comparison with the long-term average of 28.5 ± 14.5 km for randomly distributed events. The standard deviations, however, are quite large for such a comparison to be conclusive. Nonetheless, the temporal variation of the average distance between "next" events is in agreement with the results from the pair analysis. Smaller short-term values are indicated by the groups containing the aftershock sequence (2-nd to 6-th), which is to be expected, as well as around the time of the Saguenay event. In both cases, pair analysis suggested degrees of short-term spatial non-randomness (i.e., clustering) higher than the average which is in agreement with smaller distances between successive events. Conversely, the largest average distances occur mostly when degrees of spatial clustering lower than the long-term average were previously indicated. Figure 4.6.3 confirms what is already known from the analysis of the time intervals for "all" pairs, that is, that time intervals are not particularly informative. The long-term average time interval between "next" events of about 8 days is apparently undistinguishable from the long-term average time interval from a random catalog, hence the bold and thin horizontal lines coincide in the middle top frame. Their standard deviations are slightly different (bottom middle frame), but this does not make the time intervals more informative. Some variation is observed in the average time interval, but it will be shown below that it is entirely determined by the variation in the length of the periods covered by the 27 groups rather than by intrinsic differences in the occurrence of events in the different groups. The part of Figure 4.6.3 depicting the products (frames on the right) do not seem to contribute any new information.

Figure 4.6.4 shows the same variation curves as in the previous figure, but they are compared with the average values obtained from random catalogues of 100 events each (thin lines and open squares). Thus, the comparison here is made not with the long-term average value (the thin lines in Figure 4.6.3), but with the short-term values obtained from random catalogues. The top frames show the short-term average values from the real and the random groups and the lower frames show their standard deviations. The short-term values for the average distance vary very little; this slight variation is due only to the small differences between the random catalogues modelling each group. The spatial differences are negligible, since the events are randomly generated in the same volume regardless of the group number. In contrast, there is no difference between the variation curve for the average time interval from the observed and the randomly generated group catalogues. The reason is that unlike the volume in which the events occur, the time periods are different from group to group. The length of these time periods are

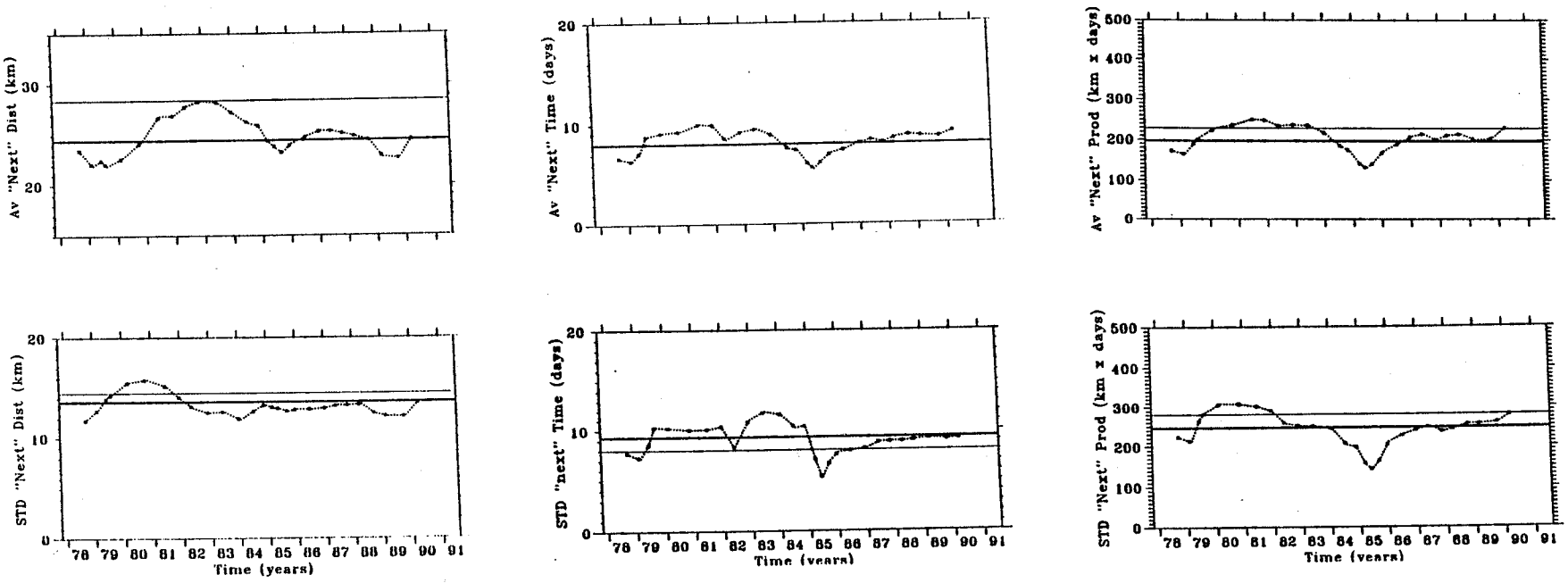

Figure 4.6.3 Temporal variations of the average group parameters (top frames) and their standard deviations (bottom frames) for the "next" pairs. From left to right: group average "next" distances, time intervals, and products. Each group average value is calculated from 99 pairs. Long-term averages are calculated from the 622 "next" pairs for the whole data set; these are shown with bold horizontal lines in each frame. Thin horizontal lines show the long-term values calculated from randomly generated catalogues of 623 events (i.e., modeling the whole data set). Note that these coincide for the group average time intervals (top middle frame). See text for more details.

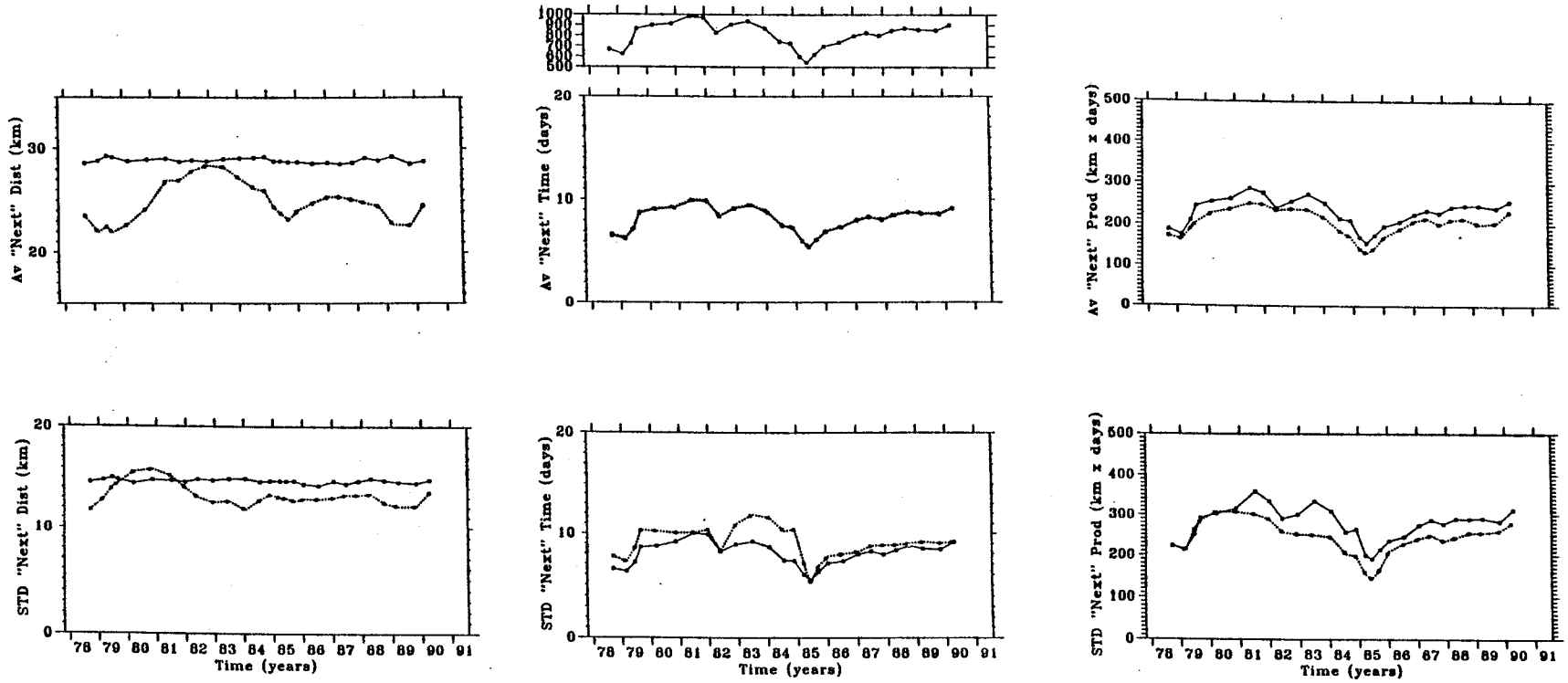

Figure 4.6.4 Temporal variations of the average group parameters (three top frames) and their standard deviations (three bottom frames) for the "next" parameters (dotted lines; same as in Figure 4.6.3) shown together with the average values obtained from random catalogues of 100 events each (solid lines; modeling the 27 groups). Narrow frame above the plots in the middle shows the temporal change in the length of group period in days. Note that the shape of this curve determines the shape of the variation curve for the group average time intervals. See text for more details.

shown above the middle frames for comparison. The longer the period, the less frequent are the randomly generated events and vice versa. This means, as mentioned above, that the variation in the average time intervals is exclusively due to the differences in the lengths of the periods covered by different groups. The events occurring in each group covering a period of a given length are otherwise distributed in such a way throughout the group that their distribution cannot be distinguished from random distribution in time. It is indeed apparent that all three curves have the same shape: the curve showing the lengths of the group periods, the one depicting the change in average time interval from the real groups, and the one showing the same for the randomly generated groups. This comes to confirm that looking at time intervals between "next" events, similar to the results of pair analysis of interevent times for "all" pairs, cannot yield any more information than the one obtained by simply comparing the lengths of the periods covered by the groups. While there is some difference between the curves for the standard deviations (bottom middle frame), the general shapes of these curves too seem to be primarily controlled by the difference in the lengths of the group periods. Finally, the products (right frames) do not suggest anything more than the previous observations.

In summary, the distances between successive events, similar to the distances from "all" pairs, appear to be most informative. In all cases, distances show larger degree of clustering than what would be expected from randomly generated catalogues. The short-term variations of the average distance between successive events have similar implications as the ones suggested by the pair analysis of "all" events. The standard deviations of these distances are, however, comparable to the distances themselves. In addition, the set of successive events is very limited by comparison with "all" pairs. It is therefore not recommended to use only the average distances for "next" pairs, although their analysis alone is technically simpler than the analysis of "all" pairs. In contrast, Purcaru and Pawelzik (1992) used similar parameters analyzing data from other areas and took much more optimistic view about their usefulness. It is possible, that in other areas, with higher levels of seismic activity, this type of parameters has greater potential than in the CSZ.

4.7 Results from "Near" Events

The use of "near" events was inspired by the work of Frohlich and Davis (1990), Davis and Frohlich (1991), and Wardlaw et al. (1991) where the so-called single-link cluster analysis was applied. It is based on examining nearest neighbours in space. This analysis was applied for various purposes, including identification of aftershocks. The most interesting result connected to the type of studies presented here is the observation of changing spatial patterns in earthquake distribution before some large events (M>7.2) reported by Wardlaw et al. (1991). Although single-link cluster analysis is not applied in the version formulated by the above authors, nearest neighbours are examined here as well. The way this is done stems directly from our other applications. **N** events form **N-1** "near" pairs. The search for the nearest event is done forward in time only, that is, the "near" events here are both "next" and "near". The figures depicting results from the analysis of the "near" pairs are similar in configuration to the figures for the "next" events in 4.6 above. The two top frames in Figure 4.7.1 show the distances and time intervals between the "near" events for the first seven groups. Each group, as before, has 100 events and hence 99 "near" pairs. It is evident that the "near distance" fluctuates around 3 or 4 km in the beginning of the groups, but it gradually increases afterwards. "Near" pairs are

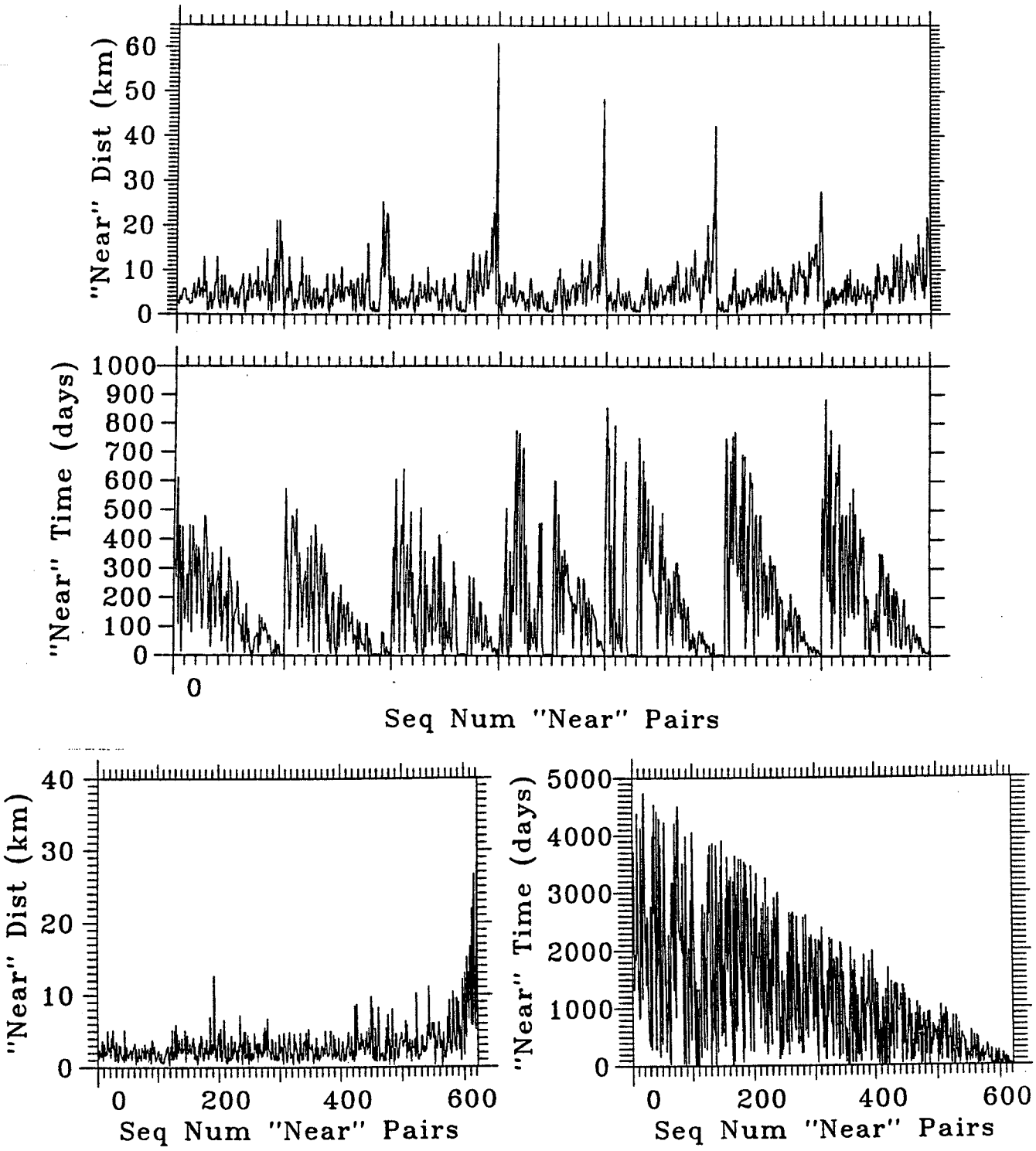

Figure 4.7.1 "Near" distances and time intervals versus sequential pair number. Top and middle frames show group "near" distances and time intervals for the first seven of the 27 groups. Each group covers 99 pairs. Frames at the bottom feature the same, but represent the whole data set.

different from "next" pairs in this respect, because the closer an event is to the end of a given group, the fewer the choices for its closest neighbour occurring at a later time. For this reason, the distances to the closest neighbour gradually increase. It appears that this increase starts taking place from the very beginning. The time intervals (middle frame) show the opposite trend; they become smaller as the end of the group period approaches. It seems that these intervals greatly fluctuate around 200 to 250 days in the beginning and become smaller and smaller afterwards. Both trends are a natural consequence of the limited time of observation. Because the trends of the distances and the time intervals between "near" events are roughly opposite, the products are slightly more stable. Yet, a compensation does not occur and the products decrease by the end of the sequence, since the trend for the time intervals is more linear-like, while the increase of the distances is more exponential- or power-like. The two lower frames in Figure 4.7.1 show the same type of plots, only they are for the whole study period. Since the whole study period is several times longer than any of the group periods, the distances between the nearest neighbours in the beginning are somewhat smaller, 2 to 3 km. It apparently takes more time for events to occur closer, so the time intervals between these "near" events fluctuate around 2000 days; a time interval more than twice longer than the longest group period. The fluctuations in all these plots are comparable with or larger than the size of the distances and time intervals between the "near" events.

The above observations already point that "near" pairs may be quite useless for the purposes of the studies discussed here. It is indeed unlikely to extract any valuable information from such highly variable data. Nonetheless, it is possible to devise some reasonable estimates of the average parameters for the "near" pairs, extracted only from the beginning of each time series. This was intended to reduce the effect of the trends. Figure 4.7.2 shows the average values calculated for the "near" distances, time intervals, and products, when only certain number of the first pairs of each group was used. Each frame shows three curves for three different choices of this number. The curves shown with dotted lines and filled squares are formed by measurements of the "near" parameters only from the first 15 pairs of each group (each group consists of 99 pairs as before). The thin solid lines and the open squares mark the variation in the "near" parameters obtained from the first 30 pairs of each group. Finally, the dashed line and the crosses mark the curves obtained by using the first 45 pairs of each group. It is apparent that none of these choices makes the curves very different from the other ones; they seem equally non-informative. The average "near" distance fluctuates around 3.5 km, while its standard deviation fluctuates around 2 km (not shown). The average "near" time interval varies around 300 days and its standard deviation - around 200 days (not shown). Both the "near" products and their standard deviations fluctuate around 1200 km x days. Since this average "near" product seems somewhat larger than the product of the average "near" distance and the average "near" time interval (i.e., $1200 > 3.5 \times 200$), it is possible that there is some hidden information in these results, which cannot be revealed at present. Such a discrepancy, if real, would indicate that smaller "near" distances tend to associate with larger "near" times, otherwise the average "near" product would not be larger than the product of the average "near" distances and average "near" time intervals. This would mean that in average, it takes more time for an event to occur closer to a location of previous earthquake occurrence. This intuitively makes a lot of sense, but cannot be verified directly at this time.

In summary, the "near" pairs are not really informative as evidenced by the type of

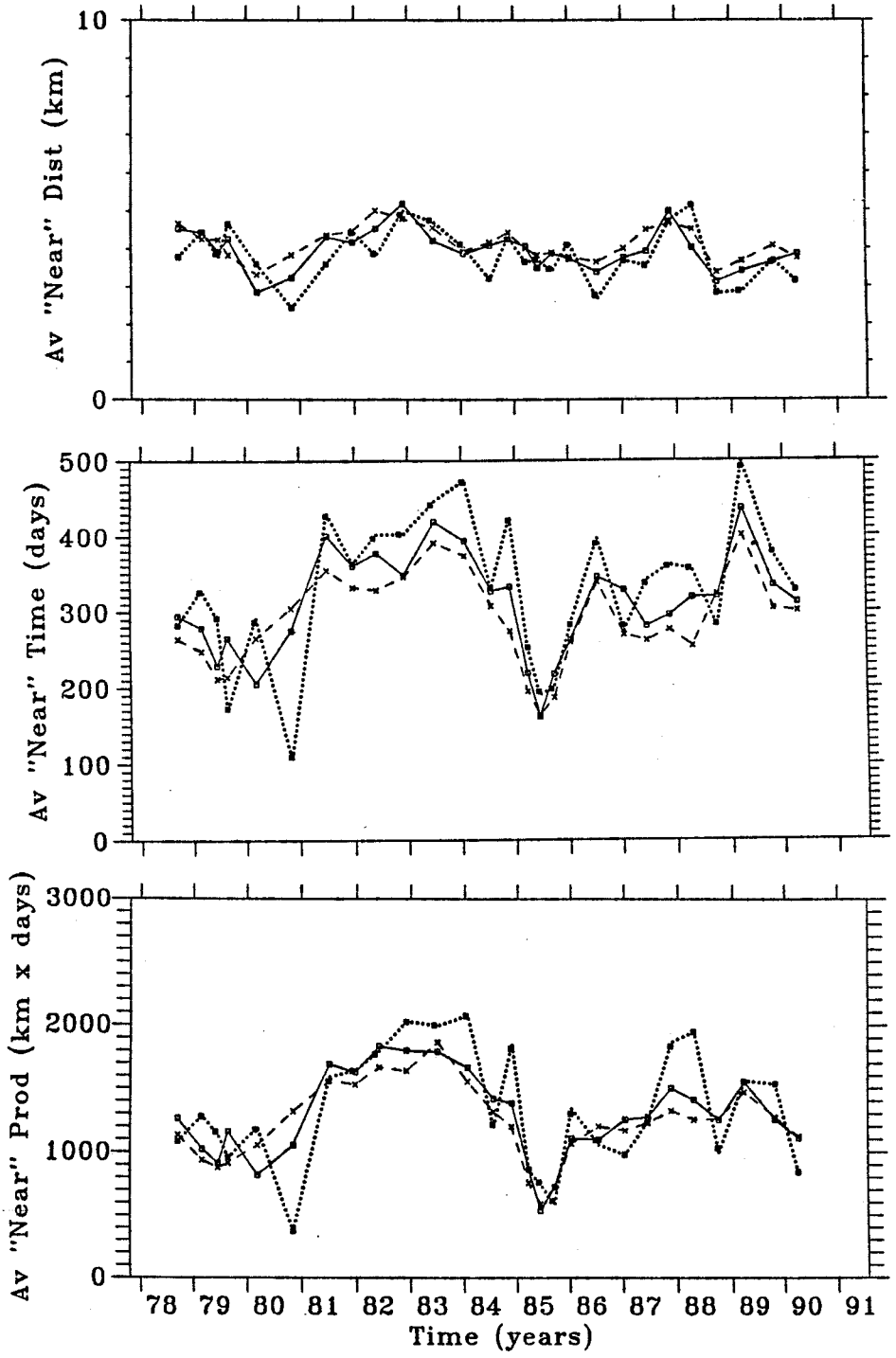

Figure 4.7.2 Temporal variations of the group average "near" parameters. Each short-term value is calculated from the first 15 (filled squares, dotted lines), 30 (open squares, solid lines), or 45 (crosses, dashed lines) pairs of the respective group. From top to bottom: group average "near" distances, time intervals, and products.

analysis presented here. This does not exclude the possibility that useful information can be still extracted from these pairs, but some other approaches should be used.

CHAPTER 5. ESTIMATES OF CORRELATION DIMENSIONS

5.1 Correlation Dimension

There has been accumulating evidence that earthquake dynamics can be studied using concepts from non-linear dynamics. For example, Rundle (1988) developed a physical model of earthquake occurrence and showed through numerical modelling that fault dynamics is chaotic. Earthquakes have been described as self-organized critical phenomena by Bak and Tang (1989) and Shaw et al. (1992). Keilis-Borok (1990) discussed the implications for earthquake prediction of a model in which the Earth's lithosphere is represented by a non-linear system. On the other hand, the concepts of self-invariance and fractal geometry have found its way in geophysics for some time now, more specifically in studying crustal fragmentation and fault geometry (Turcotte, 1986; Aviles and Scholz, 1987; Okubo and Aki, 1987; Hirata, 1989b), as well as in describing earthquake occurrence in time (e.g., Smalley and al., 1987), space (e.g., Andrews, 1980; Kagan and Knopoff, 1980; Sadovsky et al., 1987), and size (e.g., Andrews, 1980; King, 1983; Fukao and Furumoto, 1985; Rundle, 1989). Recent geophysical applications feature even newer concepts, such as multifractal distributions (e.g., Block et al., 1991; Hirata and Imoto, 1991).

Figure 5.1.1 illustrates the use of the so-called correlation integral for providing a quantitative measure of the spatial distribution. This method was introduced by Grassberger (1983) and Grassberger and Procaccia (1983) to measure the fractal dimension of the attractors associated with some time series. Further developments and modifications can be found in Kurths and Hertzel (1987) and Nerenberg and Essex (1990) among others. The quantitative aspects of this method can be used even without necessarily considering systems with fractal properties. This approach has been applied by to earthquake data by Hirata (1989a) and Radulian and Trifu (1991). In the formula shown in Figure 5.1.1, the value of the integral **C(r)** at distance **r** is simply the number of all earthquake pairs with a distance smaller than **r** normalized by the total number of earthquake pairs. It has been found that for a distribution with a fractal structure and for small values of **r**, this integral can be represented by a power law, where the power is the so-called *correlation dimension* **d**. This was found to be a number close to, but always smaller than the fractal dimension **D**. In a double logarithmic plot, where the cumulative number of pairs is shown along the vertical axis, and the distance along the horizontal axis, we obtain curves which are straight lines for certain distance range, called *scaling range*. The slope of these straight line segments is the correlation dimension **d**. The curve marked by the open squares is derived from 100 events in the CSZ, and the filled squares form a curve obtained from 50 randomly generated data sets, of 100 events each.

All too often the existence of such a scaling range has been interpreted as a proof for existence of attractors and fractal properties. For example, Hirata (1989a) directly discusses fractal dimensions, while the dimension estimated in his work is in fact the correlation dimension (i.e., an estimate that is always smaller than the fractal dimension). The correlation integral method has its limitations in this respect (Goodings, 1991) and it is not necessary to make far-fetched assumptions for fractal properties of the earthquake distribution. At this point the

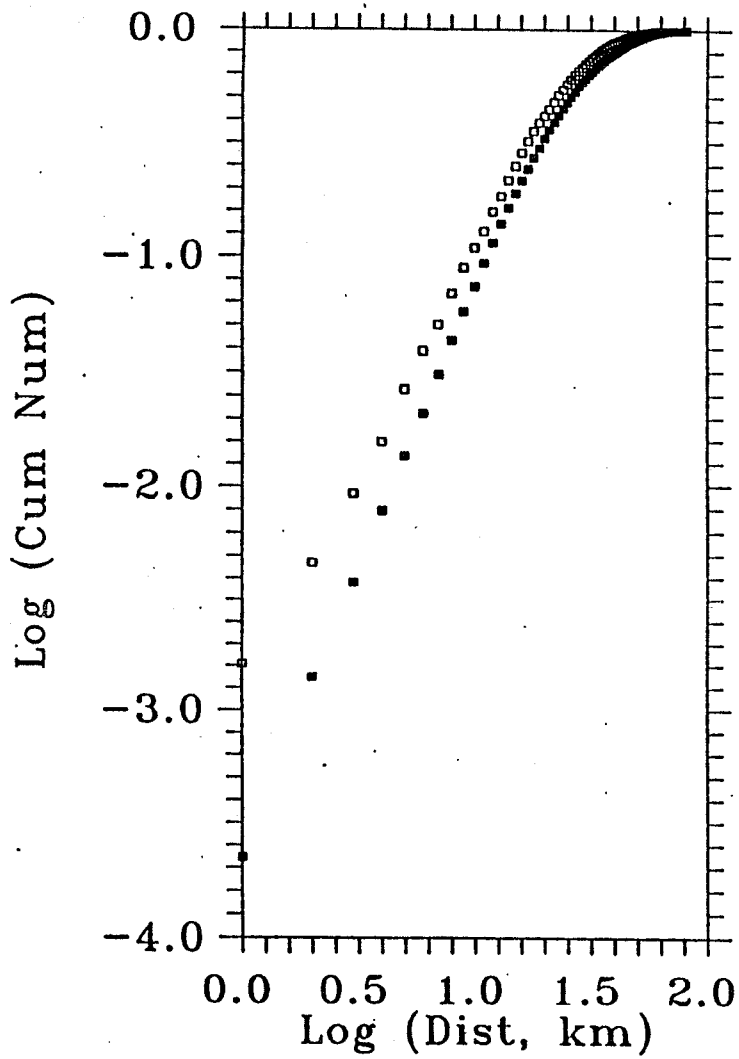

Correlation Dimension

$$C(r) = \frac{2}{N(N-1)} N(R<r)$$

$$C(r) \propto r^d$$

$$d \leq D$$

N(r) - number of pairs with distance smaller than

C(r) - correlation integral

d - correlation dimension

D - fractal dimension

Figure 5.1.1 Schematic representation of the correlation dimension technique applied to interevent distances. Open squares mark the curve obtained from observed data, filled squares mark the curve obtained from randomly generated catalogues. Formulae on the right side of the plot explain usage of the correlation integral. See text for more details.

correlation dimension is simply used as an integral measure of spatial distribution in the distance range of 1 to 10 km, since all the correlation curves seem to have straight segments over this range, represented by the 2-nd to the 10-th points of each curve on the logarithmic plots.

The same type of information is apparently used in both pair analysis and the correlation dimension estimates. There are, however, several differences between the two types of analyses:

(1) The technique of pair analysis accounts for the limited size of area and its shape by subtracting expected from observed distributions. No similar procedure has been developed to remove the effect of saturation from the correlation curve. As a result, estimates of the degree of non-randomness from pair analysis can be made over all ranges, as long as they include distances smaller than the maximum interevent distance or time intervals smaller than the maximum interevent times. This cannot be done on the basis of the correlation curves. For example, the maximum interevent distance for the CSZ is about 80 km. Estimates of the spatial degree of non-randomness can be therefore made over a number of distance ranges, as long as they involve distances smaller than 80 km. In this work, only two ranges were considered as most interesting (0-29 km and 1-10 km). Long-distance anomalies have been observed elsewhere (Eneva and Pavlis, 1988, 1991; Eneva and Hamburger, 1989) and they can be analyzed the same way as the short-distance ones. In the case of the CSZ, however, such long-distance anomalies have not been observed, but had it been necessary, distance ranges involving larger distances could be studied as well. Such an option does not exist when the correlation curves are used, since the scaling region is only over distances smaller than about 10 km.

(2) The measure of non-randomness from pair analysis over certain range is integral, i.e., it represents a total measure over the whole range; it does not contain any information about the behaviour of the pattern within the range studied. For example, the degree of spatial non-randomness measured over the distance range 1-10 km is a number characterizing this range as a whole and it does not provide any information about the relationship among the degrees of spatial non-randomness in the 1-2 km, 2-3 km, 3-4 km, etc., ranges within the original 1-10 km range. In contrast, the estimate of the correlation dimension over the same 1-10 km distance range, does not provide a total estimate over this range, and the only obvious information is that a scaling over this range is observed. However, since the slope (correlation dimension) is estimated over all the points along the straight segment, information on their mutual distribution is contained in the estimate. That is, the value of the slope does indicate what the relative spatial distribution is in the ranges < 2 km, < 3 km, < 4 km,... < 10 km. This comparison shows that although in both cases distances are used, the pair analysis and the correlation dimension analysis utilize these distances differently.

(3) The differences in (1) and (2) above also point to an important conceptual difference between pair analysis and the correlation dimension method. Correlation dimensions cannot be estimated unless scaling is present. Pair analysis does not suffer of this limitation and can be applied in all sorts of cases.

(4) Larger degree of non-randomness from pair analysis is indicated by larger values. The opposite is true for the correlation dimensions; the smaller the slope, the larger the clustering. Smaller slopes mean that relatively more pairs are concentrated at the left side of the scaling range (i.e., the smaller distances, time intervals, or products) than for the cases when the slopes are larger.

The example in Figure 5.1.1 shows that the observed curve is above the random curve,

and the slope (i.e., the correlation dimension) that would be derived from the observed curve would be smaller. That is, when compared with the dimension derived from the randomly generated data, the smaller observed dimensions are associated with clustering, in this case over distances 1-10 km. Figure 5.1.1 shows an example of distances, but the concept is the same when time intervals and products are used.

5.2 Short-Term Versus Long-Term Correlation Dimensions

Similar to the application of pair analysis, long-term correlation dimensions were estimated for the whole data set (623 events), while short-term dimensions were estimated for the same 27 groups as before. Each of the three top frames in Figure 5.2.1 shows correlation curves from the first five groups; the curves for the remaining groups are visually similar to these and are not shown. The correlation curves shown from top to bottom are for the interevent distances, time intervals, and the products. On the bottom of this Figure, the correlation curves shown from left to right are for the same quantities, but from the whole data set. The curves denoted by squares are from the real data, while the dots mark the average curves from 50 randomly generated sub-catalogues for each group (three top frames) or for the whole time period (plots on the bottom). It is apparent from these curves that larger clustering is indicated by the real data for the interevent distances when compared with the random catalogues. The time intervals and the products do not suggest similar degree of discrepancy, especially the time intervals. This already suggest that in this type of analysis too the distances might be most informative. The figures below confirm this proposition.

A. Spatial correlation dimensions. The temporal variation of the spatial correlation dimension estimated for the same 27 groups over the 1 to 10 km distance range are shown in Figure 5.2.2. The same scaling range (2-nd to 10-th points of the curves) is used for the groups and for the whole data set, since the seismically active volume is the same in all cases. The plot in Figure 5.2.2 is similar to the one in Figure 4.4.2, but the vertical axis shows the correlation dimension and lower values indicate a larger degree of spatial clustering. The thin solid line shows the correlation dimension obtained as an average value from 50 random catalogues of 623 events each. The bold line indicates the long-term value obtained from the whole data set. Because the correlation dimensions are estimated as slopes of straight lines, it is possible to also estimate their standard deviations. The long-term spatial correlation dimension (bold line) is 2.376 $\pm$ 0.017. The correlation dimension estimated from random catalogues of 623 events is 2.477 $\pm$ 0.004. This last value demonstrates the fact that the correlation dimension is lower than the fractal dimension. For points randomly distributed within a three-dimensional volume, the fractal dimension would have to be 3 (i.e, coinciding with the topological one).

When the long-term values for the real and the random data are compared, only a 4.1% smaller slope for the real data set is indicated (calculated from (2.477-2.376)/2.477). This small difference does not represent a convincing evidence that the clustering over the 1-10 km distance range is larger for the real data than for the random data when the whole time period is considered. Pair analysis apparently does much better in this respect (the long-term spatial non-randomness was about 29% for the 0-29 km distance range and about 17% for the 1-10 km range). The short-term correlation dimensions, however, when compared against the long-term estimate provide much more information. The dashed lines accompanying the variation curve in

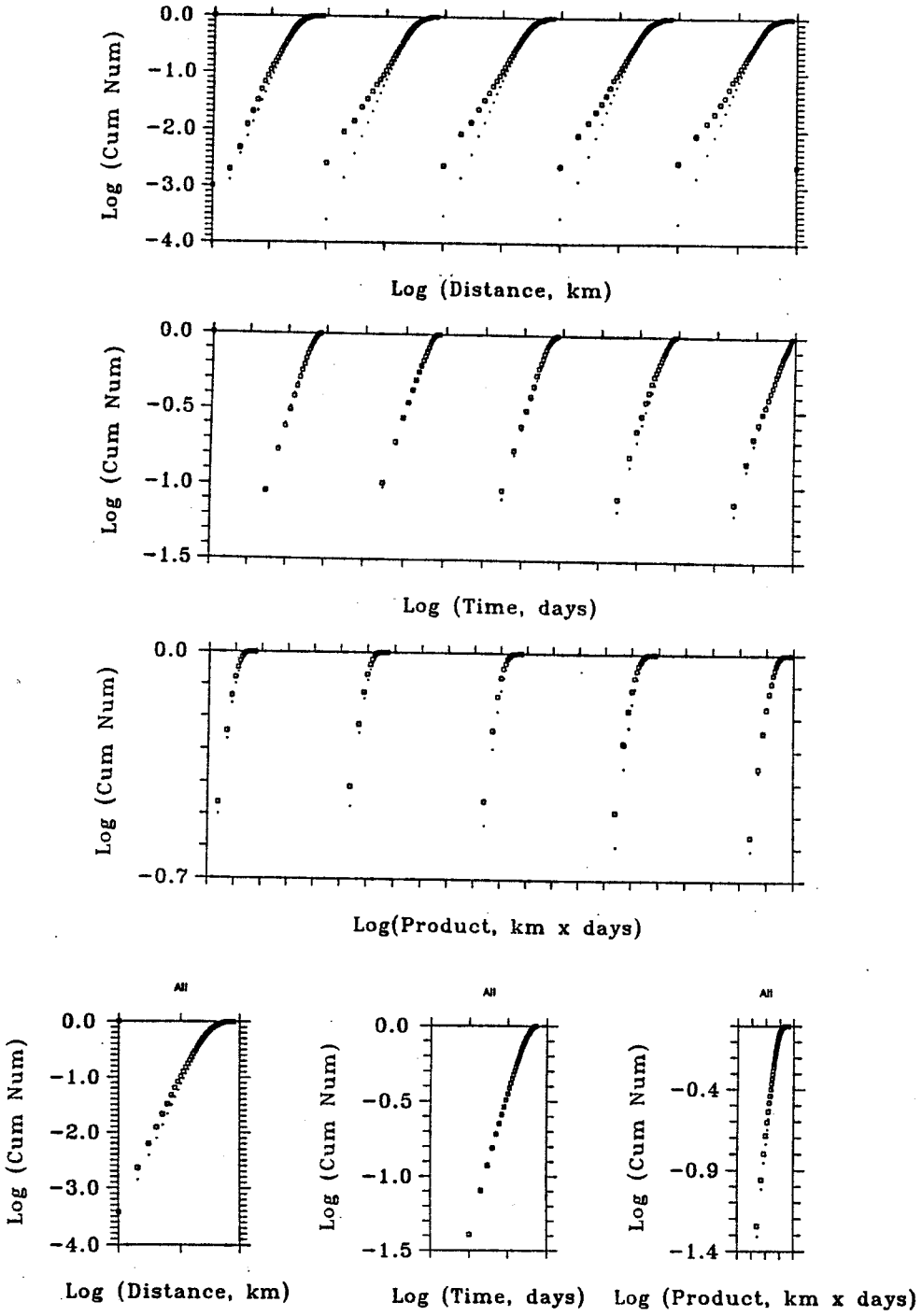

Figure 5.2.1 Correlation curves for the three types of interevent quantities studied. Group correlation curves for the interevent distances are shown in the top frame, for interevent times - in the second frame from top to bottom, and for products - third frame from top to bottom. Only correlation curves for the first five of the 27 groups are shown. Maximum distances, time intervals, and products spanned by groups are same as in Figures 4.4.1, 4.4.13, and 4.4.18, respectively. Plots on the bottom show the correlation curves for the distances (left), time intervals (middle), and products (right) obtained from the whole data set. Open squares mark curves derived from real data, dots mark curves obtained from random catalogues. Note that the difference between these is the largest for the interevent distances (top frame and bottom left plot).

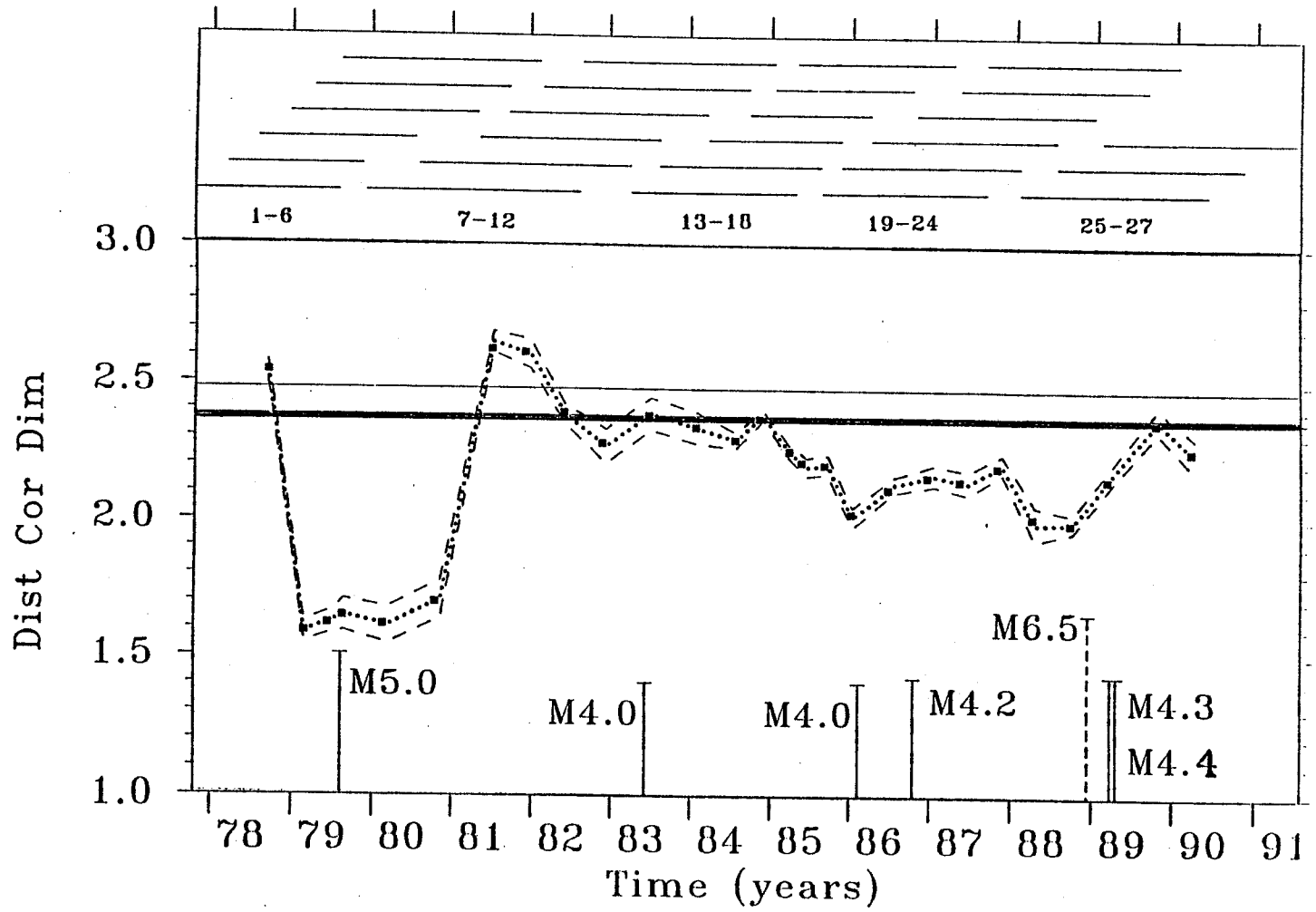

Figure 5.2.2 Temporal variation of spatial (distance) correlation dimension estimated in the 1-10 km distance range. Bold horizontal line at 2.38 represents the long-term correlation dimension estimated from the whole data set. Thin horizontal line at 2.48 marks the value of the correlation dimension estimated from randomly generated catalogues of 623 events. Dashed lines show standard deviations of the estimates of the short-term correlation dimensions. Remaining notations are the same as in Figure 4.4.2.

Figure 5.2.2 represent the standard deviations of the slopes in each group.

Similar to the results from pair analysis, it is most interesting to observe when the correlation dimensions are higher or lower than the value derived from the whole catalogue (2.376). Higher values are reached twice: for the only group preceding the 1979 M5.0 event and for a period after the end of the aftershock sequence of the same mainshock. Higher correlation dimensions presumably indicate smaller clustering or its absence. It is better to think about higher correlation dimensions as a relative lack of pairs on the left side of the scaling range, that is for the smaller distances in the 1-10 km distance range here. This appears to contradict the finding from the pair analysis that the degree of non-randomness for the 1-10 km range was relatively high before the M5.0 mainshock (see Figures 4.4.8 and 4.4.10). This difference, however, simply demonstrates the difference in the implications of the two types of analysis: the higher total relative number of pairs over the 1-10 km distance range before the M5.0 mainshock (from pair analysis), is apparently characterized by such a distribution within this range that relatively fewer pairs are at the bottom of the range than at its top. By contrast, Hirata (1989a) reported lower spatial correlation dimensions before a large event in Japan, as well as lower spatial correlation dimensions at the final stages before the destruction of laboratory specimens (Hirata et al., 1987). The results here do not support this author's findings. It must be noted, however, that the choices of the scaling regions are mostly subjective and variations in the way these choices are made may significantly influence the estimates. Pair analysis does not feature such type of subjectivity.

It is not surprising that the lowest values of correlation dimension (i.e., the highest degree of clustering) are reached for the groups that contain the M5.0 mainshock and its sequence. This observation demonstrates the capability of the correlation integral approach to account for clustering. The correlation dimension decreases by more than 30% for the 2-nd to the 6-th group, when compared with the correlation dimension for all ML $\geq$ 0.5 (MN $\geq$ 1.4) events. For example, with the baseline value of 2.38 and the correlation dimension of 1.59 for the second group, one gets a change of (2.38-1.59)/2.38) = 0.33 = 33%. For the same group, the degree of spatial non-randomness over distances up to three times larger (0-29 km) than the 1-10 km distance range here, changed by about 14% up from the long-term value (calculated from (33%-29%)/29% = 0.137, where 29% was the long-term value; see Figure 4.4.2). Similar estimate from the pair analysis of the 1-10 km distance range, the same one as here, shows even smaller change for the same (second) group, about 6%. This comparison shows that the correlation dimension approach depicts clustering at very small distances (such as the one associated with aftershocks) much better than pair analysis.

Most interesting are, however, the lowest values of correlation dimension (or the highest clustering) at other times when the cause is not so readily apparent. These are reached for the 23-d and the 24-th groups, which similarly to before, could be associated with the nearby M6.5 Saguenay event. Since the 25-th and the 26-th groups were identified as most anomalous from the pair analysis, the correlation dimension is perhaps somewhat earlier indicator of the possible association between the Saguenay event and the CSZ seismic activity. It is difficult to assess how significant this discrepancy is given the subjectivity in the choice of the scaling range.

Figure 5.2.3 compares the variations of the spatial correlation dimension for the original 27 groups (the same as in the previous figure) with the variations of the correlation dimensions after the ten aftershocks of the M5.0 main event are removed (open squares, solid line). When compared with Figure 4.4.11 demonstrating the same for the spatial non-randomness from pair

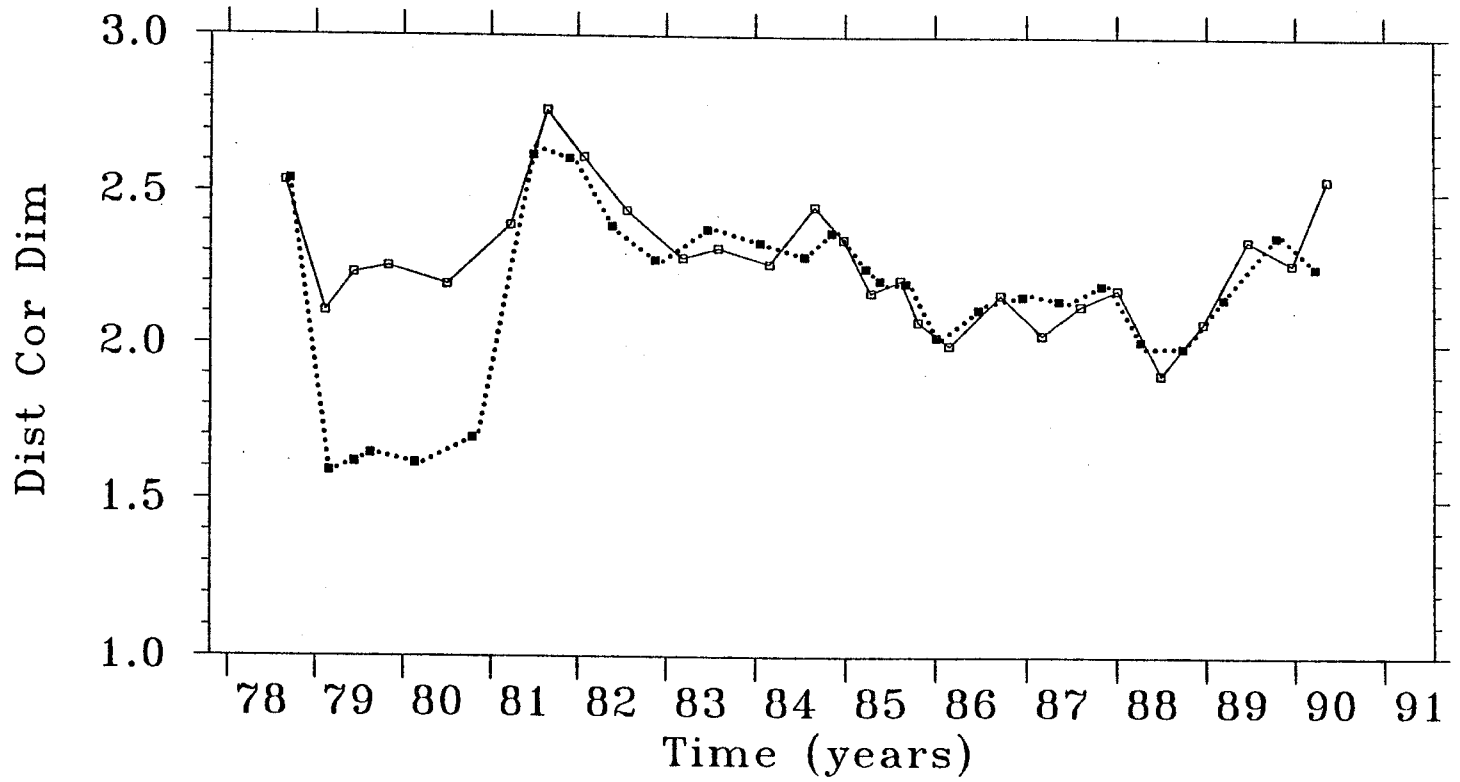

Figure 5.2.3 Temporal variations of the distance correlation dimension for the whole data set (filled squares, dotted line; same as in Figure 5.2.2) and with aftershocks of the M5.0 event removed (empty squares, solid line).

analysis, Figure 5.2.3 indicates a much larger difference. The clustering indicated for the 2-nd to the 6-th groups, i.e., the ones that originally included the sequence, is dramatically reduced (higher correlation dimensions) once the aftershocks are removed. The correlation dimensions for these groups are still lower than the long-term average, but the lowest values for this curve are around the time of the Saguenay event.

Figure 5.2.4 demonstrates the significance of the results by showing the variation curves for different choices of the number of events per group and the number of overlapping events. The choices for these variation curves are the same as in Figures 4.4.6 and 4.4.9. The character of the temporal changes of the spatial correlation dimensions is apparently preserved, although smaller clustering (higher correlation dimensions) are indicated for the groups including the aftershocks as the number of events per group increases.

B. Temporal and product correlation dimensions. Figure 5.2.5 is similar to Figure 5.2.2, but shows the temporal variations of the correlation dimensions for the times (upper frame) and for the products (lower frame). Similar to before, the thin horizontal lines show the estimates of the long-term values from the random catalogues and the bold lines show the baseline values from the whole data set. These estimates are made over scaling ranges which are different from the ones used for the groups. Unlike the spatial scaling ranges which were the same for the whole data set and for the groups, the extent of the groups in time is much smaller than the total time period and that changes drastically the position of the points of saturation of the correlation curves. The correlation curve for the time intervals from the whole dat set (see Figure 5.2.1) is calculated with a step of 100 days and appears to have a scaling range over the first 15 points, i.e., for time intervals smaller than 1500 days (equals 4.1 years which is about 1/3 of the whole period). The long-term correlation dimension estimated from this scaling range is 0.927 ± 0.006 for the real data set and 0.943 ± 0.006 for the random data set. The observed dimension is smaller than the one estimated from the random data by only 1.7%; the long-term temporal clustering indicated is therefore very weak (if at all present). It is impossible to use the same scaling range for the groups. The group correlation integrals were calculated with a step of 30 days. The correlation curves observed indicate that an appropriate scaling range to use is perhaps the one over the first six points, i.e., for time intervals smaller than 180 days. Some curves have longer scaling ranges because of the variations in the length of the group periods. The minimum scaling range is used for the sake of comparison between the groups. It appears that the short-term estimates fluctuate around the long-term one, although the scaling regions used are 0-6 months for the groups and 0-4.1 years for the whole period. This shows that the scaling over the shorter time intervals seem to be very similar to the scaling over the larger time intervals. The variation of the short-term values appears very slight, and similar to the pair analysis, one may conclude that the time intervals alone are quite uninformative.

The long-term correlation integral for the products (Figure 5.2.1) is calculated with a step of 2500 km x days. The scaling region appears to be over the first 10 points of the curve, i.e. for products smaller than 25000 km x days. The correlation dimension over this range is 0.879 ± 0.012 for the real data set and 0.910 ± 0.010 for the random data set; a clustering is indicated for the real data, but the decrease of the long-term correlation dimension for the real data is 3.4% from the one for the random data (intermediate between the decrease for the distances and for the time intervals, as could be expected). The scaling region for the group correlation integrals

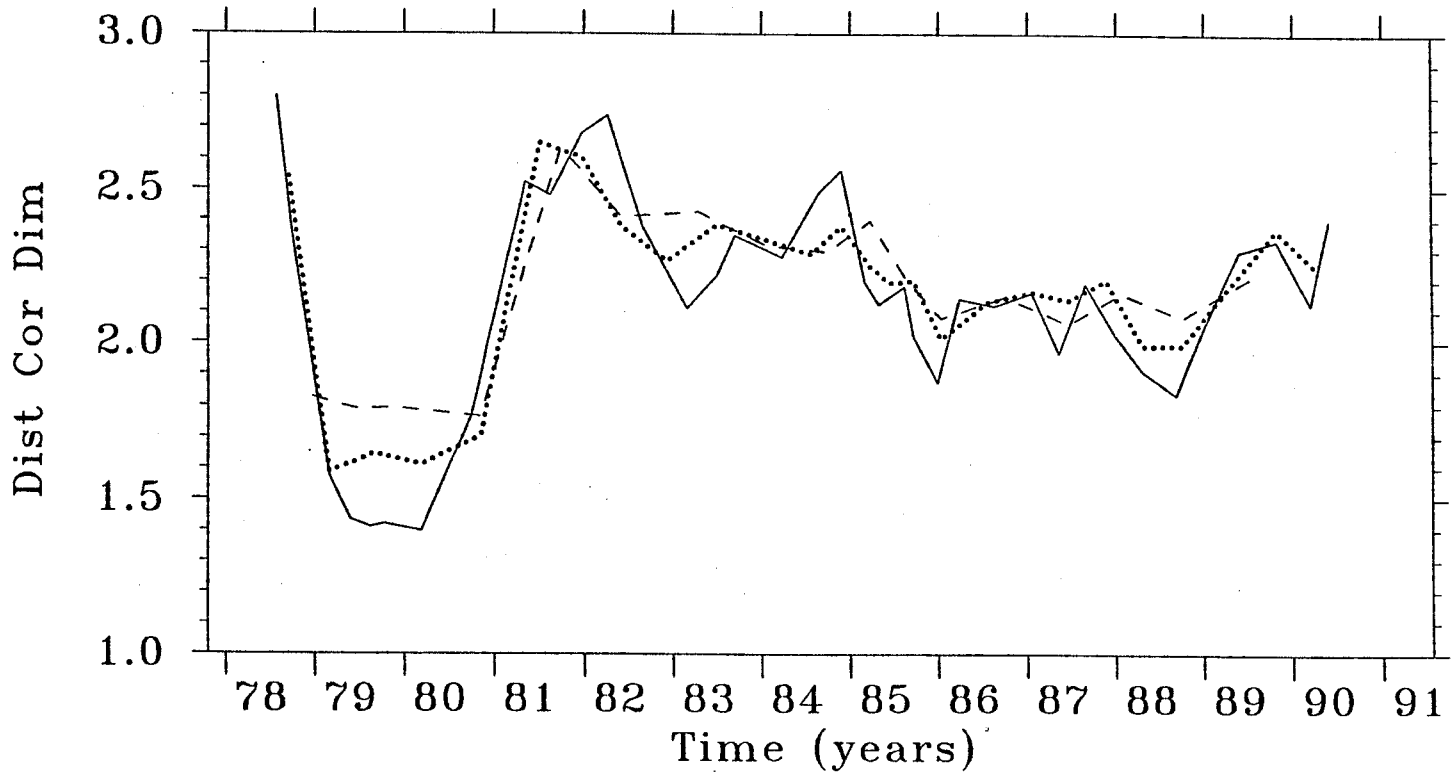

Figure 5.2.4 Temporal variations of the spatial correlation dimension for different choices of the number of events per group and number of overlapping events. Choices are the same as in Figures 4.4.6 and 4.4.9: 100 events per group and 80 overlapping events (dotted line, same as in Figure 5.2.2); 80 events per group and 65 overlapping events (solid line); and 120 events per group, 90 overlapping events (dashed line).

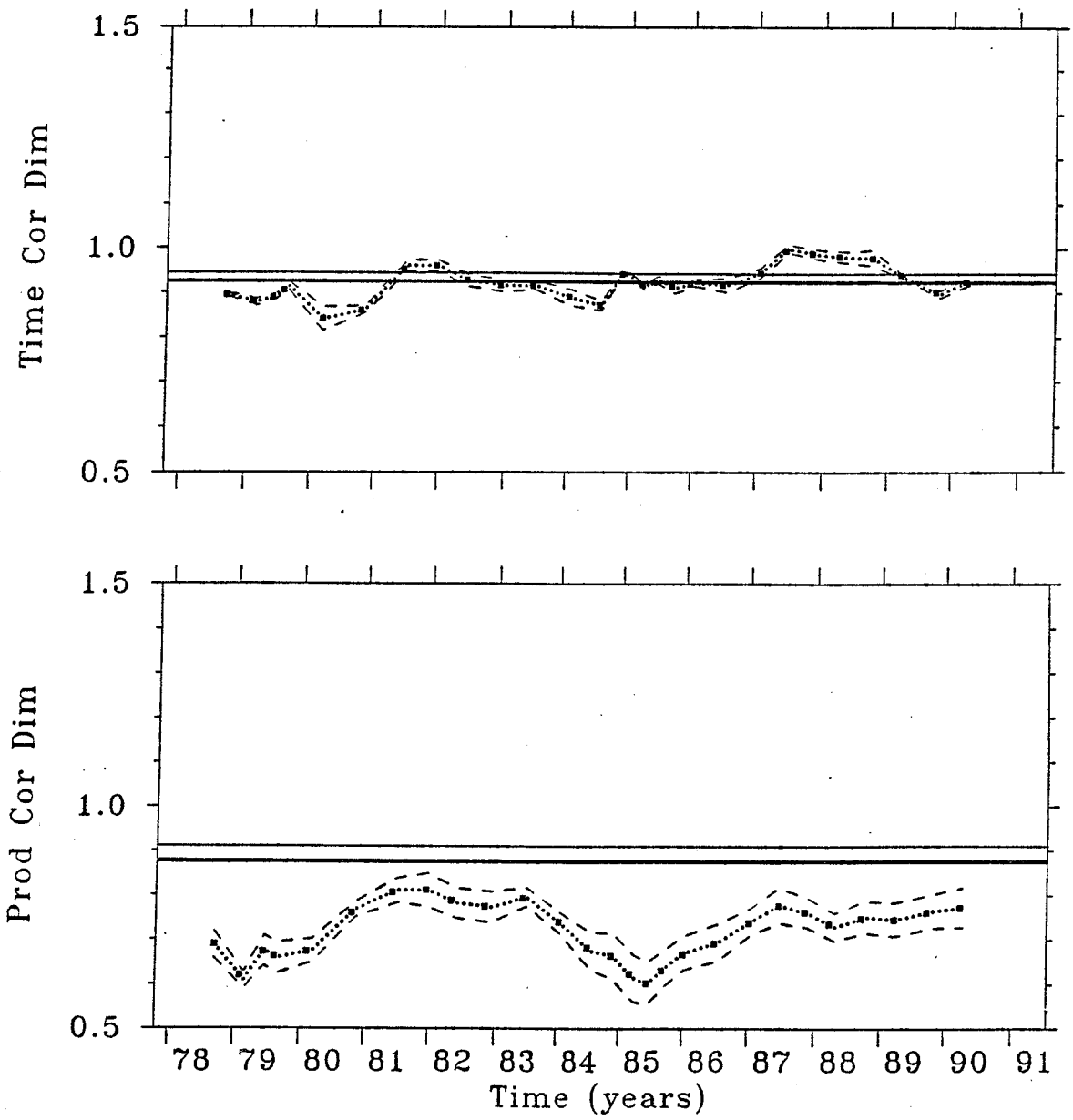

Figure 5.2.5 Temporal variations of the correlation dimensions for the interevent times (upper frame) and the interevent products (lower frame). Bold and thin horizontal lines as in Figure 5.2.2 (long-term correlation dimension from the whole data set and from randomly generated catalogues, respectively). Dashed lines mark standard deviations of the group correlation dimensions. See text for more details.

appears to be much smaller - only over the first three points (see Figure 5.2.1), i.e. for products smaller than 7500 km x days. It is doubtful how reliable the correlation dimensions estimated for such small scaling range are. The short-term values all fall below the long-term value. This hardly indicates, however, that the clustering is always higher for small products than for the larger ones; most probably the narrow scaling range used already includes elements of saturation which makes the slopes smaller.

These results indicate that in this type of approach, similar to the pair analysis, distances seem to be most informative.

5.3 Scatter Plots

The following figures show various scatter plots of the group correlation dimensions versus the quantities studied. Most of these do not indicate such correlations, but they are presented here for the sake of completeness. Figure 5.3.1 shows scatter plots showing the three types of correlation dimensions versus each other. No correlation appears to exist between the distance and the time correlation dimension, i.e., there is no evidence for connection between the clustering in space and in time. In view of the insignificant variation of the correlation dimension for the time intervals, this is expected. It appears that the other two plots, examining the product correlation dimension versus the other two types of correlation dimensions do indicate slight positive correlation. This is not surprising either, since the products by definition are not independent of the distances and the time intervals. In fact, it is more surprising that the correlation is so weak; this must be due to the specific interplay of the scaling ranges for the three types of correlation curves.

Figure 5.3.2 shows scatter plots of the group correlation dimensions versus the degrees of non-randomness estimated from pair analysis. The two top plots show the spatial non-randomness over the 1-10 km and 0-29 km distance ranges versus the spatial correlation dimension. There appears to exist a negative correlation between the correlation dimension and the degree of non-randomness over the 1-10 km distance range. Since this distance range is the same as the scaling range for the correlation curves, such a correlation is to be expected; both higher degrees of non-randomness (from pair analysis) and smaller correlation dimensions generally indicate larger clustering. The differences between the pair analysis and the correlation dimension approach, however, make this relationship not very prominent. The two plots on the bottom of this Figure show the time non-randomness versus the time correlation dimension and the product non-randomness versus the product correlation dimension. The ranges over which the degrees of non-randomness were estimated (< 90 days and < 2500 km x days) are, however, different from the scaling ranges used for the correlation dimensions (< 180 days and < 7500 km x days, respectively). No connection between these quantities is indicated by these scatter plots.

Figure 5.3.3 displays scatter plots of the three types of correlation dimensions versus the length of group periods. Some correlations with the group period were observed before (see Figures 4.4.12, 4.4.21, and 4.5.3). Here again an unexpected correlation is observed. While the distance and time correlation dimensions do not show any correlation with the length of the group period, the product correlation dimension seems to be positively correlated with the group period. This is the first time when the combination of the distances and the time intervals (i.e., the products) indicates a feature which is not suggested by either the distances or the time intervals alone. In fact, this is perhaps the strongest correlations observed by comparison with

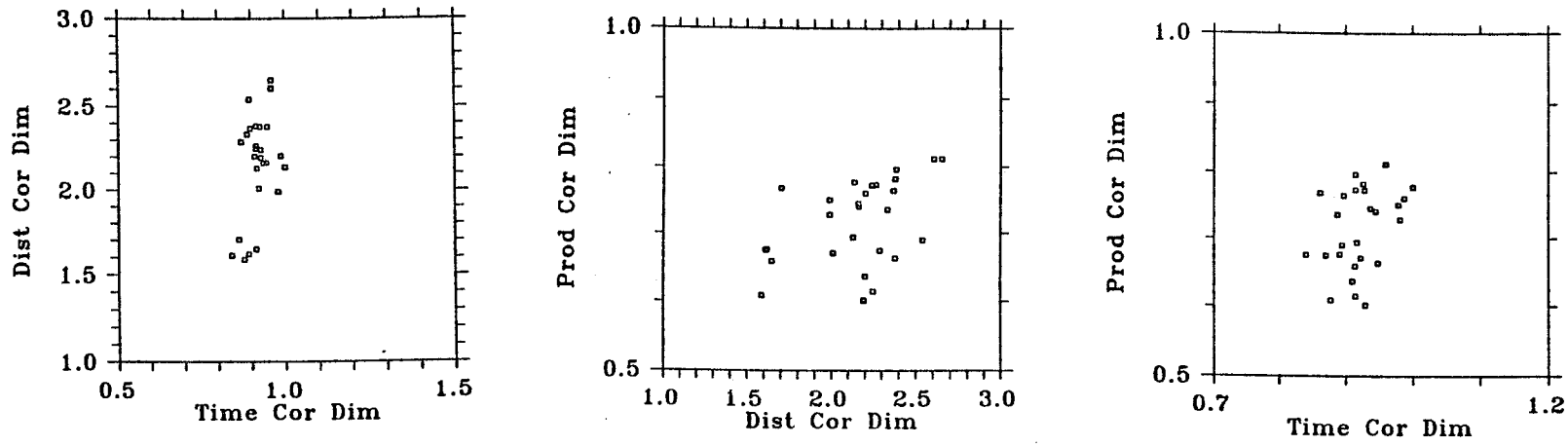

Figure 5.3.1 Scatter plots relating the three types of group correlation dimensions. From left to right: distance versus time correlation dimensions; product versus distance correlation dimensions; and product versus time correlation dimensions.

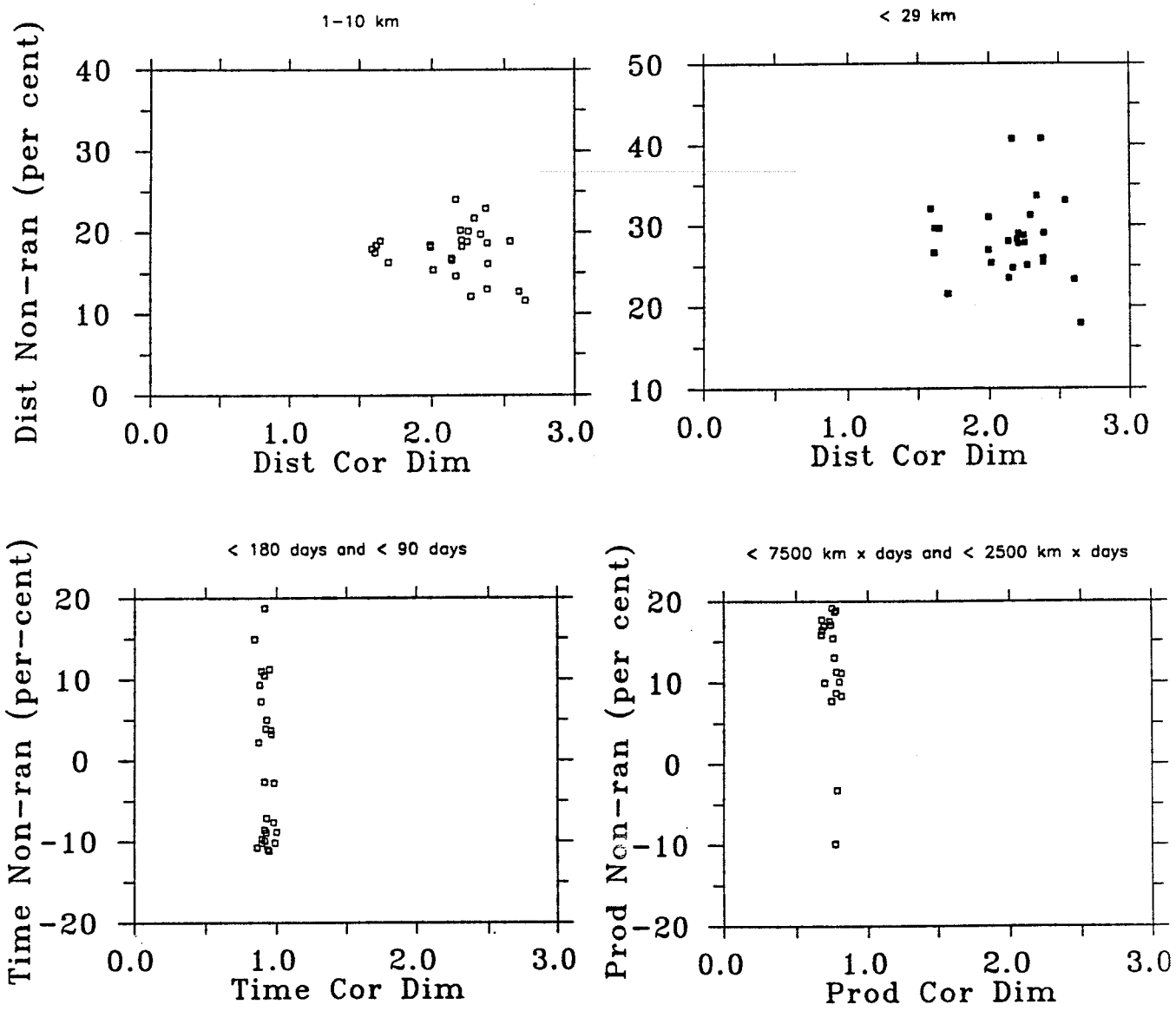

Figure 5.3.2 Scatter plots relating the three types of group degrees of non-randomness with the three types of group correlation dimensions. Two upper frames show spatial non-randomness in the distance ranges 1-10 km (left) and 0-29 km (right) versus distance correlation dimension. Lower frames show non-randomness of time intervals (left) and products (right) versus their respective correlation dimensions.

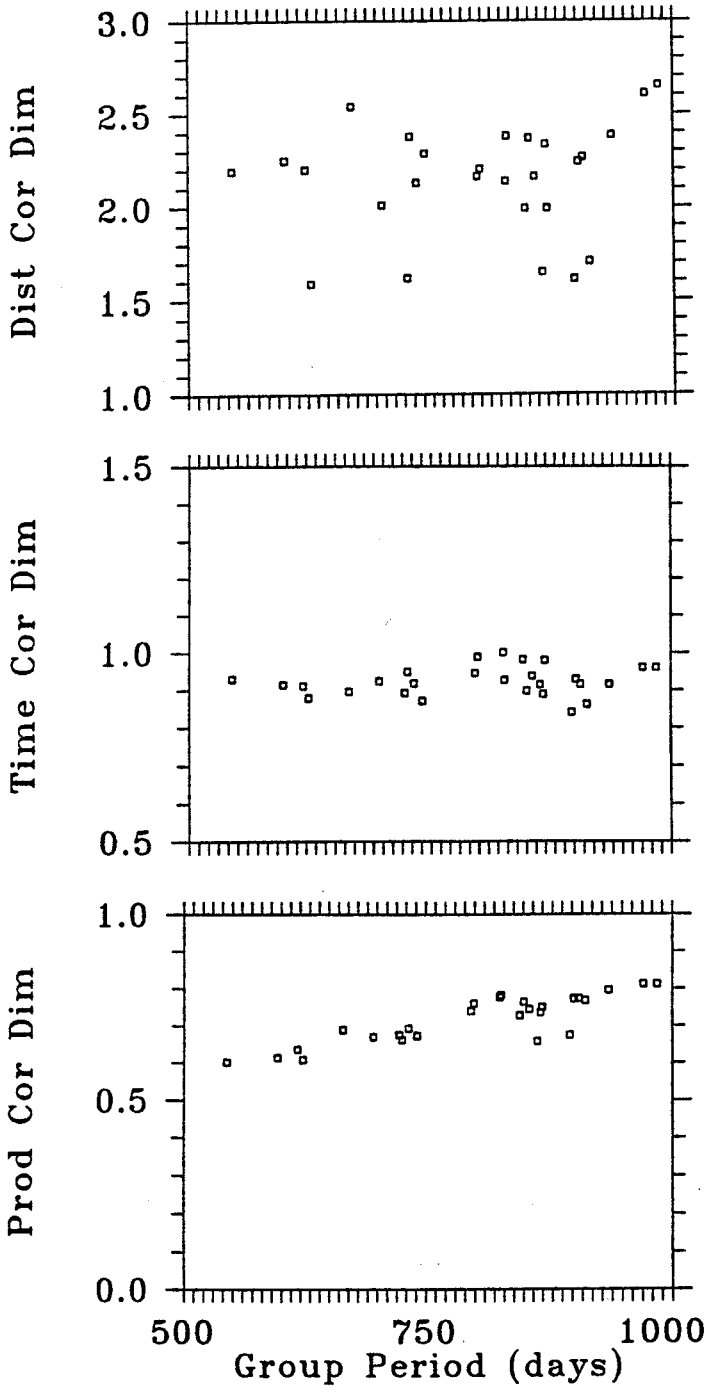

Figure 5.3.3 Scatter plots of the three types of group correlation dimensions versus length of group period. From top to bottom: spatial correlation dimensions, correlation dimensions of time intervals, and correlation dimensions of products.

all other scatter plots. This points to some hidden information that could not be revealed until now. At this point, it is unclear why when the events are more frequent (shorter group periods), the product correlation dimensions are smaller and therefore indicate more clustering in terms of products (this does not necessarily mean more spatial and temporal clustering). The scatter plot of the product non-randomness (from pair analysis) versus the group periods also indicated such correlation (see Figure 4.4.21), but it is a natural consequence of the spatial non-randomness being correlated with these periods (Figure 4.4.12). An alternative explanation here, is that this is an artifact of the way the correlation dimensions were measured. The correlation curves must saturate earlier for shorter group periods. The smaller correlation dimensions for smaller periods may be, therefore, caused by this saturation, although the curves look straight over the scaling range used for all groups. In contrast, results from pair analysis (Figures 4.4.12 and 4.4.21) are not subject of such artifacts.

Finally, Figure 5.3.4 shows scatter plots of the group b-values versus the three types of correlation dimensions. No correlation is observed between the spatial dimension and the b-values; this contradicts the results discussed by Hirata (1989a) who did find such a correlation between the same quantities. Only the product correlation dimension seems to be negatively correlated with the b-values; again a result that was not suggested by either the distance or the time correlation dimensions alone. This correlation may be, however, due to the correlation observed between the b-values and the group periods (see Figure 4.5.3). Since some doubts were expressed then about the validity of this correlation, as well as about the correlation between the product dimension and the group period (Figure 5.3.4), the same now concerns the validity of the correlation between the product dimension and the b-values.

CHAPTER 6. SOME OTHER APPLICATIONS

Several additional techniques and displays were attempted in the study of the space-time distribution of earthquakes in the CSZ. None of them provided much of an insight into this distribution. This may be, however, more a consequence of the insufficient development of these techniques rather than intrinsic lack of capabilities in this respect. For this reason, these attempts are briefly described here in the hope that at least some of them may be pursued more successfully in the future.

6.1 Randomized Catalogues and Distance-Time Interval Plots

The idea of using "randomized" catalogues for reference rather than the "random" catalogues described above stemmed from the realization that it may be conceptually better to somehow compare the observed catalogues with themselves in an averaged state rather than with arbitrary, randomly generated catalogues. For this reason, a randomization procedure was applied to the observed catalogue of the same 623 events as before ($ML \geq 0.5$, i.e., $MN \geq 1.4$). This procedure involved random shuffling of the earthquake locations, while preserving both the temporal and the spatial structures of the catalogue. If there is any relation between the spatial and the temporal structures of the data, the randomization destroys it. Technically, the times were kept the same, however the hypocentral locations assigned to them were different from the original ones. Still, these locations were derived from the real catalogue; i.e., they had really

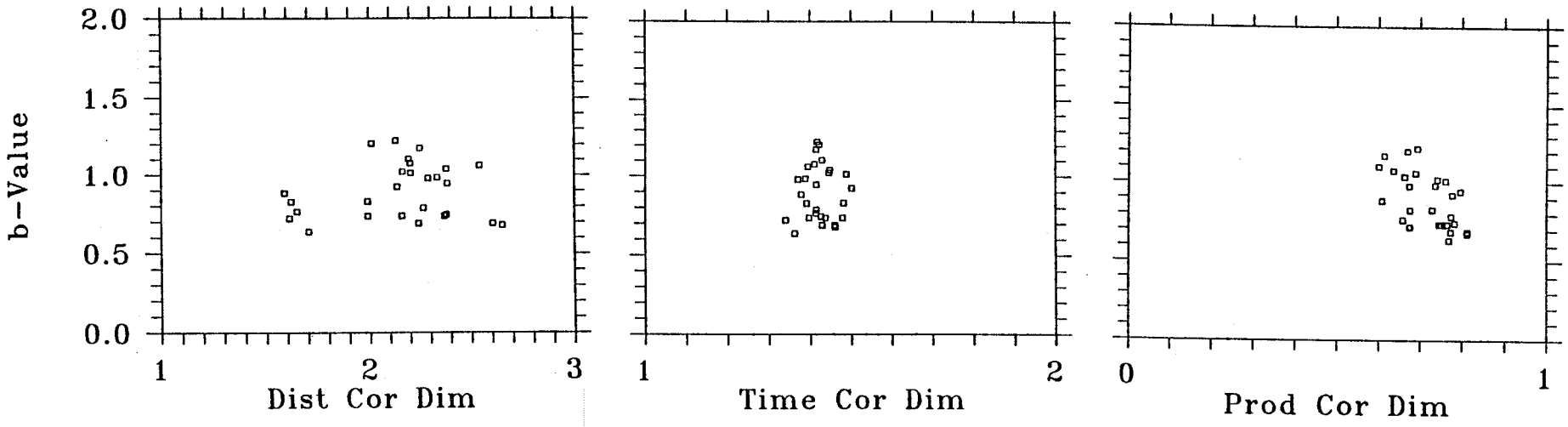

Figure 5.3.4 Scatter plots of group b-values versus the three types of group correlation dimensions: distance correlation dimension (left), correlation dimension of time intervals (middle), and product correlation dimension (right).

occurred at one time or another. Displays showing only the temporal distribution of earthquakes or only their hypocentral distribution (e.g., epicentral maps and cross-sections) would be identical for the real and the randomized catalogue. Only displays showing space and time together (e.g., space-time plots) would be different for the two types of catalogues. Figure 6.1.1 shows space-time plots along the XX' profile (see Figure 4.2.2) for the observed catalogue (top frame) and the randomized catalogue (bottom frame). An easy reference is the M5.0 event which is marked with the largest cross in the upper left corner of the space-time plot for the observed catalogue. Its aftershocks clustered around this event are also easily seen. In the randomized space-time plot, the location of the M5.0 event became randomly shifted and assigned to an existing origin time sometimes in 1985. Other applications of the randomization procedure (i.e., using different seeds) would place the same event at some other times. In all cases, however, the cluster visible in the observed space-time plot will be disintegrated. This example illustrates what happens to all remaining events.

Since the distributions of distances alone or time intervals alone are the same for the real and the randomized catalogues, only a technique mixing the time intervals and the distances has the potential to reveal any significant differences between the two types of catalogues. There are many ways this can be done, but only one approach is illustrated here. The distances of all events in a catalogue to an arbitrary point can be plotted against the time intervals between all events and the time assigned to this point. Such plots would exhibit differences between the randomized and the real catalogues. The arbitrary point can be chosen to be a major event that have already occurred, the site of an expected future event, or a set of distance-time interval plots like this can be obtained for a grid of points covering an area of interest. Figure 6.1.2 shows an example when this point is chosen to coincide with the M5.0 local event. The top frame shows a distance-time interval plot for the real catalogue, while the bottom plot shows the same type of plot for the randomized catalogue. Only distances up to 20 km are shown along the vertical axes. All events occurring before the M5.0 event are characterized by negative time intervals. The point at 0 distance and 0 time interval in the top frame simply shows the position of the M5.0 event, since it coincides with the point from which all distances and time intervals are measured. Since the randomization shifts the M5.0 event to another origin time, the bottom plot features a point at 0 distance with a non-zero time interval (2200 days for this particular randomized catalogue). This is due to the fact that the time of the arbitrary point remains the same, while the randomized time of the M5.0 event is different from the original one. Because of the disintegration of the earthquake clusters after the randomization procedure, one obvious difference between the two frames is the cluster of small epicentral distances and small time intervals (outlined with a heavy line) in the plot for the real catalogue and the absence of this cluster for the randomized catalogue.

The idea of examining such plots is to compare the neighbourhoods around the (0,0) point of these two types of plots; significant differences may indicate some precursory conditions in the real catalogues. For example, a precursory quiescence would be indicated by lack of points in the vicinity of the (0,0) point for negative time intervals, when the plots for the real and the randomized catalogues are compared. Figure 6.1.2 does not indicate, however, any significant difference in the present case. It would be necessary to devise some quantitative methods for such comparisons to be reliably performed. These methods should involve a comparison with many randomized catalogues, not with just one randomized data set (as the example in Figure 6.1.2).

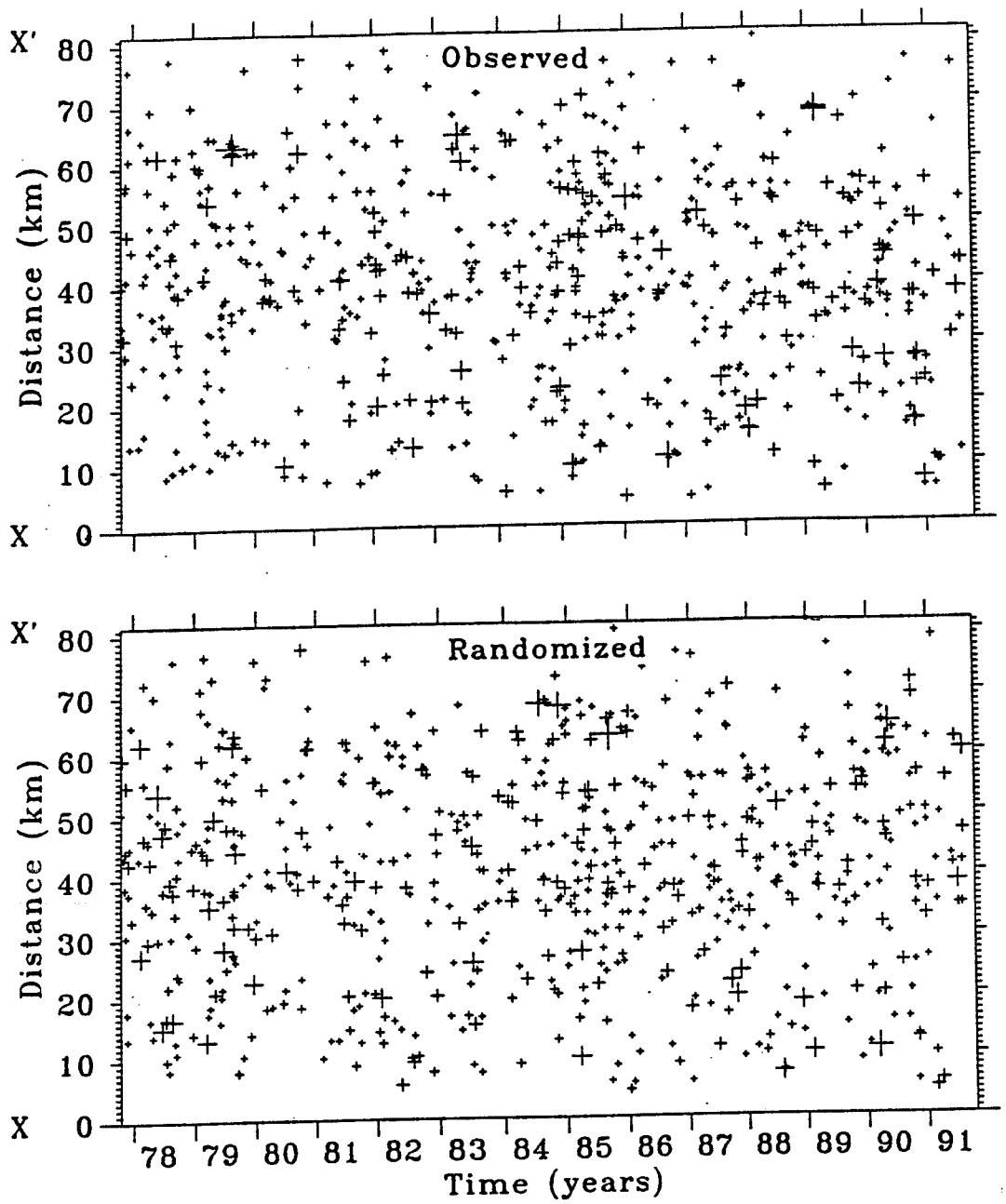

Figure 6.1.1 Space-time plots of the observed catalogue (upper frame) and of a randomized catalogue (lower frame). Distance along profile XX' from Figure 4.2.1 is along the vertical axes. See text for more detail.

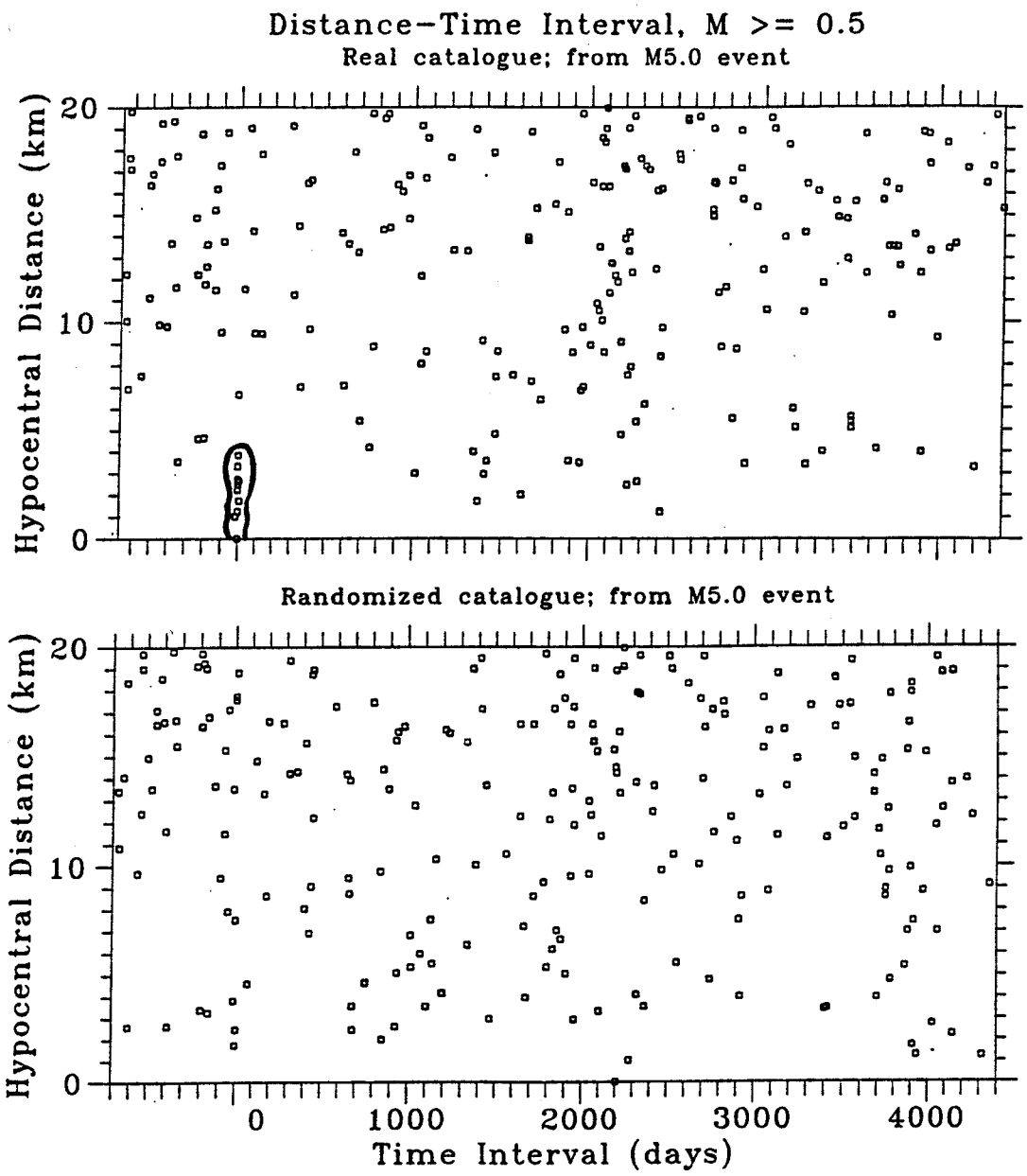

Figure 6.1.2 Plots of distances versus time intervals between all ML $\geq$ 0.5 (MN $\geq$ 1.4) events and the M5.0 earthquake. Real catalogue featured in the upper frame, randomized catalogue - in the lower frame. Area marked with solid line in the top frame outlines the aftershocks of the M5.0 event. Note that this cluster disintegrates in the randomized catalogue.

Figure 6.1.3 shows the same types of plots with a different scale: distances up to 60 km are shown along the vertical axes and time intervals up to 400 days before and 400 days after the (0,0) point are shown along the horizontal axes. The top and the middle frame depict the same types of plots as the previous figure; i.e., from the observed and the randomized catalogues, when the arbitrary point from which the distances and the time intervals are measured coincides with the M5.0 event. The bottom frame shows a distance-time interval plot for the real catalogue with an arbitrary point chosen at location and time different from the M5.0 event. The purpose is to compare the vicinity of the M5.0 event with the vicinity of whatever other point in the real catalogue. The difference between the top and the bottom plots does not seem to be more statistically significant than the difference between the top and the middle plots in terms of precursory information. It appears that the area outlined with the dashed line in the top frame, presumably representing the volume that was "quite" before the M5.0 event, is larger than the respective areas outlined in the middle and the bottom frames. This is, however, only a qualitative observation that may not be statistically significant here. In fact, this observation is a long way from a comparison with many randomized catalogues or distance-time interval plots obtained from the real catalogue for a number of arbitrary points. Yet, the potential of this approach is hopefully well demonstrated by these figures; the differences in the case of larger events may be much more dramatic.

It may be that more information is hidden in the magnitude distribution in the vicinity of the M5.0 event, than in the spatial and the temporal distribution. Looking at the magnitudes of the events which occurred within 5 km from the M5.0 mainshock at any time during the study period, some potentially important information is revealed. These events appear as points at distances 5 km or smaller in the top frames of Figures 6.1.2 and 6.1.3. The size of an area of 5 km radius is about 3% of the total area of the CSZ. The percentages of events of different magnitudes that occurred in this small area are as follows: 4.2% of the ML $\geq$ 0.5 events (26 out of 623); 4.4% of the ML $\geq$ 1.5 events (11 out of 250); 9% of the M $\geq$ 2.5 events (7 out of 77); and 67% of the M $\geq$ 4.0 events (4 out of 6). In addition, there have not been any events of magnitudes between 2.6 and 3.9 in this spot. All this suggest a strongly preferential distribution of the magnitudes of the occurring events in the vicinity of the M5.0 event. Stevens (1980) had previously pointed out that all larger events occurred either in this part of the CSZ or at its opposite end. The neighbourhood of the M5.0 event is, therefore, quite distinct and may be the spot of a future significant earthquake.

In summary, distance-time interval plots of the types presented here, combined with the event magnitudes, as well as the use of randomized catalogues, may be useful in the search for precursory phenomena. An appropriate technique should be, however, quantitatively developed and tested.

6.2 Randomized Catalogues and Difference Maps

The correlation integral technique used in the previous Chapter is widely used in non-linear dynamics to analyze strange attractors and to estimate their fractal dimensions. Other applications borrowed from non-linear dynamics may be also useful in analyzing the space-time distribution of earthquakes. One of these are the so-called difference maps. Figure 6.2.1 illustrates their use (after Fowler and Roach, 1991). A randomly generated time series of values from X_0

to X_{300} cannot be distinguished from the time series of values obtained from a logistic equation (that is, calculated in a deterministic way). In contrast, plots featuring the differences between these values, such that $X_{n+2} - X_{n+1}$ is plotted versus $X_{n+1} - X_n$ for n = 0 to 299, indicate a large difference between these time series.

Figure 6.2.2 shows plots of the distance between the (i+2)-th and the (i+1)-th event (Dist(i+1) in the Figure) versus the distance between the (i+1)-th and the i-th event (Dist(i) in the Figure), where i runs from 1 to 621 for the CSZ catalogue of 623 events. Each difference map consists of 622 points. Three difference maps are shown: for the real catalog, for one randomized catalog, and for one random catalogue. The order in which the epicentres occur in the randomized catalogue is different from the real catalogue, hence the difference map for this catalogue is not the same as the one for the real data. Only those parts of the difference maps are shown that feature distances 30 km or smaller. One obvious feature is that there are more points at smaller distances along both axes for the real catalogue than for the randomized one, while points are almost absent from the same part of the plot for the random catalogue. These points indicate small distances followed by small distances. Similar to before, the cluster in the bottom left corner for the real catalogue apparently got disintegrated in the randomized plot. The number of points in these plots is as follows: 329 for the real catalogue (about 53% of all 622 points); 306 for the randomized data (about 49%); and 238 for the random catalogue (about 38%). This apparently indicates more spatial clustering for both the real and the randomized catalogues by comparison with the random data, which is to be expected on the basis of the results discussed in earlier chapters. If one looks in the square with vertices (0,0), (0,10), (10,10), and (10,0), this same result is even more enhanced for smaller distances: 11% of all points from the real plot are in this square (36 out of 329); 6% of the points from the randomized plot (19 out of 306); and about only 1% in the random plot (3 out of 238). While differences for points representing small distances followed by small distances are easily expected when the three types of catalogues are compared, some features that are not easy to explain are also observed. For example, stripes parallel to the axes and having width of 5 km, also suggest differences between the plots for the three types of catalogues. These include the distances following distances of 5 km or smaller (along the vertical axis), as well as the distances that were followed by distances 5 km or smaller (along the horizontal axis). These stripes contain about 24% of the points for the real catalogue (78 out of 329), 13% of the points for the randomized data (40 out of 306), and less than 8% of the points from the random data (18 out of 238). If the points representing obvious clusters (for which small distances follow small distances) are removed, these percentages become 16%, 13%, and 8%, respectively. They still indicate that small distances are followed by larger ones and large distances are followed by small ones more frequently in the real data than in the randomized catalogue, and especially than in the random catalogue. This is an intriguing feature that deserves a more controlled study. These are only a few examples of the potential such studies may have.

The difference plots above do not indicate the order in which these points occur. Examining this order could provide an insight about the development of the dynamic system associated with the earthquake process. Figure 6.2.3 shows examples of the same type of difference maps as in the previous figure, however, the points are connected with lines tracing the trajectory describing the development of the system in time. The frame on the left shows a difference map for the first 21 events (20 points) in the real catalogue. The frame on the left

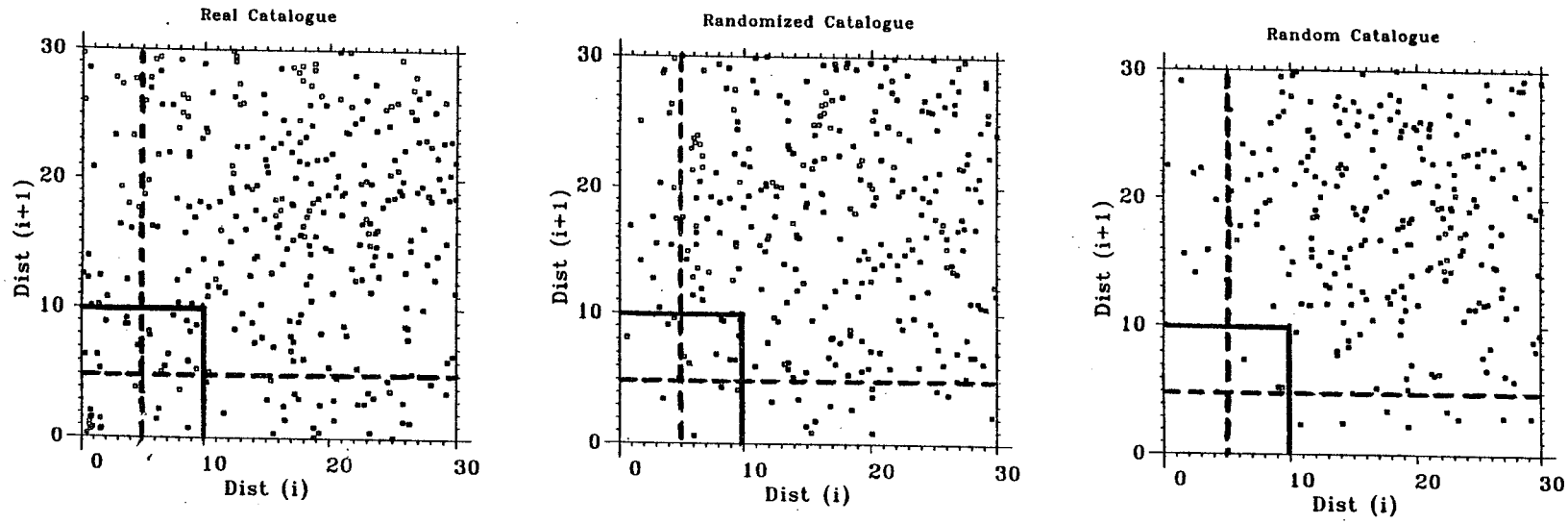

Figure 6.2.2 Difference plots showing distance between events (i+2) and (i+1) versus distance between events (i+1) and i. From left to right: real, randomized and random catalogues. Solid lines outline the region of distances $\leq$ 10 km preceded or followed by distances $\leq$ 10 km. Dashed lines mark the regions of distances followed or preceded by distances $\leq$ 5 km.

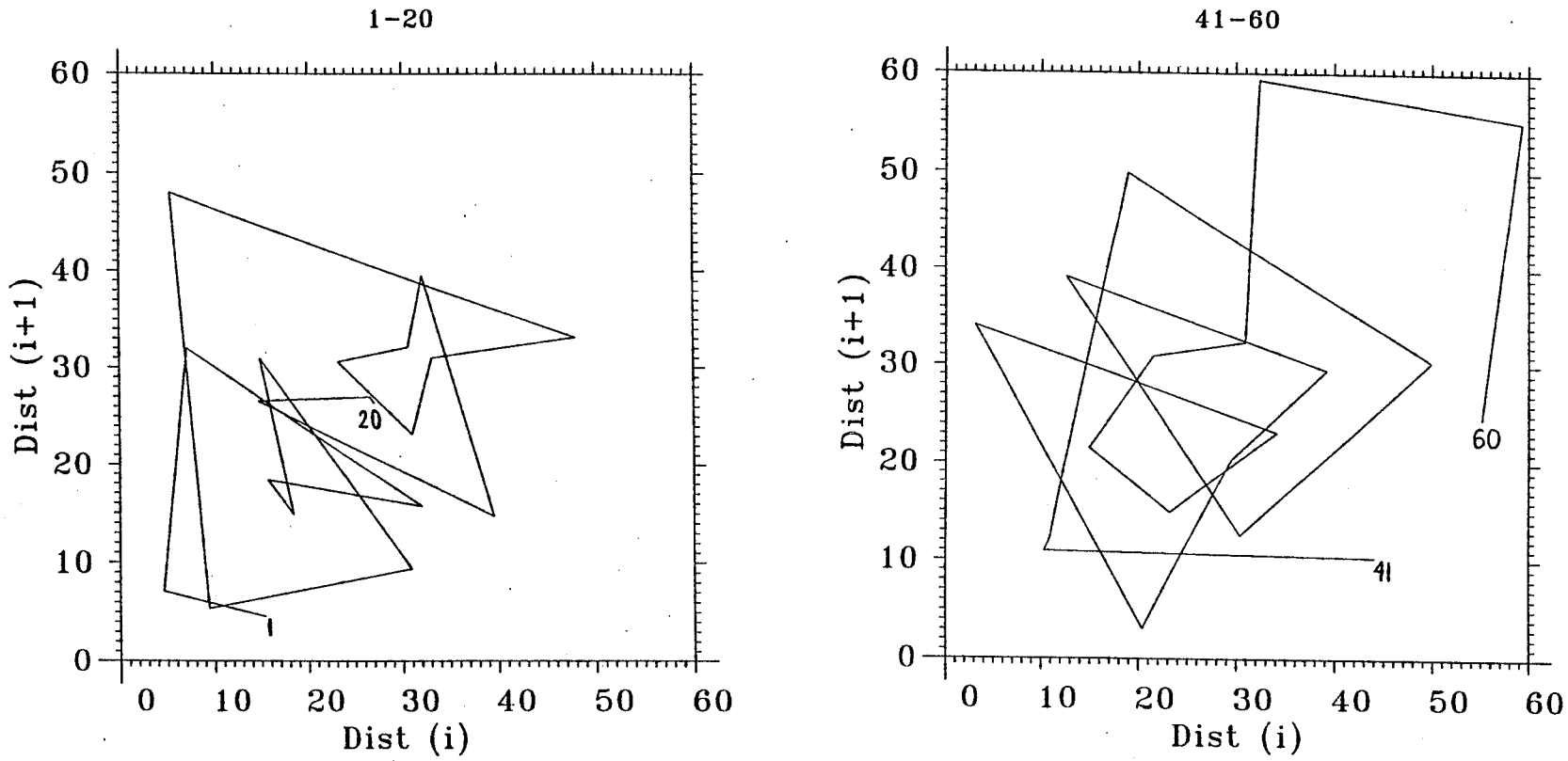

Figure 6.2.3 Examples of distance plots showing the order in which distances occur. Sequential numbers of the pairs of successive events used in these plots are shown on the top of these plots. See text for more details.

represents an example of another 20 points derived from the distances between the successive events from the 41-st to the 61-st. All these occur before the M5.0 event (102-th in the catalogue). Such trajectories are studied when strange attractors are analyzed. Hopefully some techniques can be borrowed and applied to earthquakes as well. These trajectories are shown only for the sake of insights for further study and are not analyzed here.

6.3 Other "Next" Parameters

Interevent distances, time intervals and products for events successive in time were examined in 4.6. Other parameters characterizing the distribution of such "next" events can be also considered, such as depth differences and magnitude differences. Figure 6.3.1 shows these differences versus sequential number of pair; the total number of the "next" pairs is 622 from 623 events. The arrows indicate the times of occurrence of the M5.0 event, the Saguenay event and of the $M \geq 4.0$ local events. A M4.0 earthquake (the one after the M5.0 mainshock) is followed by events exhibiting a distinct pattern of similar depths and similar magnitudes; i.e., events with small depth and magnitude differences. Figure 6.3.2 shows the same plots, but a larger scale is used in order to more clearly display the vicinity of this M4.0 event (only the "next" pairs between the 200-th and the 400-th are shown). The pattern is more distinct in the magnitudes (upper right frame). One could assume that this is perhaps a swarm of events following each other in a fast sequence and having similar locations. The bottom frames, however, show that this is not the case. They depict the hypocentral distances and the time intervals between the "next" events. The hypocentral distances for the events following the M4.0 event in question are not at all small; they vary between 4 km and 50 to 60 km. Some of the time intervals for the same events are small, but others are larger than 10 days. All in all these events are not a swarm of activity concentrated in space and time. It is not clear what the significance of this observation is and whether this is not simply a peculiar coincidence. In case it is not, it is certainly an interesting feature deserving a further study.

CHAPTER 7. CONCLUSIONS AND RECOMMENDATIONS FOR FURTHER STUDY

The Charlevoix seismic zone (CSZ) is the most seismically active area in eastern Canada. It has repeatedly been the site of events with magnitudes about 6 and larger and is the likely site for a future large event. Previous studies of various geophysical parameters have not revealed any precursory information. In particular, the earthquake catalogue featuring the CSZ microseismic activity in the period October 20, 1977 - July 31, 1991, fails to indicate precursory changes in rates of seismic activity (number of events per unit time) and b-values (the slopes of the magnitude-frequency relationships). In contrast, there have been numerous reports of changes in these parameters prior to moderate and/or large events in other seismically active areas. The CSZ catalogue for the study period is the most complete to date and features microearthquakes down to negative magnitudes. Given that even this detailed catalogue did not yield any information for precursory changes, one may become quite discouraged about the usefulness of seismicity data. The largest local event that occurred in the study period, however, is only of M5.0 and took place too early (August 1979) for an extensive monitoring to be carried out before its occurrence. Precursory changes, therefore, may still be observed before future events of larger magnitudes.

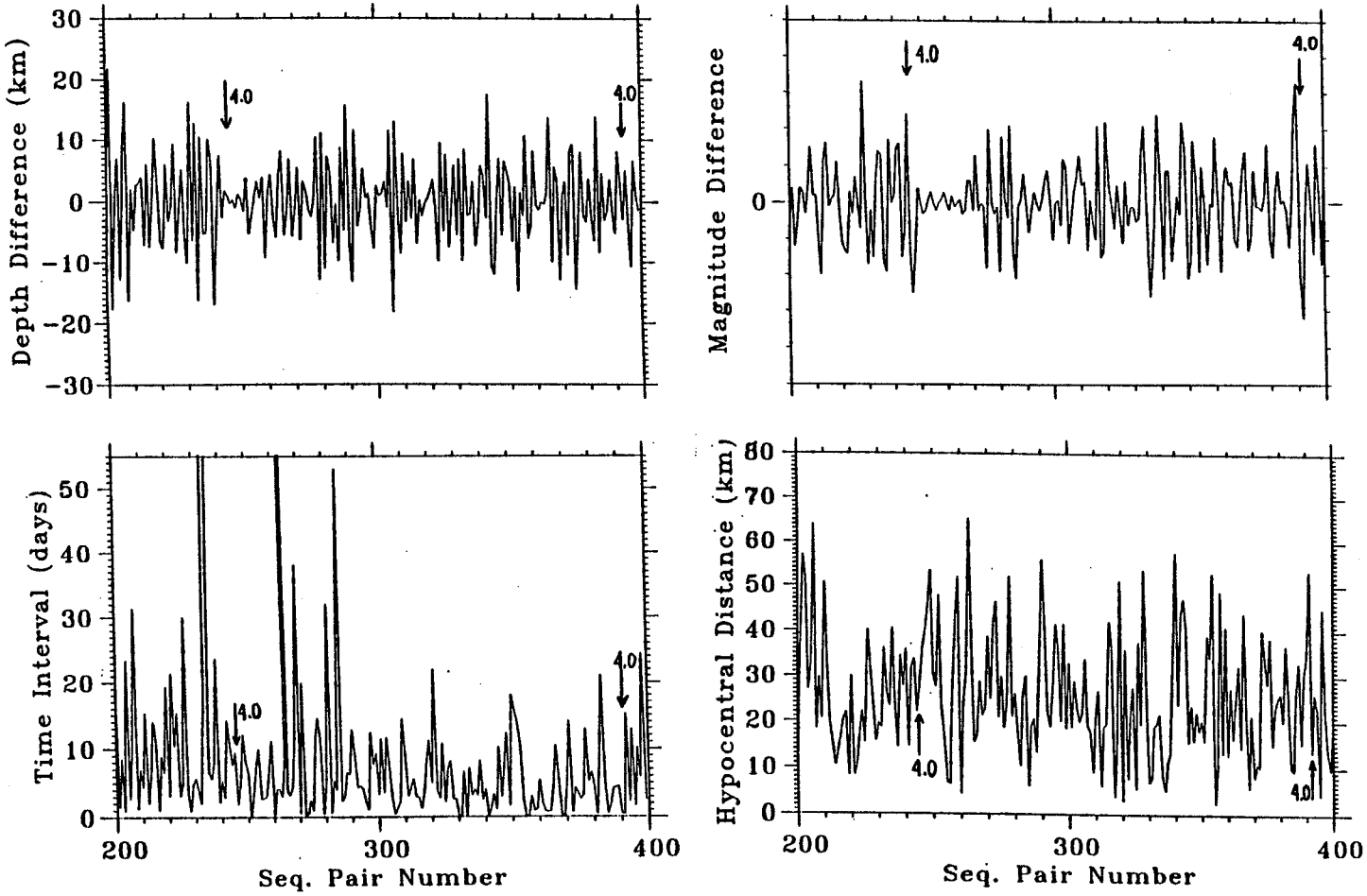

Figure 6.3.2 Plots from figure 6.3.1 zoomed in between the 200th and the 400th "next" pairs (upper frames) shown together with the time intervals (bottom left frame) and the hypocentral distances (bottom right frame) for the same pairs. Note that small magnitude and depth differences after the M4.0 around the 230th pair are not associated with small distances and time intervals.

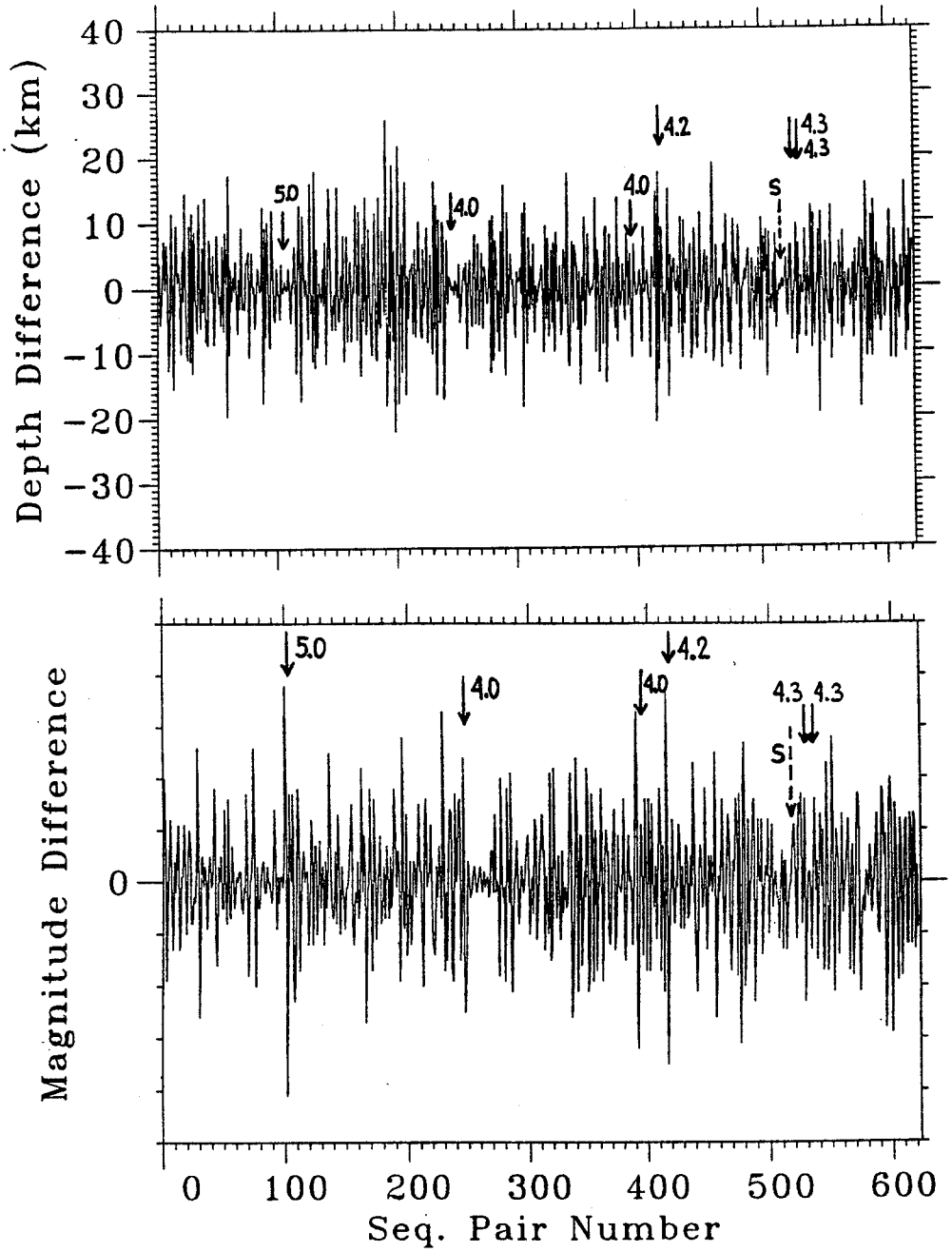

Figure 6.3.1 Depth (upper frame) and magnitude (lower frame) differences between "next" events versus sequential number of pairs. Arrows show the times of occurrence of the M≥4.0 local events. The nearby Saguenay event is marked with a dashed arrow and the letter S. Note that the M4.0 event around the 230th pair is followed by events of similar depths and magnitudes. See text for more detail.

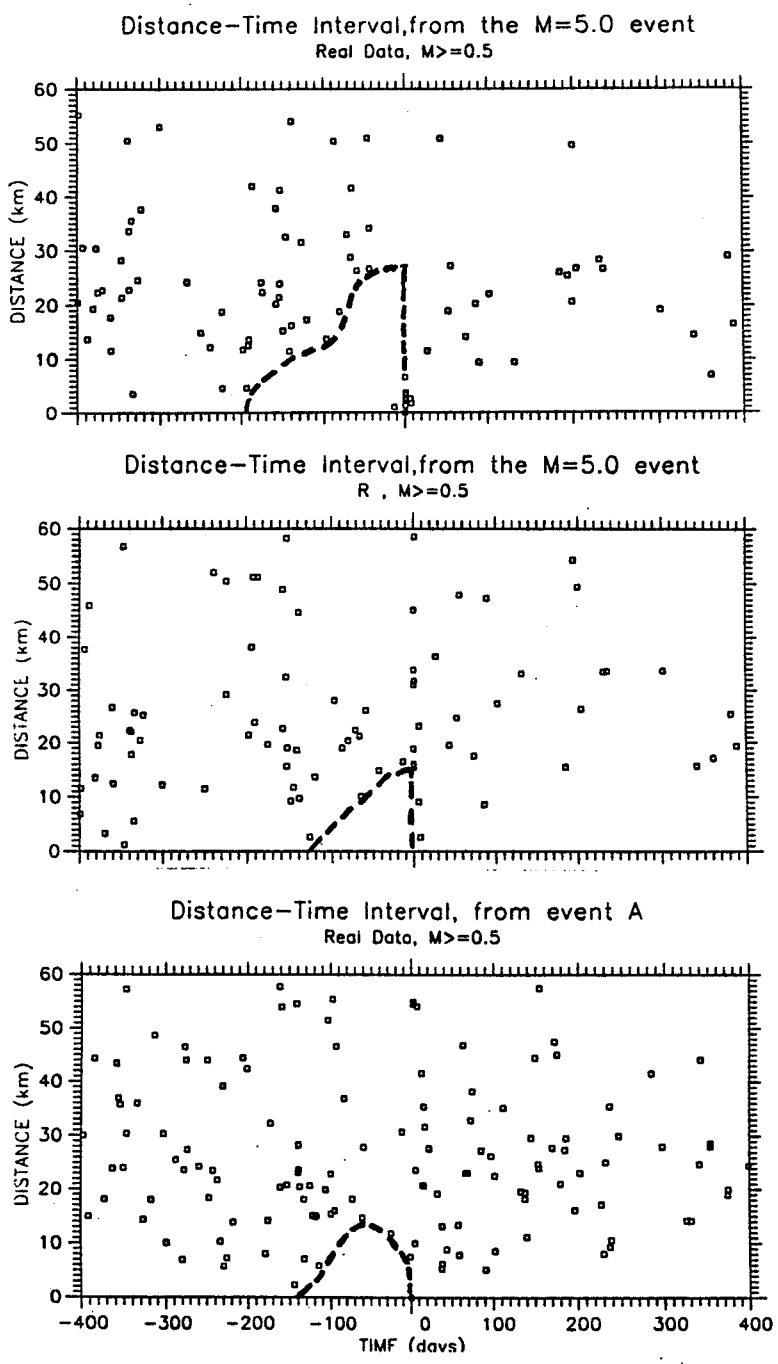

Figure 6.1.3 Distance-time interval plots for the real data in respect to the M5.0 event (upper frame); for one randomized catalogue (R) in respect to the same event (middle frame); and for the real data in respect to another arbitrary (A) event (bottom frame). Dashed lines outline "quite" regions in the distance-time interval space preceding the (0,0) point. See text for more detail.

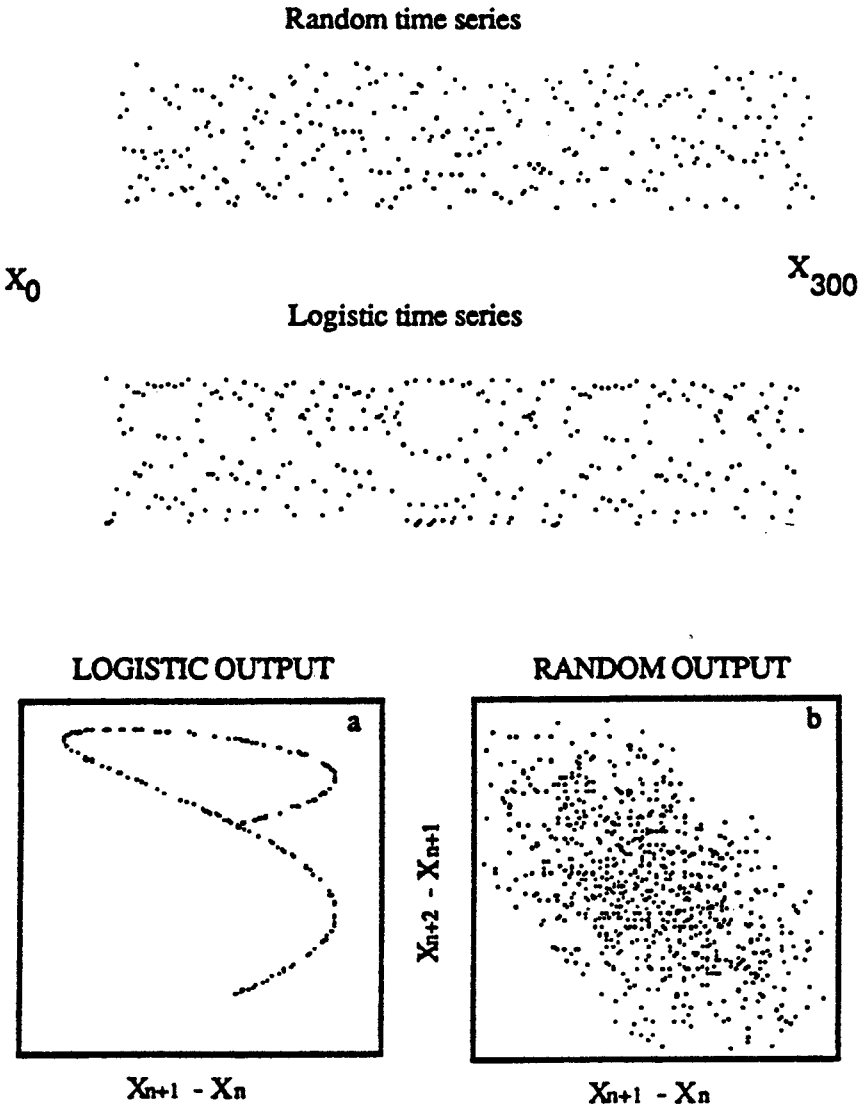

Figure 6.2.1 Difference plots used to compare random and logistic time series. The logistic equation used is $x_{n+1} = cx_n(x_{n-1})$. The value of c used in these plots is c=3.999. 301 values are shown along the vertical axes for each of the time series (two top frames). Difference plots are shown on the bottom. Note that while no difference is suggested by the time series, the difference plot for the logistic equation (bottom left) is markedly different from the plot for the random data (bottom right). After Fowler and Roach (1991).

For this reason, seismicity rates and b-values should be still closely monitored.
In addition, the present study attempts to promote the idea that earthquake catalogues can be examined beyond seismicity rates and b-values. It is unlikely that any single parameter can be found that would miraculously provide unique precursory information. It is instead necessary to monitor a number of parameters and observe their simultaneous changes, earthquake catalogues being only one of the data bases to be examined. One potential source of additional information, mostly ignored so far, is the spatial distribution of earthquakes and its temporal changes. A quantitative parameter describing this distribution can be an essential addition to the quantities previously studied.

In the present study three main quantitative techniques were applied to the CSZ catalogue:

(1) The first approach examined changes in seismicity rates depending on magnitude. This allowed us to identify six times of significant rate changes, most of which, however, seem to be artificial rather than natural. Artificial changes are due to changes in the networks rather than to natural processes. Since the local array has been known to be quite stable during the study period, this finding may be surprising. Periods when the array was down, as well as a change in the instrumentation after October 1987, may be the reasons for such artificial changes. In any case, none of these rate changes can be associated with the preparation period of any of the six local $M \geq 4.0$ earthquakes.

(2) The second technique used was pair analysis based on comparison between the frequency distributions of interevent distances, time intervals, and distance-time products derived from the real catalogue and from randomly generated catalogues. This allowed us to devise a quantitative measure for the degree of non-randomness in earthquake distribution. Long-term base values derived from the whole data set were compared with the short-term values derived from groups of events covering various periods of time. The degree of spatial non-randomness based on the interevent distances appears to be most informative. Larger degree of spatial non-randomness precedes the local M5.0 event in agreement with previous observations in other seismically active areas. The largest degree of spatial non-randomness, however, is observed around the time of a nearby large event (M6.5 Saguenay earthquake, November 1988; about 80 km away from the CSZ). This poses interesting questions about a possible effect on the CSZ of the stress changes following this event, or about the simultaneous response of the source area of the Saguenay event and the CSZ to a large-scale tectonic factor. The latter possibility is favoured at this time.

(3) The third technique used is based on correlation dimensions as applied in non-linear dynamics. Spatial correlation dimensions seem to be most informative, similar to the results from pair analysis. Higher spatial clustering is indicated around the time of the same nearby earthquake.

Pair analysis and the correlation dimension method appear to provide useful complimentary information about earthquake distribution that is different from the traditional seismicity rates and b-values. Continuous monitoring of the degree of non-randomness in earthquake distribution is highly recommended, especially monitoring of the spatial degree of non-randomness. Similarly, the correlation dimensions, more specifically the ones based on interevent distances, may help us identify clustering patterns preceding future large events. At present, the results from both pair analysis and the correlation dimension method seem to be more informative in the CSZ than the seismicity rates and the b-values. Monitoring of these new

parameters together with the traditional ones will guarantee a more complete use of the CSZ catalogue and a higher probability to identify possible precursory phenomena in the future.

In addition to this report, the results from the study of the space-time distribution of CSZ earthquakes were reported at the 1991 Fall meeting of the American Geophysical Union (AGU) in San Francisco, California (Eneva et al., 1991), the 1992 Spring AGU meeting in Montreal, Quebec (Eneva et al., 1992), as well as on seminars at the following: Geological Survey of Canada, Ottawa, Ontario; Department of Physics/University of Toronto, Toronto, Ontario; Department of Geological Sciences/Queen's University, Kingston, Ontario; Department of Physics and CIRES/University of Colorado, Boulder, Colorado; and Institute of Geophysics and Planetary Physics (IGPP) at Scripps Institute of Oceanography, La Jolla, California.

ACKNOWLEDGEMENTS

This report reflects the work done in connection with a contract funded by the Geological Survey of Canada, Geophysics Division (Energy, Mines and Resources, Canada). R.G. North and A.M. Franklin from GSC provided the data used. Discussions with John Adams, R.G. North, and A.M. Franklin, as well as with other seismologists at GSC were very important for this work to be completed. G. Buchbinder kindly provided information on the relationship between re-evaluated local and Nuttli's magnitudes for the CSZ. The study described in this report was performed at the Department of Physics/Geophysics, University of Toronto. The continuous support of Prof. G.F. West and Prof. R.M. Farquhar is highly appreciated. All plots in this report, except the ones in Chapter 3, were made using the interactive graphics package QPLOT, kindly supplied by Fred Klein from the U.S. Geological Survey, Menlo Park, California. Results and plots in Chapter 3 were obtained using programs written by Ted Habermann from the National Oceanic and Atmospheric Administration/National Geophysical Data Center, Boulder, Colorado.

REFERENCES

Adams, J., Crustal stresses in eastern Canada, in *Earthquakes at North Atlantic Passive Margin: Neotectonics and Postglacial Rebound*, Eds. S. Gregersen and P.W. Basham, Kluwer Academic Publishers, 289-297, 1989.

Adams, J. and P. Basham, The seismicity and seismotectonics of Canada east of the Cordillera, *Geoscience Canada* **16**, 3-16, 1989.

Adams,J., J. Sharp, and M. Stagg, New focal mechanisms for southeastern Canadian earthquakes, *Geological Survey of Canada, Open File 1892*, 109 pp., 1988.

Aki, K., Maximum likelihood estimate of b in the formula logN=a-bM and its confidence limits, *Bull. Earthq. Res. Inst.* **43**, 237-239, 1965.

Andrews, D.J., A stochastic fault model. 1. Static case, *J. Geophys. Res.* **85**, 3867-387, 1980.

Anglin, F.M., Seismicity and faulting in the Charlevoix zone of the St. Lawrence valley, *Bull. Seism. Soc. Amer.* **74**, 595-603, 1984.

Anglin, F.M. and G. Buchbinder, Microseismicity in the mid-St. Lawrence valley Charlevoix zone, Quebec, *Bull. Seism. Soc. Amer.* **71**, 1553-1560, 1981.

Aviles, C.A. and C.H. Scholz, Fractal analysis applied to characteristic segments of the San Andreas fault, *J. Geophys. Res.* **92**, 331-344, 1987.

Bak, P. and C. Tang, Earthquakes as a self-organized critical phenomenon, *J. Geophys. Res.* **94**, 15635-15637, 1989.

Basham, P.W., D.H. Weichert, F.M. Anglin, and M.J. Berry, New probabilistic strong seismic ground motion maps of Canada, *Bull. Seism. Soc. Amer.* **75**, 563-595, 1985.

Block, A., W. von Bloh, T. Klenke, and H.J. Schellnhuber, Multifractal analysis of the microdistribution of elements in sedimentary structures using images from scanning electron microscopy and energy dispersive X ray spectrometry, *J. Geophys. Res.* **96**, 16223-16230, 1991.

Boore, D.M. and G.M. Atkinson, Source spectra for the 1988 Saguenay, Quebec, earthquakes, *Bull. Seism. Soc. Amer.* **82**, 683-719, 1992.

Bower, D.R., Tidal and coseismic well-level observations at the Charlevoix Geophysical Observatory, Quebec, *Tectonophysics* **167**, 349-361, 1989.

Buchbinder, G.G.R., Shear-wave splitting and anisotropy in the Charlevoix seismic zone, Quebec, in 1985, *Can. J. Earth Sci.* **26**, 2691-2696, 1989.

Buchbinder, G.G.R., Velocity changes in the Charlevoix region, Quebec, in *Earthquake Prediction: An International Review*, Maurice Ewing series 4, Eds. D.W. Simpson and P.G. Richards, Amer. Geophys. Union, 367-376, 1981.

Buchbinder, G.G.R., A. Lambert, R.D. Kurtz, D.R. Bower, F.M. Anglin, and J. Peters, Twelve years of geophysical research in the Charlevoix seismic zone, *Tectonophysics* **156**, 193-224, 1988.

Davis, S.D. and C. Frohlich, Single-link cluster analysis, synthetic earthquake catalogues, and aftershock identification, *Geophys. J. Int.* **104**, 289-306, 1991.

Du Berger, R., D.W. Roy, M. Lamontagne, G. Woussen, R.G. North, and R.J. Wetmiller, The Saguenay (Quebec) earthquake of November 25, 1988: seismological data and geologic setting, *Tectonophysics* **186**, 59-74, 1991.

Ebel, J.E., P.G. Somerville, and J.D. McIver, A study of the source parameters of some large earthquakes of northeastern North America, *J. Geophys. Res.* **91**, 8231-8247, 1986.

Eneva, M., *Assessment of the Spatial, Temporal and Energetic Characteristic of Earthquakes in Regard to Seismic Zoning*, Ph.D. Thesis, Geophys. Inst., Bulg. Acad. Sci., Sofia, 178 pp., 1984.

Eneva, M., J. Adams, R.G. North, F.M. Anglin, Earthquake catalogues examined beyond seismicity rates and b-values: An example from the Charlevoix seismic zone, Quebec [abstract], *EOS trans. Amer. Geophys. Union* **73** (14), Spring Meeting Suppl., 197, 1992a.

Eneva, M. and R.M. Farquhar, *Space-Time Distribution of Earthquakes in the Charlevoix Seismic Zone, Quebec*, Proposal to GSC, 1991.

Eneva, M., R.E. Habermann, and M.W. Hamburger, Artificial and natural changes in the rates of seismic activity in the Garm region, Tadjikistan (CIS), submitted to *Geophys. J. Int.*, 1992b.

Eneva, M. and M. W. Hamburger, Spatial and temporal patterns of earthquake distribution in Soviet Central Asia: Application of pair analysis statistics, *Bull. Seism. Soc. Amer.* **79**, 4, 1475-1476, 1989.

Eneva, M., M. W. Hamburger, and G. A. Popandopulo, Spatial distribution of earthquakes in aftershock zones of the Garm region, Soviet Central Asia, *Geophys. J. Int.* **109**, 38-53, 1992c.

Eneva, M., R.G. North, J. Adams, F.M. Anglin, Space-time distribution of earthquakes in the Charlevoix seismic zone [abstract], *EOS trans. Amer. Geophys. Union* **72** (44), Fall Meeting Suppl., 336, 1991.

Eneva, M. and G. L. Pavlis, Application of pair analysis statistics to aftershocks of the 1984 Morgan Hill, California, earthquake, *J. Geophys. Res.* **93**, 9113-9125, 1988.

Eneva, M. and G. L. Pavlis, Spatial distribution of aftershocks and background seismicity in central California, *Pure Appl. Geophys.* **137**, 35-61, 1991.

Forsyth, D., P. Morel, H. Hasegawa, R. Wetmiller, J.Adams, A. Goodacre, D. Nagy, R. Coles, J. Harris, P. Basham, Comparative study of the geophysical and geological information in Timiskaming-Kapuskasing area, *At. Energy Can. Tech. Rec., TR-238*, 50 pp., 1983.

Fowler, T. and D. Roach, Dimensionality analysis of objects and series data, in *Nonlinear Dynamics, Chaos and Fractals with Applications to Geological Systems, GAC, Short Course Notes* **9**, Toronto, 59-81, 1991.

Frohlich, C. and S.D. Davis, Single-link cluster analysis as a method to evaluate spatial and temporal properties of earthquake catalogues, *Geophys. J. Int.* **100**, 19-32, 1990.

Fukao, Y. and M. Furumoto, Hierarchy in earthquake size distribution, *Phys. Earth Planet. Inter.* **37**, 149-168, 1985.

Goodings, D., Chaos in a time series, in *Nonlinear Dynamics, Chaos and Fractals with Applications to Geological Systems, GAC, Short Course Notes* **9**, Toronto, 35-46, 1991.

Grassberger, P., Generalized dimensions of strange attractors, *Phys. Lett.* **97A**, 227-230, 1983.

Grassberger, P. and I. Procaccia, Measuring the strangeness of strange attractors, *Physica* **9D**, 189-208, 1983.

Habermann, R.E., Teleseismic detection in the Aleutian island ark, *J. Geophys. Res.* **88**, 5056-5064, 1983.

Habermann, R.E., A test of two techniques for identifying systematic errors in magnitude estimates using data from the Parkfield, California region, *Bull. Seism. Soc. Amer.* **76**, 1660-1667, 1986.

Habermann, R.E., Man-made changes of seismicity rates, *Bull. Seism. Soc. Amer.* **77**, 141-159, 1987.

Habermann, R.E., Seismicity rate variations and systematic changes in magnitudes in teleseismic catalogues, *Tectonophysics* **193**, 277-290, 1991.

Habermann, R.E. and M.S. Craig, Comparison of Berkeley and CALNET magnitude estimates as a means of evaluating temporal consistency of magnitudes in California, *Bull. Seism. Soc. Amer.* **78**, 1255-1267, 1988.

Haddon, R.A., Waveform modelling of strong-motion data for the Saguenay earthquake of 25 November 1988, *Bull. Seism. Soc. Amer.* **82**, 720-754, 1992.

Hasegawa, H.S., Neotectonics and inferred movements in Canada, *Bull. Geol. Soc. Finland* **60**, Part 1, 3-25, 1988.

Hasegawa, H.S., J. Adams, and K. Yamazaki, Upper crustal stresses and vertical stress migration in eastern Canada, *J. Geophys. Res.* **90**, 3637-3648, 1985.

Hasegawa, H.S. and R.J. Wetmiller, The Charlevoix earthquake of 19 August 1979 and its seismotectonic environment, *Earthquake Notes* 51, 23-37, 1980.

Hirata, T., A correlation between the b value and the fractal dimension of earthquakes, *J. Geophys. Res.* **94**, 7507-7514, 1989a.

Hirata, T., Fractal dimension of fault systems in Japan: Fractal structure in rock fracture geometry at various scales, *Pure Appl. Geophys.* **131**, 157-170, 1989b.

Hirata, T. and M. Imoto, Multifractal analysis of spatial distribution of microearthquakes in the

Kanto region, *Geophys. J. Int.* **107**, 155-162, 1991.

Hirata, T., T. Satoh, and K. Ito, Fractal structure of spatial distribution of microfracturing in rock, *Geophys. J. R. astr. Soc.* **90**, 369-374, 1987.

Ishibashi, K., Two categories of earthquake precursors, physical and tectonic, and their roles in intermediate-term earthquake prediction, *Pure Appl. Geophys.* **126**, 687-700, 1988.

Kagan, Y. and L. Knopoff, Spatial distribution of earthquakes: the two-point correlation function, *Geophys. J. R. astr. Soc.* **62**, 303-320, 1980.

Keilis-Borok, V.I., The lithosphere of the earth as a nonlinear system with implications for earthquake prediction, *Rev. Geophys.* **28**, 19-34, 1990.

King, G., The accommodation of large strains in the upper lithosphere of the Earth and other solids by self-similar fault systems: the geometrical origin of b-value, *Pure Appl. Geophys.* **121**, 761-814, 1983.

Kurths, J. and H. Herzel, An attractor in a solar time series, *Physica* **25D**, 165-172, 1987.

Kumarapeli, P.S. and V.A. Saull, The St. Lawrence valley system: A North American equivalent of the east African rift valley system, *Can. J. Earth Sci.* **3**, 639-658, 1966.

Lambert, A. and J.O. Liard, A search for long-term earthquake precursors in gravity data in the Charlevoix region, Quebec, in *Earthquake Prediction: An International Review*, Maurice Ewing series 4, Eds. D.W. Simpson and P.G. Richards, Amer. Geophys. Union, 473-483, 1981.

Lamontagne, M., Seismic activity and structural features in the Charlevoix region, Quebec, *Can. J. Earth Sci.* **24**, 2118-2129, 1987.

Lamontagne, M., R.J. Wetmiller, and R. Du Berger, Some results from the 25 November, 1988 Saguenay, Quebec, earthquake, in *Current Research, Part B, Geological Survey of Canada*, Paper 90-1B, 115-121, 1990.

Leblanc, G. and G. Buchbinder, Second microearthquake survey of the St. Lawrence valley near La Malbaie, Quebec, *Can J. Earth Sci.* **14**, 2778-2789, 1977.

Leblanc, G., A.E. Stevens, R.J. Wetmiller, and R. Du Berger, A microearthquake survey of the St. Lawrence valley near La Malbaie, Quebec, *Can. J. Earth Sci.* **10**, 42-53, 1973.

Lyons, J.A., D.A. Forsyth, and J.A. Mair, Crustal studies in the La Malbaie region, Quebec, *Can. J. Earth Sci.* **17**, 478-490, 1980.

Matsumura, S., A one-parameter expression of seismicity patterns in space and time, *Bull. Seism.*

Soc. Amer. **74**, 2559-2576, 1984.

Meyer, S.L., *Data Analysis for Scientists and Engineers*, John Wiley and Sons, Inc., New York, 512 pp., 1975.

Milne, W.G., W.E.T. Smith, and G.C. Rogers, Canadian seismicity and micro-earthquake research in Canada, *Can. J. Earth Sci.* **7**, 591-601, 1970.

Nerenberg, M.A.H. and C. Essex, Correlation dimension and systematic geometric effects, *Phys. Rev.* **A 42**, 7065-7074, 1990.

North, R.G., Modernisation of the Canadian National Seismograph Network (unpublished manuscript, 1991).

North, R.G., Station magnitude bias - Its determination, causes, and effects, in *Technical Note #1977-24*, Lincoln Laboratory, Massachusetts Institute of Technology, Cambridge, Massachusetts, 1977.

North, R.G., R.J. Wetmiller, J. Adams, F.M. Anglin, H.S. Hasegawa, M. Lamontagne, R. Du Berger, L. Seeber, and J. Ambruster, Preliminary results from the November 25, 1988 Saguenay (Quebec) earthquake, *Seism. Res. Lett.* **60**, 89-93, 1989.

Nuttli, O.W., Seismic wave attenuation and magnitude relations for eastern North America, *J. Geophys. Res.* **78**, 876-885, 1973.

Okubo, P.G. and K. Aki, Fractal geometry in the San Andreas fault system, *J. Geophys. Res.* **92**, 345-355, 1987.

Ouchi, T. and T. Uekawa, Statistical analysis of the spatial distribution of earthquakes - variation of the spatial distribution of earthquakes before and after large earthquakes, *Phys. Earth Planet. Inter.* **44**, 211-225, 1986.

Pavlis, G.L., M.W. Hamburger, and I.L. Nersessov, Anomalies in the magnitude-frequency relation of earthquakes in the Garm region, *Bull. Seism. Soc. Amer.* 79, 1913-1926, 1989.

Purcaru, G. and K. Pawlzik, A new tool for identification of anomalous seismicity patterns, in *Int. Conf. on Earthquake Prediction: State of the art, 15-18 October 1991*, European-Mediterranean Seismological Centre, Srasburg, 108-115, 1992.

Radulian, M. and C.-I. Trifu, Would it have been possible to predict the 30 August 1986 Vrancea earthquake? *Bull. Seism. Soc. Amer.* **81**, 2498-253, 1991.

Reasenberg, P.A. and M.V. Matthews, Precursory seismic quiescence: a preliminary assessment of the hypothesis, *Pure Appl. Geophys.* **126**, 373-406, 1988.

Reasenberg, P.A. and R.W. Simpson, Response of regional seismicity to the static stress change produced by the Loma Prieta earthquake, *Science* **255**, 1687-1690, 1992.

Reyner, M., Long- and intermediate-term seismic precursors to earthquakes - state of the art, in *Earthquake Prediction: An International Review*, Maurice Ewing series 4, Eds. D.W. Simpson and P.G. Richards, Amer. Geophys. Union, 333-347, 1981.

Rondot, J., Reconnaissances geologique dans Charlevoix-Saguenay, Ministere des Richesses Naturelles, Quebec, DPV-682, 1979.

Roy, D.W. and R. Du Berger, Relations possibles entre la microseismicite recente et l'astrobleme de Charlevoix, *Can. J. Earth Sci.* **20**, 1613-1618, 1983.

Rundle, J.B., A physical model for earthquakes. 1. Fluctuations and interactions, *J. Geophys. Res.* **93**, 6237-6254, 1988.

Rundle, J.B., A physical model for earthquakes. 2. Application to southern California, *J. Geophys. Res.* **93**, 6255-6274, 1988.

Rundle, J.B., Derivation of the complete Gutenberg-Richter magnitude-frequency relation using the principle of scale invariance, *J. Geophys. Res.* **94**, 12337-12342, 1989.

Sadovsky, M.A., L.G. Bolkhovitinov, and B.F. Pisarenko, *Deformation of Geophysical Media and Seismic Process*, Nauka Publ., Moscow (in Russian), 1987.

Sanford, b.w., F.J. Thompson, G.H. McFall, Phanerozoic and recent tectonic movements in the Canadian Shield and their significance to the nuclear fuel waste management program, in *Proceedings on Workshop on transitional processes, Atom. Energy Can. Ltd.*, AECL-7822, 73-96, 1984.

Shaw, B.E., J.M. Carlson, and J.S. Langer, Patterns of seismic activity preceding large earthquakes, *J. Geophys. Res.* **97**, 479-488, 1992.

Smalley, R.F., J.-L. Chatelain, D.L. Turcotte, and R. Prevot, A fractal approach to the clustering of earthquakes: Applications to the seismicity of the New Hebrides, *Bull. Seism. Soc. Amer.* **77**, 1368-1381, 1987.

Smith, W.D., Evidence for precursory changes in the frequency-magnitude b-value, *Geophys. J. R. astr. Soc.* **86**, 815-838, 1986.

Smith, W.E.T., Earthquakes of eastern Canada and adjacent areas 1534-1927, *Publications of the Dominion Observatory* **26**, 271-301, 1962.

Somerville, P.G., J.P. McLaren, C.K. Saikia, and D.V. Helmberger, The 25 November 1988

Sagueany, Quebec earthquake: source parameters and the attenuation of strong ground motion, *Bull. Seism. Soc. Amer.* **80**, 1118-1143, 1990.

Stevens, A.E., Reexamination of some larger La Malbaie, Quebec, earthquakes (1924-1978), *Bull. Seism. Soc. Amer.* **70**, 529-557, 1980.

Turcotte, D.L., A fractal model for crustal deformation, *Tectonophysics* **132**, 261-269, 1986.

Turcotte, D.L., Fractals and fragmentation, *J. Geophys. Res.* **91**, 1921-1926, 1986.

Utsu, T., Aftershocks and earthquake statistics (III). Analysis of the distribution of earthquakes in magnitude, time, and space with special consideration to clustering characteristics of earthquake occurrence, *J. Hokkaido Univ., Ser. VII, Geophysics,* v. III, No 5, 379-441, 1971.

Wetmiller, R.J. and J. Adams, An earthquake doublet in the Charlevoix seismic zone, Quebec, in *Current Research, Part B, Geological Survey of Canada*, Paper 90-1, 105-113, 1990.

Wetmiller, R.J., J. Adams, F.M. Anglin, H.S. Hasegawa, and A.E. Stevens, Aftershock sequences of the 1982 Miramichi, New Brunswick, earthquakes, *Bull. Seism. Soc. Amer.* **74**, 621-653, 1984.

Wahlstrom, R., Focal mechanisms of earthquakes in southern Quebec, southeastern Ontario, and northeastern New York with implications for regional seismotectonics and stress field characteristics, *Bull. Seism. Soc. Amer.* **77**, 891-924, 1987.

Wardlaw, R.L., C. Frohlich, and S.D. Davis, Evaluation of precursory seismic quiescence in sixteen subduction zones using single-link cluster analysis, *Pure Appl. Geophys.* **134**, 57-78, 1990.

Wyss, M., Reporting history of the central Aleutians seismograph network and the quiescence preceding the 1986 Andreanoff Island earthquake, *Bull. Seism. Soc. Amer.* **81**, 1231-1254, 1991.

Wyss, M. and R. E. Habermann, Precursory quiescence before the August 1982 Stone Canyon, San Andreas fault, earthquakes, *Pure Appl. Geophys.* **126**, 333-356, 1988.

Yamazaki, K. and H.S. Hasegawa, Deformation of non-uniform viscous lithosphere: with special reference to seismogenic stress in southeastern Canada, *Tohoku Geophys. J.* **33**, 23-42, 1990.

Yang, J.-P. and Y.P. Aggarwal, Seismotectonics of northeastern United States and adjacent Canada, *J. Geophys. Res.* **86**, 4981-4998, 1981.